fossil studies

MDPI

Article

Pleistocene Small Mammals from Kozarnika Cave (Bulgaria): Morphology, Systematics, and Paleoecology †

Vasil Popov

Institute of Biodiversity and Ecosystem Research, Bulgarian Academy of Sciences, 1 Tsar Osvoboditel Blvd, 1000 Sofia, Bulgaria; vasilvpopov@gmail.com

† urn:lsid:zoobank.org:act:D1E9A26B-8C05-4C8C-9CAB-BE9F060105A8; urn:lsid:zoobank.org:pub:78AC7BA4-1AF5-4896-BCDF-AF9BD791CCBD.

Abstract

Kozarnika Cave revealed a lengthy archaeological sequence covering the Lower, Middle, and Upper Paleolithic periods. The site is a significant milestone in understanding the various stages of early human colonization and migration into Europe. The available paleomagnetic data indicate that the lower boundary of the deposits corresponds to the Brunhes–Matuyama reversal. During the archaeological excavations, an exceptionally rich assemblage of small mammal remains was recovered. Based on small mammals, two biozones have been delineated—lower (Biozone B) and upper (Biozone A)—which correspond to the Late Biharian and Toringian, respectively. In the present study, a total of 75 species of terrestrial small mammals (Eulipotyphla, Lagomorpha, Rodentia) are analyzed in detail. One new species, *Nannospalax sirakovi* sp. n., is described. Based on geometric analysis of the mass material of voles (Microtina and *Lagurus*), the controversial taxonomic positions of some species have been clarified. It has been proven that *Microtus arvalinus* is a distinct species. Rapid evolution within the species *Lagurus transylvanicus* towards the modern species *L. lagurus* has been demonstrated. In all layers of Biozone B, two important guide fossils, *Mimomys savini* and *M. blanci*, occur. They are indicative of the second stage of the Early Biharian, which is considered earlier than the Brunhes/Matuyama reversal. Besides this, multiple species characteristic of the Early Pleistocene (Villanyian and the Early Biharian) have been identified (*Borsodia newtoni*, *B. arankoides*, *Prolagurus pannonicus*, *Ungaromys nanus*, *Villanyia* cf. *exilis*, *Allophaiomys deucalion*, *A.* cf. *pliocaenicus*, *A.* cf. *burgondiae*, *Mimomys pitymyoides*, *M.* cf. *tornensis*, *Lagurus arankae*). Although very scarce, they occur regularly in the stratigraphic assemblages of Biozone B, which is dominated by typical Late Biharian species, such as *Allophaiomys gregaloides*, *Microtus arvalidens*, *M. nivalinus*, *M. nivaloides*, and *L. transylvanicus*. The occurrence of *Mesocricetus newtoni* and *Spermophilus citellus* in Biozone B marks the earliest known occurrence of these species. The faunal turnover within the lower part of the deposits has been analyzed in detail. A reorganization of the fauna has resulted from the gradual disappearance of the Early Pleistocene species. Paleoecological reconstructions based on stratigraphic assemblages of small mammals suggest that the faunal turnover recorded in Biozone B is associated with paleoclimatic changes during the MIS19–MIS17 interval and reflects a reorganization of the biota related to the mid-Pleistocene transition. This period was marked by significant changes in Earth's climate, shifting from low-amplitude 41,000-year obliquity-driven cycles to high-amplitude, roughly 100,000-year fluctuations that define the later Pleistocene and Holocene.

Keywords: biostratigraphy; Quaternary; climate change; taxonomy; rodents; insectivores; lagomorphs; biometry; evolution

Check for updates

Academic Editors: Dimitris S. Kostopoulos and Eric Buffetaut

Received: 16 June 2026
Revised: 8 July 2026
Accepted: 10 July 2026
Published: 13 August 2026

Copyright: © 2026 by the author. Licensee MDPI, Basel, Switzerland. This article is an open access article distributed under the terms and conditions of the Creative Commons Attribution (CC BY) license.

1. Introduction

The Kozarnika Cave (Northwest Bulgaria) contains an important sedimentary sequence spanning the entire Pleistocene. Since 1996, numerous lithic, faunal, and human remains have been discovered. It provides evidence of the presence of the genus *Homo* in Europe as early as the Early Pleistocene [1–3]. The successive Paleolithic sequences in Kozarnika Cave, the rich paleontological record, and the geographical position make this site a milestone in documenting and understanding the different phases of the earliest human settlement and faunal turnover in this region of the Balkan Peninsula.

Preliminary information on small mammals is available in our earlier publication [4], which is based on material collected during 1996–2004. It reports 68 species and provides a detailed biometric analysis of several vole species of biostratigraphic importance. After this period, an extremely abundant material was accumulated, allowing for additional insights into many aspects of the evolution of numerous species and phylogenetic lineages, as well as a detailed analysis of faunal turnover in the context of ecological changes recorded in the ecological spectra of small-mammal stratigraphic assemblages. The aim of this study is to document as thoroughly as possible the fossil material collected so far, to trace the chronological morphological variability of the mass species, to make paleoecological reconstructions, and, based on this, to track and analyze the dynamics of the fauna from the Late Biharian to the end of the Pleistocene.

2. Locality

Kozarnika Cave is located in northwestern Bulgaria (43.652 N, 22.702 E), on the border between the expansive Danube Plain and the foothills of the Stara Planina Mountain (Figure 1C). The entrance faces south and is situated on the northern slope of the valley of a small tributary of the Skomliya River at an elevation of 481 m, about 85 m above the riverbed [2]. During archaeological excavations from 1996 to 2009, a 9-m-thick stratigraphic sequence was uncovered at the cave's entrance (Figure 1A,B). Twenty-three lithological units (layers 3–14 and some subdivisions) have been identified [2,5]. The uppermost layers, 3a to 4, which are about 1 to 1.4 m thick, consist of limestone clasts (from the cave walls and ceiling) embedded in a light-brown to whitish silt matrix. The radiocarbon dates from these layers suggest a period between 13.2 and 24.5 Kya (thousand years ago) [1,3].

Layers 5a to 10c measure roughly 1.2 to 1.5 m in total thickness. The upper part of this sequence, layers 5a to 10a, features a yellowish-brown silty matrix containing limestone clasts and blocks originating from the fragmentation of the cave's walls and ceiling. The underlying layers, 10b and 10c, are composed of loose, dark brown, clayey sand containing gravels and limestone pebbles, with varying degrees of weathering. The radiocarbon age for layer 5b is approximately 31.2 Kya. A tephra horizon observed in layer 5b has been identified as the Campanian Ignimbrite tephra eruption (CI), serving as an important marker in the Balkans and eastern Mediterranean [3]. Uncalibrated radiocarbon ages for layers 6/7 range from 42.7 to 43.6 Kya [2]. Layers 9a to 10a hold archaeological assemblages characteristic of the Middle Paleolithic (Moustierian), while layers 10b and 10c include the lower part of the Mousterian sequence. Layer 10b has an optically stimulated luminescence (OSL) age of 128–183 Kya [6].

https://doi.org/10.3390/fossils4030023

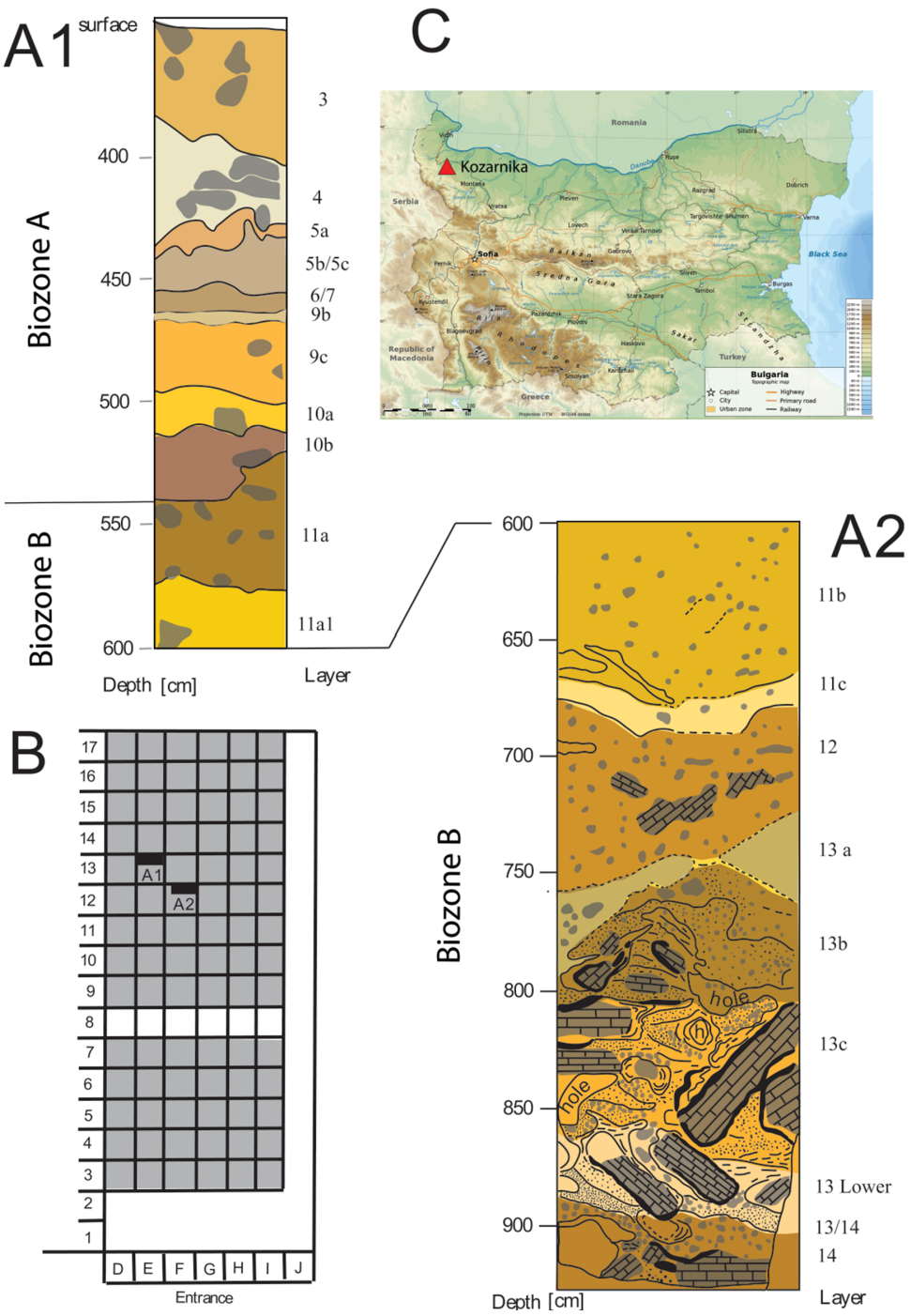


Figure 1. Kozarnika Cave. (**A1**,**A2**) Lithostratigraphy (updated after [2]), the stratigraphic ranges of Biozone A and Biozone B, based on small mammals used later in the text, are also shown. (**B**) Excavated area (shaded), positions of the stratigraphic columns (**A1**,**A2**), and the coordinate system of squares of 1 m^2 (1–17, D–J). (**C**) Map of Bulgaria, showing the location of the cave (modified from [4]).

Layers 11a to 13c have a combined thickness of about 2.5 m. They consist of relatively dense, yellowish-brown clayey sediments interspersed with dark manganese nodules and, to varying degrees, rich in boulders. These layers show significant erosion. They contain Lower Paleolithic industries that are not Acheulean. Evidence of burrowing associated with sediment erosion has been found in layer 11a [5]. Layers 13-Lower and 14 form the lowest levels of the profile, characterized by many limestone blocks with a yellowish-brown, laminated, sandy matrix between them. No archaeological artifacts have been found in these layers.

The age of the lower layers, 13a–13c, was estimated using biostratigraphy based on data from two mammal groups: large and small. The interpretation of the large mammal data assumed that these layers belong to zones 19 to 17 of the Mammalian Neogene/Quaternary (MNQ), roughly 1400 to 1600 Kya [1,2,7].

The biostratigraphic analysis of small mammals [4] showed that the Kozarnika profile can be divided into four biozones: A1 (layers 3–4–9c), A2 (layer 10a), B1 (layers 11a–11a1), and B2 (layers 13b–13c). Biozone A, which contains species similar to modern ones, was assigned to the Toringian, consistent with the available absolute dates. Biozone B, covering layers 11a–13c, features a relatively uniform small-mammal fauna typical of the Late Biharian. Since the lower boundary of the Late Biharian lies just above the Brunhes–Matuyama paleomagnetic boundary, it was suggested that the age of the deposits, at least down to layer 13c, does not exceed 1 million years. On the other hand, among the small mammals in layers 11a–13c, Villanyian and Early Biharian species were identified, although in small quantities [4]. These species are supposed to have disappeared long before the Brunhes–Matuyama boundary [8]. The age of this group aligns with the chronological framework proposed for large mammals.

Magnetostratigraphic studies [5] clarify the interpretation of mammalian biostratigraphic data. A sharp polarity change in layer 13-Lower was interpreted as the Brunhes–Matuyama boundary [5]. Given that loess is a dominant textural component in the Kozarnika sedimentary infill, down to at least layers 13 a–c, and that Kozarnika cave is located at the southwestern margin of the Bulgarian lower Danube loess belt, where loess deposition generally began sometime between the Jaramillo Subchron (990 Kya) and the Brunhes–Matuyama reversal, the magnetostratigraphic data suggest that layers 13 a–c could correspond to Loess L 6 to L 7 within the ~600 to ~750 Kya time interval. Further down, thin, short intervals of normal polarity were found within stable reverse polarity (Matuyama). The upper interval with positive inclinations at the base of layer 13-Lower might represent the Jaramillo Subchron. In contrast, the lowermost thin positive-inclination interval at 8.7 m in layer 14 could be a partial record of the Olduvai Subchron. However, these intervals are difficult to interpret due to the sedimentological complexity (Figure 1(A2)) [5].

Further in the text, biozones based on small mammals were used: Biozone A (layers 3–4–10b)—Toringian; Biozone B (layers 11a–14)—Biharian.

3. Material and Methods

During archaeological excavations, sediment samples were collected continuously at 5 cm intervals throughout the entire layer sequence. Samples were washed through a 1-mm-mesh bag. Residues were air-dried and sorted by experienced field assistants for microvertebrate bones. The bone material was examined under a binocular microscope, and all identifiable microvertebrate remains were collected. In the laboratory, these remains, consisting of isolated teeth and, more rarely, jaws or their fragments, were temporarily mounted on microscope slides with the occlusal surface facing up for further processing and identification.

The specimens were photographed with a Zeiss stereomicroscope, equipped with an AxioCam ERc5s camera and AxioVision 4.8 software. During image capture, the software displays each image on the computer screen, allowing the addition of a scale bar and text such as the sediment sample number, square, depth, and layer. It also enables the measurement of captured objects and saves the results in a separate CSV file.

The specimens and their images are stored in the Fossil Mammal Collection at the Institute of Biodiversity and Ecosystem Research of the Bulgarian Academy of Sciences. They are cataloged in the collection's database (https://iber-bas.collections.dissco-bg.eu; accessed on 22 July 2026). The database contains 25,132 object entries, mainly individual teeth, and 18,299 linked photographs. This material is described and analyzed in the

taxonomic section of this publication (Table S1). The database enables queries across multiple fields, and results can be exported to a text file, simplifying analysis.

3.1. Anatomic Nomenclature and Measurements

The teeth, the most numerous elements among the fossil remains, are designated with capital and lowercase letters for the upper and lower teeth, respectively. Anatomical terminology and respective abbreviations used in the systematic part were compiled from the following sources: Ochotonidae [9], *Apodemus* [10]; Castoridae [11]; Cricetinae [12]; Dipodidae [13]; Gliridae [14]; Hystricidae [15]; Soricidae [16]; Spalacidae [17–19]; *Spermophilus* [20]; Arvicolinae [21–26].

Since descriptive terms and abbreviations related to the specific occlusal surface of the molars of voles, Arvicolinae, have been adopted, those used later in the text are presented here for convenience: AC2/AC3—anterior cap; ACC—anteroconid complex; BSA—buccal salient angle; BRA—buccal reentrant angle, LRA—lingual reentrant angle; LSA—lingual salient angle; PL—posterior lobe; T1–T6—dentine fields of triangles. The reentrant angles and the triangles are numbered consecutively from PL towards ACC of the m1.

In most cases, teeth, the most abundant element in fossil remains, were measured for length (L) and width (W), taken along or perpendicular to the longitudinal axis of the occlusal surface, respectively. Later, depending on the needs, additional dimensions were taken from the photographs using specific schemes for a particular taxonomic group.

Soricidae [16]: AW—anterior width; BL—buccal length; HC—height of the condyle; HMd/m2—height of the horizontal ramus of the mandible, measured lingually; HPC—height of the coronoid process; LL—lingual length; LLF—length of the lower facet of the condyle; LUF—length of the lower facet of the condyle; PE—length to the posterior emargination; PW—posterior width; LI—length of upper incisive; LTI—length of the talon of upper incisive; HI—height of upper incisive; the length of some teeth [I1, i1, a1, a2(p4)] was measured along their buccal sides; (a), (c) denotes alveolar or coronar lengths, respectively.

Talpidae, humerus [27,28] H-MAXL—maximal length; H-L1—length from the baseline to the median point of the bicipital grove; H-L2—length from the baseline to the most distal point of the teres tubercle; H-L3—length from the baseline to the distal point of the pectoral tubercle; H-MINW—minimal width of the shaft; H-W—maximal width across the capitulum and the fossa for musculus flexorum digitorum ligament; H-W2—width between the most prominent points of the greater tuberosity and the median point of the bicipital groove; H-MAXW—maximal width.

Arvicolinae [21–23,26]: L—total length, W—width of the tooth across the base triangles (T4–T5) of the anteroconid complex, c—shortest distance between BRA3 and LRA3 angles, a/L [%]—relative length of the anteroconid complex, c/W [%]—relative width of the dentine connection between T4 and T5, SDQ3 [%] index representing the differentiation of enamel based on T1–T3 [29]. The method of measuring the width of the enamel stripes is illustrated in [30].

3.2. Statistical Methods for Processing Quantitative Morphological Data

The measurements were summarized using basic statistical parameters. N: sample size, Min–Max: observation range, X: arithmetic mean, SD: standard deviation. Since most samples subjected to statistical comparisons were very large, even minor differences are often statistically significant but may not reflect biologically meaningful variation. In such cases, Cohen's effect size coefficient was used to determine whether the differences are significant enough to be relevant in real-world scenarios. It measures the difference between two means in standard deviation units. Only values above 0.8, indicating large effect sizes, were considered for interpretation in the biometric analyses.

In addition to linear measurements, the mass species-specific first lower molars (m1) of voles from the subtribe Microtina and the genus *Lagurus* were analyzed using geometric morphometrics. For this purpose, 29 landmarks were digitized on each molar. The coordinates of the landmarks were recorded from the photographs using the tpsDig 3.0 software [31]. Before recording data, each image was flipped so that each appeared to be a left tooth. The landmarks were located on the anteroconid complex, which contains the most essential information for species identification. The locations of the points are shown in the figures, which illustrate the analysis results. In addition, the coordinates of a point at the most posterior part of the tooth and the endpoints of the scale bar in each photo were recorded and used to calculate standard linear dimensions using the TMorhoGen8 package from the Integrated Morphometrics Package Suite [32]. The geometric analysis presumes that the landmarks represent anatomical points inferred to be homologous among specimens. Since the analyzed species exhibit varying degrees of complexity in the anteroconid complex, simpler morphotypes lack elements present in more complex ones. In these cases, in the simplified morphotypes, semilandmarks were digitized on the homologous outline parts as in the more complex morphotypes. They are located close to one another and share the same serial number. Thus, they conform to the requirements for type I or II landmarks, according to Bookstein's [33] classification of landmarks. Landmark coordinates from specimens were superimposed using Generalized Procrustes Analysis (GPA), which translates, rotates, scales, and optimally aligns configurations to a consensus form by minimizing Procrustes distances. A bending energy matrix was computed using thin-plate spline (TPS) interpolation functions to quantify local deformation costs. Its inverse or power (coefficient alpha) allows for weights in thin-plate splines to emphasize global (alpha > 0) or local (alpha < 0) shape changes [33]. In the analyses, alpha was set to -1. Eigenvectors of the bending energy matrix yield principal warps (non-affine components) and uniform components that capture affine variation; together, these form the relative warp axes. Individual-aligned specimens were projected onto these axes. The analyses were performed using the TPSRELW program [34]. The shape variability was visualized using thin-plate spline transformation grids [35], which represent the deformation of the shape relative to the dataset's average shape. Expansions/contractions were color-coded for each network cell, with red indicating expansion and blue indicating contraction. These analyses were performed using the PAST v. 2.17c software package [36]. To identify patterns of morphological variability, the scores on the first two relative wraps (RW1 and RW2)—which account for about 50% of shape variability in the analyzed Microtina and *Lagurus* samples —were used in an unsupervised model-based clustering analysis. The goal was to yield clusters in the morphological space defined by RW1 and RW2 that represent inherent natural groups, allowing taxonomic interpretation. This approach also estimates each individual's probability of belonging to each obtained cluster and the associated uncertainty, thereby supporting biological and taxonomic interpretation. A Gaussian finite mixture model was fitted using the Expectation–Maximization (EM) algorithm, and the optimal number of clusters was determined using the Bayesian Information Criterion (BIC). The analyses were performed using the R package mclust v. 6.1.2 [37].

4. Systematic Palaeontology

Class Mammalia Linnaeus, 1758
Order Eulipotyphla Waddell, Okada and Hasegawa, 1999
Family Soricidae Fischer, 1814
Genus *Crocidura* Wagler, 1832
Crocidura leucodon (Hermann, 1780)
(Figure 2).

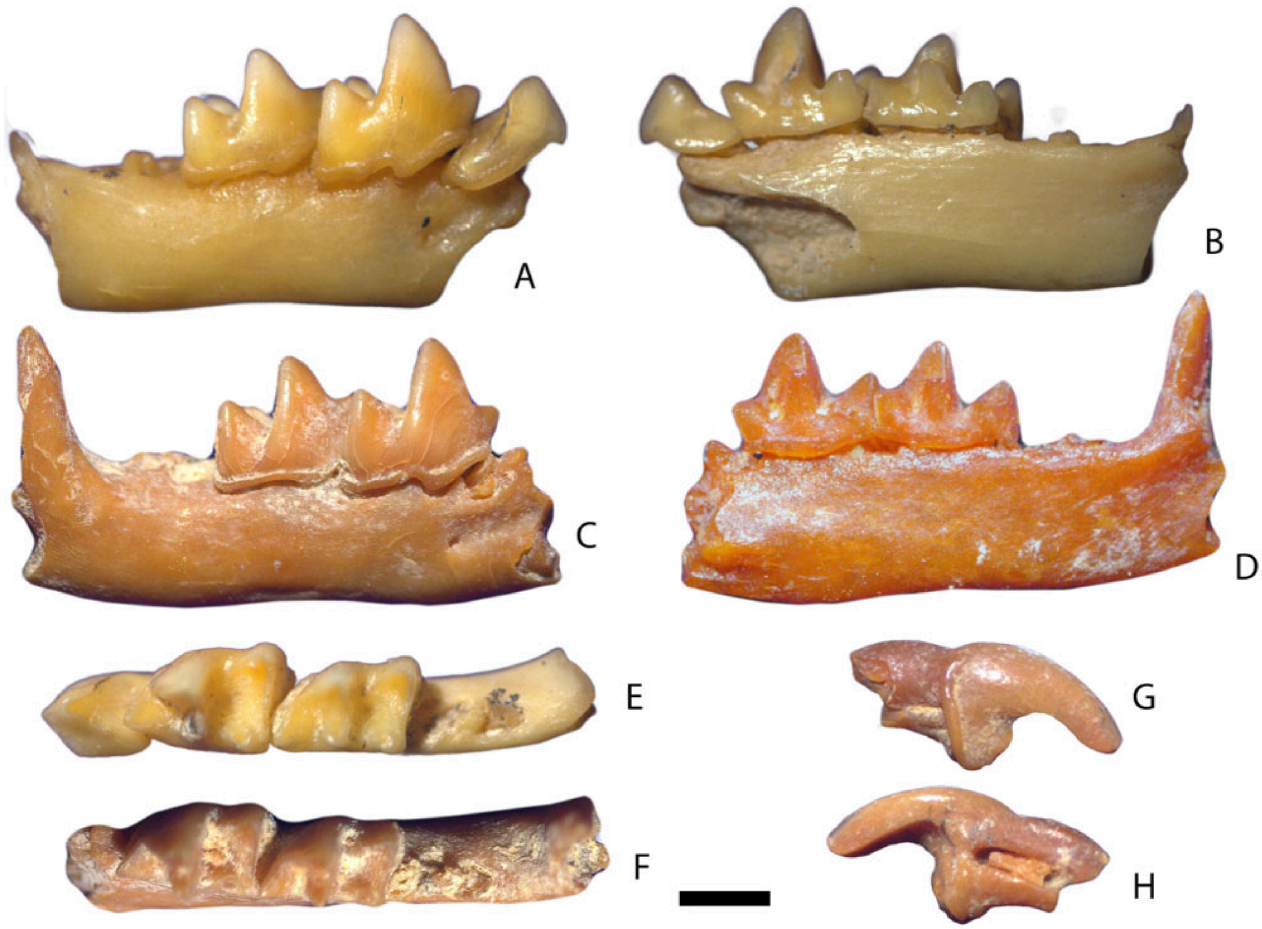


Figure 2. *Crocidura leucodon*. Fragments of right mandibles [BG-IBER-FMC-000004118, layer 11a (**A**,**B**,**E**), and BG-IBER-FMC-000003855, layer 6/7 (**C**,**D**,**F**)] in occlusal (**F**,**E**), labial (**C**,**A**), and lingual (**B**,**D**) views. Upper incisive (BG-IBER-FMC-000022017, layer 12) in labial (**G**) and lingual (**H**) views. Scale bar—1mm.

Studied material (L-layer). Biozone B: L12—upper incisive, L11a—fragment of mandible with m1 and m2; Biozone A: L9c—fragment of mandible with p4-m2; L6/7—fragment of mandible with p4-m2.

Description—The teeth are not pigmented. The upper incisor (I) has a well-developed buccal cingulum that extends nearly to the top edge of the tooth. The posterior margin of the crown behind the talon is nearly straight. The lower molars (m1–m2) are strongly compressed anteroposteriorly, resulting in a distinct upward undulation of the buccal cingulum in its middle part, especially noticeable on m1. The lingual cingulum is poorly developed, with its ventral edge slightly bent downward (m1) or almost straight (m2). The entoconid crest is very low. The mental foramen is below the contact between p4 and m1.

Measurements—Table 1.

Remarks—Based on the size of the lower molars, the mandibular fragments from layers 6/7 and 9c do not differ from the modern *Crocidura leucodon* from Bulgaria or from the Late Pleistocene fossil remains from Cave 16 [38]. The mandibular fragment from layer 11a is slightly smaller, falling within the upper end of the size variability for the m1 of *Crocidura obtusa* Kretzoi, 1938, from Somssich Hill 2 (Hungary) [39] and Betfia IX (cf.) (Romania) [40]. The very fragmentary and scarce material does not allow for more detailed comparisons. There are differing views on when the recent large species first appeared in Europe. According to some authors, it appeared in the Middle Pleistocene [41]. However, others believe it entered Europe from the Middle East only after the end of the last interglacial [42]. The large Early Pleistocene form is usually designated as *C. obtusa*, but

its differences from *C. leucodon* are unclear (for review, see [40]). That is why the material from Kozarnika is referred to as the recent species.

Table 1. Measurements [mm] of *Crocidura leucodon* from Kozarnika.

Layer	Catalog Number	p4		m1		m2		lp4-m3(a)	lm1-m3(a)	HMd/m2	LI	LTI	HI
		L	W	L	W	L	W						
layer 6/7	BG-IBER-FMC-000003855	1.43	0.99	1.79	1.27	1.66	1.11	5.56	4.63	1.75			
layer 9c	BG-IBER-FMC-000022222	1.29	1.01	1.86	1.24	1.77	1.04	5.16	4.34				
layer 11a	BG-IBER-FMC-000004118			1.76	1.09	1.73	1.05		4.28	1.47			
layer 12	BG-IBER-FMC-000022017										2.12	0.83	1.46

Genus *Sorex* Linnaeus, 1758

Among the material from the Kozarnika deposits, three size groups are clearly distinguished (Figure 3). The smallest group includes the variability of the modern species *Sorex minutissimus* and *S. minutus*, while the largest corresponds to *S. araneus*. The medium-sized group falls within the variability of the fossil species *S. runtonensis* and *S. subaraneus*.

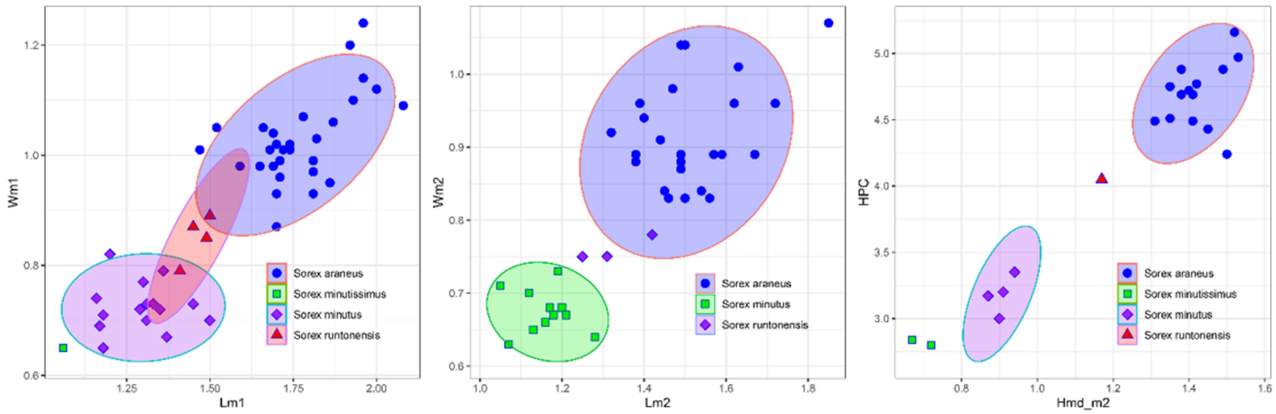


Figure 3. Scatter plot diagrams and 95% confidence ellipses of length (L) versus width (W) of lower (m1–m2) molars and height of mandible below m2 (HMd_m2) versus height of coronoid process (HPC) of representatives of the genus *Sorex* from Kozarnika.

Sorex minutissimus Zimmermann, 1780

(Figure 4A,E)

Studied material—Biozone B: L13c—fragment of mandible with m2; L13c—two fragments of mandible without teeth; Biozone A: L3–4—fragment of mandible with m2.

Description—Mandible—The upper part of the coronoid process is narrow, inclined forward, and ends in a blunt tip. The coronoid spicule is large and short, located high in the external temporal fossa, appearing as a longitudinal groove running parallel to the posterior edge of the coronoid process and extending slightly below the upper sigmoid notch. The internal temporal fossa is triangular, with its lower edge beneath the upper facet of the condyle. Inside this fossa, a longitudinal bar is present. The condyle is positioned far back, featuring a cylindrical upper facet and a lower facet that widens toward the middle. The interarticular area is broad.

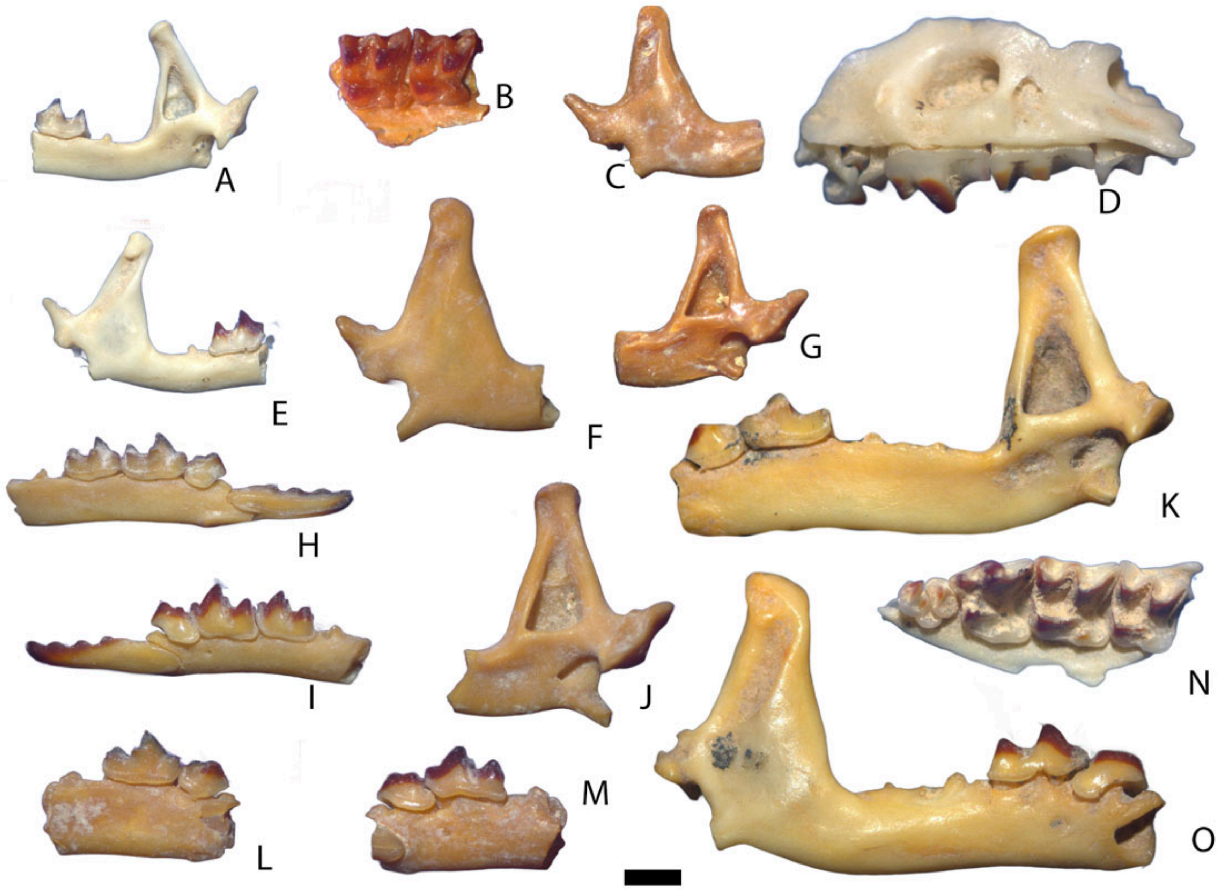


Figure 4. Mandibular and cranial fragments of *Sorex araneus* (**D**,**K**,**N**,**O**), *Sorex minutissimus* (**A**,**E**), *Sorex minutus* (**C**,**G**–**I**), and *Sorex runtonensis* (**B**,**F**,**J**,**L**,**M**) from Kozarnika. (**F**,**J**) Fragment of right mandible, lateral (**F**) and lingual (**J**) views, layer 11a (BG-IBER-FMC-000002509). (**H**,**I**) Fragment of left mandible, lateral (**I**) and lingual (**H**) views, layer 10a (BG-IBER-FMC-000003938). (**B**) Fragment of left maxilla with M1 and M2, occlusal view, layer 13c (BG-IBER-FMC-000006651). (**C**,**G**) Fragment of right mandible, lateral (**C**) and lingual (**G**) views, layer 13c (BG-IBER-FMC-000006974). (**K**,**O**) Fragment of right mandible, lateral (**O**) and lingual (**K**) views, layer 10a (BG-IBER-FMC-000007720). (**D**,**N**) Fragment of skull, lateral (**D**) and occlusal (**N**) views, layers 3–4 (BG-IBER-FMC-000011772). (**A**,**E**) Fragment of right mandible, lateral (**E**) and lingual (**A**) views, layers 3–4 (BG-IBER-FMC-000012809). (**L**,**M**) Fragment of left mandible, lateral (**M**) and lingual (**L**) views, layer 11a (BG-IBER-FMC-000021907). Scale bar = 1 mm.

m1–m2—Upper parts of the crown are stained dark red. Cingula are well-developed on both sides. The base of the buccal cingulum is straight, while the lingual one is slightly undulate.

Measurements—Table 2.

Table 2. Measurements [mm] of *Sorex minutissimus* from Kozarnika.

Biozone	Catalog Number	Lm2	Wm2	HMd/m2	HPC	HC	LUF	LLF
A	BG-IBER-FMC-000012809	1.06	0.65	0.72	2.8	1.12	0.63	0.92
B	BG-IBER-FMC-000015063	-	-	0.67	2.84	-	-	-
	BG-IBER-FMC-000022223	-	-	0.69	2.52	0.99	0.49	0.75
	BG-IBER-FMC-000022224	-	-	0.75	2.62	1.0	0.41	0.76

Remarks—The available mandibular fragments are small—below the lower limit of *Sorex minutus*—and match the size of fossil *Sorex minutissimus* from Bulgaria and neighboring regions [38,40,43]. An additional argument for assigning the remains to this species is the presence of a massive coronoid spicule, a feature noted by Rzebik-Kowalska [40]. The presence of this Boreal species in the deposits of the lower series of the Kozarnika cave is of particular interest, as many thermophilous species are also found here (see below). In neighboring Romania, a similar situation has been observed at Betfia-VII/3, an Early Pleistocene site, possibly reflecting a cold period between two mild Bavelian phases [40].

Sorex minutus Linnaeus, 1766

(Figure 4C,G–I)

Studied material—Biozone B: L13a: 3 fragm. of mandibles (fmd's); L13b: 2 fmd's L13c: 2 fmd's; L12: 2 fmd's; L11b: 2 fmd's; L11a: 1 fmd's; Biozone A: L10b: 1 fmd's; L10a: 1 fragm. of maxillae; 11 fmd's; L5c: 2 fmd's; L5b: 9 fmd's; L5a: 5 fmd's; L 3–4: 6 fmd's.

Description—Mandible—The coronoid process is large, not narrowed at the top like in *S. minutissimus*, and it gradually tapers toward the broad, rounded tip. The anterior edge forms a blunt angle with the horizontal ramus. The coronoid spicule is well developed, long, and relatively narrow, situated in the upper part of the external temporal fossa. The internal temporal fossa is triangular and quite wide, with rounded posterior and superior angles.

i—Tricuspulate, with a weak cingulum present along the buccal posterior margin. It extends posteriorly along the buccal side of the mandible to halfway along p4.

p4—Slender and tall, featuring a well-developed postero-lingual basin that typically has faint edges. It has two cusps, with the anterior cusp much higher than the posterior one. The buccal cingulum is distinct and relatively broad.

m1–m3—The lower molars feature well-defined but relatively narrow labial and lingual cingula, with the lingual cingula slightly broader. The mental foramen is located below the protoconid of the first lower molar or beneath the valley separating the protoconid from the hypoconid.

Measurements—Table 3.

Table 3. Measurements [mm] of *Sorex minutus* from Kozarnika (lab—labial, a—alveolar, c—coronal).

Measurement	N	X	Min	Max	SD
Li-lab	3	2.97	2.74	3.21	
Lp3-lab	5	0.82	0.74	0.90	0.071
Wp3	4	0.59	0.46	0.66	0.090
Lp4-lab	5	0.98	0.83	1.11	0.131
Wp4	4	0.66	0.53	0.76	0.095
Lm1	16	1.31	1.16	1.50	0.111
Wm1	15	0.72	0.65	0.82	0.044
Lm2	12	1. 17	1.05	1.28	0.065
Wm2	11	0.67	0.63	0.73	0.030
Lm3	5	0.94	0.88	1.00	0.047
Wm3	4	0.59	0.57	0.61	0.018
Li-m3(c)	1	6.58	-	-	-
Lp3-m3(c)	2	-	4.37	4.45	0.057
Lp4-m3(c)	2	-	3.89	3.98	0.064
Lm1-m3(a)	4	3.16	3.08	3.24	0.082

Table 3. *Cont.*

Measurement	N	X	Min	Max	SD
Lm1-m3(c)	3	3.11	2.95	3.24	-
HMd/m2	23	0.89	0.69	1.09	0.086
HPC	5	3.17	3.00	3.35	0.128
HC	7	1.31	1.12	1.45	0.102
LUF	7	0.62	0.57	0.72	0.051
LLF	7	0.90	0.83	0.96	0.045

Remarks—The small size and morphology allow us to assign the specimens from Kozarnika to the recent species *Sorex minutus*. The remains occur in both biozones. Comparisons between them, based on measurements presented by relatively large samples, do not reveal statistically significant differences. In terms of size, the remains are nearly identical to fossil material from other sites in Bulgaria [38,44]. The detailed morphology and synonymy of the fossil *Sorex minutus* are described in Reumer [16] and Rzebik-Kowalska [45]. The taxonomy of small fossil *Sorex* species similar to *S. minutus* (such as *Sorex bor* Reumer, 1984, *Sorex subminutus* Sulimski, 1962, *Sorex praeminutus* Heller, 1963, and *Sorex biharicus* Terzea, 1970) has been discussed by Rzebik-Kowalska [40,45]. Differentiating *S. minutus* from *S. bor* is difficult in the absence of an upper incisor. The available material can still be distinguished from *S. bor* by the better-developed coronoid spine and its position in the external temporal fossa. This structure is very poorly expressed in *S. bor* and is located high up, as described and illustrated by Reumer [16]. However, it should be noted that the available lower jaws from both biozones are characterized by a well-developed coronoid spicule, unlike the material from *S. minutus*, described by Reumer [16] (pp. 28–29) from some Hungarian localities.

Sorex runtonensis Hinton, 1911

(Figure 4B,F,J,L,M)

Studied material—Biozone B: L13c: 1 fragm. of mandible, 1 fragm. of maxillae; L13b: 1 m1, L13a: 7 fragm. of mandibles; L12: 3 fragm. of mandibles: L11b: 7 fragm. of mandibles; L11a: 2 fragm. of mandibles.

Description—Mandible—The mental foramen lies under the contact zone between p4 and m1. The anterior edge of the coronoid process forms a blunt angle with the horizontal ramus of the jaw; its upper part is almost vertical, with a broad, rounded tip. The coronoid spicule is prominent, long, and wide, but low; it connects downward to a well-defined posterior ridge that extends to the lower third of the external temporal fossa. The internal temporal fossa is triangular, relatively narrow, and high, with a horizontal bar. The mandibular foramen lies below the midpoint of the base of the internal temporal fossa. The condyle has a structure typical of the genus. It should be mentioned, however, that in specimen BG-IBER-FMC-000021985, the interarticular area is too high and relatively narrow.

p4—In buccal view, it is not particularly elongated toward the back. The buccal cingulum is prominent and relatively wide. The lingual cingulum is broad and well defined at the back of the crown. The tips are nearly the same height, or the posterior one is slightly taller.

m1–m2—The lingual cingulum is broad; the buccal one is well developed and narrow. On m1, the lower edge is wavy, with upward curves at the bases of the protoconid and hypoconid. On m2, the lower edge is almost straight.

M1–M2—The tips of the paracone, metacone, and protocone are stained in dark red or, rarely, in pale red. The hypocone is moderately developed, better than in *S. minutus* but weaker than in *S. araneus*. The metaloph is low; it branches backward, and its buccal branch closes the trigone valley from behind. Between the hypocone and protocone, there is a wide valley bordered by a well-defined, narrow lingual cingulum.

Measurements—Table 4.

Table 4. Measurements [mm] of *Sorex runtonensis* from Kozarnika.

Measurement	N	X	Min	Max	SD
Lp4-lab	1	1.10	-	-	-
Wp4	1	0.69	0.69	0.69	-
Lm1	4	1.46	1.41	1.50	0.041
Wm1	4	0.85	0.79	0.89	0.043
Lm2	3	1.33	1.25	1.42	0.086
Wm2	3	0.76	0.75	0.78	0.017
Lm3	1	0.99	-	-	-
Wm3	1	0.65	-	-	-
HMd/m2	7	1.25	1.17	1.34	0.066
HPC	4	4.04	3.80	4.19	0.167
HC	5	1.63	1.40	1.85	0.161
LUF	5	0.77	0.60	0.84	0.098
LLF	6	1.16	1.09	1.24	0.059
BL_M1	1	1.40	-	-	-
LL_M1	2	1.32	1.31	1.33	0.014
PE_M1	1	1.09	-	-	-
AW_M1	2	1.44	1.41	1.47	0.042
PW_M1	1	1.48	-	-	-
BL_M2	1	1.17	-	-	-
LL_M2	1	1.16	-	-	-
PE_M2	1	0.97	-	-	-
AW_M2	1	1.45	-	-	-
PW_M2	1	1.36	-	-	-

Remarks—Remains of a medium-sized representative of the genus were found only in the layers of Biozone B. In the Pleistocene of Europe, two widely distributed species are commonly associated with this size group: *Sorex runtonensis* and *S. subaraneus* Heller, 1958. The differences between them are small and mainly concern size, which overlaps strongly, making them difficult to distinguish. In the brief diagnosis of *S. subaraneus*, Heller [46] states only that the size is close to that of *S. araneus* Linnaeus, 1758, although slightly smaller. According to him, the Erpfingen (Germany) specimens exceed the size of other Quaternary species from Central Europe, such as *Sorex aranoides* Heller, 1930 (now a synonym of *S. runtonensis* [21,47]), *S. runtonensis*, and *S. praealpinus* Heller, 1930, and approaches the Plio/Pleistocene *S. praearaneus* Kormos, 1934 (=*Sorex* (*Drepanosorex*) *praearaneus* [16]) from Villány (Hungary), although it differs in morphology (e.g., its mental foramen is situated below the trigonid of m1, whereas in *S. praearaneus* it is below the p4).

Other studies based on mandibular and dental measurements consistently show that *Sorex runtonensis* is smaller than *S. subaraneus* [43,44,48,49]. The same is valid for *S. kennardi*, which is regarded as conspecific with *S. runtonensis* [50]. Four measurements (HPC, HMd/m2, Lm1, and Wm1) of the available material are based on relatively large samples and allow more precise comparisons with similar data for *S. runtonensis* [44] and *S. subaraneus* [43,48], from Bulgaria, using the *t*-test. The t-values show that, regarding HPC, one of the main diagnostic characters in soricids, the Kozarnika sample does not differ from *S. runtonensis* from Varshets [44] but differs significantly from samples identified as *S. subaraneus* from Varbeshnitsa [48] and Morovitsa [43], which are larger. There are no statistically significant differences in m1 size between the populations being compared, indicating that this tooth, which is most often preserved as a fossil, is of little help for distinguishing the two species. Regarding the height of the mandibular ramus below m2, comparisons yield conflicting results: no difference between Kozarnika and the two *S. subaraneus* populations, but a highly significant difference with *S. runtonensis* from Varshets. It can be assumed that, since this feature is largely age-related (adult individuals have larger jaws), it is of little help in taxonomic comparisons between similar species. Since the average HPC value from West Runton, the type locality of *S. runtonensis*, is 3.96 mm [50] and very close to that from Varshets [44], and since there is no statistically significant difference between Kozarnika and Varshets, the same can be assumed for the populations from the type locality of *S. runtonensis* and from Kozarnika. At the same time, the average HPC values from Varbeshnitsa and Morovitsa, which are significantly larger than those of Kozarnika, are close to those from Erpfingen, the type locality of *S. subaraneus* [46]. In terms of HPC and HMd/m2, the material available is very similar to the two measured jaws from the type locality, the Upper Freshwater Bed, of *S. runtonensis* [51]. Based on these comparisons, the Biozone B material from Kozarnika is assigned to *Sorex runtonensis*.

Shrews of the *S. runtonensis-subaraneus* group were widespread across Europe during the Pleistocene [40,41]. Their first occurrences are recorded in the Early Pleistocene of Austria (Deutsch Altenburg 30A, *S. runtonensis* [52]) and in the Late Pliocene of France (Mountoussé 5, *S. subaraneus* [53]). The last occurrences of these species are in the Late Pleistocene [41]. There are opinions that *S. runtonensis* could have survived into the Holocene [54,55].

Sorex araneus Linnaeus, 1758.

(Figure 4D,K,N,O)

Studied material—Biozone B: L13c: 1 fragm. of mandible (fmd); L13b: 1 fmd; L12: 1 fmd; L11a: 1 fragm. of maxillae; Biozone A: L10b: 1 fmd; L10a: 1 fragm. of maxillae; 9 fmd's; L9c: 3 fmd's; L6/7: 3 fmd's; L5a: 3 fmd's; L5b: 3 fragm. of maxillae; 15 fmd's; L3–4: 3 fragm. of maxillae; 10 fmd's.

Description—Mandible—The horizontal ramus is slightly concave below m1/m2, with the mental foramen beneath m1's trigonid. The tall ascending ramus has a straight or slightly concave anterior edge and a concave posterior edge. The broad, rounded coronoid tip leans posteriorly and lingually. The coronoid spicule varies in size and is located near the tip. The shallow external temporal fossa runs parallel to the posterior coronoid edge, being deeper below the spicule and reaching the upper sigmoid notch. There is a small pterygoid spicule. The internal temporal fossa is high and triangular, not reaching the coronoid tip. The condyloid process is low, with a cylindrical upper facet and a wide, slightly concave lower facet. Its interarticular area is narrow above and wider below, not reaching the lower facet's end.

p4—two cusps, with the anterior cusp consistently taller than the posterior; the postero-lingual basin is deep and bordered by sharp crests, and both sides of the tooth have clear, wide cingula.

m1–m2—similar in shape, although m2 is smaller; the highest cusp for both is the protoconid. Their buccal reentrant valley opens above the buccal cingulum. On the lingual side, the trigonid valley is narrow and opens low, while the metaconid/entoconid valley is wide with a long, relatively high entoconid crest. The metaconid is narrow, and the entoconid is broader—wider than the metaconid. The hypolophid is very close to the entoconid, with no groove between the entoconid and the entostylid. All molars are surrounded by a cingulum, with the buccal cingulum more prominent but narrow; on m1, the lower edge is well-developed and curves upward below the protoconid, whereas on m2 it is almost straight.

m3 features a well-developed, long-basined talonid. The hypoconid and entoconid are small, and the postero-lingual cingulum is barely visible.

The P4 shows a prominent parastyle, protocone, and hypocone, complemented by a fairly long parastylar crest. A deep valley lies between the protocone and hypocone, bordered lingually by a cingulum. The posterior cingulum is robust, whereas the buccal cingulum is weak, and there is no anterior cingulum.

The M1 has a well-developed hypocon, a metaloph, and no parastyle. A broad valley separates the protocon and hypocon, with a cingulum on its lingual side. The posterior cingulum and emargination are prominently developed, while the anterior and buccal cingula are absent.

The M2 resembles the M1 but is smaller and more trapezoidal rather than rectangular.

Measurements—Table 5.

Table 5. Measurements [mm] of *Sorex araneus* from Kozarnika.

Biozone			**A**					**B**		
Measurement	**N**	**X**	**Min**	**Max**	**SD**	**N**	**X**	**Min**	**Max**	**SD**
Li-Lab	2	3.67	3.64	3.70	-	-	-	-	-	-
Lp3-Lab	6	1.09	0.95	1.26	0.115	-	-	-	-	-
Wp3	6	0.74	0.69	0.81	0.041	-	-	-	-	-
Lp4-Lab	18	1.28	1.10	1.44	0.079	1	1.33	-	-	-
Wp4	16	0.84	0.72	0.99	0.082	1	0.89	-	-	-
Lm1	28	1.79	1.52	2.08	0.129	2	1.53	1.47	1.59	-
Wm1	27	1.03	0.87	1.24	0.082	2	1.00	0.98	1.01	-
Lm2	21	1.52	1.38	1.85	0.119	3	1.49	1.32	1.62	0.155
Wm2	21	0.92	0.83	1.07	0.073	3	0.91	0.84	0.96	0.061
Lm3	10	1.10	1.03	1.22	0.069	-	-	-	-	-
Wm3	10	0.70	0.63	0.79	0.050	-	-	-	-	-
Li-m3(c)	1	7.47	-	-	-	-	-	-	-	-
Lp3-m3(c)	5	5.35	5.20	5.53	0.141	-	-	-	-	-
Lp4-m3(c)	7	4.69	4.55	4.81	0.089	-	-	-	-	-
Lp4-m3(a)	6	4.87	4.43	5.36	0.399	-	-	-	-	-
Lm1-m3(alv)	12	4.00	3.74	4.38	0.228	-	-	-	-	-
Lm1-m3(c)	9	3.94	3.80	4.22	0.151	-	-	-	-	-
HMd/m2	39	1.40	1.16	1.69	0.118	5	1.31	1.19	1.45	0.119
HPC	14	4.74	4.24	5.18	0.263	2	4.54	4.43	4.65	-
HC	13	1.63	1.20	1.88	0.216	1	1.38	-	-	-
LUF	13	0.92	0.75	1.07	0.112	1	0.74	-	-	-

Table 5. *Cont.*

Biozone			A					B		
Measurement	**N**	**X**	**Min**	**Max**	**SD**	**N**	**X**	**Min**	**Max**	**SD**
LLF	13	1.37	1.06	1.64	0.180	1	1.25	-	-	-
BLP4	7	1.67	1.60	1.80	0.085	2	1.62	1.58	1.66	-
WP4	7	1.62	1.52	1.76	0.071	2	1.64	1.62	1.65	-
PEP4	6	1.29	1.17	1.38	0.077	2	1.27	1.24	1.29	-
LLP4	6	1.57	1.41	1.68	0.107	1	1.49	-	-	-
BLM1	9	1.56	1.44	1.65	0.060	3	1.51	1.45	1.57	0.060
LLM1	9	1.48	1.40	1.60	0.076	3	1.43	1.37	1.48	0.056
PEM1	9	1.24	1.13	1.32	0.056	3	1.22	1.18	1.29	0.059
AWM1	9	1.56	1.49	1.71	0.065	3	1.63	1.60	1.66	0.031
PWM1	9	1.65	1.54	1.80	0.073	3	1.64	1.55	1.73	0.090
BLM2	7	1.33	1.21	1.45	0.076	1	1.32	-	-	-
LLM2	7	1.26	1.19	1.32	0.058	1	1.20	-	-	-
PEM2	7	1.12	1.06	1.18	0.047	1	1.10	-	-	-
AWM2	7	1.63	1.57	1.73	0.057	1	1.59	-	-	-
PWM2	7	1.52	1.34	1.63	0.106	1	1.45	-	-	-

Remarks—Based on the data in Table 5, it can be concluded that the large *Sorex* species from Kozarnika, which falls within the size range of the modern *S. araneus*, shows clear differences between the two biozones. Those from Biozone B are smaller. Due to small sample sizes for each measurement, these differences cannot be confirmed with statistical tests. However, this difference appears in all measurements with sample sizes of three or more.

The larger form from Biozone A does not show statistically significant differences compared to the Late Pleistocene form from Cave 16 [38] in terms of HPC (t = 0.396, $p = 0.6959$) and Lm1–m3(c) (t = −1.416, $p = 0.182$). It is clearly smaller than the form from Morovitsa Cave [43] regarding HPC (t = 2.851, $p = 0.0053$), HMd/m2 (t = 4.034, $p = 0.0001$), and Lp3-m3(c) (t = 2.331, $p = 0.0272$).

S. araneus emerged in Europe during the Early Pleistocene, with earlier specimens identified as *S.* cf. *araneus* from the early Late Pliocene. *S. subaraneus* is believed to be the ancestor of *S. araneus*. It is first recorded from the late Late Pliocene (MN17) at Mountoussé 5 in France. If *S. subaraneus* was indeed the precursor, then the Late Pliocene and possibly Early Pleistocene *Sorex* fossils may have been misclassified as *S. araneus* and could actually belong to *S. subaraneus*. A reevaluation of fossils labeled as *S. subaraneus* and *S. araneus* is needed [56].

Genus *Drepanosorex* Kretzoi, 1941

Drepanosorex praearaneus (Kormos, 1934)

(Figure 5A,C)

Studied material—Biozone B: L13b: 1 upper incisive.

Description—The tips of both apex and talon colored in an intense dark red; buccally, pigmentation extends far back along the crown; the talon is well developed, extends far forward and downward, pointed, and its anterior edge forms an acute angle with the lower edge of the apex; there is a well-developed and wide buccal cingulum, especially well expressed in the lower half of the crown height, and gradually disappearing upwards; its posterior margin has a well-pronounced undulation in its middle part.

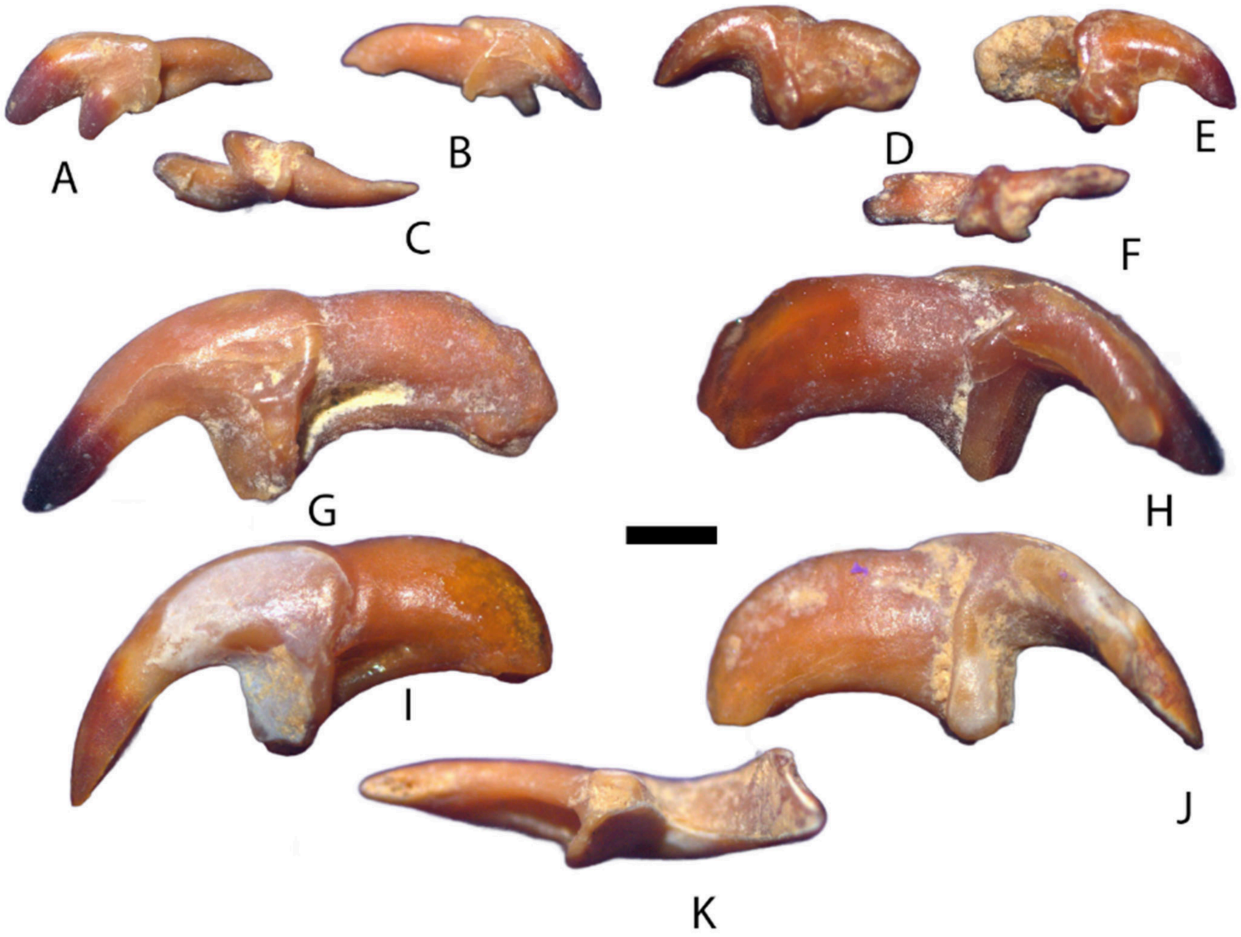


Figure 5. *Drepanosorex praearaneus* (**A**–**C**), *Asoriculus gibberodon* (**D**–**F**), *Beremendia fissidens* (**G**–**K**). (**A**–**C**)—left upper incisive (BG-IBER-FMC-000006451, L13b, buccal, lingual, and ventral views); (**D**–**F**)—right upper incisive (BG-IBER-FMC-000014710, L12, lingual, buccal, and ventral views); (**G**,**H**)—left upper incisive (BG-IBER-FMC-000007963, L12, buccal and lingual view); (**I**–**K**)—left upper incisive (BG-IBER-FMC-000006928, L13-Lower, buccal, lingual, and ventral view). Scale bar = 1 mm.

Measurements [mm]—LI = 1.77, LT = 1.02, HI = 1.16

Remarks—In terms of its qualitative characteristics and dimensions, the only tooth from Kozarnika fully corresponds to the materials from the Villanyian localities Tegelen (The Netherlands) and Osztramos 3/2 (Hungary) [16]. Known predominantly from Villanyian and Early Biharian in Europe [16,57–59], it survived into the Late Pleistocene in Ukraine [60]. It is considered the most primitive species of the genus, close to the origin of *Drepanosorex* from the *Sorex* ancestral stock. There is a clear increase in size towards the later forms, particularly in the Cromerian *Drepanosorex savini* (Hinton, 1911) [16].

Genus *Neomys* Kaup, 1829

Neomys cf. *newtoni* Hinton, 1911

(Figure 6A,C)

Studied material—Biozone B: L11a1: 1 fragment of mandible.

Description—m1–m2—The tips of the para-, proto-, and hypoconids are pigmented in light red. The pigmented part covers the upper 1/3 of the buccal side of the protoconid. The buccal and lingual cingula of m1 and m2 are narrow but well-pronounced.

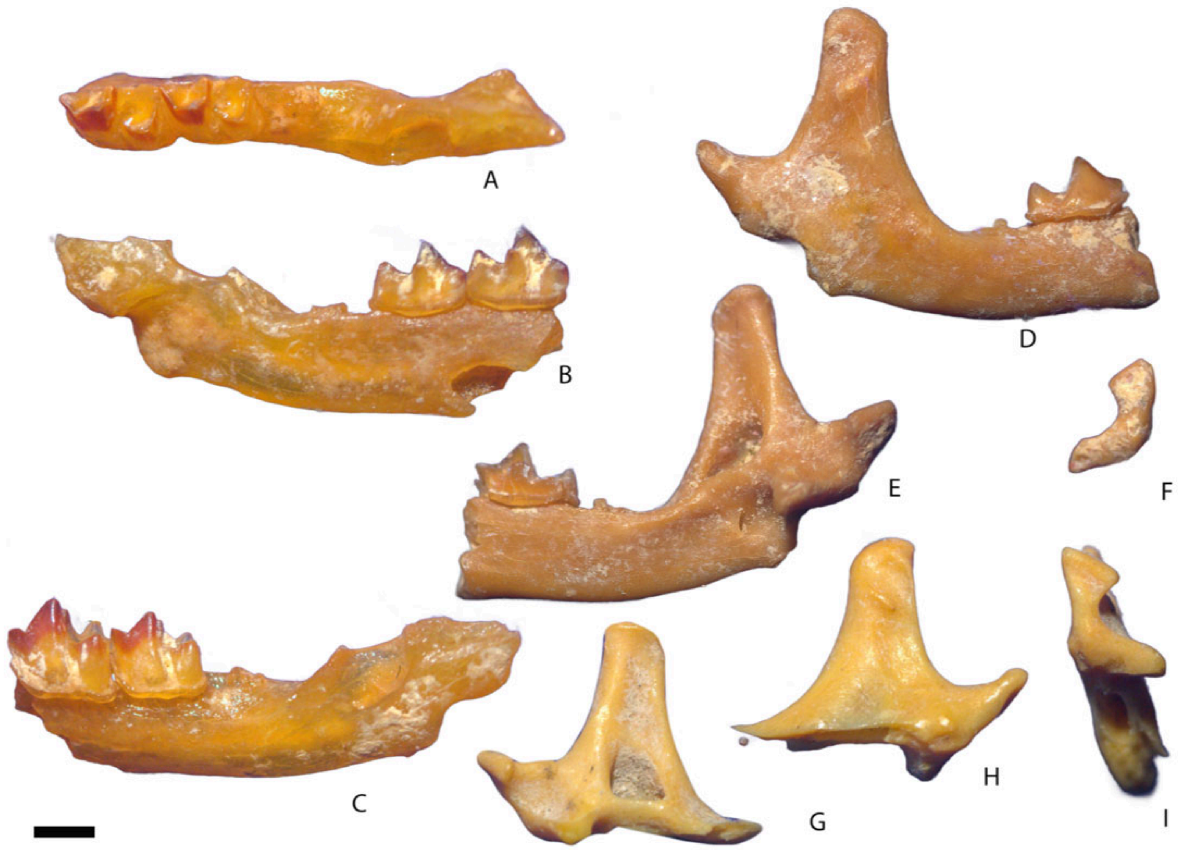


Figure 6. *Neomys* cf. *newtoni* (**A**–**C**), *Asoriculus gibberodon* (**D**–**F**), *Neomys* cf. *fodiens* (**G**–**I**). (**A**–**C**)—fragment of left mandible (BG-IBER-FMC-000004870, L11a1, (**A**)–occlusal, (**B**)–lingual, (**C**)–buccal view); (**D**–**F**)—fragment of right mandible (BG-IBER-FMC-000021997, L13-Lower, labial, lingual, caudal view); (**G**–**I**)—fragment of mandible (BG-IBER-FMC-000022025, L10b, lingual, lateral, caudal view). Scale bar = 1 mm.

Remarks—Regarding the lengths of m1 and m2, the available mandible from L11a1 is close to the average values of the recent *Neomys milleri* Mottaz, 1907 from Bulgaria. A notable difference is the well-developed lingual cingula, which are almost imperceptible in the modern species. The fossil species *Neomys newtoni* is similar in size to the modern *N. milleri* [51,56,61]. It should be noted that the available mandibular fragment is slightly larger in terms of HMd/m2 than *N. newtoni* and *N. browni* Hinton, 1911 [45], but both values fall within the variability range of modern species from Bulgaria. However, this feature is not particularly useful for identification, as there is significant overlap between modern *N. fodiens* and *N. milleri*. Since the coronoid process is missing, a definitive determination is not possible, and the material is tentatively assigned to *N. newtoni*, a common species from the Early and Middle Pleistocene of Europe (Early Biharian—early Toringian) [62].

Neomys cf. *fodiens* (Pennant, 1771)

(Figure 6G–I)

Studied material—Biozone A: L10b: 1 fragment of mandible; L10a: 2 fragments of mandible.

Description—The coronoid process is broad, with a slightly concave anterior edge. The external temporal fossa is deeper above the coronoid spicule. The coronoid spicule is well developed. The internal temporal fossa is low, and the condyloid process is high. The condyle is characterized by an interarticular area that is narrow in its middle part. The lower facet is long.

Measurements—Table 6.

Table 6. Measurements [mm] of lower molars and mandibles of *Neomys* cf. *newtoni* and *N.* cf. *fodiens* from Kozarnika.

Layer	Catalog Number	Species	Lm1	Wm1	Lm2	Wm2	HMd/m2	HC	LUF	LLF
10a	BG-IBER-FMC-000015657	*Neomys* cf. *fodiens*					2.17		1.11	
10a	BG-IBER-FMC-000015658		1.9	1.17			1.8			
10b	BG-IBER-FMC-000022025							2.24	1.11	1.84
11a1	BG-IBER-FMC-000004870	*Neomys* cf. *newtoni*	1.74	1.4	1.67	1.11	1.63			

Remarks—The fragmented mandible from L10a and L10b is assigned to the genus *Neomys* on the basis of the condyle structure and, in particular, the shape of the interarticular bridge. It is clearly narrowed in the middle, and in this respect, it differs markedly from similarly sized species of *Asoriculus*, in which such a narrowing is not pronounced. The available material is too scarce to allow for a precise determination. On the basis of the relatively high value of the length of the lower condylar facet (LLF), which is above the maximum for a large sample (N = 400) of the modern species *N. milleri* from Bulgaria (min-mean-max, mm = 1.2–1.47–1.80), the material from biozone A of Kozarnika was conditionally assigned to *Neomys fodiens*.

Genus *Asoriculus* Kretzoi, 1959

Asoriculus gibberodon (Petényi, 1864)

(Figure 5D–F and Figure 6D–F)

Studied material—Biozone B: L13-Lower: 1 fragment of mandible; L12: 1 upper incisor.

Description—I1 is fissident. The apex is stained in dark red. The buccal cingulum is well developed along almost the entire height of the crown and significantly widens in its upper part. Its posterior edge is clearly curved in the middle.

m2—A light orange pigmentation is hardly visible on the very tip of the protocone. Buccal and lingual cingula are well developed; the buccal one is slightly undulate. The buccal reentrant valley opens directly above the cingulum.

Mandible—The anterior and posterior edges of the coronoid process are slightly concave; the tip is blunt and rounded. The external temporal fossa is shallow, especially below the coronoid spicule. The coronoid spicule is long and located in the upper third of the coronoid process. The internal temporal fossa is low and narrow. The upper condylar facet is narrow, elongated, and cylindrical. The lower facet is strongly elongated lingually and points downward. The interarticular area is notched lingually and elongated.

Measurements—Table 7.

Table 7. Measurements [mm] of *Asoriculus gibberodon* from Kozarnika.

Layer	Catalog Number	Lm1	Wm1	HMd/m2	HPC	HC	LUF	LLF	LI	LTI	HI
12	BG-IBER-FMC-000014710								1.83	0.75	1.37
13 Lower	BG-IBER-FMC-000021997	1.4	0.93	1.26	3.98	1.94	0.83	1.48			

Remarks—The available mandibular fragment, in most measurements, is close to the lower limit of variability for the large form of *Asoriculus gibberodon* described from the Early Pleistocene site of Varshets. A characteristic feature of the available upper incisor is the relatively intense coloration of the apex, which is uncommon for the species and, in particular, for the comparative material from Varshets [44].

Asoriculus thenii (Malez and Rabeder, 1984)

(Figure 7)

Studied material—Biozone B: L13—Lower: 1 upper incisive; L13c: 1 fragm. of mandible; L13b: 2 fragm. of mandibles; L13a: 1 upper incisive; 4 fragm. of mandibles; layer12: 3 upper incisives, 6 fragm. of mandibles.



Figure 7. *Asoriculus thenii.* (**A**–**C**) Fragment of right mandible (BG-IBER-FMC-000022020, L12 (occlusal, buccal, lingual views). (**D**–**F**) Fragment of left mandible (BG-IBER-FMC-000010715, L13a, occlusal, buccal, lingual views). (**G**–**I**) Fragment of left mandible (BG-IBER-FMC-000003477, L13b, lingual, caudal, labial views). (**J**–**L**) Fragment of right mandible (BG-IBER-FMC-000003477, L13b, lingual, caudal, labial views). (**M**,**N**) Right upper incisive (BG-IBER-FMC-000012832, L12, lateral, lingual views). (**O**–**Q**) Left upper incisive (BG-IBER-FMC-000015135, L12, labial, lingual, ventral views). (**R**,**S**) Right upper incisive (BG-IBER-FMC-000003400, L13a, buccal, lingual views). Scale bar = 1 mm.

Description—Mandible—The coronoid process is large. Its upper part is broad and nearly vertical, with a rounded, broad tip. The anterior edge forms an obtuse angle with the horizontal shoulder of the jaw. The external temporal fossa is shallow and extends below the upper sigmoid notch. There are two coronoid spicules. The lower one is well developed and directed obliquely downward toward the posterior upper edge of the condyle, located in the upper third of the external temporal fossa. The upper one is less prominent, almost horizontal, with its posterior end slightly beyond the posterior edge of the coronoid process. The internal temporal fossa is relatively small, with a rounded triangular shape. There are one or two mandibular foramina. The condyle is of the *Neomys*-type, with a narrow interarticular bridge. The upper facet is oblique and cylindrical, and the lower one is strongly elongated medially and nearly horizontal. The mental foramen is located beneath the hypoconid of the first lower molar.

The tips of the teeth are faintly colored in pale red.

i—Bicuspulate (the weak manifestation of the cusps is due to the fact that the tooth is relatively worn). Its anterior tip is slightly raised upwards. The posterior buccal cingulum is well-pronounced.

a1—Low and elongated with a weakly developed buccal cingulum in the posterior part of the crown.

p4—Relatively high with two peaks, the posterior one being slightly lower. It has a well-developed buccal cingulum.

m1–m2—With a well-developed buccal cingulum whose lower edge is wavyly curved. The lingual cingula of the lower teeth are less pronounced than the buccal ones, but broader.

m3—The talonid is reduced as the hypoconid and entoconid are very small.

I—Fissident; the posterior edge of the buccal cingulum is strongly curved (concave) in its middle part; it is narrow and well-pronounced on its lower part, widens upward, and gradually weakens.

Measurements—Table 8.

Table 8. Measurements [mm] of molars and mandible of *Asoriculus thenii.*

Measurement	N	X	Min	Max	SD
Li	1	5.10	-	-	-
Lp3	1	1.37	-	-	-
Wp3	1	0.96	-	-	-
Lp4	1	1.72	-	-	-
Wp4	1	1.10	1.10	1.10	-
Lm1	5	1.88	1.62	2.06	0.178
Wm1	5	1.16	0.94	1.27	0.141
Lm2	3	1.60	1.56	1.63	0.035
Wm2	4	1.01	0.93	1.14	0.095
Lm3	2	1.24	1.20	1.28	0.057
Wm3	2	0.75	0.72	0.78	0.042
lm1–m3(a)	3	4.14	3.74	4.44	0.361
lm1–m3(c)	1	4.53	-	-	-
HMd/m2	7	1.53	1.32	1.69	0.138
HPC	5	4.96	4.48	5.24	0.294
HC	6	2.46	2.25	3.00	0.273
LUF	6	1.05	0.95	1.18	0.092
LLF	7	1.65	1.56	1.74	0.071
LI	4	2.56	2.43	2.65	0.100
LTI	4	0.98	0.96	1.02	0.027
HI	4	1.67	1.55	1.74	0.086

Remarks—The described remains undoubtedly belong to the tribe Soriculini sensu Reumer [16]: the upper condylar facet is cylindrical, the interarticular area is high and narrow, the upper incisor is fissident, and the teeth are pigmented. Their qualitative features clearly indicate that they belong to the genus *Asoriculus* [16] and are very similar to those of the widespread *Asoriculus gibberodon*—bicuspulate lower incisor with well-developed buccal cingulum, mental foramen situated under the posterior half of m1. They are distinguished from it, however, by being very large and massive, and by having

two coronoid spicules in the external temporal fossa. The described remains, by their quantitative features and dimensions, are practically identical to *A. thenii* from the Croatian localities Tatinja Draga (type locality) and Podumci 1 [63].

Genus *Beremendia* Kormos, 1934

Beremendia fissidens (Petényi, 1864)

(Figure 5G–K)

Studied material—Biozone B: L13—Lower: 1 upper incisive; L12: 1 upper incisive.

Description—I—The buccal cingulum is broad and well-pronounced behind the talon; it gradually thins upward, becoming progressively poor.

Measurements [mm]—LI = 3.06, 3.15; LTI = 1.06, 1.59; HI = 2.34, 2.33.

Remarks—The scarce remains available are very similar in size and qualitative features to the rich material of *Beremendia fissidens* from the Early Pleistocene site Varshets in Northwestern Bulgaria [44]. This species was widespread across Eurasia and has been present in Europe from the Early Pliocene (early Ruscinian, MN 14) until the start of the Middle Pleistocene (Late Biharian) [41,64].

Family Erinaceidae Fischer von Waldheim, 1817

Genus *Erinaceus* Linnaeus, 1758

Erinaceus sp.

(Figure 8)



Figure 8. *Erinaceus* sp. Molars in occlusal view. (**A**)—left M1 (BG-IBER-FMC-000007949, L12), (**B**)—left M1 (BG-IBER-FMC-000022000, L13a), (**C**)—left M1 (BG-IBER-FMC-000007949, L12), (**D**)—left M2 (BG-IBER-FMC-000000257, L13a), (**E**)—left m1 (BG-IBER-FMC-000001088, L13a), (**F**)—right m2 (BG-IBER-FMC-000017111, L12), (**G**)—left m2 (BG-IBER-FMC-000003695, L13c), (**H**)—left m2 (BG-IBER-FMC-000003637, L13b). Scale bar = 1 mm.

Studied material—Highly fragmented lower jaws and isolated teeth are common in the deposits of Biozone B at Kozarnika. Here, only some of the more characteristic molars are presented (Table 9).

Table 9. Measurements [mm] of molars of *Erinaceus* sp. from Kozarnika.

Layer	Specimen	Molar	L	W
11a1	BG-IBER-FMC-000002521	m1	5.76	3.57
11a	BG-IBER-FMC-000001295	m1	5.8	3.6

Table 9. *Cont.*

Layer	Specimen	Molar	L	W
13a	BG-IBER-FMC-000001088	m1	6.1	3.81
13c	BG-IBER-FMC-000003695	m2	5.17	3.61
12	BG-IBER-FMC-000019028	m2	5.32	3.3
13a	BG-IBER-FMC-000003429	m2	5.33	3.01
12	BG-IBER-FMC-000017111	m2	5.45	3.67
11a	BG-IBER-FMC-000002448	m2	5.47	3.45
13b	BG-IBER-FMC-000003637	m2	5.54	3.8
12	BG-IBER-FMC-000007949	M1	4.99	5.27
13a	BG-IBER-FMC-000001089	M1	5.1	5.34
13a	BG-IBER-FMC-000022000	M1	5.53	6.22
12	BG-IBER-FMC-000007949	M2	4.27	4.8
13a	BG-IBER-FMC-000022001	M2	4.41	5.18
13a	BG-IBER-FMC-000000257	M2	4.7	5.54

Description—M1—Large and roughly square in occlusal outline, bordered by a wide cingulum except below the protocon and hypocon; the highest cusp is the metacon; the parastyle is present, along with the oval metaconule, which closes the trigon basin.

M2—Trapezoidal occlusal outline, with a posterior margin shorter than the anterior one; the base is almost completely surrounded by a cingulum, interrupted only below the protocone and hypocone; the metacrest is short.

m1—A trigonid ending anteriorly with a small and individualized paraconid; a modest but well-defined cingulum runs along the labial base of the tooth from the paraconid to the middle of the talonid; the posterior margin has an oblique distal cingulum that almost interrupts the hypolophid.

m2—Shows a less elongated trigonid than the m1, and the paraconid ends in the form of a straight transverse ridge.

Measurements—see Table 9.

Remarks—The size of the available molars falls within the range of modern comparative samples of *Erinaceus roumanicus* Barrett-Hamilton, 1900 from Bulgaria, but approaches the upper limit. Fossil species with similar sizes include *E. davidi* Jammot, 1972, and *E. praeglacialis* Brunner, 1933. The latter, described from the Early Pleistocene of Windloch in Germany, appears slightly larger than the Middle Pleistocene *E. davidi* from La Fage (France) and the recent European species. Beyond size, *E. praeglacialis* is distinguished by an elongated metastyle on P4 and M2, as well as the unique morphology and position of the upper P3. Rabeder [61], examining material from Hundsheim (Middle Pleistocene, Austria), questioned its large size and observed that only the position of P3 and the size of M3 are useful for differentiating fossil from recent species. Due to the highly fragmented remains from Kozarnika, the relatively limited material on which European fossil species have been described, and the fact that intra-population and geographical variation, as well as their validity, are not well established [56], a definitive identification is not possible.

Family Talpidae Fischer von Waldheim, 1817

Genus *Talpa* Linnaeus, 1758

Mole remains are found in all strata, but in most cases, they are too fragmentary to allow for precise species determination. Identifying fossil mole species mainly depends on the size of postcranial bones. While dental differences have been observed, the degree of

variation within and between living and fossil *Talpa* species remains poorly understood [65]. Three relatively well-preserved humeri, whose sizes are given in Table 10, indicate that in Kozarnika two size groups are presented—small, similar to the modern *T. caeca* Savi, 1822 and the fossil *Talpa minor* Freudenberg, 1914, and larger, which in the context of the variability of both modern and fossil representatives of the genus in Europe, falls into the medium size group, to which *T. fossilis* Pétenyi, 1864, and *T. europaea* Linnaeus, 1758 belong.

Table 10. Measurements [mm] of the humeri of *Talpa* from Kozarnika.

Specimen	Layer	Species	H-MAX-L	H-MAXW	H-MINW	H-W
BG-IBER-FMC-000021901	9ab	*T. europaea*	15.72	11.19	4.25	8.53
BG-IBER-FMC-000006502	13b	*T. europaea*			4.18	8.85
BG-IBER-FMC-000006344	13b	*T. minor*			3	6.7

Talpa europaea Linnaeus, 1758
(Figure 9A–G,J,K)

Studied material—Biozone B: L13a: 1 humerus; L12: 1 m1, 1 m2, 1 M2; L11b: 1 m3; Biozone A: L9ab: 1 humerus; L6/7: 1 fragment of mandible.

Description—Based on the structural details, the medium-sized moles from Kozarnika (fragments of mandibles and humeri, isolated teeth) are indistinguishable from the recent species from Bulgaria.

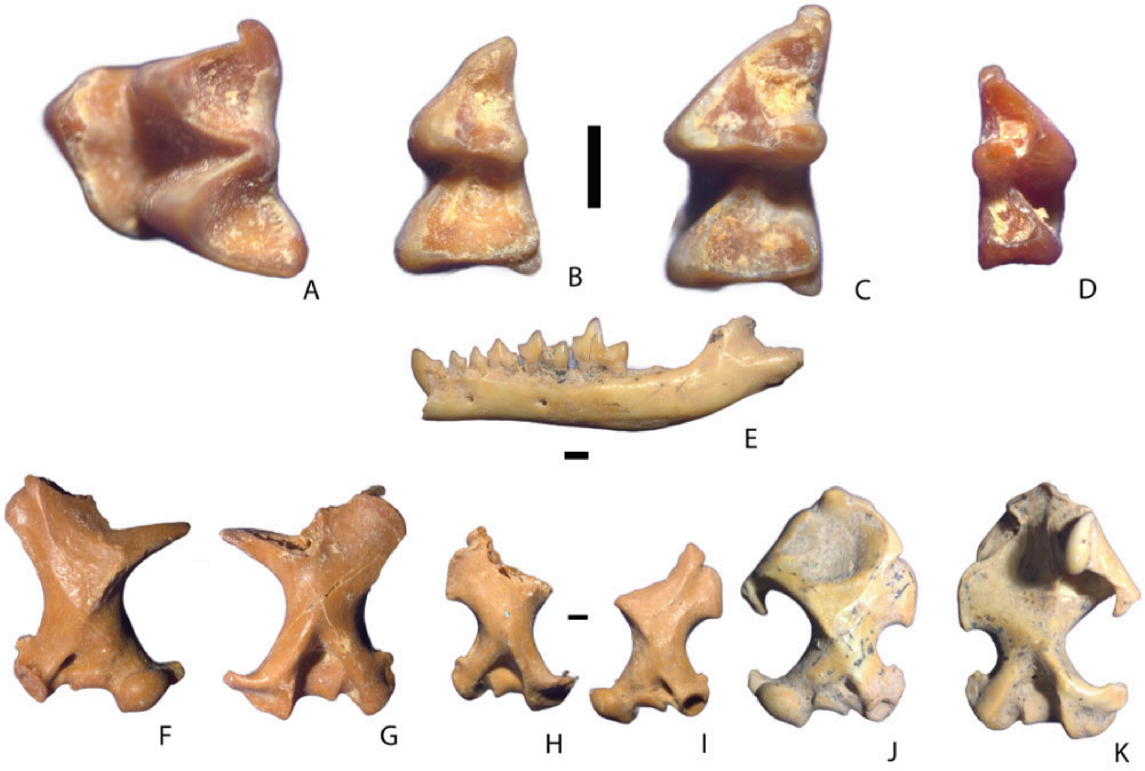


Figure 9. *Talpa europaea* (**A**–**G**,**J**,**K**), *T. minor* (**H**,**I**). (**A**)—left M2 (BG-IBER-FMC-000014689, L12), (**B**)—left m1 (BG-IBER-FMC-000010799, L12), (**C**)—left m2 (BG-IBER-FMC-000010799, L12), (**D**)—right m3 (BG-IBER-FMC-000016338, L12), (**E**)—left fragment of mandible in lateral view (BG-IBER-FMC-000003853, L6/7), (**F**,**G**)—left humerus (BG-IBER-FMC-000006502, L13b, anterior and posterior views), (**H**,**I**)—right humerus (BG-IBER-FMC-000006344, L13b, posterior, anterior views), (**J**,**K**)—right humerus (BG-IBER-FMC-000021901, L9ab, posterior, anterior views). Scale bars = 1 mm.

Measurements—Table 10.

Remarks—The limited material falls within the size variability of both *Talpa fossilis* and *T. europaea*. There are controversial opinions regarding the taxonomic validity of *T. fossilis*, partly due to its poor original description [66]. Some students do not consider it a valid species as its size falls within the range of variation of recent *T. europaea* [67,68]. Conversely, its validity was confirmed by Sansalone et al. [69]. In Europe, *T. fossilis* was recorded at localities spanning the Pliocene through the Middle Pleistocene. According to some researchers [61,70], the name *T. fossilis* refers only to a chronospecies. A revision of material from the type locality (Beremend, Hungary) is needed to determine whether *T. fossilis* and *T. europaea* are distinct forms. However, given that the remains from the Late Pleistocene layers at Kozarnika can definitely be assigned to *T. europaea* and that there are no clear differences among the remains from the lower layers (Biozone B), all remains belonging to medium-sized moles were attributed to the recent species.

Talpa minor Freudenberg, 1914

(Figure 9H,I)

Studied material—Biozone B: L12: 1 humerus.

Description—The available humerus has a morphology typical of recent *Talpa europaea*, differing only in its considerably smaller size (Table 10).

Remarks—The stratigraphic range of *Talpa minor* spans from the early Villanyian (MN 16) to the Holocene [71]. Notable localities include Erpfingen 3 [46], Petersbuch 1 [70], Hundsheim (type locality) [61], Betfia [40], Żabia Cave [71], Rivoli Veronese [72], among others.

Order Lagomorpha Brandt, 1855

Family Leporidae Gray, 1821

Genus *Hypolagus* Dice, 1917

Hypolagus cf. *petenyi* Čermák and Fladerer, 2009

(Figure 10N–R)



Figure 10. *Lepus* cf. *terraerubrae* (**A**–**M**), *Hypolagus* cf. *petenyi* (**N**–**R**), p3 in occlusal view. (**A**)—right, BG-IBER-FMC-000000398, L11a1; (**B**)—left, BG-IBER-FMC-000000679, L13b; (**C**)—left, BG-IBER-FMC-000001114, L13b; (**D**)—right, BG-IBER-FMC-000006477, L13b; (**E**)—left, BG-IBER-FMC-000010601,

L13a; (**F**)—right, BG-IBER-FMC-000014739, L11b; (**G**)—right, BG-IBER-FMC-000022251, L13c; (**H**)—left, BG-IBER-FMC-000015955, L11b; (**I**)—left, BG-IBER-FMC-000016481, L12; (**J**)—left, BG-IBER-FMC-000017119, L12; (**K**)—left, BG-IBER-FMC-000019174, L12; (**L**)—left, BG-IBER-FMC-000022015, L13-Lower; (**M**)—left, BG-IBER-FMC-000022023, L13a; (**N**)—left, BG-IBER-FMC-000014716, L13a; (**O**)—left, BG-IBER-FMC-000021993, L13-Lower; (**P**)—left, BG-IBER-FMC-000000258, L12; (**Q**)—right, BG-IBER-FMC-000019943, L12; (**R**)—right, BG-IBER-FMC-000006504, L13b. Scale bar = 1 mm.

Studied material—Only p3s were studied. Biozone B: L13-Lower: 1; L13b: 1; L13a: 2; L12: 1.

Description—The protoflexid is mostly shallow, with only one case being notably deep. The hypoflexid reaches the middle of the chewing surface, slightly obliquely oriented relative to the medial axis; the edges are almost smooth, with only two specimens showing faint crenulations on the posterior wall. In two specimens, remnants of the paraflexid are present. The hypoconid has no notch.

Measurements [mm]—N = 4, Lp3 =2.51–2.98–3.60; Wp3 = 2.67–2.84–3.07.

Remarks—The small sample does not allow for an assessment of variability or reliable comparisons in the context of the weak differences between the earlier gracile form, *H. beremendensis* (Petényi, 1864) (Late Pliocene–Early Biharian), and the more robust *H. brachignathus* (Kormos, 1930) (Biharian). The available teeth have a relatively simplified chewing surface, characterized by a weak expression of the protoflexid. The sizes are small, especially compared to data for *Hypolagus* from the Czech and Slovak Republics [73], but similar to some populations from Poland attributed to *H. beremendensis* [73]. The available teeth are very similar to those from the Pliocene site of Muselievo, which were referred to *H. beremendensis* [74]. Later, the name *Hypolagus petenyi* was proposed for this species [75].

Lepus cf. *terraerubrae* Kretzoi, 1956

(Figure 10A–M)

Studied material—Only p3's were studied. Biozone B: L13-Lower: 1; L13c: 2; L13b: 4; L13a: 3; L12: 6; L11b: 7; layer 11a1: 1; L11a: 1.

Description—The asymmetry between the labial and lingual anteroconids is clearly expressed—the labial is better developed. The anteroflexid, which separates them, is shallow. The protoflexid is shallow, except for one specimen. The hypoflexid reaches the lingual wall; the anterior edge is smooth, or more often has a few undulations, and the posterior edge is smooth. The hypoconid is more often weakly projecting labially. The entoconid is mostly strongly rounded.

Measurements [mm]—N = 14 (Min-X-Max), Lp3 = 2.81–3.60–4.06, Wp3 = 2.61–3.17–3.70.

Remarks—Based on the asymmetry between the lingual and buccal anteroconids, resulting from their different sizes, the available teeth undoubtedly belong to the genus *Lepus* rather than *Oryctolagus*. The poorly developed and rounded entoconid and the shallow antero- and protoflexids allow it to be distinguished from the modern *L. europaeus* Pallas, 1778, and *L. timidus* Linnaeus, 1758. Currently, the oldest known hare was named *L. terraerubrae*, described on the basis of Biharian materials from Hungary, whose diagnosis is limited to (translation from the German original) "A species of hare with, like *L. europaeus* and *L. timidus*, divergent limb proportions, a simple occlusal surface of the p3, and a divergent cross-section of the incisors" [76], p. 167. This species was cited in the Lower and Middle Biharian of Beremend 9 and 10, Nagyharsanyhegy 4, Villány 6, and Voigtstedt [76], and in the Lower Biharian of Monte Peglia (Italy) [21], where the author provides a drawing of the occlusal surface of the p3. In this drawing [21] (p. 27, Figure 8), one can find characters that are still poorly pronounced, but which foreshadow *L. europaeus* (reduced anterior lobe, shallow protoflexid), or which may be primitive stages compared to other morphotypes of p3 of later *L. europaeus* [77]. The material from Kozarnika is very similar to several teeth from Monte Peglia, identified as belonging to *Lepus terraerubrae*, in terms of size and shape

of the occlusal surface. As the material from Monte Peglia has been directly compared with that from Betfia 2 (Romania) and full agreement has been established, and since the material from Kozarnika is very similar to that from Monte Peglia, it has been tentatively classified as this species.

Family Ochotonidae Thomas, 1897

Genus *Ochotona* Link, 1795

Ochotona cf. *transcaucasica* (Vekua, 1967)

(Figure 11A–C)

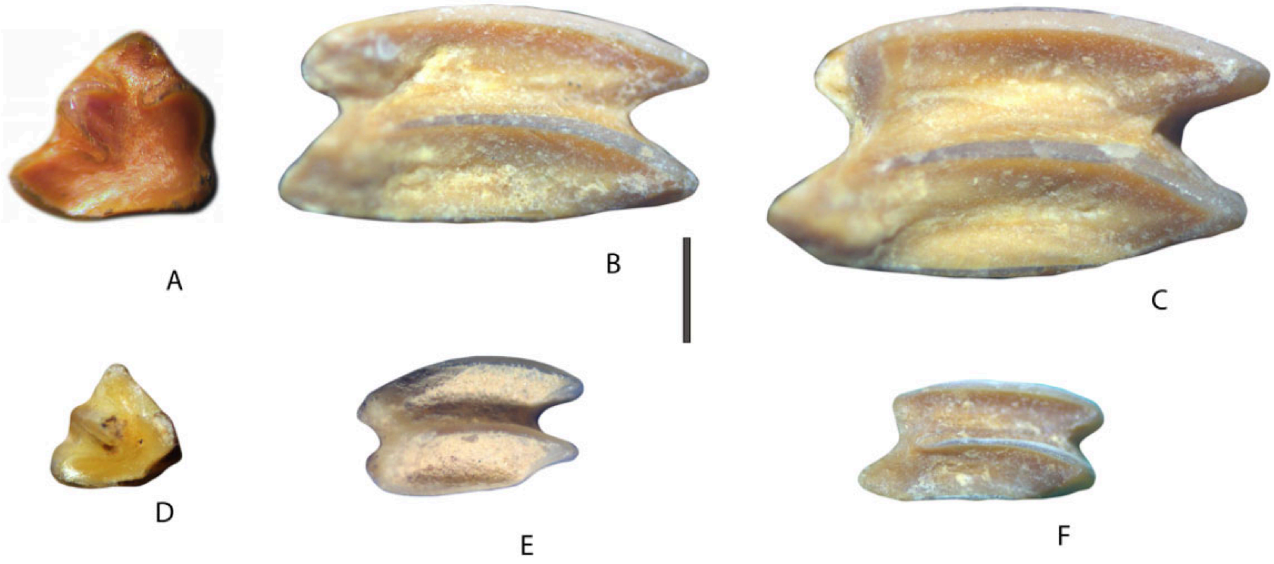


Figure 11. *Ochotona* cf. *transcaucasica* (**A**–**C**), *Ochotona pusilla* (**D**–**F**), left cheek teeth. (**A**)—p3, BG-IBER-FMC-000000550, L13a; (**B**)—P4/M1, BG-IBER-FMC-000016340, L12; (**C**)—P4/M1, BG-IBER-FMC-000016341, L12; (**D**)—p3, BG-IBER-FMC-000021764, L9ab; (**E**)—P4/M1, BG-IBER-FMC-000013013, L5a; (**F**)—P4/M1, BG-IBER-FMC-000013179, L5b. Scale bar = 1mm.

Studied material—1 p3, 2 P4/M1.

Measurements [mm]—(L × W). p3: 2.07 × 2.1; P4/M1: 2.15 × 3.85; 2.09 × 4.07)

Description—p3. The occlusal surface possesses a relatively small anteroconid with a rounded top; there is a trace of anterolingual fold. Para- and protoflexid have smooth walls, are short, and are nearly the same depth. The confluence between anteroconid and posteroconid is moderately broad. The lingual margin of the posteroconid is slightly concave.

P4/M1. The teeth are similar to those of *Ochotona pusilla* (Pallas, 1769) but are twice as large.

Remarks—The shape of the available p3 is similar to the teeth of *Ochotona transcaucasica* from Azyh (Azerbaijan) [78]. This species has p3 morphology akin to *O. pusilla* but is notably larger, more than twice the size of *O. pusilla* [79]. It was originally described from Copi (Georgia) as *Ochotonoides transcaucasica* [80] and was later reclassified into the genus *Ochotona* [79]. Due to the lack of detailed descriptions, making precise comparisons is challenging.

Ochotona sp.

Studied material—(number of molariform teeth). Biozone B: L13—Lower: 1; L13c: 15; L13b: 71; L13a: 65; L12: 90; L11c: 20; L11b: 89; L11a1: 167; L11a: 104.

Remarks—The available upper and lower molariforms do not differ in size or morphology from the corresponding teeth of *Ochotona pusilla*. However, due to the absence of the diagnostic p3, the exact species determination is not possible, having in mind the

possible occurrence of *O. polonica* Sych, 1980 [48], *O. kormosi* Fostowicz-Frelik, Frelik, and Gasparik, 2010 [81], or *O. valerotae* Erbaeva, Montuire, and Chaline, 2001 [82].

Ochotona pusilla (Pallas, 1768)

(Figure 11D,E)

Studied material—Biozone A (number of molariform teeth). L10b: 1; L10a: 23; L9c: 10; L9ab: 5; L9a: 1 fragment of mandible with p3; L6/7: 15; L5c: 8; L5b: 84; L5a: 12; L3–4: 1.

Description—p3. The outline of the chewing surface is triangular. The anterocone is asymmetrical, resulting from uneven depths of the proto- and paracone. The connection between the anterocone and the posterocone is most often wide. The lingual margin of the posteroconid is slightly concave.

Measurements [mm]—p3: L= 1.2; W= 1.26.

Remarks—The available remains of Biozone A are very similar to those of *Ochotona pusilla* from nearby Late Pleistocene sites [38,83].

Order Rodentia Bowdich, 1821

Family Sciuridae Fischer, 1817

Genus *Marmota* Blumenbach, 1779

Marmota marmota Linnaeus, 1758

(Figure 12)

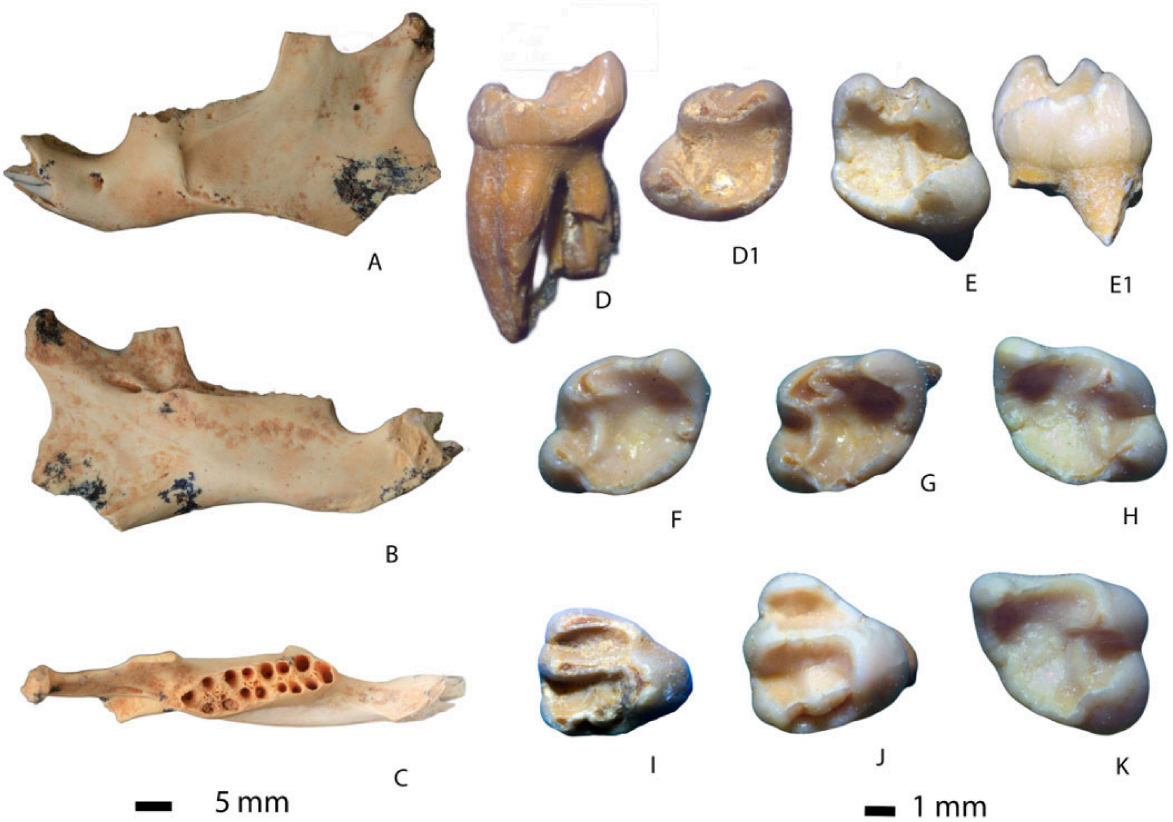


Figure 12. *Marmota marmota*. (**A**–**C**) Fragment of left mandible—kz1563, L13-Lower (labial, lingual, occlusal views); (**D**,**D1**) left p4—BG-IBER-FMC-000000655, L13b (occlusal, posterior views); (**E**,**E1**) right p4—kz1256, L11a (occlusal, posterior views). (**F**–**K**) Upper and lower cheek teeth in occlusal view, kz838, L13c (**F**,**G**)—m1/2, (**H**,**K**)—m3, (**I**)—M1/2, (**J**)—P4.

Studied material—L11a: 2 M1/2; L11a1: 1 m3; L11b: 2 P4, 2 M1/2, 2 M3, 3 p4, 1 m1/2, 5 m3; L12: 2 P2, 5 P4, 2 M1/2, 4 p4, 4 m1/2, 2 m3.

Measurements—Table 11.

Table 11. Measurements [mm] of cheek teeth of *Marmota marmota* from Kozarnika.

Tooth	N	L			W		
		X	Min	Max	X	Min	Max
P2	2	4.12	4.10	4.15	5.01	4.99	5.0
m3	8	5.10	4.38	5.62	5.44	4.98	5.9
M1/2	6	4.28	4.11	4.61	5.13	4.75	5.6
m1/2	5	4.38	4.15	4.85	5.09	4.68	5.4
p4	7	4.15	3.60	4.68	4.28	3.47	5.1
P4	7	4.41	3.61	5.06	4.65	3.49	5.6
M3	2	5.14	5.11	5.17	5.31	5.16	5.5

Description—M1–2. All available teeth have a mesostyle, with some being very well developed. The metaconule is well expressed. One tooth also has a well-developed paraconule.

m1–m3 always have a mesostylid, which in most cases appears as a wide and low tubercle, in a few as a high and conical one, and in one it is very faintly expressed. The metalophid is weakly developed and appears to form independently, very close to the protoconid.

p4—The anteroconulid is well developed, protruding forward. Among the few available p4s with preserved roots, in one, the posterior root is single but formed by the fusion of two roots; on another tooth, although the roots are broken, the presence of two roots can be inferred. On a well-preserved lower jaw (Figure 12C), three well-defined alveoli for the p4 roots are visible, indicating the presence of two posterior roots.

Remarks—During the Pleistocene, two species are known from Europe—in Western and Southwestern Europe, the remains are most often identified as *Marmota marmota*, and in Eastern, Northeastern, and Northern Central Europe, as *M. bobak* (Müller, 1776). Differentiating them based on morphology is difficult [84]. Based on the presence of p4 with two posterior roots among the material from Kozarnika, the entire material is attributed to *Marmota marmota*. Among the material from Kozarnika, the remains have been found only in the lower layers (Biozone B). They can be grouped into two taphonomic groups. One consists of well-preserved light-colored skeletal elements, always found in the lowest layers, but in a sedimentary context different from that of the main one for the respective layer, and clearly representing secondary intrusions. It can be assumed that these are holes where marmots hibernated, and the well-preserved skeletal remains are of animals that died during hibernation. Judging by the color of the bones and the intrusions containing them, this material is synchronous with the uppermost layers of biozone B—layers 11 and 11a1. The other taphonomic group consists of isolated teeth found in intact sediments of Biozone B. In terms of color and preservation, they are similar to the other bone materials from the respective layers.

Genus *Spermophilus* F. Cuvier, 1825

Spermophilus citellus (Linnaeus, 1766)

(Figure 13A–P)

Studied material (number of cheek teeth)—Biozone B: L13-Lower: 4; L13c: 49; L13b: 151; L13a: 134; L12: 157; L11c: 44; L11b: 119; L11a1: 172; L11a: 177; L10b: 7; Biozone A. L10a: 48; L9c: 8; L9ab: 46; L6/7: 14; L5c: 17; L5b: 64; L5a: 5; L3–4: 8.

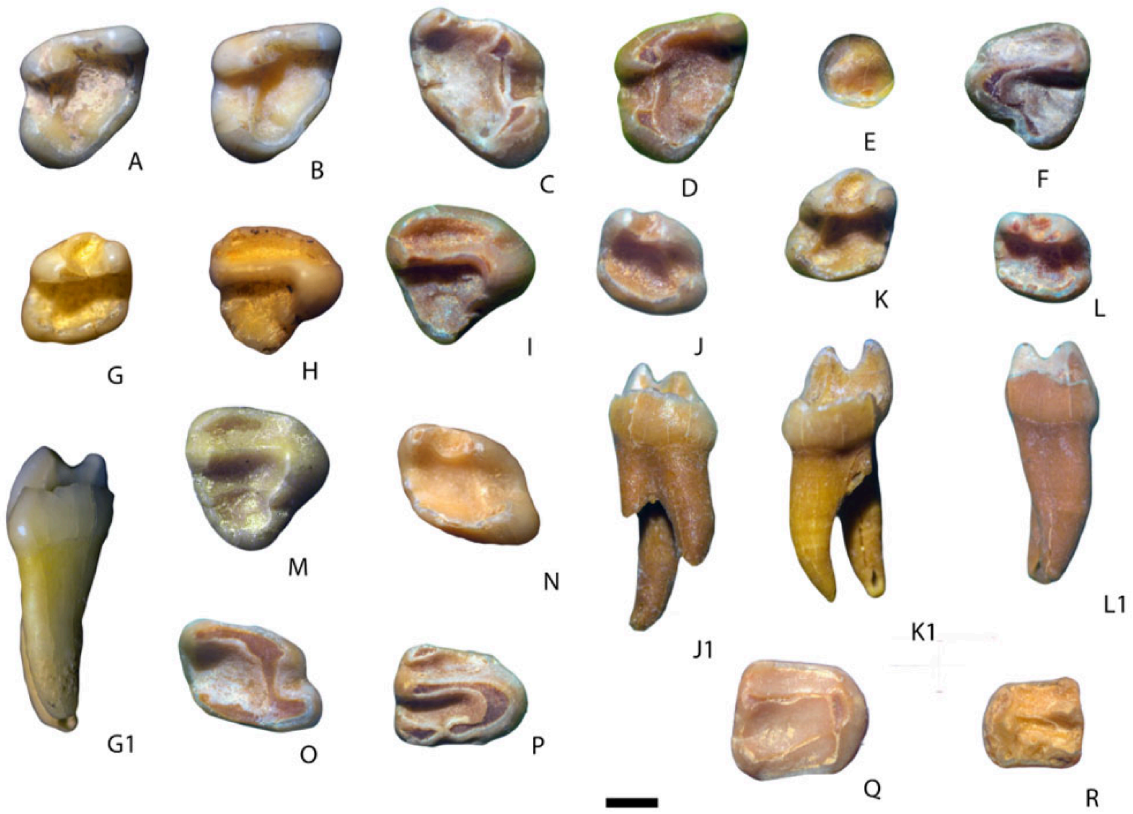


Figure 13. *Spermophilus citellus* (**A**–**P**), *Sciurus* sp. (**Q**), *Tamias orlovi* (**R**). (**A**)—left m3, BG-IBER-FMC-000013713, L10a; (**B**)—left m3, BG-IBER-FMC-000013523, L10a; (**C**)—right m3, BG-IBER-FMC-000017051, L12; (**D**)—left m3, BG-IBER-FMC-000016876, L12; (**E**)—P3, BG-IBER-FMC-000016879, L12; (**F**)—left M3, BG-IBER-FMC-000018347, L11b; (**G**,**G1**)—left p4 (occlusal, posterior views), BG-IBER-FMC-000013918, L5b; (**H**)—right M3, BG-IBER-FMC-000012137, L3–4; (**I**)—right M3, BG-IBER-FMC-000018871, L13a; (**J**,**J1**)—right p4 (occlusal, posterior views), BG-IBER-FMC-000017050, L12; (**K**,**K1**)—left p4 (occlusal, posterior views), BG-IBER-FMC-000019789, L12; (**L**,**L1**)—right p4 (occlusal, posterior views), BG-IBER-FMC-000019790, L12; (**M**)—right M3, BG-IBER-FMC-000000009, L11b; (**N**)—right m1/2, BG-IBER-FMC-000013753, L11a; (**O**)—right m1/2, BG-IBER-FMC-000016878, L12; (**P**)—right M1/2, BG-IBER-FMC-000019794, L12; (**Q**)—right M2, BG-IBER-FMC-000001147, L13b; (**R**)—left M2, BG-IBER-FMC-000012829, L12. Scale bar = 1 mm.

Description—p4. The outline in the occlusal view is trapezoidal, and as a result, the trigonid basin is narrow and small. The anteroconulid is small or absent. The labial anterolophid is weak. There is mesostylid, but sometimes very poor. Out of a sample of 30, where the roots are preserved, 24 have only one posterior root, 2 have one and traces of an additional root, completely fused with the main one, 2 have a very small additional root, and 2 have two posterior roots, a large one and a smaller one, which is partially fused with the main posterior root.

m1–2. The metalophid is developed to varying degrees but is sometimes completely absent. The entoconid is most often well expressed, separated from the hypoconid. The mesostylid is well expressed, conical, and separated from the entoconid. The ectolophid is often high and connected to the protoconid; less frequently, it is low and does not reach the protoconid base. The hypoconid is compressed anteroposteriorly, separated from the protoconid by a large valley. On some teeth, the mesoconid is slightly marked, with negligible traces of the entoconulid.

m3. The ectostylid is poorly developed. The hypoconid is relatively underdeveloped. The entoconulid is missing, but is rarely present as a small enamel plication. The entoconid is very weak or missing. The mesostylid is observed only on one tooth, and the ectostylid

is absent. The metalophid is reduced, appearing near the protoconid. On several teeth, the ectolophid is low.

P4—M1/2. The anterostyle is rarely well pronounced. The metaconule is weak. The anterosinus is lacking or only slightly marked.

M3. The shape of the tooth is a rounded triangle; its posterior margin is relatively narrow. The metacone is poorly developed, and on the worn tooth, it is not visible. Metaloph is either absent or very low and barely noticeable on the worn teeth.

Measurements—Table 12.

Table 12. Measurements [mm] of cheek teeth of *Spermophilus citellus* from Kozarnika.

Biozone	Measurement	N	L				W			
			X	SD	Min	Max	X	SD	Min	Max
A	P4	9	1.98	0.125	1.74	2.15	2.52	0.082	2.40	2.65
	M1/2	21	2.10	0.151	1.89	2.61	2.77	0.243	2.05	3.04
	M3	10	2.61	0.108	2.37	2.75	2.61	0.193	2.34	2.89
	p4	8	1.97	0.317	1.31	2.35	2.08	0.388	1.23	2.45
	m1/2	16	2.23	0.228	1.80	2.72	2.74	0.270	1.86	2.98
	m3	17	2.77	0.241	2.25	3.23	2.56	0.197	1.92	2.82
B	P4	7	1.97	0.059	1.91	2.07	2.51	0.258	2.08	2.91
	M1/2	25	2.11	0.195	1.62	2.54	2.78	0.244	2.05	3.06
	M3	13	2.59	0.221	2.05	2.82	2.60	0.205	2.10	2.91
	p4	22	2.03	0.168	1.72	2.45	2.03	0.146	1.72	2.35
	m1/2	21	2.21	0.258	1.74	2.94	2.87	0.277	2.08	3.26
	m3	11	2.98	0.234	2.64	3.38	2.56	0.154	2.29	2.71

Remarks—In terms of tooth size, there is no difference between the two biozones. The material from Kozarnika belongs to a small form of the genus—the size is definitely smaller compared to those of *Spermophilus nogaici* Topachevski, 1957 (Nogajsk), *S. primigenius* (Kormos, 1934) (Villány 3), and *S. polonicus* (Kamyk, Kozi Grzbiet) [85] and similar to those in modern *S. citellus*, *C. suslicus* (Güldenstaedt, 1770), and the fossil *S. citelloides* (Kormos, 1916) [86,87]. It is believed that the bifurcated posterior root of p4 is a characteristic feature of the first species [88]. Based on this, the Late Pleistocene material from Bacho Kiro cave (Bulgaria) has been attributed to *S. citellus* [89]. However, two-rooted p4 also occur within the *citelloides* group [88], but the posterior root is always distinctly flattened in the sagittal plane, unlike those in the *Citellus suslicus* group. In this regard, the available material is more similar to *S. citelloides*, e.g., as in the form from Burgtonna [87]. It should be noted that such a structure of the posterior root is common among the modern comparative material from Bulgaria (11 p4s). The material from Kozarnika differs from *S. citelloides* and *S. suslicus* in its simpler chewing-surface structure. The Kozarnika material lacks a well-developed metaloph and metaconul on M3. In *S. citelloides*, the structure of the occlusal surface of m3 is more complex, as the central part of the talonid basin contains a voluminous structure formed by the entoconulid and entolophid, which are closely appressed and partially fused with the lingual side of the entoconid. The groove, delimiting the bulging from the ectolophid and the labial cusps, is well-excavated [90]. All these features are missing or poorly pronounced in the material from Kozarnika. There are also significant differences in the shape of p4. In *S. citelloides*, the maximal width most often exceeds the length, and the tooth has a rectangular outline in occlusal view, while in the described material, the shape

is trapezoidal with a narrowed front part. According to these features, it is very similar to the modern *S. citellus*. It is also closely related to this species by the high frequency of M1–2, which has a mesostyle. *S. xanthoprimnus* (Bennett, 1835) also has a simplified structure of the occlusal surface, but unlike *S. citellus*, p4 has two posterior roots [91]. Overall, based on the features observed in the isolated fossil teeth, the material from Kozarnika does not differ from later populations attributed to the modern species [43] or from the modern comparative material.

For the Balkan Peninsula and adjacent regions of Asia Minor, fossil evidence for ground squirrels is scarce, and they are generally either not identified to species or are tentatively attributed to some modern species, mostly based on indirect arguments (general morphological similarity, ranges of modern species, presumed ranges of fossil similar species, etc.). So far, the earliest material definitely attributed to *S. citellus* is from the lower layers of the Morovitsa Cave (Holsteinian) [43]. In this context, the material from Kozarnika fills a significant gap in the history of *S. citellus*. These results are consistent with genetic data, which show that the species has existed independently for at least the last 5 million years [92].

Genus *Tamias* Illiger, 1811

Tamias orlovi (Sulimski, 1964)

(Figure 13R)

Studied material—Biozone B: L11d: 1 right M1/2.

Description. The available tooth is rather worn, but nevertheless, the morphology is clearly discernible. Proto-, metaloph, para-, and metacone are all well pronounced. The protocone and the hypocone form a well-developed ridge. There is a parastyle in the anterolabial corner of the occlusal surface. The anteroloph and the posteroloph are weak.

Measurements [mm] (L × W)—1.81 × 2.0.

Remarks. In terms of the structure of the chewing surface and size, the available molar is very similar to the material from Veže 2 (Poland, Late Pliocene MN 16b, 2900–2600 Kya). *Tamias orlovi* is known from several Pliocene and Early Pleistocene (?*Tamias* sp.) sites [74], [93,94]. Its presence in Biozone B of Kozarnika extends its stratigraphic range to the end of the Early Pleistocene.

Genus *Sciurus* Linnaeus, 1758

Sciurus sp.

(Figure 13Q)

Studied material—Biozone B: L13b: 1 M2; L11a1: 1 m1

Description—M2. The metaloph is straight and develops obliquely relative to the anteroloph; the mesostyle is low, separated from the metaconid by a well-defined, though shallow sinus.

m1. The mesoconid is low, and the metastylid is very small.

Measurements [mm] (L × W). M2: 2.44 × 2.74; m1: 2.19 × 2.39.

Remarks—In terms of size, the available teeth are within the range of variability of *S. wartae* Sulimski, 1964 [95] or slightly below it, and are very similar to the modern comparative material of *S. vulgaris* Linnaeus, 1758, but differ in the less pronounced mesoconid and metastylid of m1. The limited available material does not allow for an exact identification.

Family Sminthidae Brandt, 1855

Genus *Sicista* Gray, 1827

Sicista subtilis (Pallas, 1773)

(Figure 14)

Studied material—Biozone B: L11a: 1 M1; L11a1: 1 M1; L11b: 1 m1; L12: 2 M1, 1 M2. Biozone A: L5b: 2 m1, 1 m2; L9c: 1 m1; L10a: 1 m1.

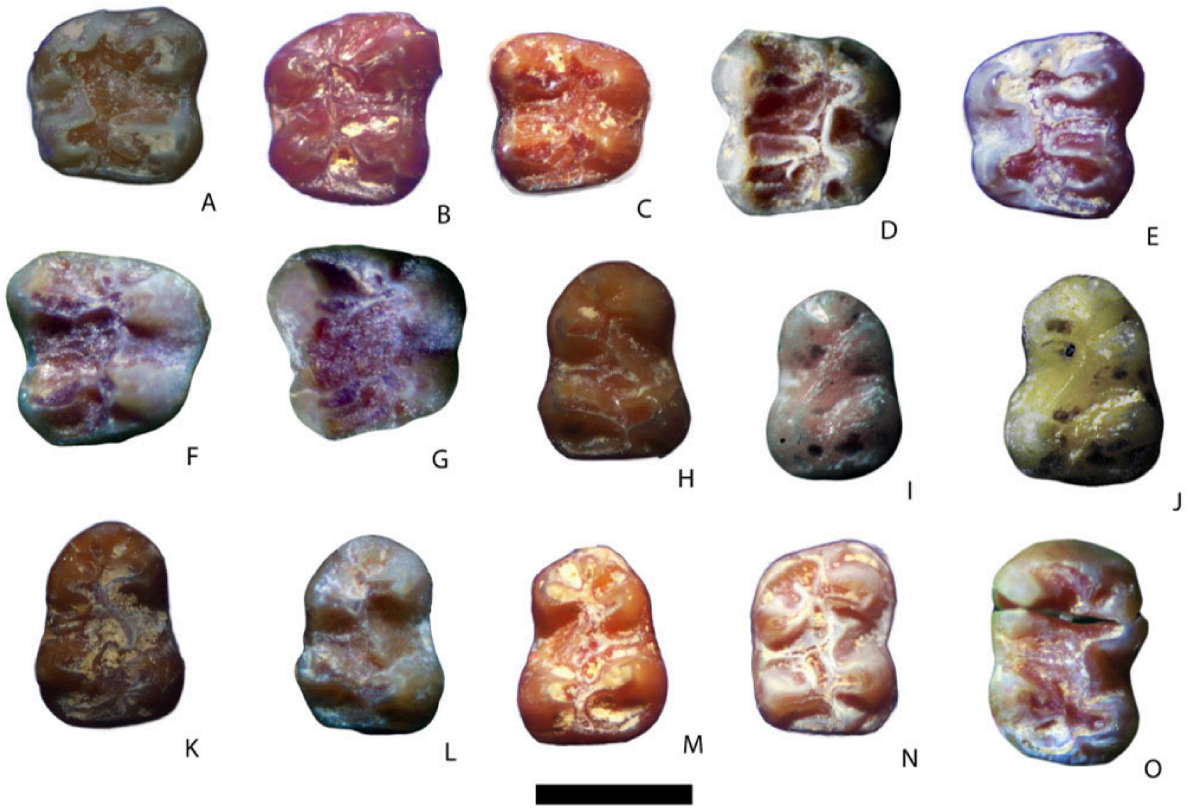


Figure 14. *Sicista subtilis*, molars in occlusal view. (**A**)—left M1, BG-IBER-FMC-000002493, L11a; (**B**)—left M1, BG-IBER-FMC-000003461, L13a; (**C**)—right M1, BG-IBER-FMC-000006538, L13b; (**D**)—left M2, BG-IBER-FMC-000017613, L12; (**E**)—left M1, BG-IBER-FMC-000021949, L11a1; (**F**)—right M1, BG-IBER-FMC-000017049, L12; (**G**)—right M1, BG-IBER-FMC-000016872, L12; (**H**)—right m1, BG-IBER-FMC-000004294, 11a; (**I**)—left m1, BG-IBER-FMC-000001816, L10a; (**J**)—left m1, BG-IBER-FMC-000005156, L5b; (**K**)—right m1, BG-IBER-FMC-000004327, L11a; (**L**)—right m1, BG-IBER-FMC-000015915, L11b; (**M**)—left m1, BG-IBER-FMC-000006576, L13b; (**N**)—right m2, BG-IBER-FMC-000022010, L13b; (**O**)—right m2, kz1296, L11a1. Scale bar = 1 mm.

Description—M1. The anterocone is well developed, connected to the paracone and protocone. This three-lobed structure is connected to the metacone and hypocone via an endoloph, and the metacone and hypocone, in turn, are connected through a well-developed metaloph. The hypocone is connected to a well-developed posteroloph. Between the posteroloph and metacone, there is a well-defined valley that closes into a mark as the tooth wears down. The mesolophid is well developed. The valleys that separate it from the protocone and metacone, when the tooth is worn, close into marks (mesofossette), starting with the posterior one.

M2. Similar to M1, but lacks an anterocone; instead, it has a well-developed anteroloph.

m1. In occlusal view, the outline of the tooth is rounded and narrowed anteriorly, with a well-defined, shallow lateral concavity. The well-developed anteroconid connects with the metaconid and protoconid, forming a three-lobed structure. The mesolophid is low. The posterolophid is well developed and separated from the entoconid by a deep valley. Behind the hypoconid, there is a well-defined but short valley. There are no additional spurs on the entoconid.

m2. No anteroconid. The anterolophid is well developed. In front of the protoconid, there is a wide and short incoming valley. The mesolophid and posterolophid are well defined. The posterolophid is separated from the entoconid by a wide valley, which closes into a mark when the tooth is worn down.

Measurements—Table 13.

Table 13. Measurements [mm] of molars of *Sicista subtilis* from Kozarnika.

Molar	N	X	Min	Max	X	Min	Max
M2	1	1.23			1.2		
M1	4	1.24	1.21	1.3	1.3	1.24	1.33
m1	5	1.25	1.19	1.31	0.9	0.9	1.01
m2	1	1.1			0.9		

Remarks—Several Pleistocene species of the genus *Sicista* are known in Europe, but their classification is debated. The status of *Sicista vinogradovi* Topachevsky, 1965, from the Early and Early/Middle Pleistocene at Nogajsk (Ukraine) and neighboring sites [96] needs confirmation. *S. montana* Méhely, 1913, is now considered a synonym of S. *betulina* Pallas, 1779 [97]. The most common European Pleistocene species are *S. praeloriger* Kormos, 1930, *S. subtilis*, and *S. betulina.* The first species is probably an ancestor of *S. subtilis* [97]. It was described by Somlyóbérg near Püspökfürdő (Hungary, Upper Pliocene, Middle „Cromerian") based on a lower jaw and a complete dental row. However, the diagnosis and description do not provide detailed information about the structure of the occlusal surface [98]. According to the original description, m1 is relatively large, similar to *S. subtilis* but with a more complex occlusal structure, as evidenced by additional spurs connected to the entoconid. Distinguishing *S. betulina* from *S. subtilis* is difficult due to limited collections, but morphometric criteria based on molar size and complexity aid in differentiation. *S. subtilis* is larger and has somewhat simpler molar morphology [99]. *S. subtilis* has a distinct shallow concavity on the lateral margin of m1, while *S. betulina* shows a more oval and rounded occlusal outline [100]. Due to their relatively large size, simplified lower molar structure, and the well-visible lateral concavity of m1, the available material is identified as *S. subtilis*. It cannot be distinguished from other Pleistocene records from Bulgaria [101].

Genus *Allactaga* F. Cuvier, 1837

Allactaga major (Kerr, 1792) (= *Allactaga jaculus*)

(Figure 15)

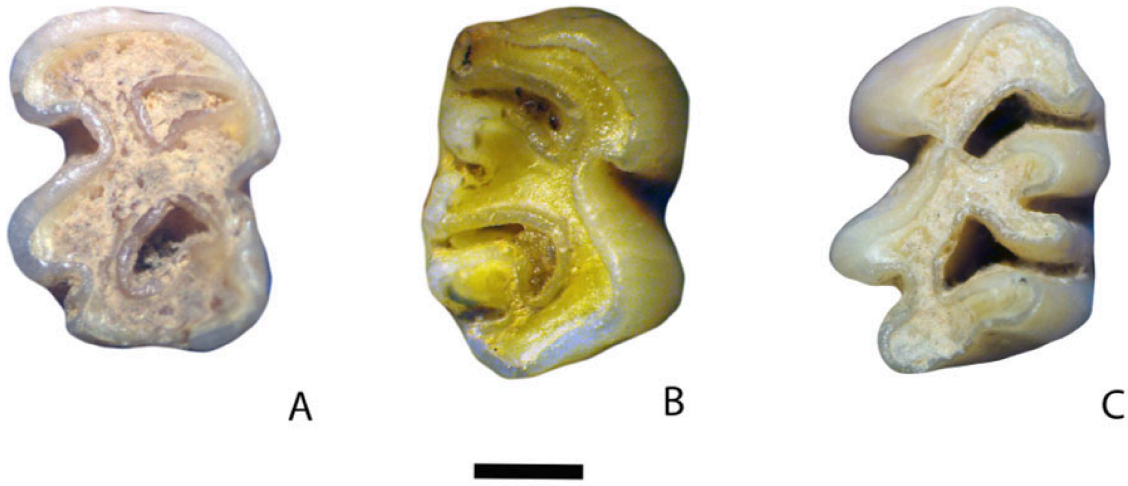


Figure 15. *Allactaga major*, upper molars in occlusal view. (**A**)—left M2, BG-IBER-FMC-000014055, L5b; (**B**)—right M1, BG-IBER-FMC-000005131, L5b; (**C**)—left M1, BG-IBER-FMC-000008881, L5a. Scale bar = 1 mm.

Studied material and Measurements [mm]: L5a: 1 M1 (3.46 × 2.47), 1 M2 (3.11 × 2.53); L5b: 1 M1 (3.46 × 2.27).

Description—M1–M2. The crown is relatively tall, with three roots. There are four buccal incoming folds, but the most posterior one is very weakly expressed. During wear, the first and third folds close into marks, while the middle (between the paracone and mesocone) and the posterior disappear. On the lingual side, there are two incoming folds.

Remarks—In structure and size, the available teeth do not differ from those of *Allactaga major* from other Late Pleistocene sites in Bulgaria [38].

Family Cricetidae Fischer, 1817

Subfamily Cricetinae Fischer, 1817

Based on tooth size, the Cricetinae material from Kozarnika forms three well-defined groups (Figure 16). The smallest group is the most abundant and falls within the range of variability of small hamsters, similar to the modern species *Nothotcricetulus migratorius* (Pallas, 1773) and to the fossil species, usually assigned to the genus *Allocricetus*. The systematics of small fossil hamsters in Europe is a subject of discussion, given the remarkable similarity in the size and structure of the occlusal surfaces of the molars [102]. The two largest molars from Kozarnika in this group can certainly be attributed to *Allocricetus ehiki* Schaub, 1930. A more detailed analysis of the changes in the sizes of the remaining molars in the stratigraphic plan allows us to assess variability and clarify their taxonomic composition. Statistical comparisons between Biozones A and B using the *t*-test reveal that the teeth from Biozone A are significantly smaller than those from Biozone B in all tooth measurements. Clearly, the mass material of small hamsters from Kozarnika forms two size groups with a clear stratigraphic separation. This pattern aligns with the traditional idea of two species that replace each other over time—*Allocricetus bursae* Schaub, 1930 (Late Pliocene, Early to Middle Pleistocene) and *Nothocricetulus migratorius* (Late Pleistocene to Holocene) [103–105]. The size characteristics of these two groups from Kozarnika correspond to data for the two species from Bulgaria [38,43,48].

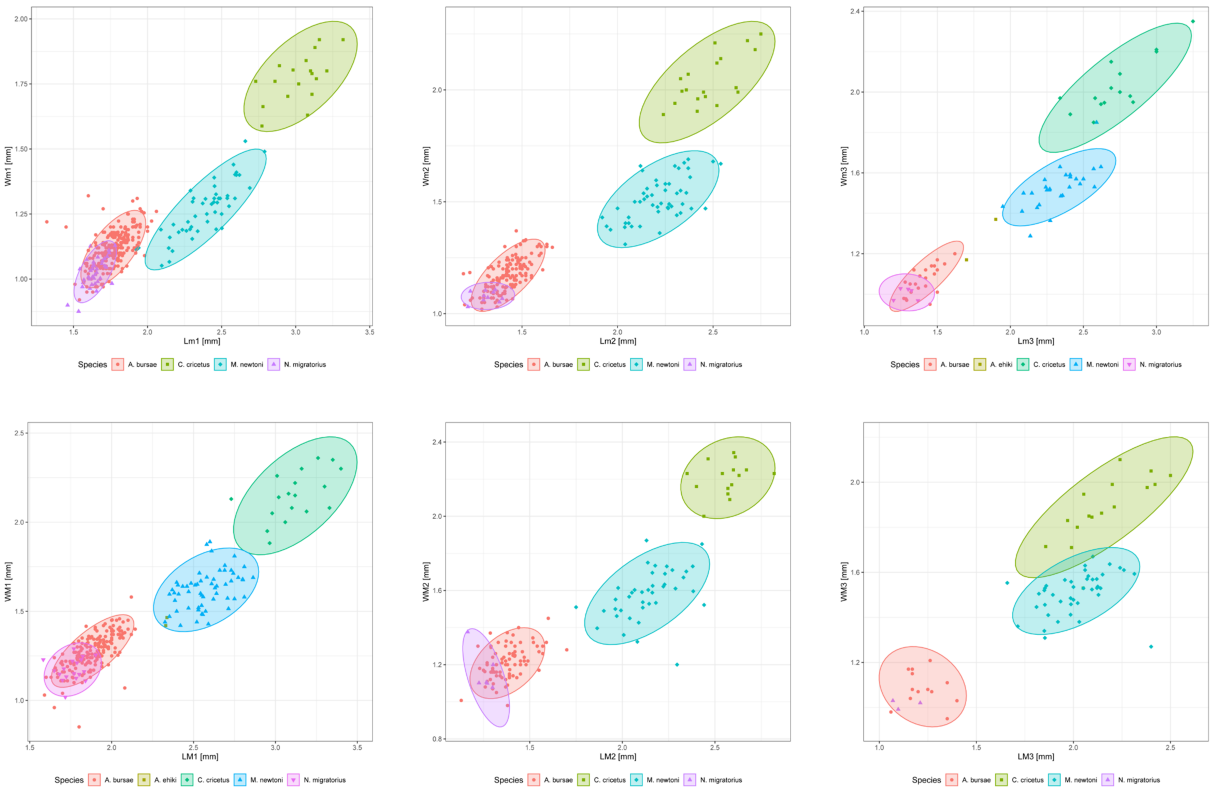


Figure 16. Scatter plot diagrams and 95% confidence ellipses of length (L) versus width (W) for upper (M1–M3) and lower (m1–m3) molars of hamsters from Kozarnika.

The well-defined medium-sized group is also characterized by a more elongated shape, particularly evident in m1 and m2. So, the size and shape clearly show that these remains belong to the genus *Mesocricetus*.

The large-sized group falls within the range of variability observed in modern representatives of the genus *Cricetus*.

Genus *Allocricetus* Schaub, 1930

Allocricetus ehiki Schaub, 1930

(Figure 17K)

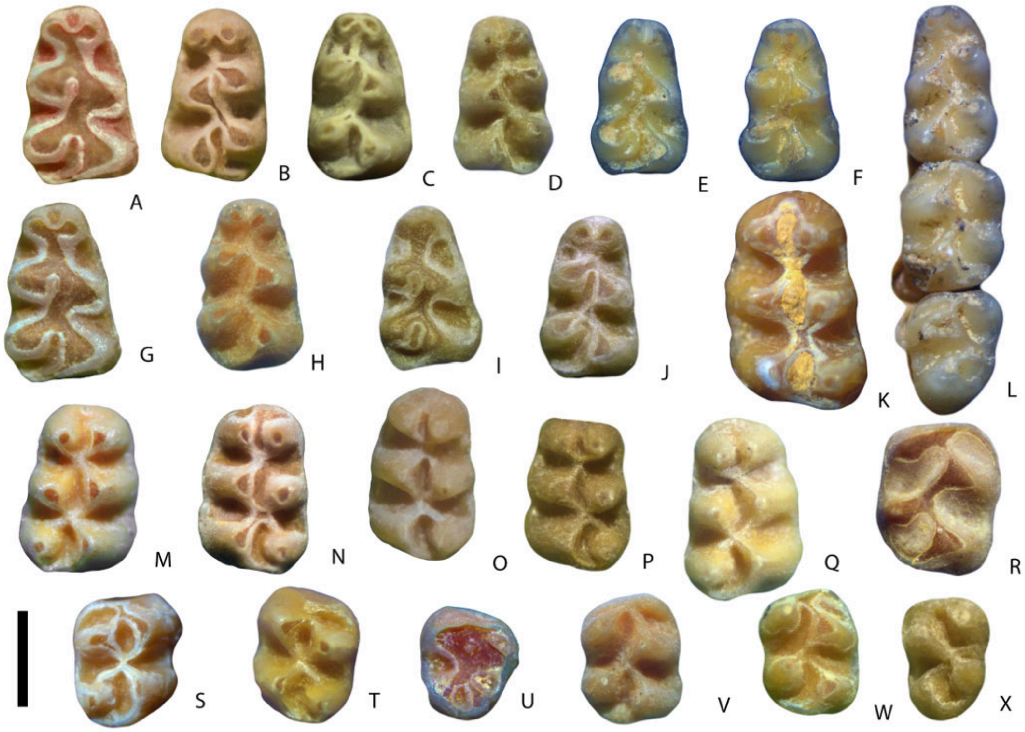


Figure 17. *Allocricetus bursae* (**A**–**D**,**G**–**J**,**M**–**X**), *A. ehiki* (**K**), *Nothocricetulus migratorius* (**E**,**F**,**L**). (**A**)—right m1, BG-IBER-FMC-000017740, L11b; (**B**)—left m1, BG-IBER-FMC-000019891, L12; (**C**)—right m1, BG-IBER-FMC-000016276, L12; (**D**)—left m1, BG-IBER-FMC-000017053, L11d; (**E**)—right m1, BG-IBER-FMC-000008906, L5b; (**F**)—right m1, BG-IBER-FMC-000008904, L5b; (**G**)—right m1, BG-IBER-FMC-000017740, L11b; (**H**)—right m1, BG-IBER-FMC-000017057, L11d; (**I**)—right m1, BG-IBER-FMC-000017066, L11d; (**J**)—right m1, BG-IBER-FMC-000017078, L11d; (**K**)—left M1, BG-IBER-FMC-000013717, L11a; (**L**)—right m1-m3, BG-IBER-FMC-000010897, L3/4; (**M**)—right M1, BG-IBER-FMC-000016538, L12; (**N**)—left M1, BG-IBER-FMC-000017742, L11b; (**O**)—left M1, BG-IBER-FMC-000017747, L11b; (**P**)—left M1, BG-IBER-FMC-000017079, L11d; (**Q**)—right M1, BG-IBER-FMC-000018995, L12; (**R**)—right m2, BG-IBER-FMC-000018984, L12; (**S**)—right M2, BG-IBER-FMC-000014564, L11b; (**T**)—left M2, BG-IBER-FMC-000018365, L12; (**U**)—left M3, BG-IBER-FMC-000019866, L12; (**V**)—right m2, BG-IBER-FMC-000017060, L11d; (**W**)—right m2, BG-IBER-FMC-000018942, L12; (**X**)—left m3, BG-IBER-FMC-000017085, L11d. Scale bar = 1 mm.

Studied material—Biozone B: L11b:1 M1; L11a1: 1 M1; L11a: 1 M1.

Description—M1. The tooth is characterized by a relatively complex structure, expressed by well-developed anterolophus and entolophus, and the associated spurs that connect them to the main tubercles.

Measurements—Table 14.

Table 14. Measurements [mm] of molars of hamsters (Cricetinae) from Kozarnika.

Molar	Species	N	L				W			
			X	SD	Min	Max	X	SD	Min	Max
M1	*A. bursae*	154	1.87	0.117	1.59	2.14	1.26	0.104	0.85	1.58
	A. ehiki	2	-	-	2.33	2.34	-	-	1.42	1.46
	N. migratorius	17	1.75	0.077	1.58	1.90	1.17	0.061	1.02	1.25
	C. cricetus	9	3.09	0.178	2.73	3.33	2.14	0.152	1.88	2.36
	M. newtoni	42	2.55	0.129	2.33	2.86	1.61	0.098	1.43	1.88
M2	*A. bursae*	66	1.38	0.093	1.13	1.70	1.20	0.089	0.98	1.40
	N. migratorius	5	1.25	0.058	1.16	1.30	1.17	0.123	1.08	1.38
	C. cricetus	11	2.54	0.127	2.35	2.82	2.20	0.106	2.00	2.34
	M. newtoni	32	2.13	0.129	1.86	2.44	1.56	0.130	1.20	1.87
M3	*A. bursae*	9	1.24	0.109	1.06	1.40	1.06	0.075	0.95	1.21
	N. migratorius	2	1.15	0.080	1.10	1.21	1.01	0.020	0.99	1.02
	C. cricetus	10	2.13	0.202	1.82	2.42	1.87	0.177	1.50	2.10
	M. newtoni	30	1.99	0.169	1.50	2.31	1.53	0.127	1.31	1.92
m1	*A. bursae*	189	1.76	0.101	1.51	2.06	1.11	0.068	0.92	1.31
	N. migratorius	13	3.02	0.167	2.77	3.32	1.77	0.095	1.59	1.92
	C. cricetus	31	2.34	0.155	1.92	2.60	1.23	0.090	1.05	1.40
	M. newtoni	36	1.64	0.067	1.46	1.78	1.02	0.056	0.88	1.13
m2	*A. bursae*	120	1.42	0.092	1.19	1.66	1.17	0.075	1.02	1.33
	N. migratorius	11	1.34	0.056	1.22	1.42	1.08	0.026	1.03	1.11
	C. cricetus	13	2.46	0.155	2.24	2.75	2.02	0.116	1.89	2.25
	M. newtoni	31	2.17	0.116	1.94	2.39	1.48	0.079	1.36	1.67
m3	*A. bursae*	16	1.38	0.085	1.27	1.50	1.06	0.063	0.97	1.17
	N. migratorius	4	1.31	0.050	1.25	1.37	1.01	0.028	0.97	1.03
	C. cricetus	9	2.72	0.143	2.57	3.00	2.00	0.112	1.85	2.21
	M. newtoni	16	2.28	0.150	1.95	2.58	1.48	0.078	1.29	1.59

Remarks—In terms of the structure of the occlusal surface, the available molars are identical to those of *Allocricetus ehiki* from Poland [104]. However, the dimensions of M1 are slightly above the upper limit for the Polish materials. In this regard, it falls at the lower end of the variability range for *Mesocricetus newtoni* (Nehring, 1898). However, in this species, the protocone is strongly developed, prominently bulging lingually, and the anterior width of the tooth, across the two tubercles of the anterocone, is much smaller. The outline of the tooth in occlusal view is elongated and curved. In *A. ehiki*, the protocone is not strongly developed, and the anterior part is not as distinctly narrow.

Allocricetus bursae Schaub, 1930

(Figure 17A–D,G–J,M–X)

Studied material (number of molars)—Biozone B: L13/14: 5; L13—Lower: 36; L11c: 90; L13c: 380; L11b: 398; L11a1: 490; L11a: 649; L13a: 970; L12: 1010; L13b: 1433.

Description—m1. The posterolophid is always present, but it never terminates with a true posterostylid. The mesolophid is absent; the anterior cingulum is sometimes very poorly developed. The anterolophulid is most often well developed.

m2. The mesolophid is absent; it appears as a weak ridge on only one tooth.

m3. The mesolophid is usually absent.

M1. The posteroloph descending from the hypocone is well developed, reaches the metacone, and sometimes continues beyond it as a small spur.

M2. The lingual branch of the anterior cingulum is often absent or is sometimes represented as a weak ridge.

M3. The mesostyle is well developed.

Measurements—Table 14.

Remarks—Some authors have challenged the validity of the genus *Allocricetus* [106,107]. The described material, along with other data from Bulgaria [38] and Central Europe [105,108], demonstrates that there are well-established differences between the two commonly compared species, *A. bursae* and *N. migratorius*. In addition to size differences, which are clearly visible in our material, a notable simplification of the occlusal surface in the smaller forms has been observed [108]. This trend is also evident when comparing materials from the two biozones of Kozarnika (Figure 17). These features and their changes over time support the opinion that *Allocricetus* warrants its own genus.

Allocricetus appears in Central European deposits at the end of the Pliocene (Villány 3; Osztramos 3, Hungary) [108,109]. Later, *A. bursae* is found in Biharian deposits at Villány 8 and Brassö [104], and at the start of the Middle Pleistocene in France at Balaruc [84]. It co-occurs with *A. ehiki* at Monte la Mesa in Italy [57]. *A. bursae* is known in Spain up to the Upper Pleistocene [110], in Hungary at Lambrecht Cave [111], and extends farthest west at Caldeirão Cave, Portugal [112]. Cuenca-Bescós [113] studied speciation in small hamsters during the Pleistocene, revealing three lineages: *A. bursae*, *Cricetulus*, and *A. correzensis* (initially a subspecies of *A. bursae* [84]). Its widespread presence in mid-Middle Pleistocene Western Europe indicates that it could be a characteristic taxon of that period. From the Early Pleistocene of the western Balkan Peninsula (crevice fill near Razvodje close to Knin, southern Croatia), the species *Allocricetus croaticus* Paunovic and Rabeder, 1996 has been described, distinguished by its larger size compared to *A. bursae* [114]. A comparison with the data in Figure 16 and Table 14 shows that the tooth measurements of this species' type series fall within the upper range of variability in our material.

Genus *Nothocricetulus* Lebedev, Bannikova, Neumann, Ushakova, Ivanova, Surov, 2018

Nothocricetulus migratorius (Pallas, 1773)

(Figure 17E,F,L)

Studied material (number of molars)—Biozone A: L10a: 2; L10b: 2; L9ab: 4; L6/7: 9; L5a: 12; L5c: 21; L3–4: 25; L5b: 81.

Description—m1. The general structure of the occlusal surface is similar to that in *A. bursae*. However, the simplified structure features a weakly expressed or absent anterolophulid. The posterolophid is most often well developed. There is no mesolophid.

m2–m3. The mesolophid on m2 is usually absent, but it is relatively well developed on m3.

M1. The posteroloph rarely reaches the facial wall of the tooth.

Measurements—Table 14.

Remarks—Apart from the sizes, the simplified structure of the teeth, especially the first lower molar (Figure 17), corresponds with what is known about the evolution of this species [108]. The available material is very similar to the modern comparative material from Bulgaria.

Genus *Cricetus* Leske, 1779

Cricetus cricetus (Linnaeus, 1758)

(Figure 18A,B,F,H,J–L)

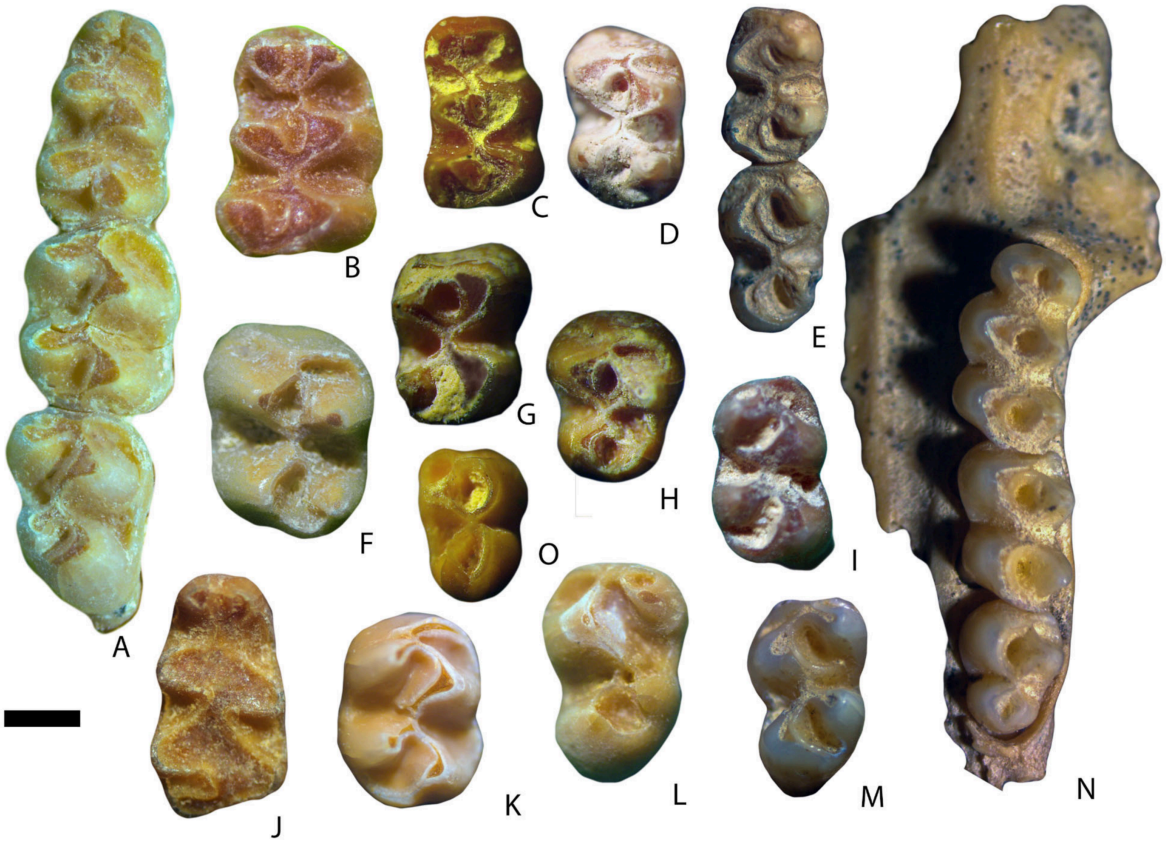


Figure 18. *Cricetus cricetus* (**A**,**B**,**F**,**H**,**J**–**L**), *Mesocricetus newtoni* (**C**,**D**,**E**,**G**,**I**,**M**,**N**,**O**). Molars in occlusal view. (**A**)—right m1-m3, BG-IBER-FMC-000017768, L11b: (**B**)—right M1, BG-IBER-FMC-000017766, L11b: (**C**)—right M1, BG-IBER-FMC-000004070, L11a: (**D**)—left M2, BG-IBER-FMC-000004738, L11a: (**E**)—left m2-m3, BG-IBER-FMC-000012042, L3–4: (**F**)—left M2, BG-IBER-FMC-000017767, L11b: (**G**)—right M2, BG-IBER-FMC-000004738, L11a: (**H**)—left M3, BG-IBER-FMC-000004738, L11a: (**I**)—right m2, BG-IBER-FMC-000016559, L12: (**J**)—right m1, BG-IBER-FMC-000015986, L11b: (**K**)—right m2, BG-IBER-FMC-000016286, L12: (**L**)—left m3, BG-IBER-FMC-000018431, L13a: (**M**)—left m3, BG-IBER-FMC-000012961, L5a: (**N**)—left M1-M3, BG-IBER-FMC-000013176, L5b, (**O**)—right M3, BG-IBER-FMC-000004070. Scale bar = 1 mm.

Studied material (number of molars)—Biozone B. L13—Lower: 1; L5b: 3; L13c: 21; L13b: 107; L13a: 96; L12: 116; L11c: 29; L11b: 89; L11a1: 96; L11a: 96; L9ab: 2; L9c: 2.

Measurements—Table 14.

Description—M1. The labial spur of the anterolophule and the mesoloph are weak. An anterior ridge is present on some teeth.

M2. The labial anteroloph and the posteroloph are well developed, while the lingual anterior cingulum is weak. The mesoloph is short.

M3. Only the labial branch of anterolophus is developed. Between pairs of the main tubercles, there are closed enamel atolls.

m1. Simplified. The anterolophid is low. No mesolophid. The posterolophid is well developed.

m2. The labial branch of the anterolophid is well developed, while the lingual branch is only faintly marked. The posterolophid is well developed. On only one unworn tooth is a trace of the mesolophid visible.

m3. The posterolophid is relatively short, and the posterosinusid is sometimes open lingually.

Remarks—Regarding the size of m1 (Table 14), the hamster from Kozarnika falls within the variability of modern European species [65]. The average sizes of M1, M2, and

m1 are at the lower end of the variability range for *Cricetus praeglacialis* Shaub, 1930 from Villány [115].

Genus *Mesocricetus* Nehring, 1898

Mesocricetus newtoni (Nehring, 1898)

(Figure 18C–E,G,I,M,N,O)

Studied material (number of molars)—Biozone B: L13a: 2; L12: 2; L11b: 13; L11a1: 28; L11a: 33. Biozone A: L10b: 20; L10a: 115; L9c: 32; L9ab: 194; L6/7: 49; L5b: 332; L5c: 44; L5a: 40; L3–4: 46.

Description—The teeth, especially m1 and M1, are elongated. Upper molars have a well-defined posteroloph. The primary tubercles are positioned opposite each other. The spurs of the anterolophule and entoloph are well developed, and there are enamel marks between the pairs of main tubercles. On M2, the labial anteroloph is well developed, while the lingual anterior cingulum is very poor. Lower molars show a consistently well-pronounced mesolophid. The primary tubercles are arranged sequentially, and no marks are left during abrasion.

Measurements—Table 14.

Remarks—In terms of its quantitative and qualitative characteristics, the available material is uniform and very similar to the comparative material of recent *Mesocricetus newtoni* from Bulgaria. The small number of remains from layers 13a–11a indicates the earliest appearance of this species. Until now, the earliest finds of this species were known from the Holsteinian interglacial (Middle-Riss Interglacial, MIS 11) in the lower layers of the Morovitsa cave [43], Casian Cave in Romania [97], and the Middle Pleistocene of Yarimburgaz Cave in Turkish Thrace [116].

Subfamily Arvicolinae (Gray, 1821)

Tribe Arvicolini Gray, 1821

Subtribe Arvicolina

Genus *Arvicola* Lacépède, 1799

Arvicola amphibius (Linnaeus, 1758)

Studied material—Biozone A. L10b: 1 m1; L10a: 1 M3; L9c: 1M3; L5b: 2 M3; L5a: 1 m1, 1 M3; L3–4: 1 m1.

Description—Large size. Abundant cement in the reentrant angles. The enamel is weakly differentiated, with slight thinning at the tips of the reentrant folds.

m1. The triangles of the anteroconid complex are broadly fused with each other and with the anterior cap, which is wide, rounded, and slightly asymmetrical.

M3. The dentine fields of AL, T2, and T3 are well separated from each other. T4 is connected to the posterior field to varying degrees depending on the depth of LRA3. LSA4 is weakly developed and rounded.

Measurements—Table 15.

Table 15. Measurements [mm] of molars of *Arvicola amphibius* from Kozarnika.

Molar	N	L			W			a		
		M	Min	Max	M	Min	Max	M	Min	Max
m1	2	3.68	3.32	4.03	1.54	1.45	1.7	1.47	1.3	1.63
M3	5	2.55	2.45	2.75	1.3	1.24	1.34	-	-	-

Remarks—The genus *Arvicola* originated in the early Middle Pleistocene (Toringian) and developed through anagenesis from the mimomyid lineage [85,117]. Primitive forms from the Toringian are associated with *A. mosbachensis* (Schmidtgen, 1911), which has negative enamel differentiation, whereas modern *A. amphibius* shows positive enamel

differentiation. Recent research [118] indicates that the type of enamel differentiation is more closely related to intraspecific differences than to a clear chronological trend. The available molars have poorly differentiated enamel, as the teeth probably belong to young individuals. In their characteristics, they are similar to materials from other Late Pleistocene sites in Bulgaria [38,83].

Subtribe Microtina

The predominant part of the material from Kozarnika consists of vole teeth without roots and with cement at the reentrance angles, belonging to the subtribe Microtina. Given the significant variability in the shape of the species-diagnostic anteroconid complex (ACC) of m1, definitive identification of each tooth can be problematic, even for Late Pleistocene material (Biozone A), which consists of modern species. Often, features characteristic of a given species can occur at low frequency in other species. For example, morphotypes characteristic of *Chionomys nivalis* (Martins, 1842) occur infrequently in populations of *Alexandromys oeconomus* Pallas, 1776; in many populations of *Stenocranius gregalis* Pallas, 1779, morphotypes characteristic of *Microtus* (s. str.) and *M. (Terricola*) were recorded [84,119]. Such difficulties are even more pronounced when identifying materials from the lower Early Pleistocene layers at Kozarnika (Biozone B), which are composed of extinct primitive vole species. At these early stages of radiation, the species were not yet sufficiently morphologically distinct, and there was broader overlap in the morphological features of the ACC among them than among modern ones. This is why, historically, during their studies—particularly in early stages when the typological approach in systematics was prevalent—individual morphotypes, often chosen subjectively, were described as separate species. However, this classification became controversial as more material was gathered, revealing significant morphological variability. A typical example of this concerns the voles from West Runton (Norfolk, Great Britain), a site of comparable age. Some of the species described from this locality, such as *Microtus arvalinus* Hinton, 1923, *M. nivalinus* Hinton, 1923, *M. nivaloides* Forsyth Major, 1902, and *M. ratticepoides* Hinton, 1923 [120,121], are difficult to distinguish from one another, and their taxonomic status is a subject of discussion [122]. Similar morphotypes also occur in the material from Biozone B of Kozarnika. During initial sorting, assigning some specimens to one species or another proved difficult. Due to the extensive material, a large subsample of 2212 m1 was examined using geometric analysis with Relative Warp Analysis (RWA). This was followed by unsupervised model-based clustering, aiming to produce a quantitative variability description and objective criteria for classifying all 19,883 m1 specimens. Relative warps are orthogonal axes (like those of Principal Component Analysis) that capture major patterns of shape change in the landmark data (Figure 19). In the present analysis, the first relative warp explains 35% of the non-affine variation, while the second (RW2) explains 15%. The first axis (RW1) represents the complexity of ACC. Higher positive values indicate a complicated ACC with well-developed T6, T7, and AC3, whereas negative values indicate a simpler ACC with only T4, T5, and AC2. This axis clearly reflects the main evolutionary trend in voles—an increase in ACC complexity through the formation of new triangles in front of T4 and T5. The second axis (RW2) captures a morphological gradient related to the degree of isolation of the dentine fields. On the right side of the graph, it compares the degree of fusion between T5 and T4, whereas on the left side, it shows differences in the width of the connection between T5 and AC2. Negative scores denote specimens with highly isolated dentine fields, indicating a more advanced evolutionary stage, whereas positive scores indicate primitive forms with less isolated dentine fields.

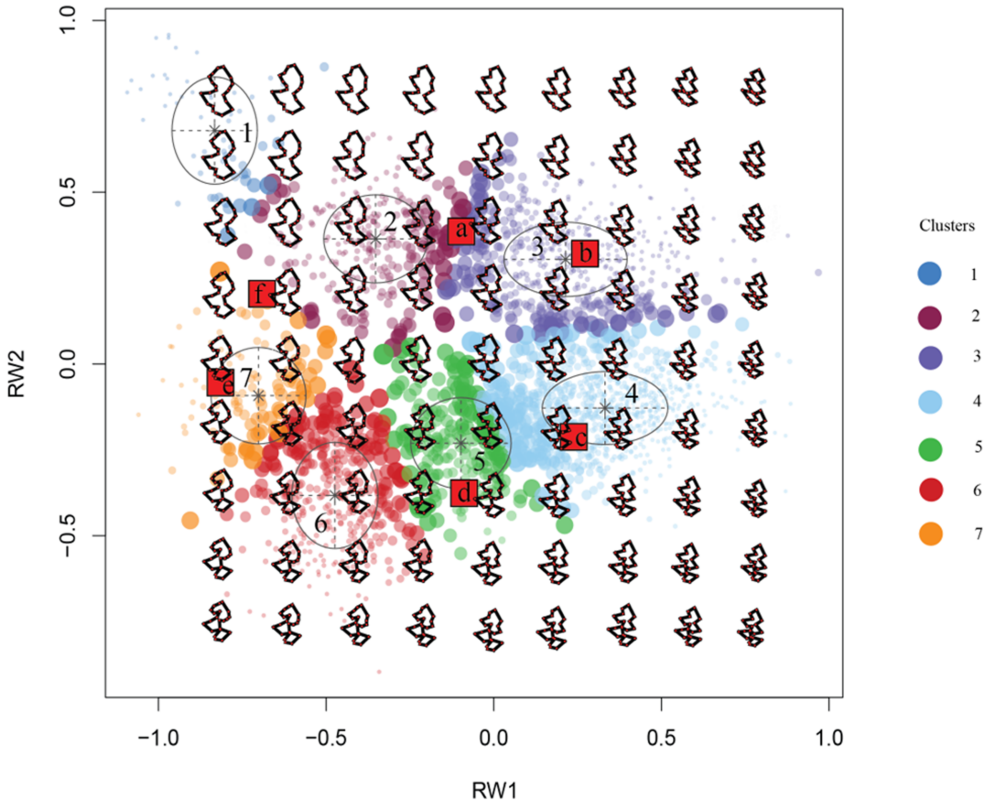


Figure 19. Position of 2212 m1 of Microtina from Kozarnika in the morphological space formed by the first two Relative Warps (RW1, RW2). Colors, point symbols, and 95% confidence ellipses, their centroids (asterisks) and axes (dashed lines) represent the results of model-based clustering. The size of the points is proportional to uncertainty. Red squares represent the type specimens of *M. gregaloides*—a, *P. arvaloides* (=*M. arvalidens*)—b, *M. arvalinus*—c, *M. nivaloides*—d, *M. nivalinus*—e, and a specimen of *M. ratticepoides*—f from West Runton (UK) [117,121].

To assess the relationship between features derived from geometric analysis (RW1 and RW2) and those from the conventional linear measurements and indices derived from them, correlations between the two groups of features were calculated (Table 16).

Table 16. Correlations of the first two Relative Warps (RW1, RW2) with linear measurements and indices of m1.

Character	L	a	W	c	b	a/L	c/W
RW1	0.13	0.55	−0.16	−0.16	−0.84	0.79	−0.12
RW2	−0.48	−0.42	−0.58	0.89	−0.29	−0.17	0.89

As expected, the linear measurements characterizing the overall size of the tooth (L, W, a) are weakly correlated with RW1 and RW2. This reflects a key feature of geometric analysis: it characterizes shape regardless of size. Based on these correlations, RW1 clearly reflects the complexity of the anteroconid complex, as expressed by its relative elongation (a/L) [21]. The correlations between linear measurements and indices derived from them, with RW2, confirm that this axis reflects the degree of isolation of the dentine fields of T4 and T5, traditionally represented by the index c/W [21]. The strong correlation of this axis with the linear measurement (c) is due to the fact that, within the studied morphological group, overall size, as represented by W, has little variability—all forms have similar overall sizes.

The variability within the morphological space (Figure 19), defined by the first two Relative Warps (RW1 and RW2), was analyzed using model-based clustering. It is expected that this unsupervised classification technique will identify morphological groups corresponding to real biological species. Thus, this approach turns qualitative shape impressions into a quantifiable, visual morphological space that makes species boundaries and intraspecific variation explicit and statistically testable. The fact that material from Biozone A consists of recent species may help assess the feasibility of using this approach to identify real species. This is especially important in interpreting clusters defined in the material of the lower layers (Biozone B), which consists of extinct morphologically similar forms with controversial taxonomic status and poorly defined morphological boundaries. To facilitate the taxonomic interpretation of the obtained clusters, the type specimens of the species described from West Runton were included in RWA [*P. arvaloides* (=*M. arvalidens*), *M. arvalinus*, *M. nivaloides*, *M. nivalinus*, *M. gregaloides*]. The coordinates of the landmarks were taken from the figures in [121], the original descriptions [120], or a later publication by the same author [117]. Since no illustration of the type specimen of *M. ratticepoides* is provided, the digitization was based on Figure 65/29 on p. 128 of [117].

The clustering algorithm selected a diagonal, equal-volume, varying-shape (EVI) model as the best. It reveals 7 clusters (Figure 19). As expected, many specimens have uncertain assignments to one cluster or another. To further interpret the clusters in terms of their taxonomic affiliations, they were analyzed in a stratigraphic context—separately for each biozone (A, B) (Figure 20). To assist with the taxonomic interpretation of the obtained clusters, alongside the traditional linear measurements and indices presented above, the enamel differentiation index based on T1–T3—SDQ3 [29] has also been calculated.

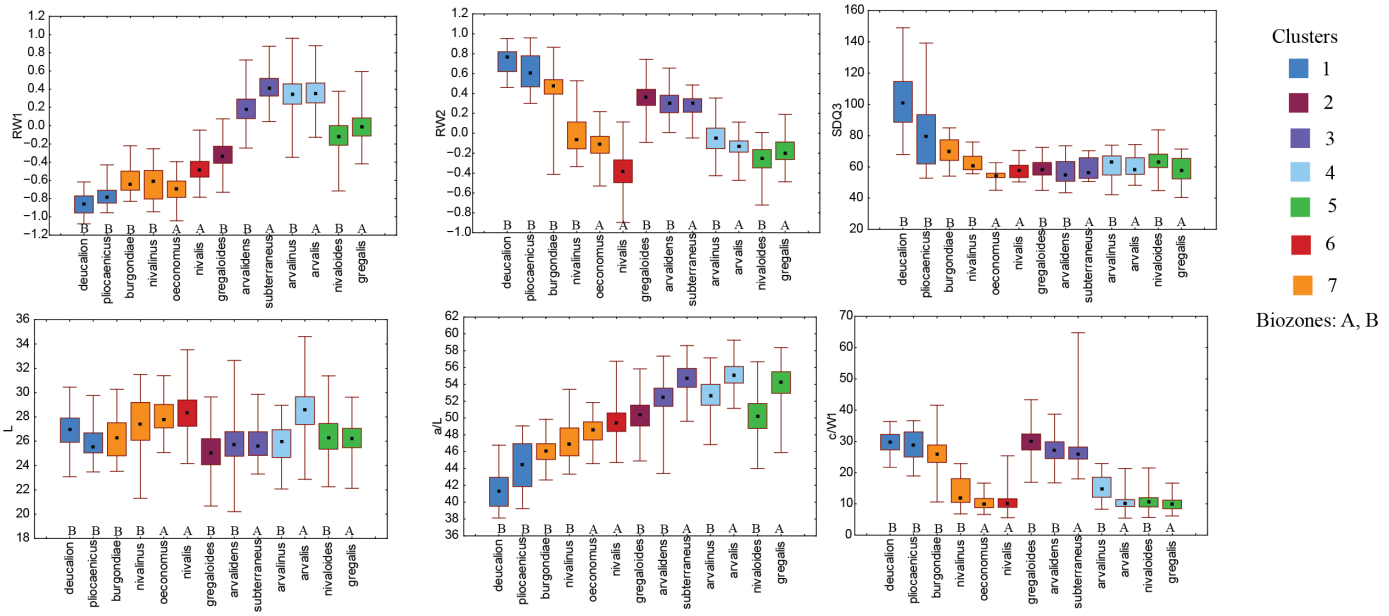


Figure 20. Box and whiskers plots showing the differences between the two biozones (A, B) within the clusters (1–7) obtained from model-based clustering and their species identification concerning the first two Relative Warps (RW1, RW2), the enamel differentiation index (SDQ3), total length of m1 (L), relative length of the anteroconid complex (a/L), and the index of confluence between T5 and T5 (c/W1). The black squares represent medians, the boxes—the 25–75% interval, and the whiskers—the limits of variability.

Cluster 1 is well-defined (low uncertainty for most specimens assigned to this cluster; Figure 19). It comprises specimens from Biozone B only and represents a primitive arvicolid [21] morphotype with a weakly differentiated anteroconid complex (ACC), as

indicated by extreme negative and positive values along the RW1 and RW2 axes, respectively, and by low and high a/L and c/W values, respectively (Figure 20). The enamel is poorly differentiated (Figure 20), and SDQ3 has significantly higher values than in the other clusters ($p < 0.05$). Overall size is moderate (Figure 20). Based on these characteristics, specimens confidently assigned to this cluster were referred to the most primitive species in the subtribe, *Allophaiomys deucalion*.

Cluster 2 is well-defined (Figure 19), including specimens from Biozone B that belong to hintonid and gregalid morphotypes [21]. ACC exhibits greater complexity compared to cluster 1, characterized by a narrow connection between AC2 and the widely fused T4 and T5. AC2 is complicated by a well-defined LSA5. The ACC outline is similar to that of the gregaloid forms known from the end of the Early Pleistocene, such as *M. hintoni*, *M. thenii*, and *M. gregaloides*. These are considered stages in an evolutionary sequence, with the first species the most primitive, characterized by a shortened anterior unpaired field. Conversely, *M. gregaloides* is at a higher evolutionary level, with an elongated anterior field and a well-developed LSA5, often followed by an LRA5. This is evident from the position of the holotype of *M. gregaloides* within the morphological space defined by RW1 and RW2 (Figure 19). Based on these peculiarities, the specimens assigned to cluster 2 were attributed to *Microtus gregaloides*. Given its simple ACC, this species is referred to as *Allophaiomys* in the remainder of the text.

Cluster 3 is clearly distinct from cluster 2, despite the presence of a relatively large number of uncertain specimens. This cluster represents an arvalid morphotype [21] with a complex ACC—presence of T5, T6, and AC3—but with widely fused posterior triangles (T4 and T5) (Figures 19 and 20). There are well-defined differences between the two biozones within this cluster, with Biozone A's form showing significantly higher RW1 and a/L values (Figure 20). Since the form from Biozone A undoubtedly belongs to *M. subterraneus*, the one from Biozone B, being more primitive, was referred to *M. arvaloides*, based on the position of the West Runton holotype. Later, the name *Microtus arvalidens* was adopted for this form [123].

Cluster 4 is well-defined, although many specimens are assigned to it with considerable uncertainty, showing similarities to clusters 3 and 5 (Figure 19). Cluster 4 comprises arvalid morphotypes with the highest degree of complexity, as shown by both RW1 and RW2. Across all features compared (Figure 20), there is a statistically significant difference between biozones A and B, especially with respect to overall size (L) and indices a/L and c/W (Figure 20). Based on the index values, the form from Biozone A is more advanced, with a relatively longer ACC and well-separated T4 and T5 (Figure 20). It is also larger. These differences are consistent with the time intervals represented by the two biozones and support treating them as two species in an evolutionary sequence. The form from the Late Pleistocene (Biozone A) can certainly be attributed to *Microtus arvalis* in a broad sense. Based on the position of the holotype of *Microtus arvalinus* in the morphological space defined by RW1 and RW2 (Figure 19), and on its geological age, the form from Biozone B is attributed to *Microtus arvalinus*.

Cluster 5 consists entirely of specimens with uncertain classification, exhibiting transitional features between clusters 4 and 6. It includes forms of the gregalid and arvalid [21] morphotypes. Predominate specimens with well-isolated dentine fields, especially T4 and T5, but with a weakly differentiated anterior part, with poorly defined T6 and T7, and an underdeveloped AC3. Comparisons between biozones show significant differences in a/L, with the form from Biozone B having a relatively shorter ACC (Figure 20). This cluster was considered to comprise two species at a similar evolutionary level in terms of ACC complexity, as indicated by RW1 and RW2. The form from Biozone B is more primitive, as evidenced by the relative length of the ACC (a/L). The form from Biozone A undoubtedly

belongs to *Stenocranius gregalis*—many specimens have an asymmetrical anterior field, due to a well-developed LSA5 and a missing or weakly developed BSA4. Because of variability in the degree of development of BSA4, some specimens of *S. gregalis* cannot be reliably distinguished from those of the *Microtus arvalis* group, as noted above. The more primitive form represented by cluster 5B, although indistinguishable from 5A in terms of RW1 and RW2 values, is not identical to 5A. Since the holotype of *Microtus nivaloides* falls within this cluster, the material from Biozone B was attributed to this species. Some argue that the type specimens of *Microtus arvalinus* and *M. nivaloides* fall within the morphological variability of a single species, with *M. nivaloides* having formal priority [122]. The current analysis shows that this is not the case.

Cluster 6 comprises specimens from Biozone A (Figure 19), belonging to the nivalid morphotype [21] and exhibiting a high degree of differentiation, with a narrow link between the simplified anterior complex—where AC3 is almost absent—and the posterior triangles (T4 and T5), which are well separated. Numerous transitional specimens exist between this cluster and cluster 7. Based on these features, the specimens belonging to this cluster from Biozone A were identified as *Chionomys nivalis*. The few specimens from Biozone B are linked to cluster 6 with high uncertainty. They occupy an intermediate position between clusters 5 and 6. Additionally, there is a statistically significant difference between the two biozones across all features. In particular, the form from Biozone B is distinctly smaller and, in this respect, aligns with cluster 5B, which corresponds to *M. nivaloides*. Considering these peculiarities and the relatively high uncertainty, specimens from cluster 6 from Biozone B were regarded as extreme variants of *M. nivaloides*.

Cluster 7 features a simplified ACC, with well-isolated T4 and T5, but AC2 and T5 are widely fused, and the fourth buccal salient angle (BSA4) is lacking. Based on the shape of the anteroconid complex, this cluster can be identified as ratticepid [21]. Between the two biozones, statistically significant differences were observed in a/L and SDQ3, with the form in Biozone B being more primitive. Considering the relatively high uncertainty in assigning this cluster by the clustering algorithm, especially given the small sample from Biozone B, these peculiarities suggest it may comprise two closely related species. The specimens from Biozone A can certainly be attributed to *A. oeconomus*. The small sample from Biozone B can be identified as a more primitive species on the evolutionary lineage leading to modern species. In some specimens referred to this group, there is a narrow connection between T4 and T5, a feature that was not observed in specimens from Biozone A. In one specimen (BG-IBER-FMC-000022291), the anterior field is somewhat similar to that of *Chionomys nivalis*, but it is relatively widely connected to T5, similar to that of *Microtus malei*. This morphotype is often classified as a separate species belonging to *Chionomys*, or even as a distinct genus, *Suranomys*, or as a "variant" of *A. oeconomus* [122,124]. Based on its position in the morphological space, the second opinion was accepted. The holotypes of two species described from West Runton, *M. nivalinus* and *M. ratticepoides*, fall within the morphological space occupied by cluster 7 (Figure 19). This confirms the prevailing view that these two names should be treated as synonyms, with the name *M. nivalinus* having formal priority [122]. Based on this, the material from cluster 7B was identified as belonging to *M. nivalinus*.

Special attention is warranted for a small group of specimens that fall into the morphological space between clusters 1, 2, 5, and 7. These are conditionally considered within two species, based on both the shape of the ACC and additional features such as enamel differentiation and overall size. The specimens, similar in ACC outline to *Allophaiomys deucalion* and uncertainly assigned to cluster 1, were tentatively regarded as belonging to *Allophaiomys pliocaenicus*. The differences from specimens confidently assigned to cluster 1 involve smaller sizes, enamel differentiation, which is definitively of a positive type [25],

unlike that in specimens assigned to cluster 1 with greater certainty, which is neutral or negative, and a more complex structure of the anterior part of the anterocone complex, expressed by an elongation of the anterior field (AC2) and a tendency to form a weak LSA5, highlighted by a more pronounced LRA4. The other group of specimens is characterized by a better-differentiated anterior field (AC2), featuring a well-developed LSA5, often with a well-developed BSA4, and a tendency to narrow the connection to the broadly fused main triangles T4 and T5. The extreme variants resemble *Chionomys nivalis*, but with the T4 and T5 broadly fused. These specimens were tentatively assigned to *Allophaiomys burgondiae*. These two groups were not identified by the clustering algorithm due to the small number of specimens.

In conclusion, by using geometric analysis and unsupervised model-based clustering of 2212 m1s belonging to subtribe Microtina, the following species were identified: *Allophaiomys deucalion*, *A.* cf. *pliocaenicus*, *A.* cf. *burgondiae*, *A. gregaloides*, *Alexandromys nivalinus*, *A. oeconomus*, *Chionomys nivalis*, *Microtus arvalidens*, *M. subterraneus*, *M. arvalinus*, *M. arvalis*, *M. nivaloides*, and *Stenocranius gregalis*.

Genus *Allophaiomys* Kormos, 1930

Allophaiomys deucalion Kretzoi, 1969

(Figure 21)

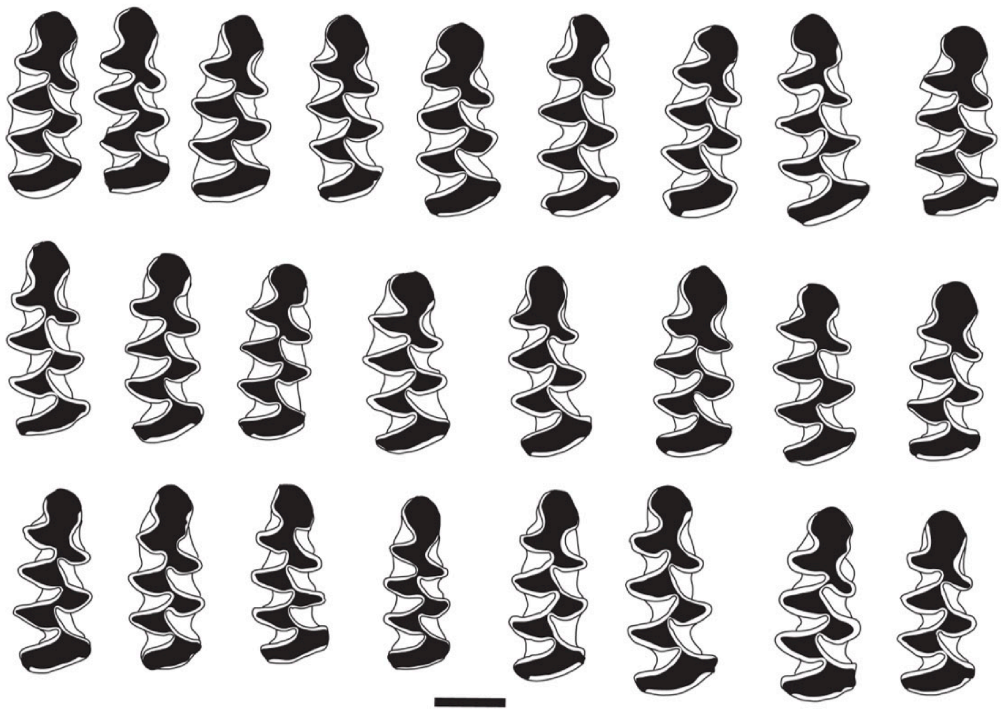


Figure 21. *Allophaiomys deucalion*. Kozarnika, Biozone B. m1s in occlusal view; all figured as right specimens. Scale bar = 1 mm.

Studied material (m1)—Biozone B: L13—Lower: 6; L13c: 16; L13b: 23; L13a: 15; L12: 4; L11b: 3; L11a1: 7.

Description—The parts of the anteroconid complex are widely fused. The anterior cap (AC2) is short and rounded. The enamel differentiation is variable. In some specimens, it is negative, while in others, it is weakly positive. The enamel at the tips of the reentrant angles is thinner.

Measurements—Table 17.

Table 17. Measurements [mm × 10] and indices [%] of m1 of *Allophaiomys deucalion* (N = 36).

Characters	X	SD	Min	Max
L	26.79	1.4918	23.09	30.45
SDQ3	103.3	19.780	67.88	149.0
a/L	41.43	2.275	38.12	46.77
c/W	29.71	3.358	21.74	36.34

Remarks—This species was described from Villány 5 (Hungary), based on a single specimen [125] (p. 181), as larger and with a simpler anterior cap of m1 than in *A. pliocaenicus*, and simpler than that of *A. ruffoi* (Pasa, 1947). The available material corresponds to this description, except that the size is rather moderate. However, the length of the type specimen [21] is slightly above the maximum recorded here (Table 17), yet larger than that of Kozarnika referred to *A.* cf. *pliocaenicus*, consistent with the original diagnosis. The study of a larger sample from the type locality [126] indicates that *A. deucalion* differs from *A. pliocaenicus* by its type of enamel differentiation. This difference is also clearly visible in the material from Kozarnika (Figure 20; Tables 17 and 18). Comparisons with the material from *A. deucalion* from Kamyk and Zabia Cave show that these populations differ from the Kozarnika material in having slightly larger sizes and higher a/L values [127]. *Microtus (Allophaiomys) valerotensis*, described from Valerots (France), shows variability encompassing morphotypes here attributed to *A. deucalion* and *A. pliocaenicus*, but it is much smaller, and the a/L = 48.41 values are higher (note that "a" values were calculated rather than measured directly [128]). Additionally, the enamel is clearly and strongly positively differentiated [128]. Two m1s from Deutsch-Altenburg 10, attributed to *A. deucalion*, are of medium size [22] as in Kozarnika. *Tibericola sakaryaensis* Ünay, Emre, Erkal, and Keçer, 2001, described from the late Early Biharian locality Degirmendere (Anatolia), is similar to the material from Kozarnika in terms of the shape of the occlusal surface, the relative length of the ACC, and the degree of enamel differentiation, but it differs in larger sizes and a well-defined tendency of narrowing the T4 and T5 connection [129].

Table 18. Measurements [mm × 10] and indices [%] of m1 of *Allophaiomys* cf. *pliocaenicus* (N = 14) from Kozarnika.

	X	SD	Min	Max
L	25.88	1.573	23.48	29.76
SDQ3	81.7	23.924	52.80	139.2
a/L	44.64	2.896	39.25	49.07
c/W	28.43	5.942	18.93	36.65

Allophaiomys deucalion and *A. pliocaenicus* can formally be differentiated on the basis of average a/L values—*A. deucalion*—A/L ≤ 42.0; *A. pliocaenicus*—A/L = 42.0–44.5 [22,130]. In this respect, the form from Kozarnika fits well in the range of *A. deucalion*.

Allophaiomys cf. *pliocaenicus* (Kormos, 1933)

(Figure 22)

Studied material (m1)—Biozone B: L13-Lower: 4; L13c: 1; L13b: 16; L13a: 14; L12: 11; L11c: 5; L11b: 1; L11a1: 4; L11a: 1.

Description—The parts of the anteroconid complex are broadly fused. In most cases, the anterior field (AC2) is elongated and asymmetrical, with a more or less pronounced LSA5; in some specimens, it is rounded and poorly protruded, while in others, it is well developed but not followed by even a shallow LRA5. In most cases, the buccal side is

rounded and lacks BSA4, except for one specimen (Figure 22). The enamel bands are poorly positively differentiated.

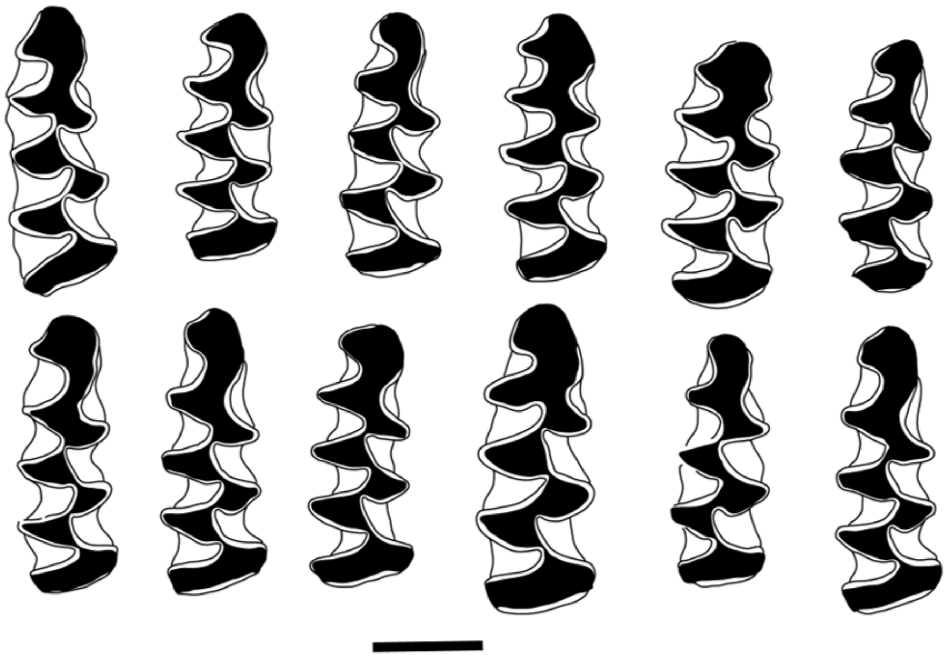


Figure 22. *Allophaiomys* cf. *pliocaenicus*. Kozarnika, Biozone B. m1s in occlusal view; all figured as right specimens. Scale bar = 1 mm.

Measurements—Table 18.

Remarks—The species is described from Betfia 2 (Romania). In size and proportions, the m1s from Kozarnika correspond to the specimens from the type locality [127], differing only in slightly smaller sizes and slightly larger average values of a/L and c/W. The forms from several localities in Russia (Shamin, Karaj Dubina, Port Katon, Zapadnye Kairy) have similar average a/L values in the range 43.65–45.33 [131]. These sites fall within the Brunhes–Jaramillo interval. However, it should be noted that these values are based on small samples and represent a broader interpretation of the species' variability than that accepted here and include morphotypes considered here to belong to *A. burgondiae*, which, as shown below, has a higher mean a/L (see Table 19). Probably the latest occurrence of *A. pliocaenicus* is reported from Nagornoye 1 section (Moldova, Kagul liman, the 7th terrace of the Danube River) [132]. The indices a/L and c/W are nearly identical to those of the material from Kozarnika.

Table 19. Measurements [mm × 10] and indices [%] of m1 of *Allophaiomys* cf. *burgondiae* (N = 24) from Kozarnika.

Characters	X	SD	Min	Max
L	26.35	1.782	23.52	30.27
SDQ3	70.4	8.749	54.11	85.0
a/L	46.10	1.809	42.64	49.85
c/W	26.84	6.257	10.64	41.61

The stratigraphic ranges of *A. deucalion* and *A. pliocaenicus* are poorly known. A possible coexistence is assumed to have occurred immediately after the Olduvai polarity reversal, during the interval between 1.8 and 1.7 million years ago [8]. The co-occurrence of both species was documented in the Early Biharian Romanian locality Betfia IX [133]. The

situation at Kozarnika can be interpreted as evidence that *A. deucalion* and *A. pliocaenicus* are representatives of parallel phylogenetic lineages that, in some parts of Southeast Europe, coexisted rather than replaced one another over time. The fact that, in Kozarnika, a more progressive *A. pliocaenicus* also occurs, but in combination with its much more abundant "descendants", such as *Alexandromys nivalinus*, *Allophaiomys gregaloides*, *Microtus arvalidens*, and *M. nivaloides*, contradicts the widely accepted model of gradual evolution in the *Allophaiomys–Microtus* (s.l.) lineages. Most likely, it is not about anagenetic evolution but about the parallel existence of phyletic lineages that probably arose through allopatric speciation. Different lines have varying chronological ranges in different geographic regions. Over large areas of the Holarctic, the more primitive ones quickly disappear, probably due to global cooling and competition from their more advanced relatives, which are better adapted to the new conditions. However, in some places, primitive forms persist for longer, as in Kozarnika. A situation similar to that in Kozarnika has been recorded on the Iberian Peninsula, in the slightly earlier deposits of the Trinchera Dolina section (layers TD3–TD6a) in Sierra de Atapuerca (Burgos, Spain), where a form of a similar evolutionary level, *Allophaiomys chalinei* Alcalde, Agusti, Villalta, 1981 (=*Victoriamys chalinei* in Martin, 2012), is found together with *Stenocranius gregaloides* and *Microtus (Terricola) arvalidens* [134,135]. Even today, there are species with dental structures very similar to those of *Allophaiomys*. They have limited, relic-like ranges in the southern parts of the overall Microtini range, and their evolution is slower [136]. Furthermore, the co-occurrence of *A. pliocaenicus* together with representatives of more advanced descendants in Kozarnika supports the view that *Allophaiomys* should be considered a separate genus [83,84], rather than a subgenus of *Microtus* [10,21,83,84].

Allophaiomys cf. *burgondiae* (Chaline, 1972)
(Figure 23)

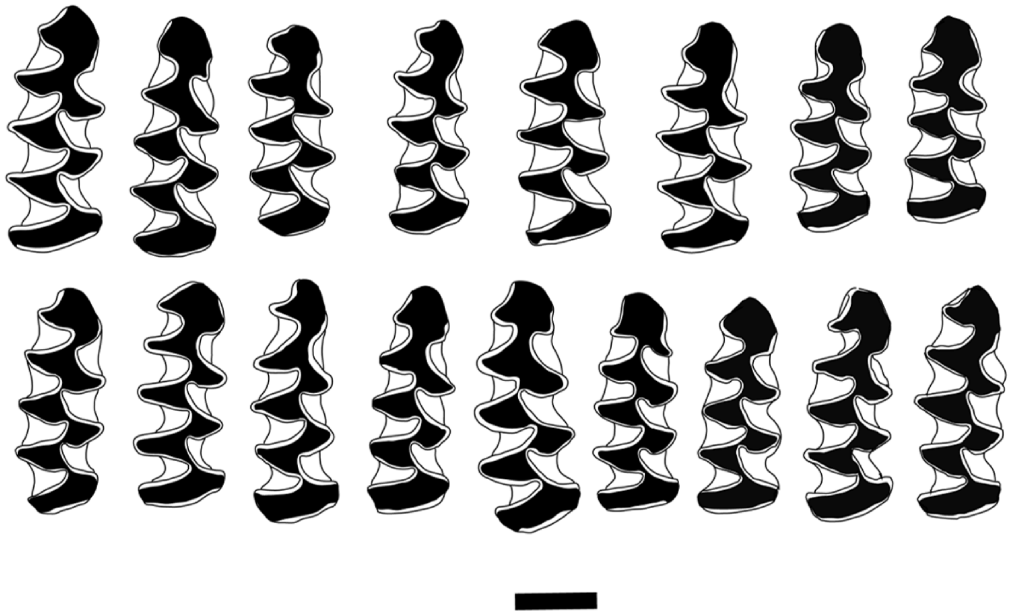


Figure 23. *Allophaiomys* cf. *burgondiae*. Kozarnika, Biozone B. m1s in occlusal view; all figured as right specimens. Scale bar = 1 mm.

Studied material (m1)—Biozone B: L13-Lower: 1; L13b: 1; L13a-3; L12–9; L11a1: 3.

Description—The material tentatively referred to this species is characterized by widely fused T4 and T5. The connection of the T4–T5 complex with the anterior part of the ACC varies, ranging from wide to very narrow. The anterior field (AC2) always has a well-developed LSA5, resulting in asymmetry. BSA4 may be absent; in such cases, if the

connection with T5 is wide, it resembles ratticepid morphotypes, differing by the more broadly connected T4 and T5. In some cases, BSA4 is well developed, and AC2 takes on a more or less symmetrical shape. In these cases, when the connection between the anterior field and the T4–T5 complex is narrow, they resemble nivalid morphotypes but differ in having a wide T4–T5 connection. The enamel is weakly positively differentiated.

Measurements—Table 19.

Remarks—In terms of ACC shape, the described material is similar to *Allophaiomys* sp. B from Monte Peglia 2–8 [21,137], and *Microtus (Allophaiomys) burgondiae* from Valerots [128], but it differs from them in being slightly smaller. The variability of the material from the lower layers of Kozarnika attributed to this species is great, comprising simpler morphotypes, similar to *M. (A.) pliocaenicus*, as well as more complicated nivalis-like ones, and corresponds with the views on its possible evolutionary connection with *Chionomys* [21,84,124].

The type specimen of *Microtus eoratticeps* Paunovic and Rabeder, 1996, described from Tatinja Draga in South Croatia and illustrated in Figure 6 of the original publication [114], falls within the variability of *Allophaiomys burgondiae* from Valerots, e.g., Figure 5A in [128] and Kozarnika. From the description of the material from Tatinja Draga, it can be concluded that the entire material corresponds to the variability of *Allophaiomys burgondiae* from the type locality.

Microtus (Allophaiomys) burgondiae is reported in Europe, from Spain, France, Italy, Croatia (as *M. eoratticeps*), Bulgaria [83], and Romania [132]. Its presence in the Atapuerca sequences (Spain) marks early Biharian faunas before the Jaramillo Subchron [135,138].

Allophaiomys gregaloides (Hinton, 1923)

(Figure 24)

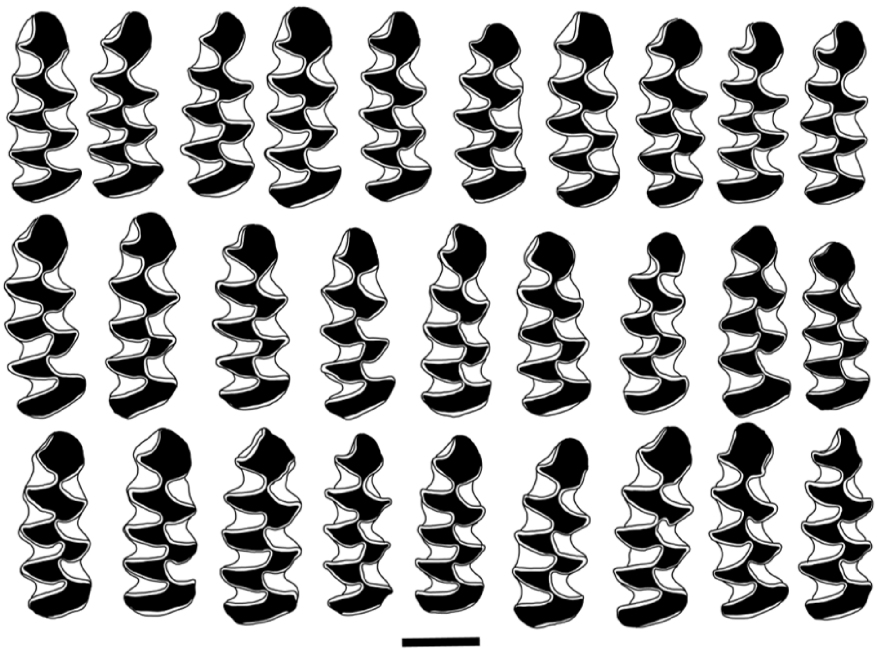


Figure 24. *Allophaiomys gregaloides*. Kozarnika, Biozone B. The m1s in occlusal view; all figured as right specimens. Scale bar = 1 mm.

Studied material (m1)—Biozone B. L13—Lower: 13; L13c: 86; L13b: 416; L13a: 432; L13/14: 2; L12: 526; L11c: 84; L11b: 117; L11a1: 164; L11a: 204.

Description—The dentine fields of T4 and T5 are extensively fused and separated from the anterior part of the anteroconid complex, which is asymmetrical and has a well-developed LSA5. LRA5 is developed to varying degrees—from almost absent, in which

case AC2 is shortened (morphotype "*hintoni*"[22]), to well-developed and elongated AC2, morphotype "*gregaloides*" [22].

Measurements—Table 20.

Table 20. Measurements [mm × 10] and indices [%] of m1 of *Allophaiomys gregaloides* from Kozarnika.

Character	X	N	SD	Min	Max
L	25.13	254	1.483	20.66	29.65
SDQ3	58.5	58	6.126	44.95	72.6
a/L	50.30	254	1.919	44.90	55.83
c/W	29.84	254	4.066	16.93	43.35

Remarks—In terms of the ACC shape, this form can be characterized as gregalid [21]. This generalized morphotype includes various forms with conflicting taxonomic status, most of which are treated as species or subspecies. From Western, Central, and Southern Europe, the following species/subspecies are most frequently mentioned: *Pitymys hintoni* Kretzoi, 1941; *Microtus (Allophaiomys) pliocaenicus nutiensis* Chaline, 1972; *Microtus thenii* Malez and Rabeder, 1984; and *Pitymys gregaloides* Hinton, 1923. Within this group, a well-defined trend of elongation of the anteroconid complex over time is observed [139]. According to the a/L values, the form from Kozarnika corresponds to *Microtus gregaloides* from the Hungarian sites Villány 8/III-VII and Nagyharsanyhegy 4 [21]. These sites belong to the Templohegyian substage of Hungarian biostratigraphy and, with respect to faunal composition, are similar to Biozone B, but *Mimomys pusillus/blanci* does not occur there [111]. In the type locality of *Pitymys gregaloides*, West Runton, where *Mimomys savini* is also found, the value of the a/L index is higher—almost 52 [65]. The average a/L value from Kozarnika is similar to that from Atapuerca layers TD5-TD3 (Spain) [140] and Hohensülzen (Germany) [65,141], which range from 49 to 51. These sites are within the time interval between the Brunhes and Jaramillo [139]. Comparisons with *Microtus thenii* from Podumci 1 (Croatia) [63] and Untermassfeld (Germany) [67] indicate that they have lower a/L values, suggesting they are at an earlier evolutionary stage within the *hintoni–gregaloides* lineage. Untermassfeld falls within the Jaramillo Subchron [139].

It should be noted that the a/L values for the Biozone B form presented in this study are higher than those reported in the previous publication [4]. This is because geometric analysis and subsequent clustering have placed some specimens of the morphotype *hintoni* in "nearby" clusters. The high variability among voles in this group introduces subjectivity in assigning individual specimens to one species or another, which, in turn, affects the values of biometric indices widely used for biostratigraphic correlations. In this sense, comparisons of a/L with data from the literature can be regarded only as approximate with respect to the exact biostratigraphic allocation of a particular locality.

Genus *Alexandromys* Ognev, 1914

Alexandromys nivalinus (Hinton, 1923)

(Figure 25)

Studied material (m1)—Biozone B: L13c: 1; L13a: 6; L12: 5; L11b: 11; L11a: 1; L11a1: 1.

Description—A typical ratticepid [21] morphotype of the anteroconid complex predominates, in which the dentine fields of T4 and T5 are well separated, and T5 is broadly associated with the anterior lobe, which most often has a well-developed LSA5. Variability affects the degree of fusion of T4 and T5—they can be fused to varying degrees—and the development of BSA4—in some cases it is well developed, sometimes accentuated by shallow BRA4.

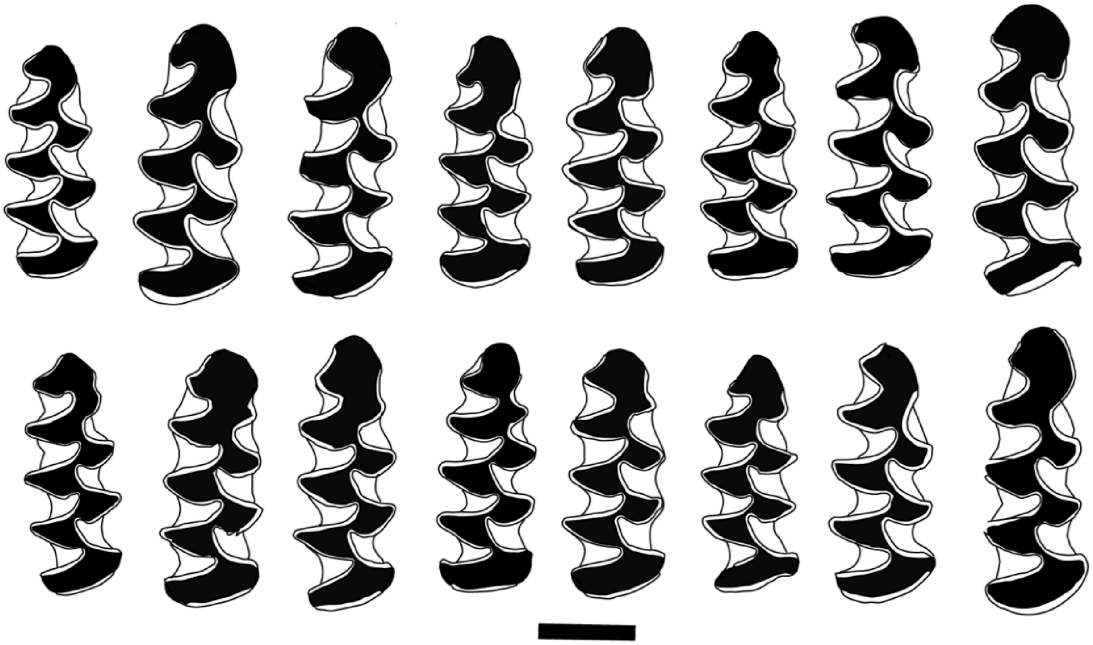


Figure 25. *Alexandromys nivalinus*. Kozarnika, Biozone B. m1s in occlusal view; all figured as right specimens. Scale bar = 1 mm.

Measurements—Table 21.

Table 21. Measurements [mm × 10] and indices [%] of m1 of *Alexandromys nivalinus* from Kozarnika.

Character	X	N	SD	Min	Max
L	27.46	20	2.4500	21.30	31.48
SDQ3	63.5	17	6.432	55.66	75.9
a/L	47.26	20	2.465	43.33	53.40
c/W	13.60	20	4.748	6.80	22.85

Remarks—The morphological peculiarities of the material from Biozone B, referred to this species, and the comparison with *Alexandromys oeconomus* from Biozone A align with the diagnoses of *M. nivalinus* and *M. ratticepoides* [120]: "*M. nivalinus* sp. n. m1 agrees exactly in form and structure of the anterior loop of recent *M. nivalis*. Size smaller. *M. ratticepoides* sp. n., m1 resembling that of *M. ratticeps*, but with the fourth outer prism less reduced, the fifth inner prism more reduced, and the anterior loop shortened. Size smaller." The differences between *A. oeconomus* and *A. nivalinus* from Biozones A and B, respectively, are small but correspond to general trends in the evolution of this phylogenetic lineage—increasing size, an increase in the relative length of the anteroconid complex (a/L), and a narrowing of the connection between T4 and T5. Regarding the a/L index, the values for the Kozarnika sample are higher than those for *M. nivalinus* and *M. ratticepoides* from Voigtstedt, West Runton, and Přezletice, whereas the SDQ3 values are lower than those reported in Voigtstedt [29,65,141]. In this regard, the form from Kozarnika is more derived. The mentioned localities are associated with faunas from the Brunhes Chron that contain *M. savini* [139]. In Central Europe, the earliest records of *Microtus nivalinus* are from Holstein, a site that predates the end of the Jaramillo Subchron, where it is found alongside *Mimomys pusillus* and advanced *Allophaiomys*. The latest known occurrence is from Tarkő/unit 2–15. In Eastern Europe, the earliest form of this lineage, *Microtus protoeconomus*, has been identified at Karaj Dubina (A/L = 45), dating to the very end of the Matuyama Chron (MIS 20–21) within the Petropavlovkian assemblage. In Petropavlovka 2 (MIS 21–18), *Microtus protoeconomus* co-exists with *Prolagurus pannonicus* [8].

Alexandromys oeconomus Pallas, 1776
(Figure 26)

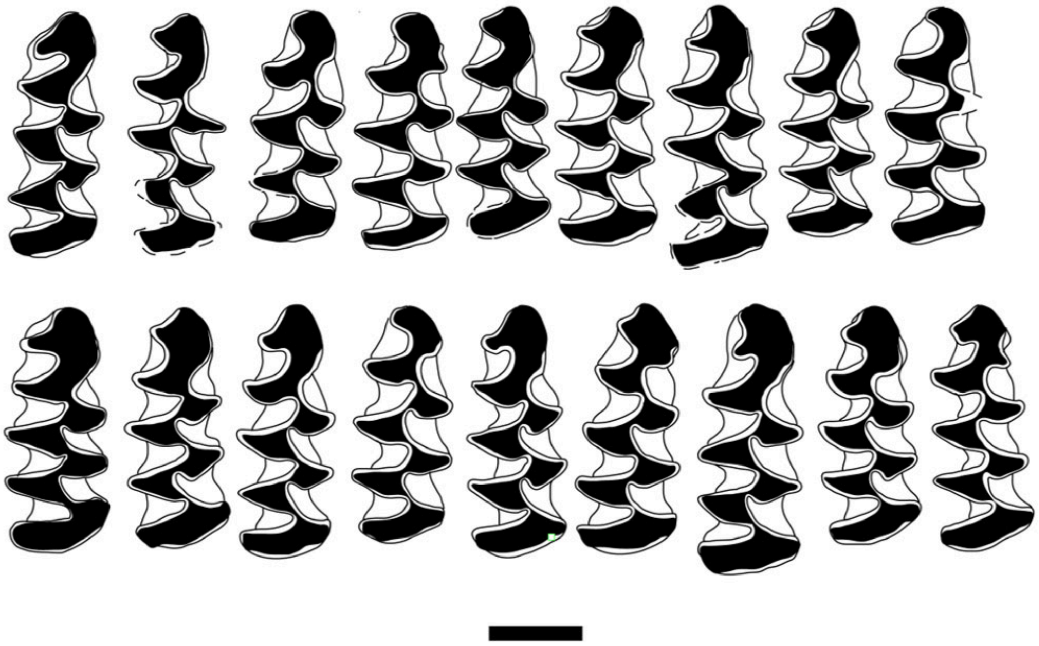


Figure 26. *Alexandromys oeconomus*. Kozarnika, Biozone A. m1s in occlusal view; all figured as right specimens. Scale bar = 1 mm.

Studied material (m1)—Biozone A: L10a: 3; L9c: 1; L9ab: 11; L5b: 15; L5a: 8; L3–4: 14.

Description—T4 and T5 are isolated, and the connection between T5 and the asymmetric AC2 is always wide.

Measurements—Table 22.

Table 22. Measurements [mm × 10] and indices [%] of m1 of *Alexandromys oeconomus* from Kozarnika.

Character	X	N	SD	Min	Max
L	28.02	78	1.336	25.08	31.39
SDQ3	54.8	15	4.441	45.18	62.8
a/L	48.45	78	1.479	44.59	51.83
c/W	10.31	78	2.200	6.61	16.67

Remarks. The first *Alexandromys oeconomus* was recorded in the Hungarian locality of Solymar of a Saalian age [8].

Genus *Chionomys* Miller, 1912

Chionomys nivalis (Martins, 1842)

(Figure 27)

Studied material (m1)—Biozone A: L10b: 21; L10a: 204; L9c: 13; L9ab: 32; L6/7: 38; L5c: 38; L5b: 240; L5a: 120; L3–4: 176.

Description—T4 and T5 are well separated, while T5 is separated from the front part of the anteroconid complex, which exhibits high variability. Usually, BSA4 and LSA5 are rounded and poorly defined due to the absence of BRA4 and LRA5. Less often, they are weakly expressed and shallow.

Measurements—Table 23.

Remarks—An apparent decrease in size toward the upper layers is observed (Figure 28). Since layers 3–4 correspond to the Last Glacial Maximum, this response likely

reflects unfavorable climatic conditions. *Chionomys nivalis* appears and evolves in Europe and Asia Minor at the beginning of the Middle Pleistocene [43,142].

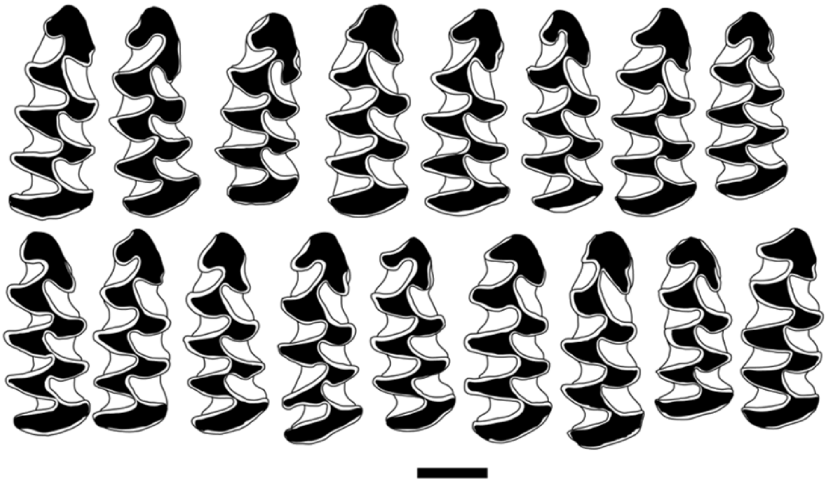


Figure 27. *Chionomys nivalis*. Kozarnika, Biozone A. m1; all figured as right specimens; occlusal view. Scale bar = 1 mm.

Table 23. Measurements (mm × 10) and indices (%) of m1 of *Chionomys nivalis* from Kozarnika.

Character	X	N	SD	Min	Max
L	28.41	298	1.6596	24.17	33.52
SDQ3	58.4	19	5.925	50.43	70.6
a/L	49.51	298	1.832	44.71	56.75
c/W	10.48	298	2.499	5.59	25.39

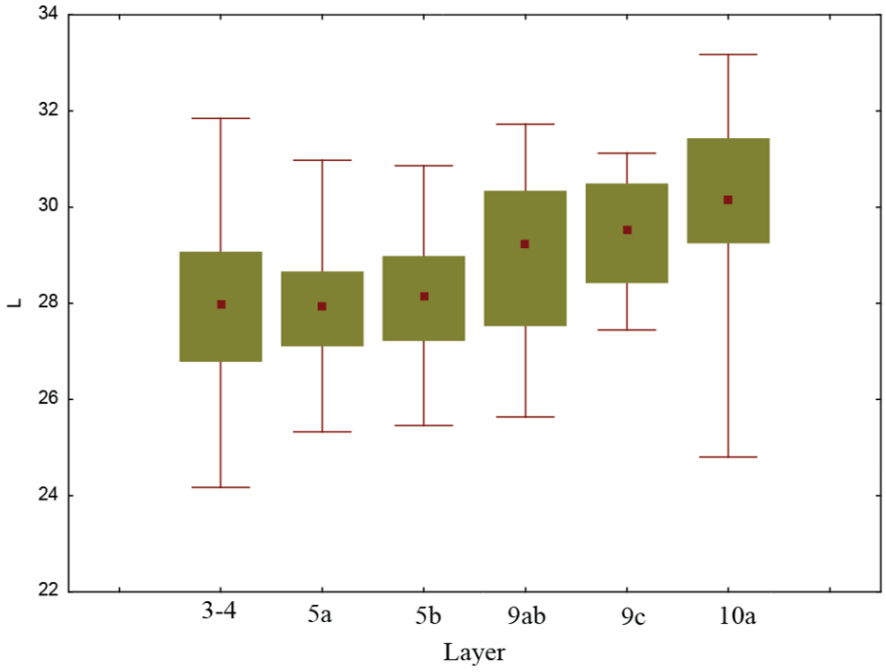


Figure 28. Box—and—whisker plots (median, 25–75%, Min–Max) showing the stratigraphic changes in the length (L [mm × 10]) of m1 of *Chionomys nivalis*.

Genus *Microtus* Schrank, 1798
Microtus arvalidens Kretzoi, 1958

(Figure 29)

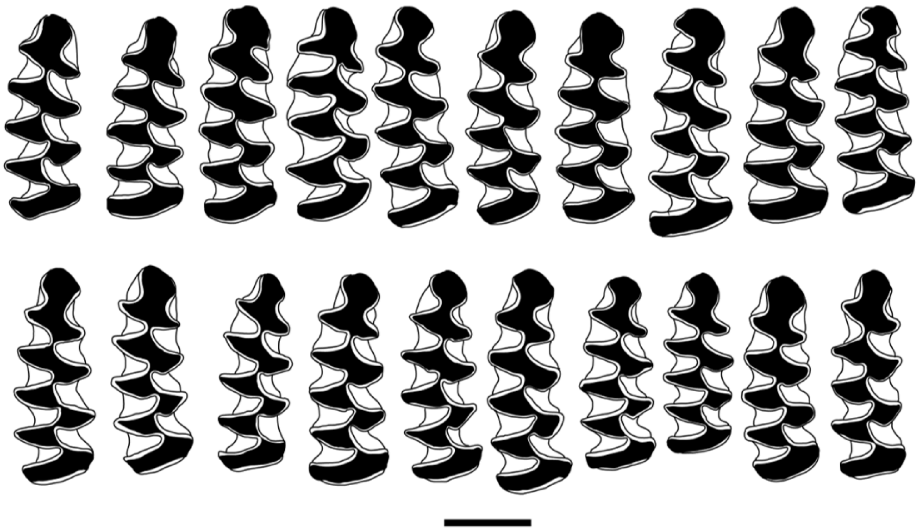


Figure 29. *Microtus arvalidens*. Kozarnika, Biozone B. m1s in occlusal view; all figured as right specimens. Scale bar = 1 mm.

Studied material (m1)—Biozone B. L13—Lower: 60; L13c: 368; L13b: 1541; L13a: 1311; L13/14: 1; L12: 2540; L11c: 500; L11b: 1115; L11a1: 1137; L11a: 927.

Description—T4 and T5 are widely connected and well separated from the front part of the anteroconid complex, whose parts are fused, forming a common dentine field—i.e., the 'neck' of the anterior cap (AC3) is always broad. AC3 is rounded and asymmetrical, similar to that of *M. arvalis*.

Measurements—Table 24.

Table 24. Measurements (in mm × 10) and indices (%) of m1 of *Microtus arvalidens* from Kozarnika.

	X	N	SD	Min	Max
L	25.76	420	1.5142	20.20	32.65
SDQ3	57.5	23	8.352	43.50	73.5
a/L	52.41	420	1.799	43.43	57.36
c/W	27.26	420	3.952	16.75	38.70

Remarks—Regarding the a/L index, the materials from Biozone B at Kozarnika fall within the variability range of materials from Brunhes Chron localities, including *Mimomys savini*—West Runton, Přezletice, and Rifreddo, and to Spanish localities Atapuerca TD4 and 5, but lower than in Atapuerca TD6 [26], localities belonging to the time interval between Brunhes and Jaramillo [139]. *Microtus arvalidens* appeared in Central Europe before the Matuyama/Brunhes boundary. In Villány 6, it coexists with *Mimomys pusillus*. Since *M. pusillus* disappears from Central Europe after the Jaramillo Subchron and before the 'Cromerian Interglacial II,' the first occurrence of *M. arvalidens* must be within this timeframe [8].

Microtus subterraneus (Sélys-Longchamps, 1836)

(Figure 30)

Studied material (m1)—Biozone A: L10a: 7; L9ab: 4; L6/7: 7; L5c: 5; L5b: 21; L5a: 11; L3–4: 19.

Description—The structure of m1 is similar to that of the previous species, but the neck of the anterior field is narrower.

Measurements—Table 25

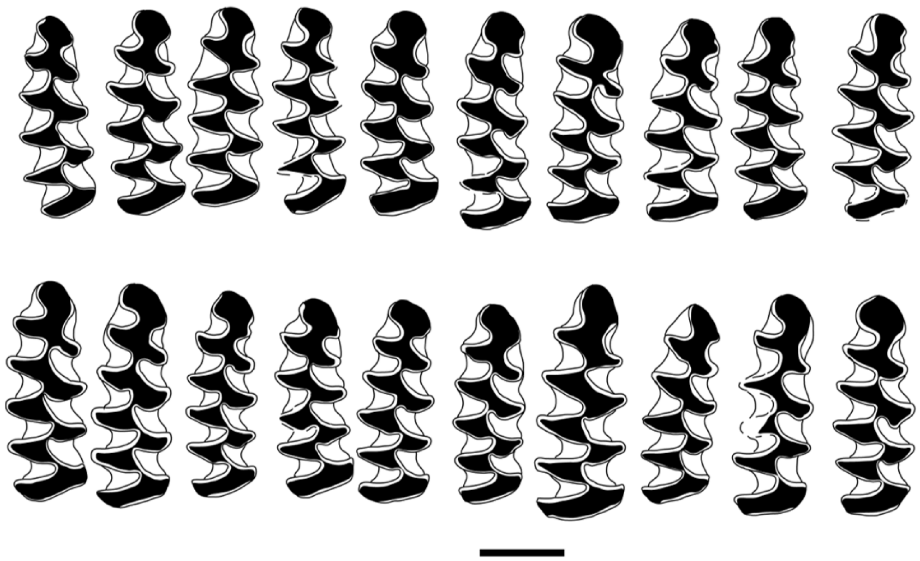


Figure 30. *Microtus subterraneus*. Kozarnika, Biozone A. m1s in occlusal view; all figured as right specimens. Scale bar = 1 mm.

Table 25. Measurements (in mm × 10) and indices (%) of m1 of *Microtus subterraneus* from Kozarnika.

Character	X	N	SD	Min	Max
L	25.85	50	1.4867	23.30	29.85
SDQ3	58.2	20	6.829	50.71	70.4
a/L	54.76	50	1.849	49.60	58.60
c/W	27.00	50	6.362	18.02	64.79

Remarks—The values of the a/L index are above 53 and are typical of modern populations of *Microtus subterraneus* [65]. The earliest *M. subterraneus* fossils are from Maastricht-Belvedere 4, dating to the Early Saalian [8].

Microtus ex gr. *arvalis* (Pallas, 1778)

(Figure 31)

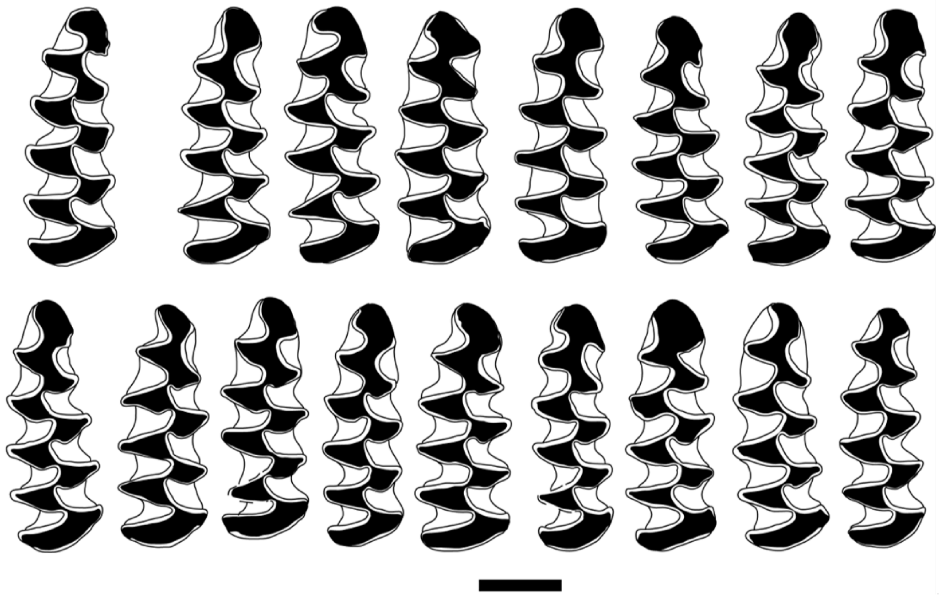


Figure 31. *Microtus ex gr. arvalis*. Kozarnika, Biozone A. m1s in occlusal view; all figured as right specimens. Scale bar = 1 mm.

Studied material (m1)—Biozone A. L10b: 75; L10a: 1019; L9c: 97; L9ab: 253; L6/7: 377; L5c: 484; L5b: 1038; L5a: 550; L3–4: 801.

Description—The m1 features a transversely elongated posterior loop, three closed triangles in the posterior complex, an anteroconid complex consisting of four more-or-less closed triangles, and a variable AC3. The dominant morphotype is characterized by a wide-necked, asymmetrical anterior cap and confluent, opposing T6 and T7.

Measurements—Table 26.

Table 26. Measurements (mm × 10) and indices (%) of m1 of *Microtus ex gr. arvalis* from Kozarnika.

Character	X	N	SD	Min	Max
L	28.57	646	1.636	22.87	34.60
SDQ3	59.9	17	7.570	48.28	74.3
a/L	55.13	646	1.375	51.15	59.26
c/W	10.36	646	1.850	5.47	21.33

Remarks—Two recent species, *Microtus arvalis* and *M. agrestis*, look similar and are difficult to distinguish, especially in fossils. Studies show that *M. agrestis* m1s are larger, and triangles T4/T5 and T6/T7 show more asymmetry than in *M. arvalis* [143]. Paleogenetic studies, however, indicate that size (m1 length) is not a reliable criterion. Recent paleo DNA analyses revealed that some populations of phyletic lineages within the superspecies *M. arvalis* are also large. The available material from Kozarnika, in terms of size, is more similar to the smaller form from Cave 16 [38], which, according to genetic data, belongs to *M. arvalis*, rather than to the large form from the same locality, which is genetically close to *Microtus ilaeus*. At the same time, a population from Ukraine, based on genetic data, belongs to the *ilaeus* group, which is small, similar to *M. arvalis* [144].

A reliable way to distinguish *Microtus agrestis* from *M. arvalis* is the presence of an extra posterior triangle on M2. This feature was not seen in a sample of 56 M2 specimens from layer 5b. Given this, along with the absence or faintness of asymmetry in the triangles of m1 and the relatively small size, it is likely that *Microtus agrestis* is not present in the sample, and all the specimens were classified as *Microtus* ex gr. *arvalis*.

The earliest *M. arvalis* is probably from 'Cromerian Interglacial III or IV' [8]. Given that the species is not found in Biozone B deposits, it can be argued that the upper chronological boundary of this biozone is below 600,000 years. Based on paleomagnetic data that record the Brunhes/Matuyama boundary in layer 13—Lower, and confirmed by the presence and evolutionary levels of other *Microtus* species, the deposits in Biozone B formed over an interval of approximately 200,000 years.

Microtus arvalinus Hinton, 1923

(Figure 32)

Studied material—Biozone B. L13c: 1; L13a: 17; L12: 13; L11a1: 1; L11b: 49; L11a: 6.

Description—The anteroconid complex is complicated, similar to that of modern *M. arvalis*. The dentine fields of T4 and T5 are most often well isolated from each other; less frequently, there is a narrow connection between them. T6, T7, and the anterior cap (AC3) are widely connected. AC3 is often asymmetrical, with a more developed LSA6.

Measurements—Table 27.

Remarks—Compared to *Microtus arvalis* from Biozone A, *M. arvalinus* from Biozone B is smaller. Lower a/L and higher c/W values indicate a more primitive form within the general evolutionary trends of Microtina.

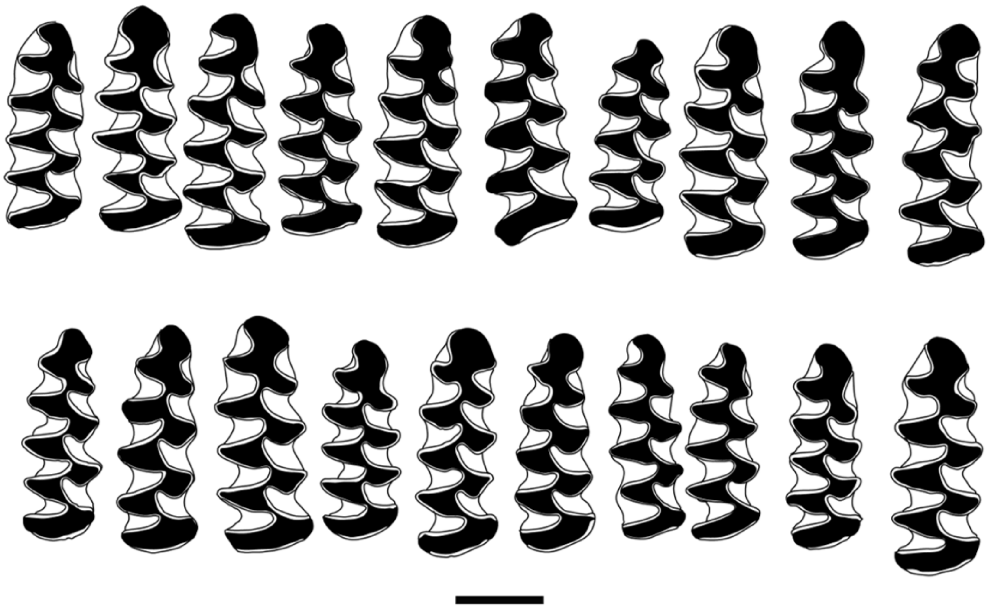


Figure 32. *Microtus arvalinus*. Kozarnika, Biozone B. m1s in occlusal view; all figured as right specimens. Scale bar = 1 mm.

Table 27. Measurements (mm × 10) and indices (%) of m1 of *Microtus arvalinus* from Kozarnika.

Character	X	N	SD	Min	Max
L	25.81	96	1.5242	22.08	28.96
SDQ3	61.2	34	8.345	42.21	73.9
a/L	52.62	96	1.963	46.84	57.14
c/W	15.22	96	3.843	8.32	22.93

The material classified under this species closely corresponds to Hinton's [120] diagnosis, "m1 in adults agreeing in form with that of *M. arvalis*; its size somewhat smaller. . .". The characteristics of the material assigned to this species align with Heller's [145] opinion that *Microtus arvalinus* is a smaller member of the *M. arvalis-agrestis* complex, with transitional forms toward the latter, and that *Microtus subarvalis* Heller, 1933, also belongs to this group; therefore, it is most accurate to refer to the complex as *M. arvalinus-subarvalis-arvalis-agrestis*. *M. arvalinus* is commonly interpreted as a primitive member of this group. The distinction between *Microtus arvalis* and its proposed 'ancestor', *M. arvalinus*, is not well defined. Lower A/L values are typical for *M. 'arvalinus'* (Hohensülzen: 48.1, Somssichhegy 2: 50.4, Voigtstedt: 50.9) compared to contemporary *M. arvalis* (Poland: 54; Germany: 54) [8]. Kozarnika's data support this trend, although the index values are slightly higher. This discrepancy likely arises because the cited values were based on mixed samples of *M. arvalinus* and *M. nivaloides* (see below).

Microtus nivaloides Forsyth Major, 1902

(Figure 33)

Studied material (m1)—Biozone B. L13—Lower: 9; L13c: 43; L13b: 227; L13a: 186; L12: 321; L11c: 112; L11b: 176; L11a1: 220; L11a: 276.

Description—The shape of the anteroconid complex varies greatly. Most commonly, the well-separated T4 and T5 are isolated from the anterior triangles (T6 and T7), which are fused, and from the usually shortened anterior field (AC2/AC3), which can sometimes be clearly asymmetrical. The degree of differentiation of T6 and T7 varies among these morphotypes. In some specimens, T7 is well distinguished, forming a well-developed LSA5, followed by a

deep LRA5, highlighting a well-defined AC3 with an asymmetrical shape (well-developed LSA6); T6 is less developed, with a very shallow BRA4. In other cases, BRA4 and LRA5 are shallow, and the anterior cap is not well distinguished—an AC2-state. Extreme variants show a clearly separated anterior part of the ACC, but T6 and T7 are poorly distinguished and fused with AC2, resembling *A. nivalinus*. However, in that species, T4 and T5 are broadly connected to the poorly differentiated anterior parts of the ACC.

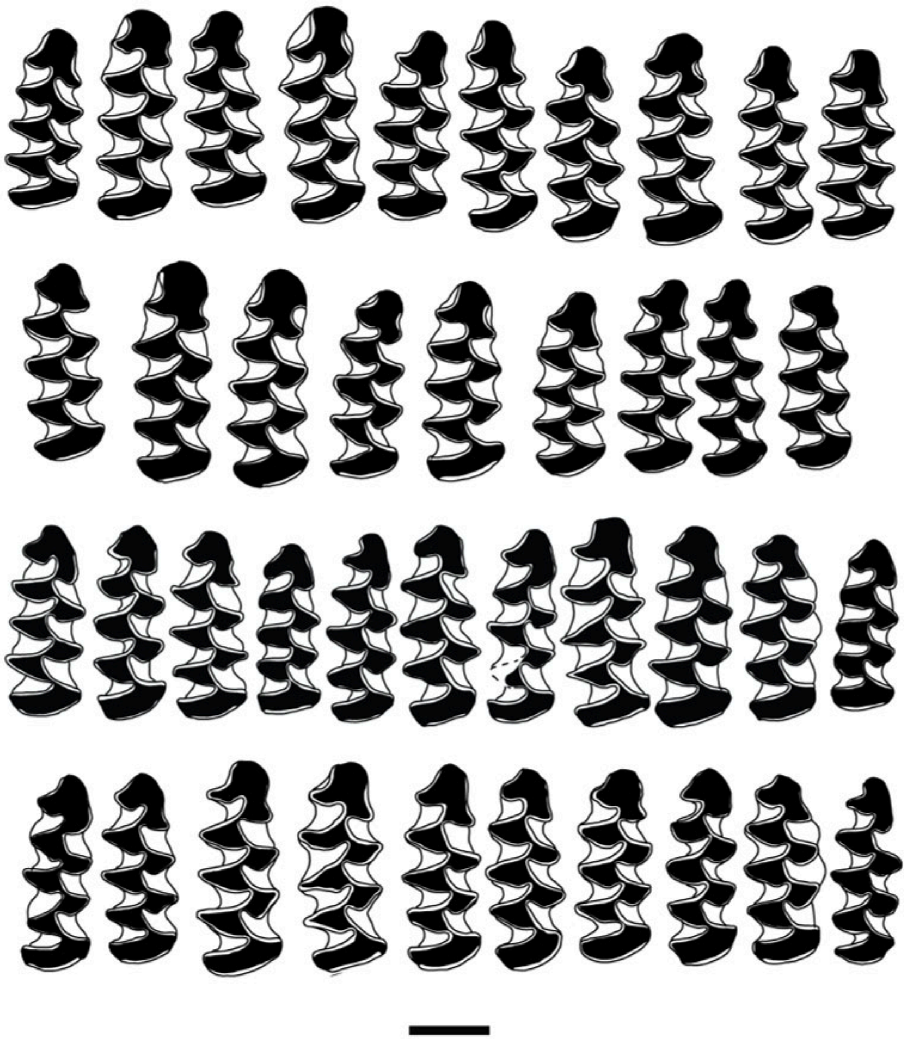


Figure 33. *Microtus nivaloides*. Kozarnika, Biozone B. m1s in occlusal view; all figured as right specimens. Scale bar = 1 mm.

Measurements—Table 28.

Table 28. Measurements (mm × 10) and indices (%) of m1 of *Microtus nivaloides* from Kozarnika.

	X	N	SD	Min	Max
L	26.37	154	1.5617	22.26	31.38
SDQ3	63.9	35	7.578	44.85	83.7
a/L	50.17	154	2.040	44.02	56.69
c/W	10.93	154	2.875	5.73	21.49

Remarks—The majority of specimens, classified under this species based on model-based clustering (Figure 19), align with Hinton's diagnosis: "m1 with the anterior loop

shortened, the fourth outer and fifth inner prisms somewhat reduced," and with the type specimen figured by Forsyth Major [121] (p. 106, Figure 19). There is an opinion that *Microtus arvalinus* should be considered a junior synonym of *M. nivaloides* because the holotypes of both species are considered extreme variants of a single highly variable species [21,127,133–135]. In particular, the view [122] that the type specimen of *M. nivaloides* Hinton, 1923, has the same morphology as *M. arvalinus* is not supported by the analyses presented above (Figures 19 and 20). Instead, the results correspond to Hinton's [120] original opinion. The presence of transient specimens is not a ground for synonymization. This is a common phenomenon and makes it difficult to distinguish between species, even those belonging to different genera, as shown by the results of the above analyses regarding *M. arvalis/S. gregalis* and *Ch. nivalis/A. oeconomus*. When comparing clustering results between the two biozones, it is evident that *M. arvalinus* and *M. nivaloides* are more clearly distinguished from each other than *M. arvalis* and *S. gregalis*. In this context, the differences between *M. arvalinus* and *M. nivaloides* from Kozarnika are so clearly manifested, despite the presence of transitional specimens, that they cannot be ignored, and both should be regarded as separate species. Moreover, according to Nadachowski's [124] observations, the material from West Runton is dominated by morphotype "*arvalis*" (56.1%), followed by "*nivalis*" (32.9%). In Kozarnika, the situation is reversed; apparently, the nivaloid morphotype prevails. These differences indicate that they are two species, probably with different environmental requirements. Due to the trend of merging *M. arvalinus* with *M. nivaloides*, comparisons with other sites in Europe are difficult. Taken together, the features of the material from Kozarnika correspond well to the morphological characteristics of the combined material from the type locality of both species—a small form (L = 2.62 mm) with relatively high values of the a/L index (on average, 50.5). Both species cluster separately from the *Chionomys* and *A. oeconomus* groups [124]. The analysis of material from Kozarnika supports the view that, with respect to the characteristics of the anteroconid complex, *M. nivaloides* is at a higher evolutionary level than the modern *Ch. nivalis* and is not its predecessor [22]. Its characters place it more closely within the *Microtus arvalis/agrestis* group [124,146].

In Central Europe, the oldest records of *Microtus 'arvalinus/nivaloides'* come from Villány 6, Sackdillingen, and Hohensülzen, where these forms occur alongside *Mimomys pusillus*. Because the latter species disappears from the region after the Jaramillo Subchron and before the 'Cromerian Interglacial II', the earliest occurrence of *M. 'arvalinus/nivaloides'* must also fall within this timeframe. The earliest likely record of *Microtus arvalis* may be from Hundsheim (A/L 53.0) and Miesenheim 1 [8]. However, the a/L values reported are identical to those reported by Kozarnika for *M. arvalinus* (Table 27), so these findings may represent a pure sample of *M. arvalinus* rather than *M. arvalis*.

Genus *Stenocranius* Kastschenko, 1901

Stenocranius gregalis Pallas, 1779

(Figure 34)

Studied material (m1)—Biozone A: L10a: 7; L9c: 1; L9ab: 3; L6/7: 3; L5c: 11; L5b: 32; L5a: 15; L3–4: 43.

Description—The posterior loop and the five triangles in front of it are well isolated from one another. The anterior part of the anteroconid complex is most often asymmetrical, with a well-developed LSA5 and a missing or weakly indicated BRA4. In the highly deviating variants, BSA4 is well expressed but remains weaker than LSA5, with asymmetry persisting.

Measurements—Table 29.

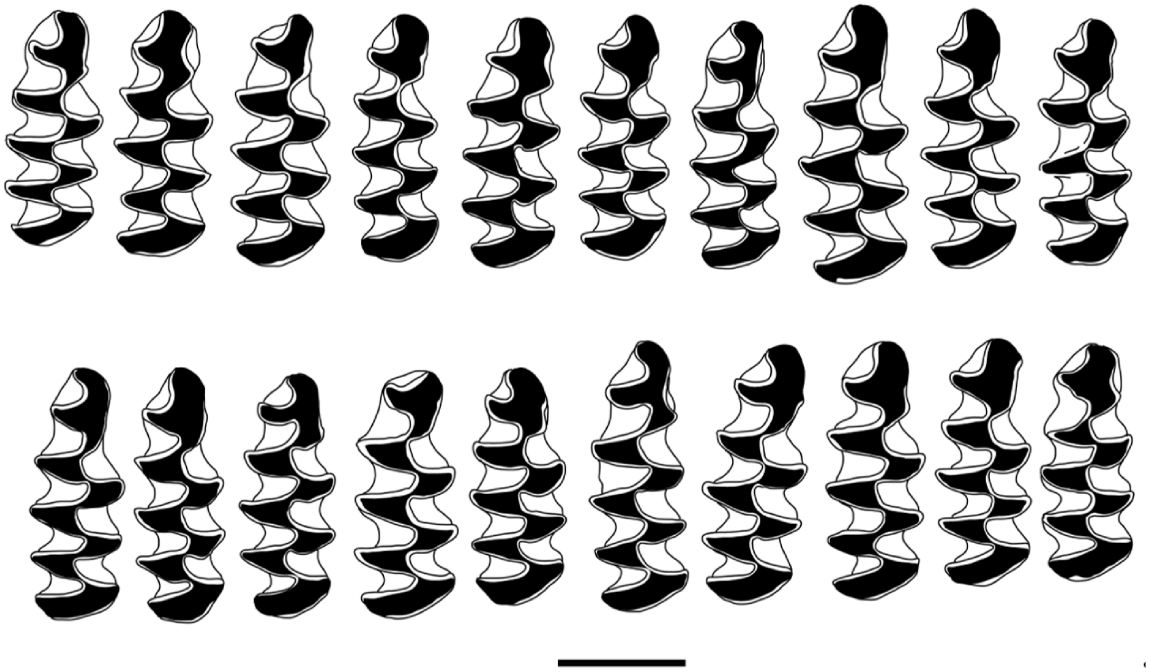


Figure 34. *Stenocranius gregalis*. Kozarnika, Biozone A. m1; all figured as right specimens; occlusal view. Scale bar = 1 mm.

Table 29. Measurements (mm × 10) and indices (%) of m1 of *Stenocranius gregalis* from Kozarnika.

Character	X	N	SD	Min	Max
L	26.29	122	1.251	22.13	29.62
SDQ3	57.5	21	8.286	40.39	71.5
a/L	54.01	122	2.137	45.90	58.35
c/W	10.01	122	1.989	6.17	16.67

Remarks—*Stenocranius gregalis* likely appeared in Europe during the Middle Pleistocene [97], probably in MIS 17, an equivalent of Cromerian Interglacial II [8], or in MIS 15, correlated with Muchkap Stage Interglacial, ca. 0.7–0.5 Mya [147]. The earliest Bulgarian records are from Morovitsa Cave [43].

The fossil record shows that during Pleistocene glacial periods, *S. gregalis* expanded its range across treeless, temperate landscapes, including much of Europe. However, modeling the species' distribution under the climate conditions of the last glacial maximum (LGM) reveals a lack of suitable habitat across much of Western and Central Europe, where the species is known to have existed during much of the Pleistocene [148]. Recent paleogenetic data indicate a significant divergence between Central European narrow-headed voles and Asian lineages, dating back at least 230,000 years. This challenges existing biogeographic ideas, suggesting that during interglacial periods, the narrow-headed vole did not retreat from Europe but persisted in refugial areas. Based on this, a cryptic species status was proposed for the Late Pleistocene European narrow-headed vole, named *S. anglicus*. Its distinctiveness also helps explain the controversial modeling results [149]. These data question the precise identification of the abundant material from Kozarnika, given that the uppermost layers 3–4, according to available calibrated radiocarbon dates, fall within the Last Glacial Maximum. Here, due to the lack of morphological differences in m1 between *S. anglicus* and *S. gregalis*, it is assigned to the latter species based on indirect evidence. The predictive model [148] indicates that Bulgaria borders the westernmost extent of the

LGM suitable habitat for *M. gregalis*, suggesting that its occurrence in Kozarnika is quite plausible. Considering its ecological requirements, this aligns with the presence of many eastern steppe species, including *Lagurus lagurus*, *Mesocricetus newtoni*, *Allactaga major*, *N. migratorius*, *Spermophilus citellus*, and *Nannospalax leucodon*.

Genus *Mimomys* Forsyth Major, 1902

In the Kozarnika material of this genus, two size groups clearly stand out (Table 30). The larger form can unquestionably be attributed to *Mimomys savini*. Differentiating species within the smaller-size group is somewhat challenging due to similarities in occlusal surface structure. Among this group, several teeth can be distinctly separated by the broad fusion of T2 and T3 and the well-developed *Mimomys* ridge, which matches the description of *Mimomys pitymyoides*. The remaining first lower molars show a simplified anteroconid complex and relatively well-differentiated main triangles (T1–T3). Species such as *Mimomys pusillus*, *M. blanci*, and *M. tornensis* possess these features. The first two species are slightly smaller, but there is substantial overlap in size among them and *M. tornensis*. The differences are much more noticeable in the outline of the occlusal surface of the third upper molar. *M. tornensis* has a deep LRA3 [22,150]. For *M. pusillus* and *M. blanci*, as well as for the primitive related forms such as *M. hintoni* and *M. reidi*, a simplified M3 occlusal surface, due to insulation-induced reduction of the inner part of LRA3, is characteristic. In more advanced forms, such as *M. blanci*, the enamel islet resulting from this reduction is a temporary feature visible only in unworn teeth; the posterior part of the occlusal surface is a single dentine field, with LRA3 barely marked. In the Kozarnika material, seven M3s exhibit a simplified structure, and two have a deep LRA3, confirming the presence of *M. pusillus/blanci* and *M. newtoni*.

Table 30. Measurements [mm] and m1 indices [%] of *Mimomys* species from Kozarnika.

Species	N	L		W		a/L	
		X	SD	X	SD	X	SD
M. pitymyoides	9	2.62	0.18	1.03	0.11	40.4	2.14
M. blanci	20	2.58	0.13	1.06	0.03	36.8	2.63
M. savini	21	2.87	0.162	1.36	0.09	37.1	0.97
M. tornensis	7	2.73	0.09	1.07	0.037	40.0	2.39

Mimomys blanci Van der Meulen, 1973

(Figure 35)

Studied material—Biozone B. L13—Lower: 1 m1; L13c: 20 m1; L13b: 1 M3; L13b: 42 m1; L13a: 3 M3, 40 m1; L12: 4 M3, 36 m1; L11c: 4 m1; L11b: 5 M3, 22 m1; L11a1: 29 m1; L11a: 3 M3, 18 m1.

Description—The teeth attributed to this species represent a medium-sized vole with high-crowned teeth and moderate crown cement and feature strongly negatively differentiated enamel.

m1. The *Mimomys* ridge is weakly expressed in occlusal view; the islet fold is only a faint depression; the prism fold is shallow but sometimes filled with crown cementum; there is no enamel island. The dentine fields of T1 and T2 are often connected. The enamel-free tracks are high, with the posterior, buccal, and lingual ones reaching the occlusal surface even in unworn teeth.

M3. AL1 is widely connected to T2; T3, the poorly pronounced T4, and PC1 are also widely connected, forming a single dentine field separated from the AL1-T2 complex. Anterosinus and protosinus are high, reaching the occlusal surface even on unworn teeth. The enamel islet is very rare, occurring only in a few unworn teeth.

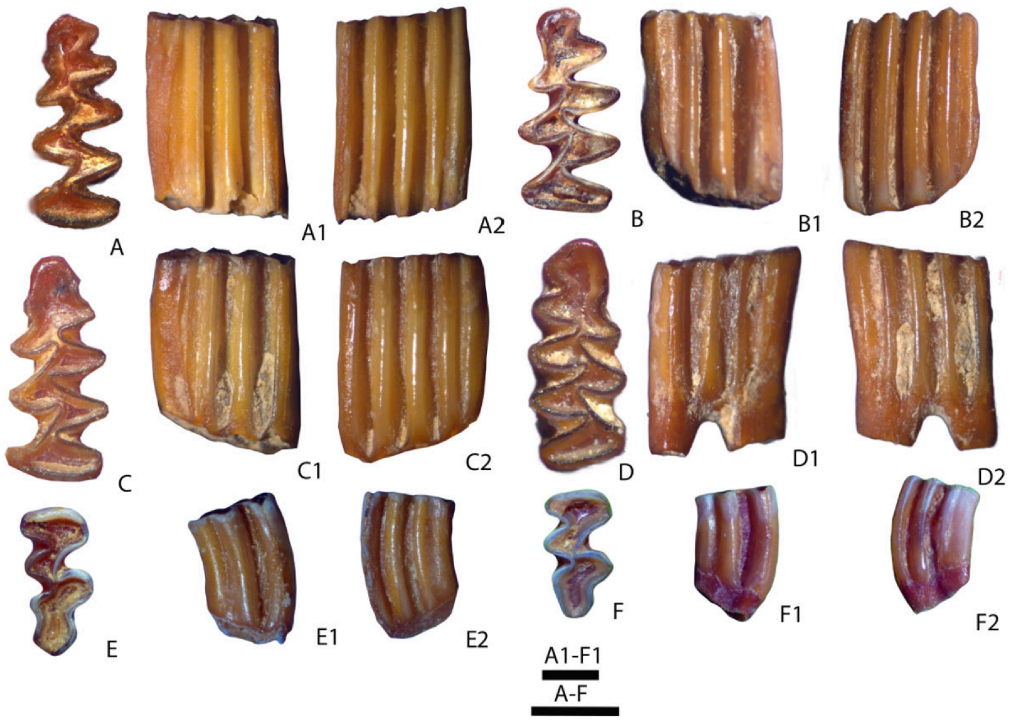


Figure 35. *Mimomys blanci*. (**A**)—left m1, BG-IBER-FMC-000006667, L13c; (**B**)—left m1, BG-IBER-FMC-000000636, L13b; (**C**)—left m1, BG-IBER-FMC-000006375, L13b; (**D**)—right m1, BG-IBER-FMC-000001322, L11a; (**E**)—right M3, BG-IBER-FMC-000018624, L13a; (**F**)—right M3, BG-IBER-FMC-000016672, L12 ((**A**–**F**)—occlusal, (**A1**–**F1**)—lingual, (**A2**–**F2**) buccal view). Scale bars = 1 mm.

Measurements—Table 30.

Remarks—The species was described from the lower levels of Monte Peglia (Italy) [21]. It closely resembles *Mimomys pusillus* and is regarded as a more advanced stage within the *M. reidi-pusillus* lineage [22]. Its taxonomic status remains debated. Some researchers have recognized it as a valid species, reporting it from France [151,152], England [153], and the Netherlands [154], and confirming it for Monte Peglia [137]. Tentative references include Spain [155] and Bulgaria [156]. Samples of varying ages (from late Early Biharian or latest Villányian to earliest Biharian) have been classified as *M. blanci*. The older fossils from England and the Netherlands previously assigned to *M. blanci* were later referred to another species, *Mimomys tigliensis* Tesakov, 1998 [157]. Kowalski [97], citing studies that group small-sized *Mimomys* populations from the latest Villányian as *M. blanci*, considers it a "primitive" form of *M. pusillus*. Other researchers regard *M. blanci* as a synonym of *M. pusillus* [8,29,158–160].

M. pusillus/blanci likely went extinct in Eastern Europe later than in Central Europe. In Eastern Europe, it persisted until the early part of the Ilinka Interglacial, corresponding to Marine Isotope Stages (MIS) 17–18. Sites in Western and Central Europe, like West Runton and Voigtstedt, probably corresponding to 'Cromerian Interglacial II' and MIS 17, do not contain *M. pusillus* [8].

Mimomys cf. *tornensis* Jánossy et van der Meulen, 1975

(Figure 36)

Studied material—*Biozone B.* L13—Lower: 1 m1; L13c: 1 m1; L13b: 5 m1; L13a: 1 M3, 1 m1; L12:1 M3, 3 m1; L11a1: 2 m1.

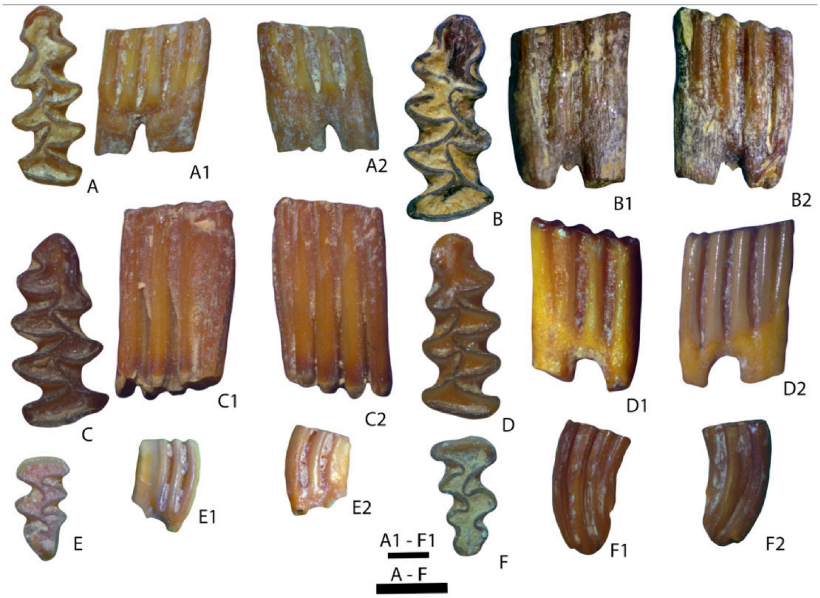


Figure 36. *Mimomys* cf. *tornensis*. (**A**)—left m1, BG-IBER-FMC-000003774, L13-Lower; (**B**)—right m1, BG-IBER-FMC-000018623, L13a; (**C**)—right m1, BG-IBER-FMC-000003518, L13b; (**D**)—left m1, BG-IBER-FMC-000001164, L13b; (**E**)—right M3, BG-IBER-FMC-000016815, L12; (**F**)—left M3, BG-IBER-FMC-000018777, L13a ((**A**–**F**)—occlusal, (**A1**–**F1**)—buccal, (**A2**–**F2**)—lingual views). Scale bar = 1 mm.

Description—The scarce material referred to this species is distinguished by the following features: the enamel is negatively differentiated; the cement in the entrance angles is abundant, filling more than half of them, and visible from the side.

m1. The basic triangles (T1–T3) are well separated. The ACC is simple, formed by widely confluent T4, T5, and AC2. On the labial side, a remnant of the *Mimomys* ridge, fairly shifted forward, can sometimes be observed. The prism fold is well-pronounced, wide, and filled with crown cementum. The isle fold is rudimentary, expressed as a small undulation in front of BSA4. LSA5, although small and rounded, is well-pronounced. The dentine tracks are high and extend to the occlusal surface, even when the roots are not yet developed.

M3. AL1, T2, and T3 are well separated. LRA3 is deep, filled with crown cementum. BSA3 is sometimes followed by a shallow BRA3 not filled with crown cementum.

Measurements—Table 30.

Remarks—This species is similar to *Mimomys blanci* but differs in larger size and in the structure of m1—a *Mimomys* ridge strongly displaced forward, a well-developed, wide prism fold, and practically no islet fold; and in the structure of the posterior part of M3. The diagnosis notes that there is no *Mimomys* ridge, but one of the illustrated specimens ([150] Figure 4a) has a well-developed BSA4, followed by a shallow BRA4, which can be interpreted as a rudimentary *Mimomys* ridge and an isle fold, respectively. The species described from Croatia, *M. malezi* Rabeder, 1983, is considered to belong to the *Mimomys tornensis* group [157,161], but it is markedly different in the structure of the anteroconid complex [63]. The material from Kozarnika generally corresponds to the type specimen of *M. tornensis* [150] and the type population from Osztramos 3 [162], but is somewhat smaller, with the *Mimomys* ridge more reduced and shifted forward, and the insle fold much more reduced. With respect to size, however, it is similar to the populations of Schernfeld and Kamyk [23,127,162]. The structure of m1 is very similar to that of Deutsch-Altenburg 3, 10, 2 C1, and 4 [22]. The differences concern the smaller sizes—the length of m1—of the teeth from Kozarnika and higher enamel-free areas on m1. In young individuals with roots in the initial stage of formation, from Deutsch-Altenburg [22] (Figure 108), the enamel-free

areas do not reach the occlusal surface. The same can be observed in the specimens from the type locality, illustrated in Figure 4 in [162]. As for the height of the dentine tracts and the structure of the anteroconid complex, the Kozarnika population is similar to that of Schernfeld but differs in the structure of the occlusal surface of M3, which is simplified in this locality [23]. Regarding the height of the anterior sinus and the sizes, the form from Kozarnika is similar to the material from the Villanyian site Bıçakçı (Anatolia), described as *Mimomys* gr. *tornensis* [163]. However, it has a more developed, posteriorly displaced *Mimomys* ridge, similar to that of other early populations. The features exhibited by the Kozarnika population suggest it is likely a derived form of *M. tornensis*. Due to the small sample size, these differences cannot be fully evaluated, and the material is tentatively assigned to *M. tornensis*. The presence of this species in the lower layers of Kozarnika (Biozone B) is particularly interesting, as it was previously thought to occur mainly in the Late Pliocene faunas (Osztramos 3, Schernfeld) that lack *Allophaiomys deucalion* and the latest records reported from some Late Pliocene/earliest Pleistocene localities (Deutsch Altenburg 10, Neuleiningen 2, 3, and 13, Kamyk, Kolinany 3, Kadzielnia, and Kielniki 3/A, together with *Borsodia newtoni*, *Lagurodon*, and *A. deucalion* [8].

Mimomys pitymyoides Jánossy and van der Meulen, 1975
(Figure 37)

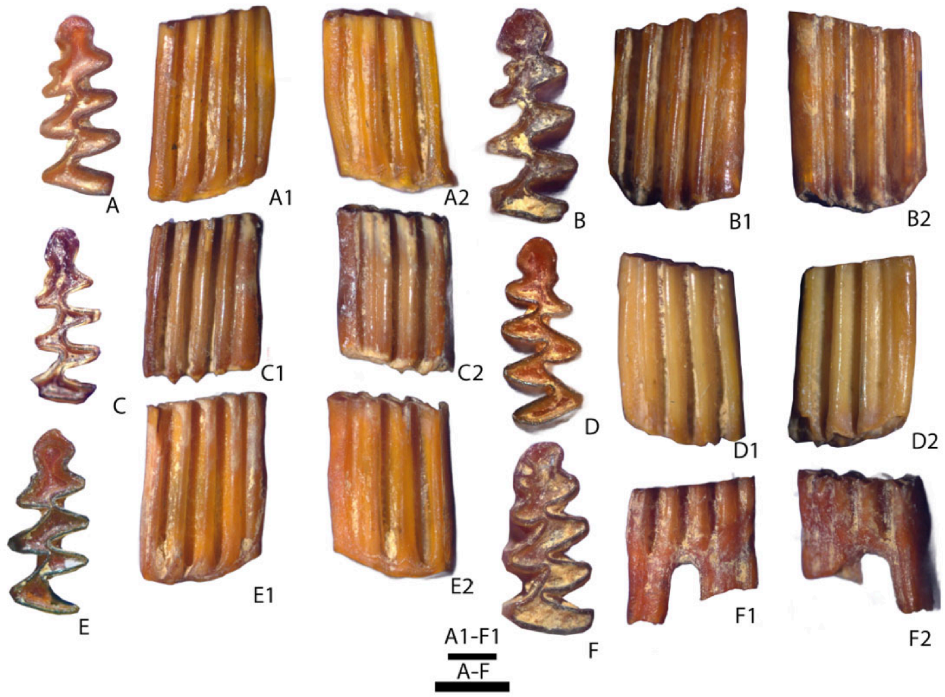


Figure 37. *Mimomys pitymyoides.* (**A**)—left m1, BG-IBER-FMC-000001133, L13b; (**B**)—left m1, BG-IBER-FMC-000003626, L13b; (**C**)—left m1, BG-IBER-FMC-000022013, L13b; (**D**)—right m1, BG-IBER-FMC-000006304, L13a; (**E**)—left m1, BG-IBER-FMC-000014704, L12; (**F**)—left m1, L13b (**A**–**F**)—occlusal, ((**A1**–**F1**)—lingual, (**A2**–**F2**)—buccal views). Scale bars = 1 mm.

Studied material (m1): Biozone B: L13–Lower, 1; L13c, 2; L13b, 13; L13a, 9; L12, 2; L11c, 2; L11b, 2; L11a1, 4.

Description—m1—In most specimens, cement is present in the reentrant folds, and the enamel is negatively differentiated in adult specimens; however, in very young specimens in which the roots are not yet developed, there is no cementum, and the enamel is not yet differentiated. The enamel-free areas are high, with the posterior, buccal, and lingual ones almost reaching the occlusal surface in the unworn teeth. The *Mimomys* ridge is well-pronounced and sometimes shifted forward. It extends downwards up to the base

of the crown. The prism fold descends almost to the base of the crown. The islet fold is well developed, reaching nearly to the base of the crown on one tooth, and only about one-third of its height on the other. The dentine fields of the main triangles are broadly fused, especially in T2 and T3; on one tooth of a young individual, the fusion is less prominent.

Remarks—The material from Kozarnika fits the diagnosis of *Mimomys pitymyoides*, as far as the morphology of the occlusal surface of m1 is concerned [150]. In size, hypsodonty, and in the linea sinuosa of m1, it is very similar to the highly evolved forms from Deutsch-Altenburg 3 and 10 and Schernfeld [23]. It seems more advanced than the form from the type locality, Osztramos 3 (Hungary), in having a higher anterosinusid on m1, reaching the occlusal surface at earlier stages of root formation. To some extent, the hypsodont teeth assigned to this species are similar to those of *M. malezi* Rabeder, 1983, described from the Early Biharian Croatien localities Tatinja Draga, Razvodje, and Podumci 1 [63,161,162]. The material from Kozarnika, however, differs in several important taxonomic features, such as reduced cement in reentrant folds, especially in young individuals, widely fused T2 and T3, a less-developed *Mimomys* ridge, which is not pronounced as a separate triangle, and a wider neck connecting the anterior field with the T4–T5 complex.

M. pitymyoides is known from many Villanyian localities in Europe, extending into the Early Biharian [8,164]. At Kozarnika, this species is regularly found in all layers of Biozone B, except for the two lowest layers (its absence here is probably due to relatively small sample sizes in these layers) and the topmost layer, 11a. In the context of the paleomagnetic data and the accompanying dominant vole species, its presence at Kozarnika is unusual. However, here it is part of a group of species also considered much older than the Biozone B layers at Kozarnika. Since there is no evidence of redeposition or mechanical contamination from older sediments—which have not been observed in the excavated area—it can be said that their presence at Kozarnika extends the stratigraphic distribution to the end of the Biharian.

Mimomys savini Hinton, 1910

(Figure 38)

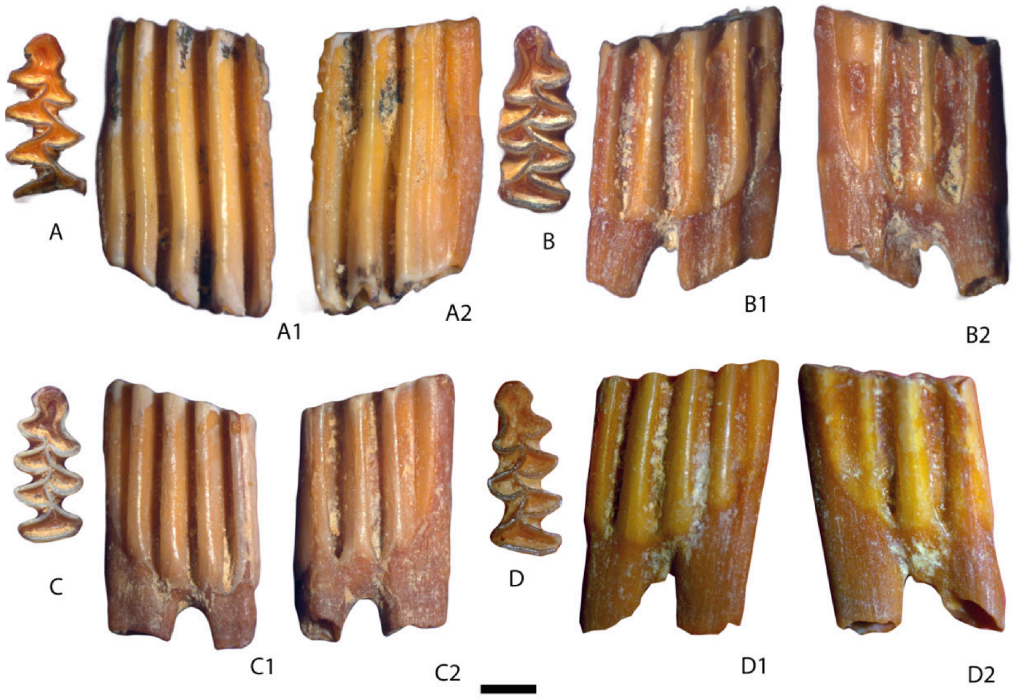


Figure 38. *Mimomys savini*. (**A**)—left m1, BG-IBER-FMC-000001104-1, L13a; (**B**)—left m1, BG-IBER-FMC-000021986, L13a; (**C**)—right m1, BG-IBER-FMC-000001104-2, L13a; (**D**)—left m1, BG-IBER-FMC-000004492, L13b, ((**A**–**D**)—occlusal, (**A1**–**D1**)– lingual, (**A2**–**D2**)—buccal). Scale bar = 1 mm.

Material—Biozone B. L13_Lower: 1 m1; L13c: 6 m1; L13b: 6 M3, 36 m1; L13a: 7 M3, 44 m1; L12: 6 M3, 57 m1; L11c: 37 m1; L11b: 1 M2, 1 m2, 8 M1, 17 M3, 64 m1; L11a1: 82 m1; L11a: 1 M1, 1 M2, 4 M3, 76 m1.

Description—The molars have roots, except in a few very young specimens. The enamel is negatively differentiated. There are abundant cement deposits in the reentrant angles. Dentine tracts reach the wear surface, even in younger teeth in which the roots are just forming.

m1: The wear surface consists of a posterior lobe (PL), three triangles with fully separated dentine fields, a simplified anteroconid complex, whose elements (T4–T5-AC2) are broadly fused. There is no enamel island. Only in one specimen is there a faint curvature of the enamel, which can be interpreted as a remnant of a *Mimomys* ridge.

M3: The triangle T2 is separated from the anterior lobe by a deep reentrant fold, and between triangle T3 and the posterior field, there is a narrow dentine bridge. There is no enamel island.

Measurements—Table 30.

Remarks—The stratigraphic range of *Mimomys savini* spans the entire Biharian. The co-occurrence of *M. savini* and *M. pusillus* marks the Early Biharian, whereas *M. savini* and some *Microtus* species (excluding *Allophaiomys*) characterize the Late Biharian. In Western and Central Europe, the upper stratigraphic boundary is the early part of MIS 15 [65]. In Eastern Europe, *M. savini* persists much longer, up to the Muchkap Stage Interglacial [8]. Based on size, it can be said that in the lower layers of Kozarnika, a relatively small form occurs compared with the late populations from the Western and Central European sites of Voigtstedt, Kozi Grzbiet, West Runton, and Prezletice, which belong to the Brunhes paleomagnetic epoch. In this regard, the material from Kozarnika is more similar to the forms from earlier Eastern European sites, Karaj Dubina and Port Katon, which fall within the Brunhes–Jaramillo interval, as well as earlier sites dating to approximately 0.99–1 million years ago [139]. The biostratigraphic significance of these differences is difficult to assess, as size is often correlated with climate. The comparisons presented above correspond to climate cooling at the end of the Biharian, but there is undoubtedly also a geographic component to this variability, which accounts for the smaller size of southern forms in warmer climates.

Tribe Clethrionomyini Hooper & Hart, 1962

Genus *Clethrionomys* Tilesius, 1850

Remains of representatives of the genus *Clethrionomys* were found throughout the entire Kozarnika sequence. There are pronounced, statistically significant biometric differences between the two biozones in size (L, W) and in the c/W index of m1 (Table 31). The c/W index reflects the degree of confluence between T4 and T5. In the form from Biozone B, these triangles are widely confluent, whereas in the form from Biozone A, the dentine connection is narrow. These differences are so pronounced (Figure 39) that, without doubt, two distinct species can be said to occur in Kozarnika. Given that the evolution of the anteroconid complex is directional toward increasing differentiation, the form from Biozone B can be considered more primitive. A well-defined phylogenetic line is traced across Europe, including the species *C. kretzoii*, *C. hintonianus*, *C. acrorhiza*, and *C. glareolus*. The form from Biozone A is practically indistinguishable from the modern species, while that from Biozone B is consistent with the diagnostic features of *C. hintonianus* [23] (Abb. 16).

Table 31. Measurements [mm] and indices [%] of m1 of *Clethrionomys* species from Kozarnika.

Biozone (Species)	N	L		W		a/L		c/W	
		X	SD	X	SD	X	SD	X	SD
A (*C. glareolus*)	41	2.41	0.128	1.03	0.059	41.0	2.624	11.2	2.862
B (*C. hintonianus*)	18	2.19	0.106	0.94	0.057	41.9	3.684	14.5	3.769

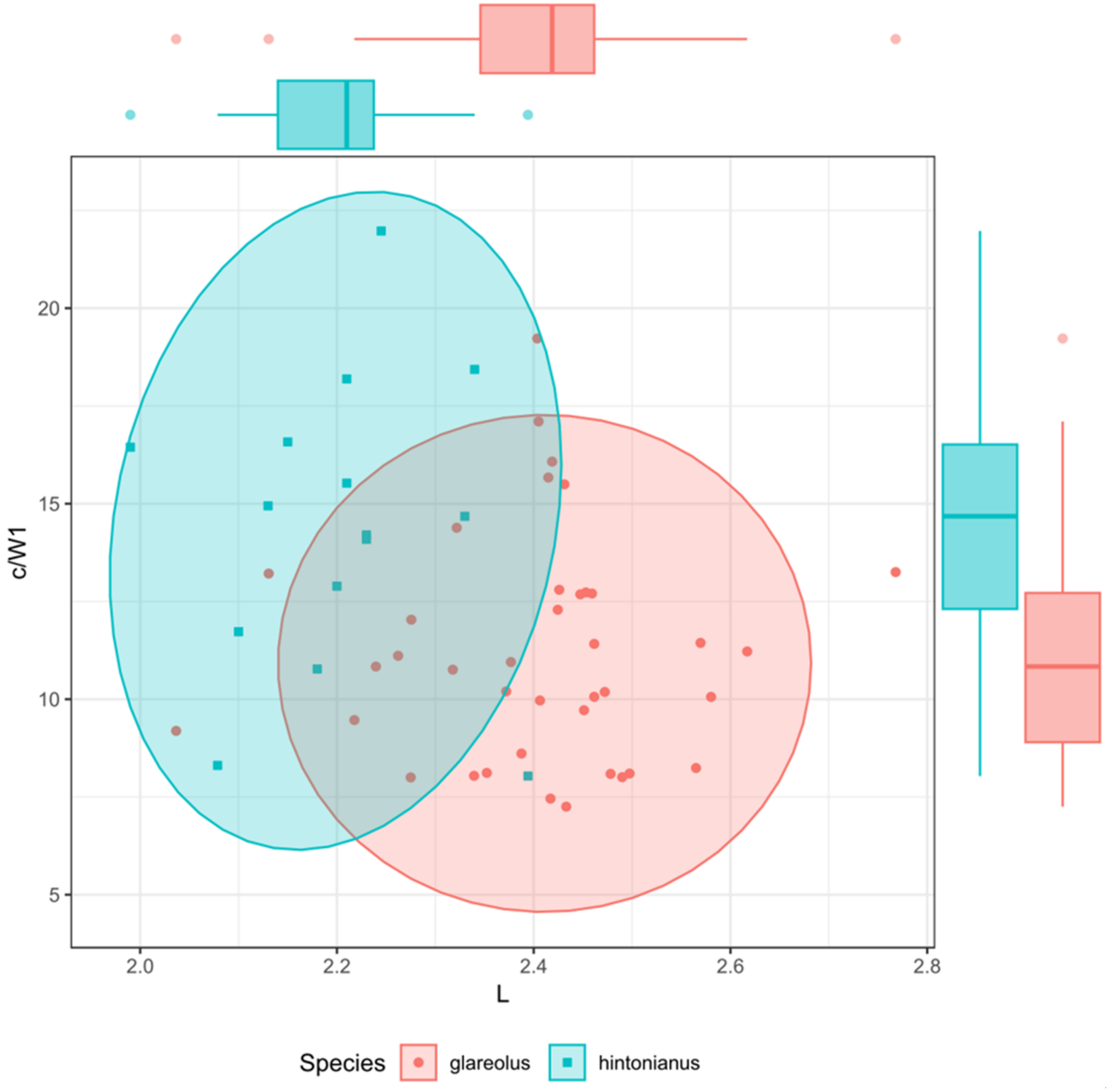


Figure 39. Scatter plot diagrams and 95% confidence ellipses of length (L, mm) versus the c/W1 [%] index of first lower molars of representatives of the genus *Clethrionomys* from Kozarnika.

Clethrionomys hintonianus Kretzoi, 1958

(Figure 40F–J)

Studied material—Biozone B. L13a: 1 m1; L12: 2 m1; L11b: 11 m1; L11a: 1 m1; L11b: 1 M1; L11b: 2 M3; L12: 1 M3.

Description—m1. The enamel-free areas are high. The enamel is slightly negatively differentiated. T4 and T5 are widely merged. T5 is widely connected to AC2, which, in turn, is shortened.

Measurements—Table 31.

Remarks—The Pliocene and Pleistocene *Clethrionomys* probably form a phylogenetic lineage composed of successively replacing species: *C. kretzoii* Kowalski, 1958—*C. hintonianus* Kretzoi, 1958—*C. acrorhiza* Kormos, 1933—*C. glareolus* [22]. The evolution is toward increasing the hypsodonty of the molars, thereby increasing the height of the linea sinuosa and the differentiation of the occlusal surface, as is well expressed on the first lower molar. The Middle Pleistocene species *C. hintonianus* is distinguished from the Late Pleistocene forms of *C. glareolus* by the wide fusion between T4 and T5 of m1 [22]. Apart from the shape of the chewing surface, this species is also characterized by the smaller size of m1

(Table 31). In this regard, the material from Kozarnika is very similar to *C. hintonianus* from Deutsch Altenburg [22], Voigtstedt, and West Runton [65]. In this respect, it is similar to material from the Polish Biharian locality of Kozi Grzbiet, identified as *C. glareolus* [165]. The latest representatives of this species in Central Europe are known from normally polarized sediments, together with *Mimomys savini*, *Microtus 'arvalinus'*, and *Microtus 'ratticepoides'*. It can therefore be said that its last occurrence corresponds to the "*Mimomys savini*" zone, which is equated with the "Cromerian Interglacial II" [8].

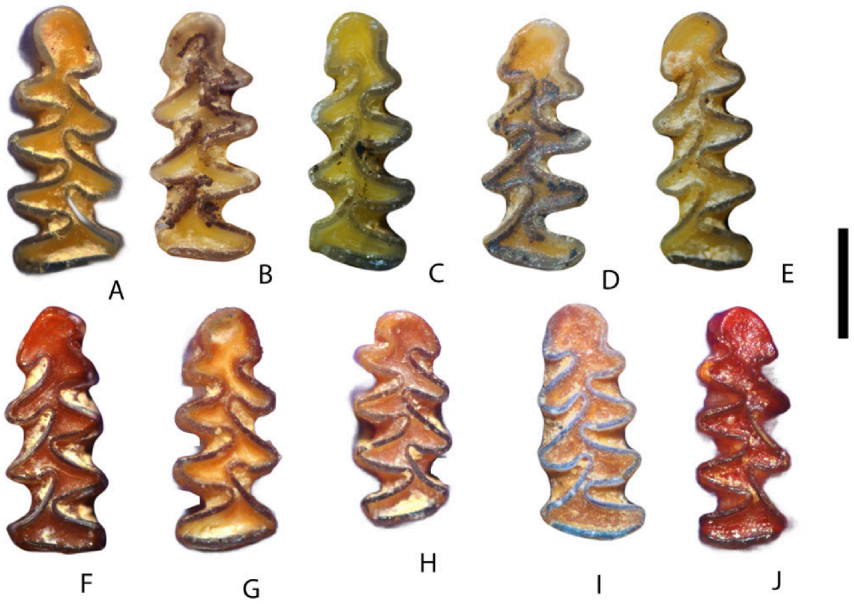


Figure 40. *Clethrionomys glareolus* (**A**–**E**), *C. hintonianus* (**F**–**J**). m1, occlusal view. (**A**)—BG-IBER-FMC-000003913,L6/7; (**B**)—BG-IBER-FMC-000021892, L9ab; (**C**)—BG-IBER-FMC-000021893, L9ab; (**D**)—BG-IBER-FMC-000021894, L9ab; (**E**)—BG-IBER-FMC-000021895, L9ab; (**F**)—BG-IBER-FMC-000006322, 1, L13a; (**G**)—BG-IBER-FMC-000006322, 2, L13a; (**H**)—BG-IBER-FMC-000006661, L13c; (**I**)—BG-IBER-FMC-000015968, L11b; (**J**)—BG-IBER-FMC-000003410, L13a. Scale bar = 1 mm.

Clethrionomys glareolus (Schreber, 1780)

(Figure 40A–E)

Studied material (m1)—Biozone A. L9ab: 4; L6/7: 4; L5c: 3; L5b: 22; L5a: 11; L3–4: 11.

Description—m1. The enamel-free areas are high. The enamel is slightly negatively differentiated. T4 and T5 are narrowly connected. The connection between T5 and AC2 varies from wide to very narrow. The ASC2 is more elongated than in previous species.

Measurements—Table 31.

Remarks—In terms of size and structure of the chewing surface, the available material from Biozone A of Kozarnika is very similar to Late Pleistocene remains from numerous sites in Bulgaria [101].

Tribe Pliomyini Kretzoi, 1969

Genus *Pliomys* Méhely, 1914

Pliomys episcopalis Méhely, 1914

(Figure 41)

Studied material (m1)—Biozone B. L11a: 19; L11a1: 44; L11b: 26; L11c: 10; L12: 107; L13a: 74; L13b: 79; L13c: 21; L13-Lower: 3.

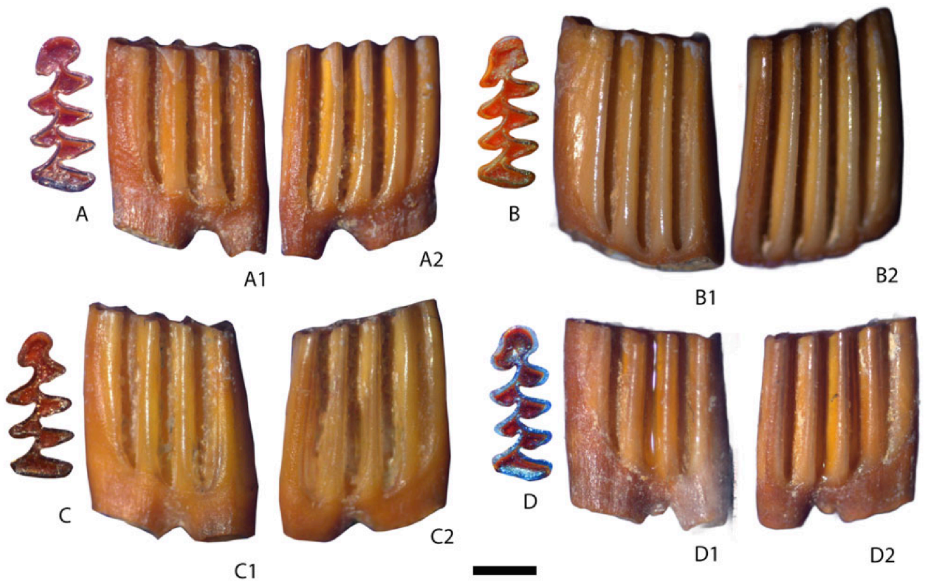


Figure 41. *Pliomys episcopalis*, left m1s. (**A**)—BG-IBER-FMC-000000276, L13a; (**B**)—BG-IBER-FMC-000000664, L13b; (**C**)—BG-IBER-FMC-000000276, L13a; (**D**)—BG-IBER-FMC-000006352, L13b; (**A**–**D**)—occlusal, (**A1**–**D1**)—buccal, (**A2**–**D2**)—lingual views). Scale bar = 1 mm.

Description—m1. Positive enamel differentiation. No crown cementum. The dentine fields behind AC2 are well isolated or have very tight connections. Most often, AC2 is clearly separated from T5, and wide connections are very rare. BSA4 is well developed and is sometimes followed by a shallow BRA3. Enamel-free areas are very high, but the posterior buccal and lingual ones do not reach the occlusal surface on unworn teeth.

Measurements [mm] and indices [%]—N = 37, min-mean-max, SD: L: 2.30–2.51–2.72, 0.111; W: 0.97–1.11–1.25, 0.061; a/L: 42.55–46.65–50.41, 2.001.

Remarks—In terms of size, the first lower molars from Kozarnika do not differ from those found at other sites from the beginning of the Middle Pleistocene, for example, Kozi Grzbiet [165]. It is definitely smaller than *Pliomys bolkayi* (Kormos, 1931) and similar to *P.* cf. *hollitzeri* Rabeder, 1981, from Podumci 1 [63]. At the same time, however, the molars from Kozarnika are larger than those of *P. hollitzeri* from Deutsch-Altenburg 4 (type locality) [22].

In Central Europe, the first *P. episcopalis* appears alongside *Allophaiomys deucalion* and persists into the Middle Pleistocene, whereas in Eastern Europe, it is found exclusively in *A. pliocaenicus* assemblages [8].

Pliomys coronensis (Méhely, 1914)

(Figure 42)

Studied material (m1)—Biozone B: Layer 13c: 5; layer 13b: 22; layer 13a: 25; layer 12: 10; layer 11c: 5; layer 11b: 12; layer 11a1:13; layer 11a: 7.

Description—The m1s assigned to this species have two roots, five closed triangles, no cement at the reentrant angles, and a variable anterior complex in which T6 and T7 are alternating and confluent. The enamel is positively differentiated. The enamel-free areas are prominent. On unworn teeth, the posterior dentine tracts reach slightly below the chewing surface.

Measurements [mm] and index [%]—N = 5, Min–X–Max, SD. L: 2.39–2.71–3.09, 0.254; W: 0.88–1.14–1.39, 0.193; a/L: 44.66–48.03–51.09, 2.291.

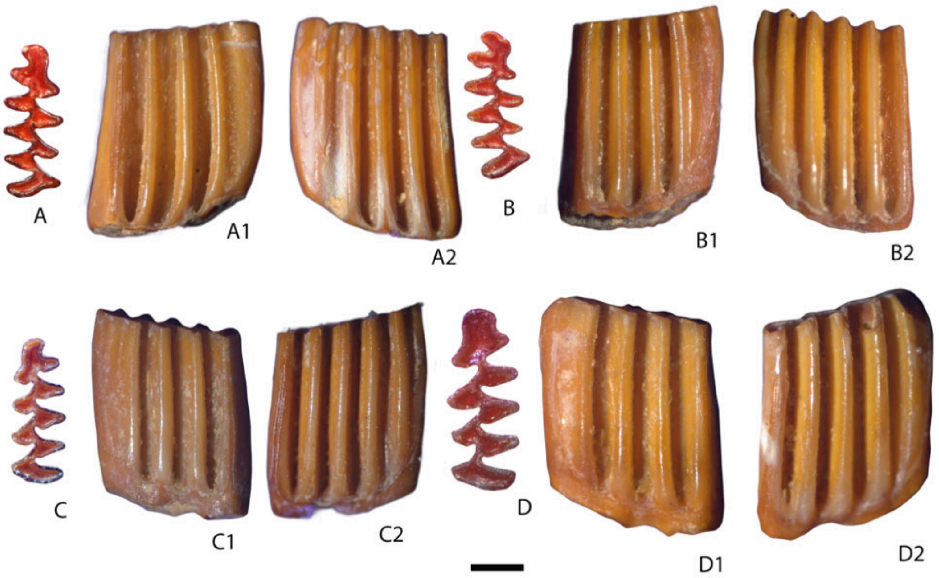


Figure 42. *Pliomys coronensis*. right (**A**,**B**), left (**C**,**D**) m1s. (**A**)—BG-IBER-FMC-000000277-1, L13a; (**B**)—BG-IBER-FMC-000000602, L13b; (**C**)—BG-IBER-FMC-000000665, L13b; (**D**)—BG-IBER-FMC-000001127, L13b; ((**A**–**D**)—occlusal, (**A1**–**D1**)—buccal, (**A2**–**D2**)—lingual views). Scale bar = 1 mm.

Remarks—During the Pleistocene, *Pliomys coronensis* [= *P. lenki* (Heller, 1930)] evolved greater hypsodonty, a longer m1, and cementum at reentrant angles, with earlier breakdown of enamel bands. The species has been extensively studied across Europe [166]. Three subspecies were recognized: *lenki*, present in Europe at the start of the Middle Pleistocene; *ultimus*, typical of the end of this period; and *relictus*, associated with larger-sized 'relict' populations of the Upper Pleistocene. The available material differs from the Middle Pleistocene sample from the lower layers of the Morovitsa Cave in being smaller and having a shorter anteroconid complex relative length. In this sense, it is much more primitive [43]. It is similar to the population from Betfia-V and VII, identified as *Pliomys coronensis lenki* [167].

Genus *Dinaromys* Kretzoi, 1955

Dinaromys dalmatinus (Kormos, 1931)

(Figure 43)

Studied material (m1)—Biozone B. Layer 13—Lower: 3; layer 13c: 8; layer 13b: 8; layer 13a: 14; layer 12: 9; layer 11c: 10; layer 11b: 10; layer 11a1: 13; layer 11a: 16.

Description—The dentine fields are isolated from each other, except for the anterior (AC2), which is sometimes relatively widely connected to T5. The anterior field is broad and short, with well-defined LSA5 and BSA4; the first is rounded and the second pointed, sometimes followed by a very shallow LRA4. In less-worn teeth (e.g., BG-IBER-FMC-000000662 and BG-IBER-FMC-000020425), it can be seen that BSA4 is, in fact, a well-developed *Mimomys* ridge that extends only a short distance downward and must, therefore, have disappeared due to erosion. From this, it follows that LRA3 is a strongly developed prism fold, and the weakly expressed LRA4 can be considered a remnant of an isle fold. The enamel is strongly positively differentiated. The dentine tracts are high, but in unworn teeth, they do not reach the chewing surface. There is no cementum.

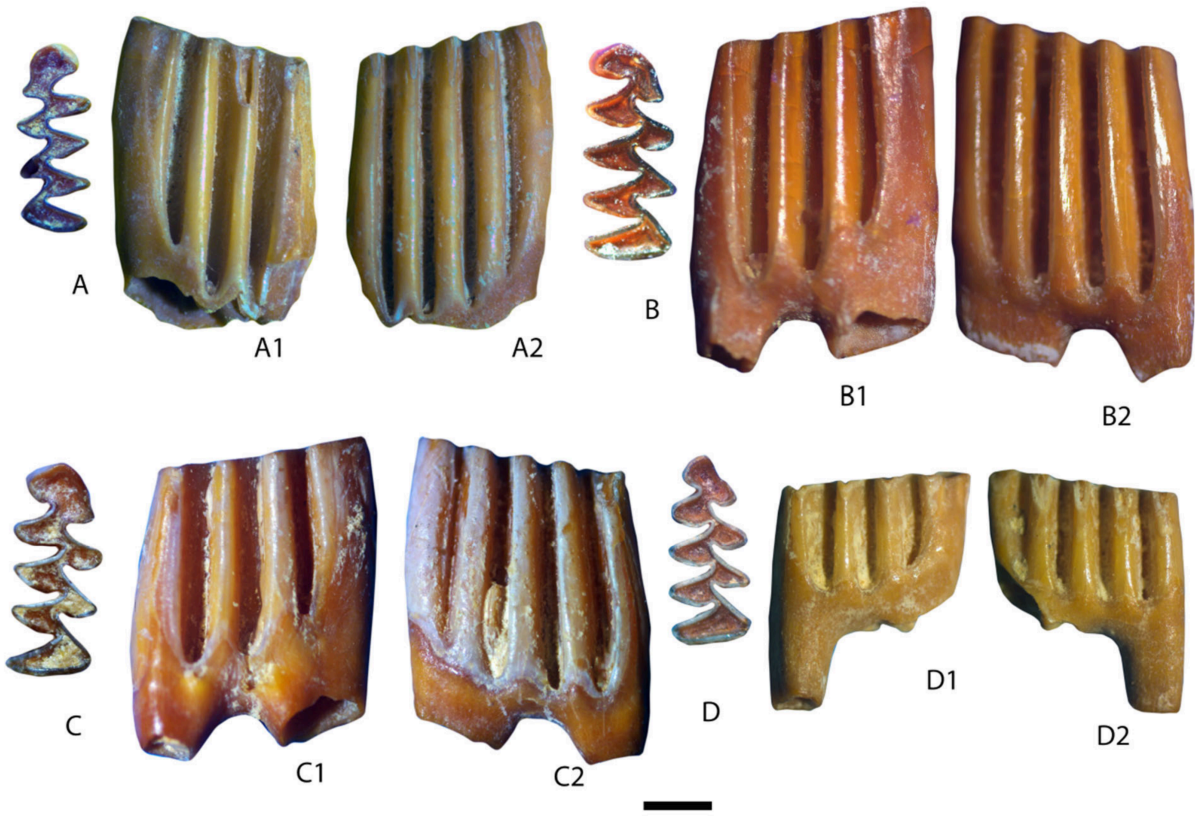


Figure 43. *Dinaromys dalmatinus.* left (**A**), right (**D**) m1s. (**A**)—BG-IBER-FMC-000020425, L13a; (**B**)—BG-IBER-FMC-000000662, L13b; (**C**)—BG-IBER-FMC-000017774, L11b; (**D**)—BG-IBER-FMC-000017109, L12, ((**A**–**D**)—occlusal, (**A1**–**D1**)—buccal, (**A2**–**D2**)—lingual views). Scale bar = 1 mm.

Measurements [mm] and index [%]—N = 4–6, Min–X–Max, SD: L: 2.85–3.14–3.43, 0.290; W: 1.23–1.40–1.64, 0.153; a/L: 43.73–45.55–48.42, 2.057.

Remarks—The described material is almost identical to the form from Podumci 1 (Croatia) [63]. The differences concern the absence of cement in the teeth from Kozarnika. It is similar to *Dinaromys allgranzii* (Sala, 1996) but is larger and has a well-defined enamel differentiation [168]. In this respect, it also differs from *D. topachevskii* Nesin and Scoric, 1989, which, in addition, has a different configuration of AC2 and widely fused T4 and T5 [169]. *D. dalmatinus* was described from Podumci, north Dalmatia [170]. Thus far, it is known from the Early Pleistocene of Southern Europe—Croatia: Razvođe, Podumci-1, Tatinja Draga (Early Biharian), Rava, Ugljan, Dubci (Late Biharian), and Italy (Monte Lama–Early Biharian) [97]. Kozarnika is the easternmost locality in which this species has been found.

Tribe Ellobiini Gill, 1872

Ungaromys nanus Kormos, 1933

(Figure 44A,A1)

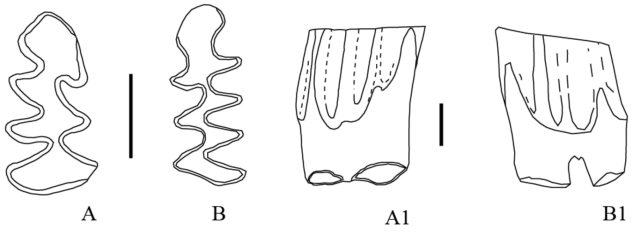


Figure 44. *Ungaromys nanus* (**A**) and *Villanyia* cf. *exilis* (**B**) from Kozarnika. (**A**,**B**)—occlusal view; (**A1**,**B1**)—buccal view. Scale bars = 1 mm.

Studied material and Measurements [mm]—L12: 1 m1 (2.2 × 1.1).

Description—The molar has two roots and lacks crown cementum in the reentrant folds. On the wear surface, the dentine fields in front of the posterior loop are broadly connected. The enamel bands are thick. The anterosinoid and hyposinoid are tall, reaching the wear surface. On the lingual side, the tracts are shorter and do not reach the occlusal surface.

Remarks—*Ungaromys* is an extinct genus whose members lived in Europe from the Early Pliocene to the Early Biharian. The genus *Germanomys* was introduced for the Ruscinian and Villanyian forms, which are similar to *Ungaromys* but probably less derived [97]. Specific names are assigned to forms from different geological ages based on the level of hypsodonty within a single evolutionary lineage [22]. Based on the height of the dentine tracts, the available tooth is more primitive than that of *Ungaromys meuleni* Rabeder, 1981 from Monte Peglia (Italy) and nearly identical to that of *Ungaromys nanus* from the type locality [22]. The species is described from the Early Biharian locality Betfia 2 in Romania and is known from many Villanyian and Early Biharian sites across Europe [97]. Its upper chronological range extends to the Jaramillo Subchron [8].

Tribe Lagurini Kretzoi, 1955

This tribe includes species that lack cementum in the reentrant angles. The most primitive species that possess rooted molars are usually assigned to the genus *Borsodia*. In this genus, two main lineages can be traced. One bearing *Mimomys* ridge stems from *B. petenyii* (Méhely, 1914) and continues into *B. arankoides*. The other consists of forms lacking the *Mimomys* ridge, the late form being *B. newtoni*. They can be considered hypothetical ancestors of the tribe's rootless species, but the exact mechanisms, timing, and location of the latter's origin, as well as its phylogenetic relationships, remain unclear and debatable. One of the main reasons for the existing taxonomic problems is the unclear definition of the species *Prolagurus pannonicus* Kormos, 1930, described from Püspökhfürdő (Betfia). The holotype is a skull fragment [171] that lacks diagnostic features sufficient to assign this species to any of the m1 morphotypes occurring at this site [171], some of which were later described as separate species. Rabeder [22] redefined the genus *Prolagurus*, of which *P. pannonicus* constitutes the type species. Based on m1 morphology, he established distinguishing features of *Lagurus* (*arankae*), including the absence of the "Mimomyskante" and the "Mimosinuide". According to Rabeder's view, *P. pannonicus* comprised two distinct evolutionary stages in chronological succession: *P. praepannonicus* and *P. pannonicus*. Later, Terzea [172] amended the diagnosis of *P. pannonicus* and designated the specimen figured in Chaline [84] as a paralectotype, representing m1 with an ovoid anterior lobe, a closed neck, and T4–T5 opposite-confluent. The taxonomy and evolutionary concepts adopted here generally follow those of Rabeder [22] and Terzea [172], which can be summarized as follows. At the boundary between the Villanyian and Biharian, the *Borsodia* lineages represented by *B. arankoides* and *B. newtoni* give rise to two evolutionary sequences of rootless forms. The line with a *Mimomys* ridge consists of *B. arankoides—Lagurus arankae—L. transylvanicus—L. transiens—L. lagurus*. The second line is represented by a sequence of forms lacking a *Mimomys* ridge—*Borsodia newtoni—Prolagurus ternopolitanus (praepannonicus)—P. (s. str.) pannonicus—P. posterior*. The coexistence of forms at different evolutionary levels, both in Kozarnika (*B. arankoides/L. arankae*, *L. arankae/L. transylvanicus*, *B. newtoni/P. ternopolitanus*, *P. ternopolitanus/P. pannonicus*) and in the earlier site Temnata Cave (*B. arankoides/L. arankae*, *B. newtoni/P. ternopolitanus*) [173], indicates that evolution within these two phylogenetic lineages is not anagenetic. Rather, it corresponds to the punctuated equilibrial model, which explains the persistence of ancestral species alongside their descendant species. Accordingly, the macroevolutionary trend arises from species selection [174] rather than from natural selection within populations.

Genus *Borsodia* Jánossy and van der Meulen, 1975

Borsodia arankoides (Alexandrova, 1976)
(Figure 45)

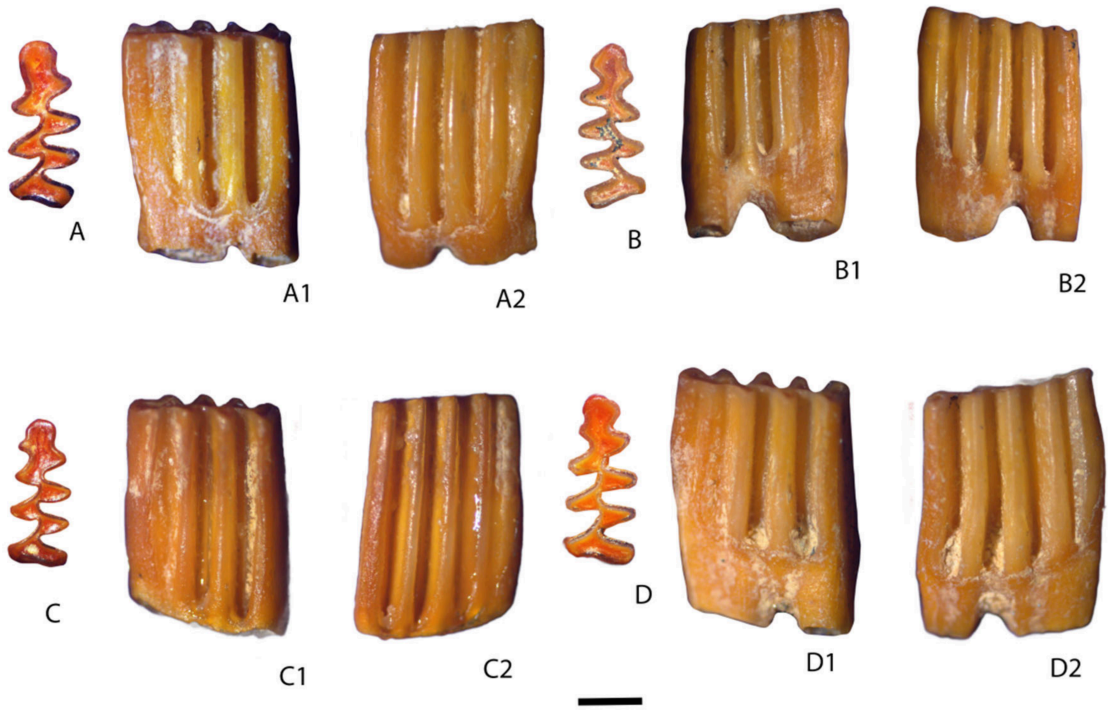


Figure 45. *Borsodia arankoides.* Left (**A**,**C**,**D**), right (**B**) m1s. (**A**)—BG-IBER-FMC-000000603, L13b; (**B**)—BG-IBER-FMC-000006941, L13-Lower; (**C**)—BG-IBER-FMC-000003686, L13c; (**D**)—BG-IBER-FMC-000006488, L13b, ((**A**–**D**)—occlusal, (**A1**–**D1**)—buccal, (**A2**–**D2**)—lingual views). Scale bar = 1 mm.

Studied material (m1)—Biozone B. L13-Lower: 2; L13c: 1; L13b: 5; L13a: 7; L12: 3; L11b: 2; L11a1: 1; L11a: 2.

Description—No crown cementum, two roots, strongly positively differentiated enamel. Dentine tracts are high but do not reach the occlusal surface in teeth with roots not yet fully developed. There is a *Mimomys* ridge, but it is not very prominent (in one specimen, BG-IBER-FMC-000000603, it is poorly pronounced and not visible in occlusal view), extending downward to about 1/3 of the crown height. The Mimosinuide [22] does not reach the occlusal surface even in specimens with moderately developed roots, and as a result, there is no enamel interruption at the tip of the *Mimomys* ridge in occlusal view.

Measurements [mm] and indices [%]—N = 5, Min–X–Max, SD. L: 2.29–2.44–2.60, 0.155; W: 0.90–0.99–1.07, 0.065; a/L: 43.85–45.01–47.16, 1.311.

Remarks—The described teeth from Biozone B at Kozarnika are very similar to the materials from Kryzhanovka 4, Liventzovka 1–4 sites, representing the transition between the Villanyian and Biharian [24]. A representative of the genus *Borsodia* is reported from a much later locality: Litvin (Krasnodar Territory, Taman Peninsula). The fossiliferous horizon was found in the Chauda transgression deposits and therefore may be dated to the beginning of the Brunhes epoch [132].

Borsodia newtoni (Forsyth Major, 1902)

Studied material (m1)—Biozone B: L13Lower: 1; L13b: 2; L13a: 2.

Description—m1. Two roots, high dentine tracks, and a positively differentiated enamel band. The occlusal surface consists of a posterior loop, three basic triangles (T1, T2, and T3), and a simple anteroconid complex. The dentine fields of the basic triangles show narrow connections. The connection between the cap (AC2) and the rest of the anteroconid complex (T4 and T5) is broad.

(Figure 46)

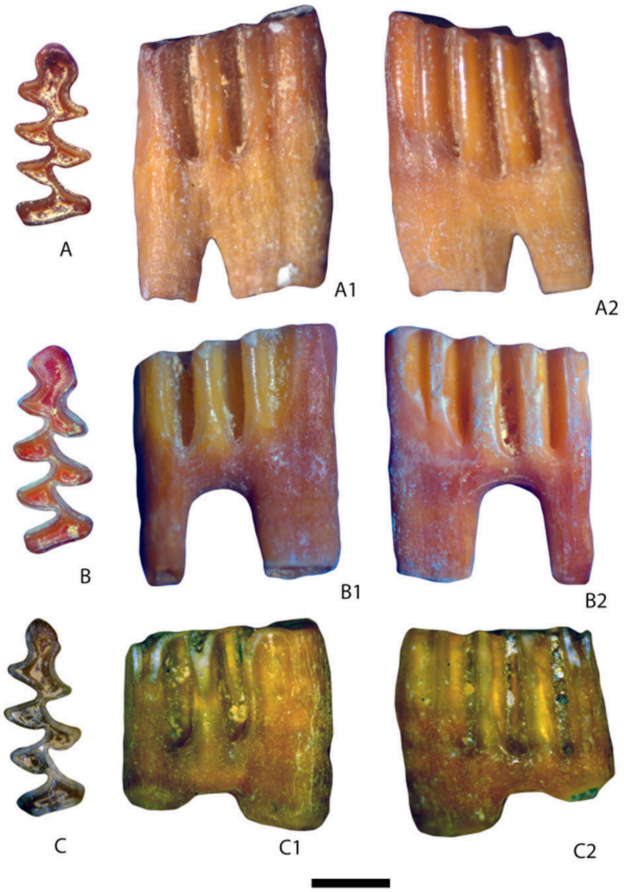


Figure 46. *Borsodia newtoni.* Right m1s. (**A**)—BG-IBER-FMC-000003597, L13b; (**B**)—BG-IBER-FMC-000018425, L13a; (**C**)—BG-IBER-FMC-000004615, L13)—Lower; ((**A**–**C**)—occlusal, (**A1**–**C1**)—buccal, (**A2**–**C2**)—lingual views). Scale bar = 1 mm.

Measurements [mm] and index [%], N = 5. Min–X–Max, SD. L: 2.44–2.59–2.73, 0.108; W: 0.94–1.01–1.07, 0.053; a/L: 41.29–42.83–45.88, 1.996.

Remarks—The available molars are similar to *Borsodia newtoni*, as they share key features with specimens from East Runton and Schernfeld [23,153], such as positively differentiated enamel, lack of crown cement, and nearly closed dentine fields. It is also very similar to the materials from Liventzovka1–4, Kryzhanovka 4 [24]. *B. newtoni* is a senior synonym of *Mimomys newtoni hungaricus* Kormos, 1938 [153], and *Mimomys simplex* Kretzoi, 1954 [175]. It is known from localities lacking advanced *Microtus* but with *Prolagurus ternopolitanus*, *Microtus deucalion*, and *Mimomys pitymyoides* of earliest Pleistocene or latest Pliocene age [8]. In Bulgaria, the species is reported as *Borsodia hungarica* from Temnata Cave in a similar faunistic context [173]. Its occurrence in the lowest layers of Kozarnika, within assemblages dominated by advanced *Microtus*, extends its stratigraphic range.

Genus *Lagurus* Gloger, 1841

In this study, m1s with a well-defined dentine tract along the ridge of BSA4, reaching the chewing surface, resulting in a consistent break in the enamel band at the tip of this salient angle in occlusal view, were referred to. From a comparative anatomical perspective, this angle should be considered a highly modified *Mimomys* ridge, and the dentine tract a homolog of Mimosinuid; BRA3 and BRA4 represent a prism fold and an island fold, respectively [63]. Among the diagnostic first lower molars referred to this genus, two groups can be distinguished based on their evolutionary level. One group, represented by a very primitive form indistinguishable from *L. arankae*, is relatively rare and occurs only

in the lower layers—Biozone B. The other group that dominates the material referred to this genus (8679 m1s) comprises more advanced forms that exhibit features characteristic of the species *L. transylvanicus*, *L. transiens*, and *L. lagurus*, [22,176,177]. These species are assumed to mark stages in evolution within an anagenetic phylogenetic lineage [4] and, in this sense, have important biostratigraphic significance. Because the transitions between these forms are gradual, it is difficult to draw sharp boundaries between them. To provide a basis for more objective taxonomic interpretation and separation, Relative Warp Analysis and unsupervised model-based clustering were applied to a subsample of 1743 m1.

The first Relative Wrap (RW1), explaining 28.86% of the variability in the outline of the anteroconid complex (ACC), presents a morphological gradient of increasing complexity through the addition of new triangles, T6 and T7, and the differentiation of the anterior cap (AC3). Along this axis, two clear groups are observable—a primitive group on the left side of the graph and a progressive group on the right (Figure 47). The second axis (RW2), which explains 16.54% of the variability in the shape of ACC, represents the degree of differentiation of the dentine fields within each group defined by RW1. In the more primitive group, on the left side of the graph, this trend reflects the degree of isolation of the main ACC triangles (T4 and T5). In the group on the right side of the graph, the degree of differentiation involves separating AC3 from the T6–T7 complex by deepening BRA4 and LRA5. Clearly, these two axes represent the main evolutionary trends in voles with rootless molars. In the subsequent model-based clustering, RW1 and RW2 were used as two quantitative variables representing the shape, supplemented by the length of m1 (L) as a feature representing the overall size. The best model, VVE (ellipsoidal, equal-orientation mode), defines four clusters in the morphological space of the first two Relative Warps (Figure 47). Cluster 1 is undoubtedly the most primitive and represents m1s with broadly merged T4 and T5. Cluster 2 is more derived, showing a tendency towards isolation of the dentinal fields of the main triangles of the ACC and the development of LSA5. Based on the shape of the anterocone complex, these two clusters correspond to *L. transylvanicus* and can be interpreted as primitive and derived forms within this species. Clusters 3 and 4 represent two degrees of complexity among the progressive forms. Cluster 3, more primitive, has relatively shallow BRA4 and LRA5 and shows similarity to *L. transiens*. In cluster 4, these folds are well developed, and AC3 shows a tendency toward isolation—features characteristic of the most evolved form in this phylogenetic line—*L. lagurus*. For better taxonomic interpretation, the relative proportions of teeth from each cluster in the stratigraphic sequence are shown in Figure 48.

In the lower layers of the sequence—Biozone B—representatives mainly from clusters 1 and 2 occur, with those from clusters 3 and 4 making up a negligible proportion. In this biozone, a clear trend of decreasing relative proportion of the primitive form (cluster 1) is observed. It is evident that in the lower part of the Kozarnika sequence, an evolution of *L. transylvanicus* has been recorded. In the upper part of the sedimentary sequence (Biozone A), similar changes are observed among the progressive forms, but they are not as well expressed. The relative proportion of primitive morphotypes, similar to *L. transiens* (Cluster 3), gradually decreases from layer 10a to layer 5a, but in the topmost layers 3–4, their share increases again. As for the primitive morphotypes from cluster 3, although similar to *L. transiens*, they are more progressive than the typical Middle Pleistocene form of this species, such as the one recorded in the lower layers of the Morovitsa Cave [43]. As a consequence, the stratigraphic changes in the upper part of the Kozarnika sequence were interpreted as weakly expressed evolutionary changes within the modern species, *L. lagurus.*

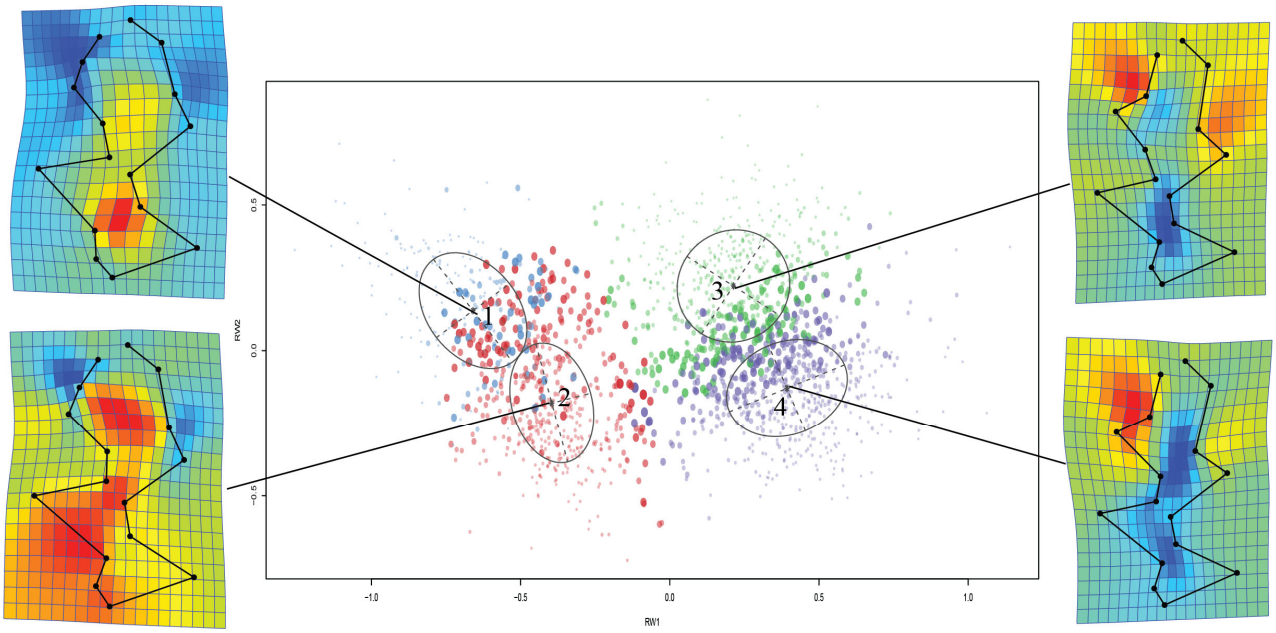


Figure 47. Position of 1743 m1s of *Lagurus* from Kozarnika in the morphological space formed by the first two Relative Warps (RW1, RW2). Colors, point symbols, and 95% confidence ellipses (1–4), their centroids (asterisks) and axes (dashed lines) represent the results of model-based clustering. The size of the points is proportional to uncertainty. The shape deformations of the centroid specimen of each cluster relative to the overall mean shape as the reference are also shown; expansions are color-coded in red and contractions in blue.

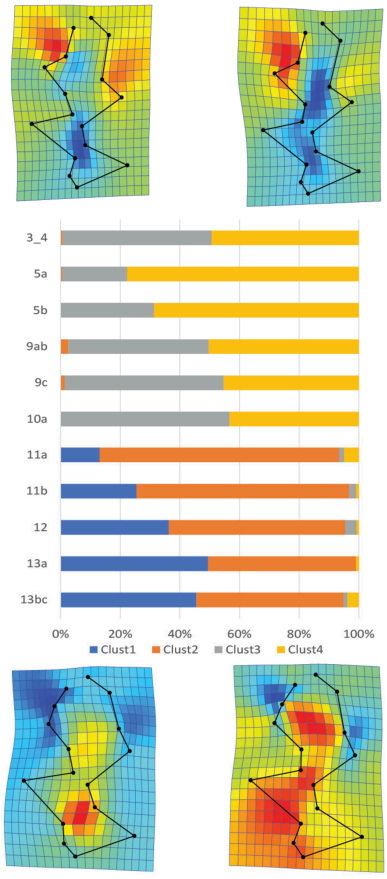


Figure 48. Stratigraphic changes in the percentage share of the m1 clusters identified through model-based clustering. The deformation grids illustrate the centroid shape characteristics of each cluster (see Figure 47).

Based on this analysis, it can be said that, in addition to the scarce remains of *L. arankae*, the mass material from m1 in the Kozarnika sequence represents two other species of the genus—*L. transylvanicus* and *L. lagurus*.

Lagurus arankae (Kretzoi, 1954)

(Figure 49)

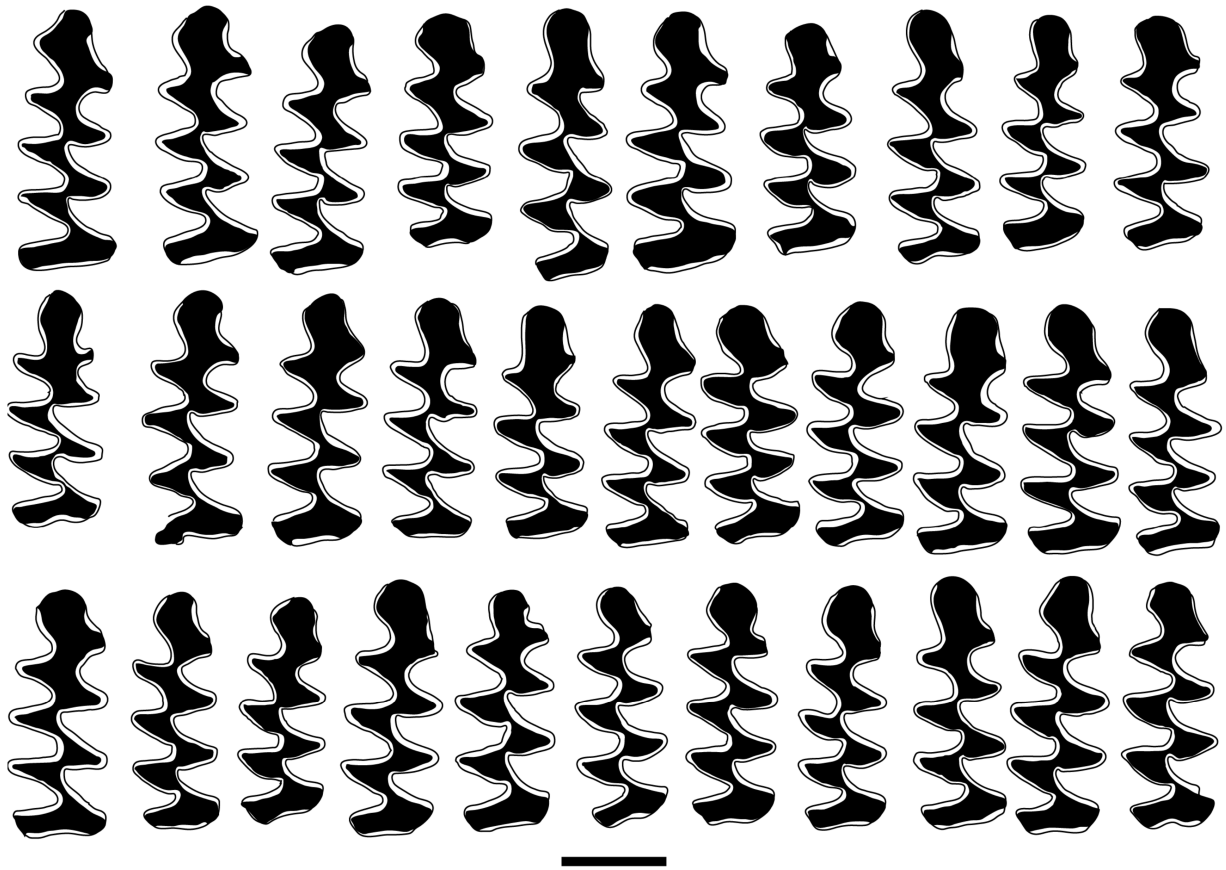


Figure 49. *Lagurus arankae.* Biozone B, right m1s in occlusal view. Scale bar = 1 mm.

Studied material (m1)—L11b: 2; L12: 14; L13a: 3; L13—Lower: 2; L14: 1.

Description—The posterior field (PL) and the basic triangles (T1–T3) are well isolated from each other. The elements of the anteroconid complex are most often in broad connection; less frequently, there is narrowing of the connections between T4 and T5 and/or between T5 and AC2 in various combinations. Such morphotypes resemble *L. transylvanicus* but show lower a/L values.

Measurements [mm] and index [%]—N = 24. X, SD. L: 2.34, 0.095; W: 0.88, 0.07; a/L: 47.96, 3.26.

Remarks—The presence of transitional forms to the next species indicates that the population from Kozarnika represents a highly evolved form of *L. arankae*. This is also confirmed by the significantly greater a/L value compared to that of *L. arankae* from the nearby Villanyian site, Temnata Cave [173]. A progressive form, similar to the one from Kozarnika, is described from Podumci 1 as a chronosubspecies of *L. arankae podumcensis* Malez and Rabeder, 1984 [63]. In Central Europe, the latest known occurrences of *L. arankae* are reported from localities dated to before the end of the Jaramillo [8]. In Eastern Europe, it persists until later periods. It has been reported from sediments occurring immediately above the Matuyama–Brunhes reversal—Priazovsky small mammal locality (Taman Peninsula) [132]. The vole spectrum in this locality is identical to that in Biozone B of Kozarnika.

Lagurus transylvanicus Terzea, 1989
(Figure 50)

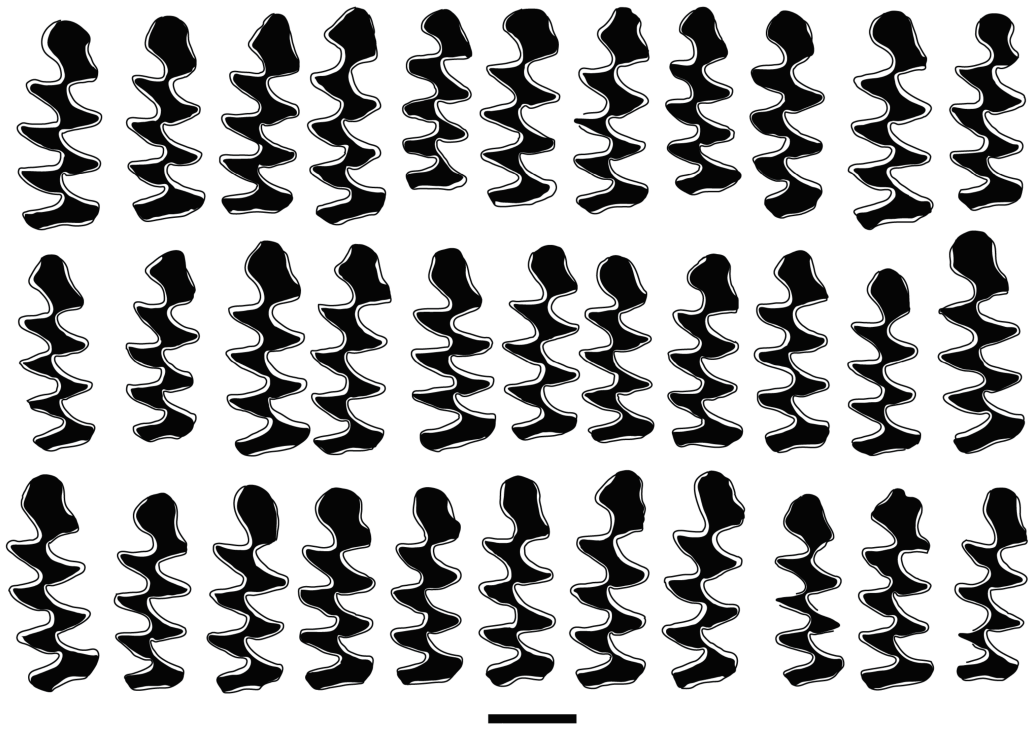


Figure 50. *Lagurus transylvanicus.* Biozone B, right m1s in occlusal view. Scale bar = 1 mm.

Studied material (m1)—L13/14: 2; L13—Lower: 82; L13c: 320; L13b: 1190; L13a: 1112; L12: 1540; L11c: 334; L11b: 691; L11a1: 786; L11a: 689.

Description—Four lingual and four labial reentrant angles; 3 alternating well-isolated enamel triangles; and an elongated anteroconid complex with a rhomboidal posterior field, resulting from the confluence of the opposing T4–T5, and a long, closed anterior lobe (AC2) with a prominent BSA4 ("*Mimomys*-ridge"). The AC2, with rounded lingual and mesial faces, exhibits a slight labial concavity, resulting in a shallow BRA4. At the apex of BSA4, there is an enamel interruption caused by Mimosinuid extending the entire height of the crown.

Measurements—Table 32.

Table 32. Measurements (mm × 10) and indices (%) of m1 of *L. transylvanicus* from Kozarnika.

Layer	N	L		W		a/L		c/W	
		X	SD	X	SD	X	SD	X	SD
11a	49	23.95	1.175	9.23	0.552	51.55	1.555	18.33	4.325
11a1	12	24.14	1.410	9.05	0.649	50.98	1.690	19.85	6.722
11b	313	23.78	1.287	9.07	0.554	51.16	1.381	20.91	6.208
12	132	23.44	1.183	8.92	0.545	50.75	1.698	21.88	7.354
13a	105	23.33	1.179	8.91	0.645	50.79	1.702	23.95	7.797
13b	57	23.73	1.065	9.09	0.526	50.40	1.522	25.59	7.698
13c	22	23.44	1.018	8.91	0.557	51.09	1.467	19.53	7.771

Remarks—The m1s from the lower layers of Kozarnika (Biozone B), consisting of the bulk of Lagurini material, fit perfectly with the diagnosis and description of *L. transylvanicus* from the Middle Pleistocene type locality Ciscau-1 (Romania) [176].

Lagurus lagurus (Pallas, 1773)

(Figure 51)

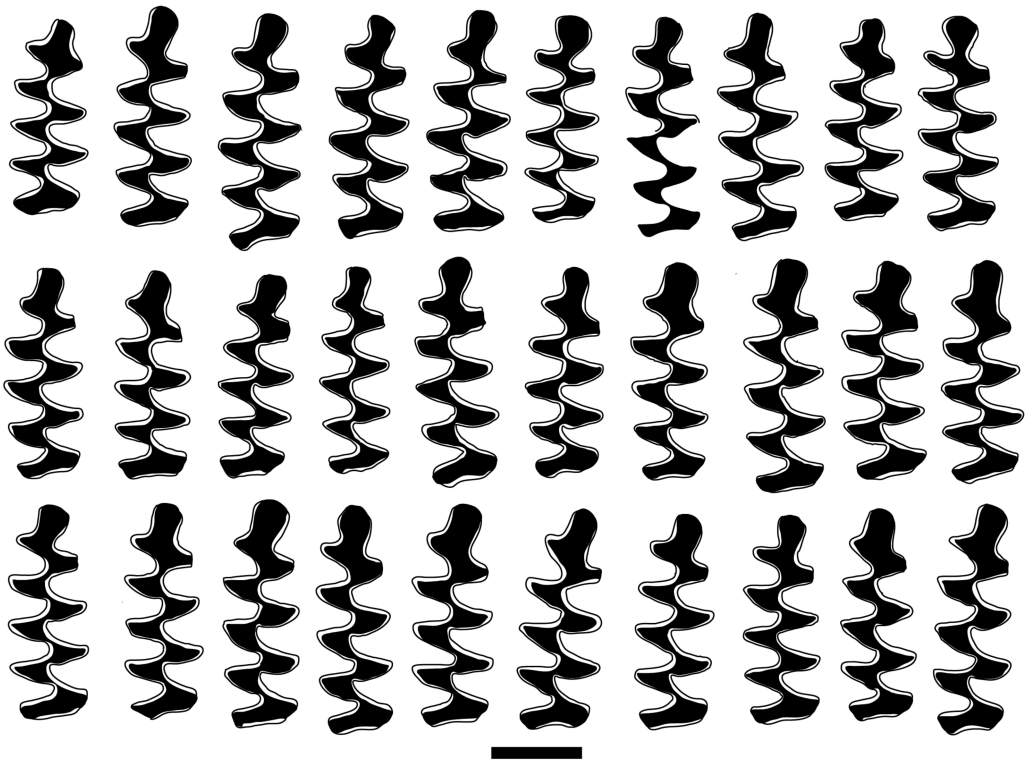


Figure 51. *Lagurus lagurus.* Biozone A, right m1s in occlusal view. Scale bar = 1 mm.

Studied material (m1)—Biozone A: L10b: 26; L10a: 651; L9c: 139; L9b: 58; L9ab: 255; L6/7: 43; L5c: 149; L5b: 344; L5a: 98; L3–4: 161.

Description—The rear field, the main triangles (T1–T3), and the basic triangles of the ACC are isolated from one another. T5 is isolated from the front part of the ACC, which is complex and, in addition to BSA4 (*Mimomys* ridge), also includes LSA5, in front of which are BRA4 and LRA5, expressed to varying degrees—shallow (*transient* morphotype) or deep (*lagurus* morphotype).

Measurements—Table 33.

Table 33. Measurements (mm × 10) and indices of m1 of *L. lagurus* from Kozarnika.

Layer	N	L		W		a/L		c/W	
		X	SD	X	SD	X	SD	X	SD
3–4	154	24.31	1.294	8.892	0.578	53.84	1.373	15.88	2.548
5a	197	24.30	1.229	8.944	0.607	54.08	1.369	15.86	2.683
5b	83	24.14	1.253	8.988	0.633	53.96	1.357	15.47	2.245
6–7-9ab-c	45	25.67	1.176	9.132	0.556	54.16	1.373	16.54	2.516
9ab	155	25.37	1.256	9.109	0.543	54.24	1.314	16.37	2.362
9c	148	25.57	1.212	9.045	0.534	54.28	1.296	15.80	2.396
10a	187	25.36	1.214	9.077	0.525	54.21	1.389	15.15	2.420

Remarks—In its characteristics, the material referred to this species shows no differences compared to other Late Pleistocene populations from Bulgaria, for example, those from caves in the nearby karst region near Karlukovo [38,83]. *L. lagurus* appears in Europe during the late Holsteinian Stage, ca 300–250 Kya (MIS 7–8) [8]. Since the species is abundant across all layers of Biozone A, this age is the lowermost possible temporal boundary for this biozone.

Genus *Prolagurus* Kormos, 1938

Prolagurus pannonicus (Kormos, 1930)

(Figure 52)

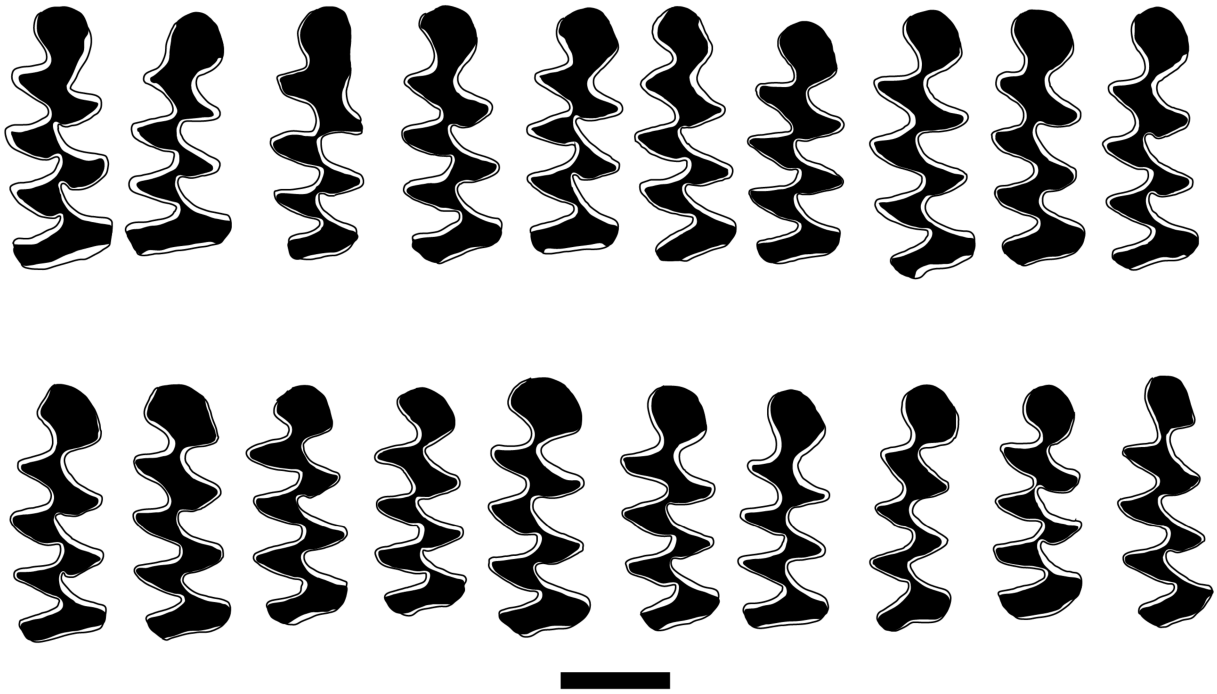


Figure 52. *Prolagurus pannonicus.* Biozone B, right m1s in occlusal view. Scale bar = 1 mm.

Studied material (m1)—Biozone B. L13c: 7; L13b: 26; L13a: 15; L12: 6.

Description (m1)—The enamel band is positively differentiated, but in some specimens, this differentiation is not well-pronounced. The anterior cap is significantly shortened and simplified compared to *Lagurus arankae*: the BRA3 (prism fold) is widened, shifting BSA4 further mesially. The enamel band terminates slightly anterior to LSA5 and resumes on the lingual side at BRA4, so the obliquely outwardly directed anterior surface is enamel-free; T4 and T5 are always broadly confluent, forming a rhombus whose longitudinal axis is obliquely mesiolingually directed. The anterior cap is broadly confluent with the rhombus T4 + T5 (*ternopolitanus*-morphotype) or separated from it by a narrow neck (*pannonicus*-morphotype).

Measurements [mm] and indices [%]—N = 15, X, SD. L: 2.36, 0.11; W: 0.91, 0.08; a/L: 46.9, 2.14; c/W = 29.2; 2.8; b/W = 11.5, 2.9.

Remarks—The more frequent morphotype *pannonicus* fits the amended diagnosis of *Prolagurus pannonicus*, and the designated paralectotype [172], figured on p. 182, Figure 67—3 in [84]. It is shown that the connection between AC2 and the T4–T5 complex decreases over time from 50% in the older fauna of Deutsch-Altenburg 2 C to 75% in the younger faunas of Deutsch-Altenburg 4 B and 4 A, where the "narrow-necked" types increase to 75% and 100%, respectively [22]. Although the small sample from Kozarnika does not permit a detailed stratigraphic analysis in this regard, it can be said that, in biozone B, a highly progressive form is represented, dominated by the morphotype *pannonicus*. The

stratigraphic range of *P. pannonicus* is not well known, as it is often not distinguished from *L. transylvanicus*. The transition between *P. ternopolitanus* and *P. pannonicus* likely occurred immediately before the Jaramillo Subchron, and the upper stratigraphic extension of *P. pannonicus/L. transylvanicus* is tentatively placed around the Brunhes/Matuyama boundary [8]. Data from Kozarnika indicate that both species definitely occur after this date.

Genus *Villanyia* Kretzoi, 1956

Villanyia cf. *exilis* Kretzoi, 1956

(Figure 44B,B1)

Studied material—Layer 11d: 1 m1.

Description—No cement. There are two roots. The enamel is not differentiated. The enamel-free areas do not reach the occlusal surface. The reentrant angles are broadly rounded. The dentine fields of the main triangles, T1–T3, are widely confluent. They are separated from the anteroconid complex, whose dentine fields are also broadly fused. The anterior cap is rounded and slightly asymmetrical.

Measurements [mm]—L = 2.17, W = 0.95, a = 0.87

Remarks—The height of the dentine tracts is greater than that of specimen GIH V-12702 Vt95#2 from Villány-5, which is accepted as the genotype and type of *V. exilis* [178]. Considering the age of layer 11d, it can be assumed that the form from Kozarnika is more progressive than that from the type locality. The limited material does not allow for more detailed comparisons, so the determination is tentative. The last occurrences of *Villanyia exilis* are recorded in localities of the latest Pliocene or earliest Pleistocene age together with *Mimomys tornensis*, *M. pitymyoides*, *Borsodia*, and *Microtus deucalion* [8].

Family Muridae Illiger, 1811

Genus *Apodemus* Kaup, 1829

Species belonging to two subgenera, *Sylvaemus* Ognev, 1924, and *Karstomys* Martino, 1939, currently occur in Europe. The latter subgenus includes the modern species *Apodemus epimelas*, which is distinguished by its larger size and several features of tooth structure. Species in the subgenus *Sylvaemus* are very similar to one another, and species identification is generally challenging. For fragmentary remains, characteristic of the fossil record, this problem becomes even more pronounced. Both fossil and recent species show considerable variability in size and morphology over time [179,180]. According to the fossil record of Central Europe [181,182], the genus is absent from MIS 3–MIS 2 assemblages but occurs regularly during the Late Vistulian. The Late Vistulian remains belong to *A. flavicollis*, which dominates the fossil record until the Late Holocene. *A. uralensis* accompanies it until the late Boreal, when it disappears from the fossil record. *A. sylvaticus* appears in the Early Holocene and remains relatively rare until the Atlantic period. *A. agrarius* appears sparsely from the Boreal, with maximum frequency during the post-Neolithic period. The Late Pleistocene fossil record from Cave 16 in Northwestern Bulgaria shows similar patterns regarding *A. uralensis*, *A. sylvaticus*, and *A. flavicollis* [38,101]. During a warm period, probably at the end of the Eemian, two species, clearly distinguishable in size, were abundant in the deposits. The smaller one was identified as *A. uralensis* (*microps*), and the larger one as *A. flavicollis*. In the upper part of the deposits, which covers a cold climatic phase from the end of the Pleistocene, only *A. uralensis* is represented by isolated remains. The abundant material from the lower part of the deposits of Cave 16 enabled us to identify features of the occlusal surface in *A. flavicollis* that clearly distinguish it from *A. sylvaticus*, despite the broad overlap in size. *A. flavicollis* has a relatively simplified tooth structure, especially evident on the first lower molar. The antero-central cusp (acc) of m1 is comparatively small and rarely protrudes forward. The accessory cusps on the labial cingulum are often reduced. In this respect, this species is more similar to *A. uralensis* than to *A. sylvaticus*. However, the two species (*A. uralensis* and *A. flavicollis*) are clearly

distinguishable by size. *A. sylvaticus* usually has a well-developed acc, and the lateral accessory cusps on the labial cingulum are well developed. The differences in the upper teeth are less apparent, and those of intermediate size cannot be definitively attributed to either species. Based on these observations, it was concluded that *A. sylvaticus* is absent from the deposits of Cave 16 [38].

The fossil forms from the Pliocene and Early and Middle Pleistocene of Europe are often not clearly diagnosed. Their actual status and relationships to extant taxa, and consequently, the history of extant species, should be considered somewhat unclear. *A. atavus* Heller, 1936, is a species described from Gundersheim (MN 16), Germany, and also reported in Villanyian and Biharian localities within Germany and Austria [97]. According to some authors, the geographic range of *A. atavus* extends across the entire Palaearctic region [183,184], from the latest Miocene to the Early Pleistocene [185]. The species is characterized by consistently well-developed t7 and t12, t3 with a short backward-directed spur, separated t4 and t7 until a relatively advanced stage of wear, three roots on the slender M1, a consistently well-developed accessory cusp, and a variable number of labial accessory cusps on the m1. Since no m2 from the type locality is available, Rietschel and Storch [186] added the large posterior accessory cusp (c1) of m2 as a diagnostic trait; however, in larger samples, this trait appears to be highly variable [185]. The species is considered a direct ancestor of the living species *A. sylvaticus* [184,186,187], because the only difference between them is the more prominent t12 in M1 and M2 in *A. atavus*. Other researchers considered *A. atavus* the common ancestor of *A. sylvaticus* and *A. flavicollis* in Europe during the Early Pleistocene [184]. According to Marchetti et al. [57], *A. atavus* could be an Early Pleistocene species present in Europe up until the Late Biharian.

A. dominans Kretzoi, 1959 (type locality Csarnóta 2; MN 15b), synonymized later with *A. occitanus* [188], was reported in Europe from the latest Miocene to the Pleistocene. The species shows some primitive features, including a prominent t12 on M1 and M2, upper molars with three roots, and a rearward-facing c1 on m1 and m2 [187]. Some authors consider it an ancestor of *A. flavicollis* [179,186]. Since *A. flavicollis* is slightly larger than *A. atavus*, in analogy with the current situation, the first species is considered the ancestor of modern *A. flavicollis*, and the second is considered the ancestor of *A. sylvaticus*. However, Fejfar and Storch [187] argued that the minor size differences between the two forms are not sufficient to support their species status, considering *Apodemus dominans* as a junior synonym of *Apodemus atavus*, an opinion later accepted by other authors [184,186].

A. maastrichtiensis van Kolfschoten, 1985, described from the Middle Pleistocene of Maastricht-Belvedere, is a fossil form characterized by a small size. The other diagnostic features include the M1 with mainly three roots, t9 smaller than t6, and a narrow, elongated t7. The t3 of the M2 is incipient or absent, and t7 and t9 are small. The acc of m1 is isolated in most of the specimens. The m2 antero-labial cusp is small. It differs from *A. uralensis* by the reduced t3 of M2 and the t9 of M1 and M2.

Based on molar size, the material from Kozarnika forms two well-defined groups (Figure 53). The group with large molars, above the upper limit of the modern species *Apodemus sylvaticus* and *A. flavicollis*, undoubtedly refers to the large representatives of the genus, members of the subgenus *Karstomys*. The small-sized group encompasses the range of variability among the three modern species in the subgenus *Sylvaemus*: *A. uralensis*, *A. sylvaticus*, and *A. flavicollis*. A significant part of the teeth falls below the range of variability of the modern *A. sylvaticus*. It undoubtedly belongs to a small species, similar to the modern *A. uralensis*. Since there is a wide overlap in size between the three *Sylvaemus* species, for species determination, in addition to size, the features of the structure of the occlusal surface were used in the context of existing knowledge about the morphological peculiarities of the teeth in modern and fossil representatives of the genus, briefly outlined above.

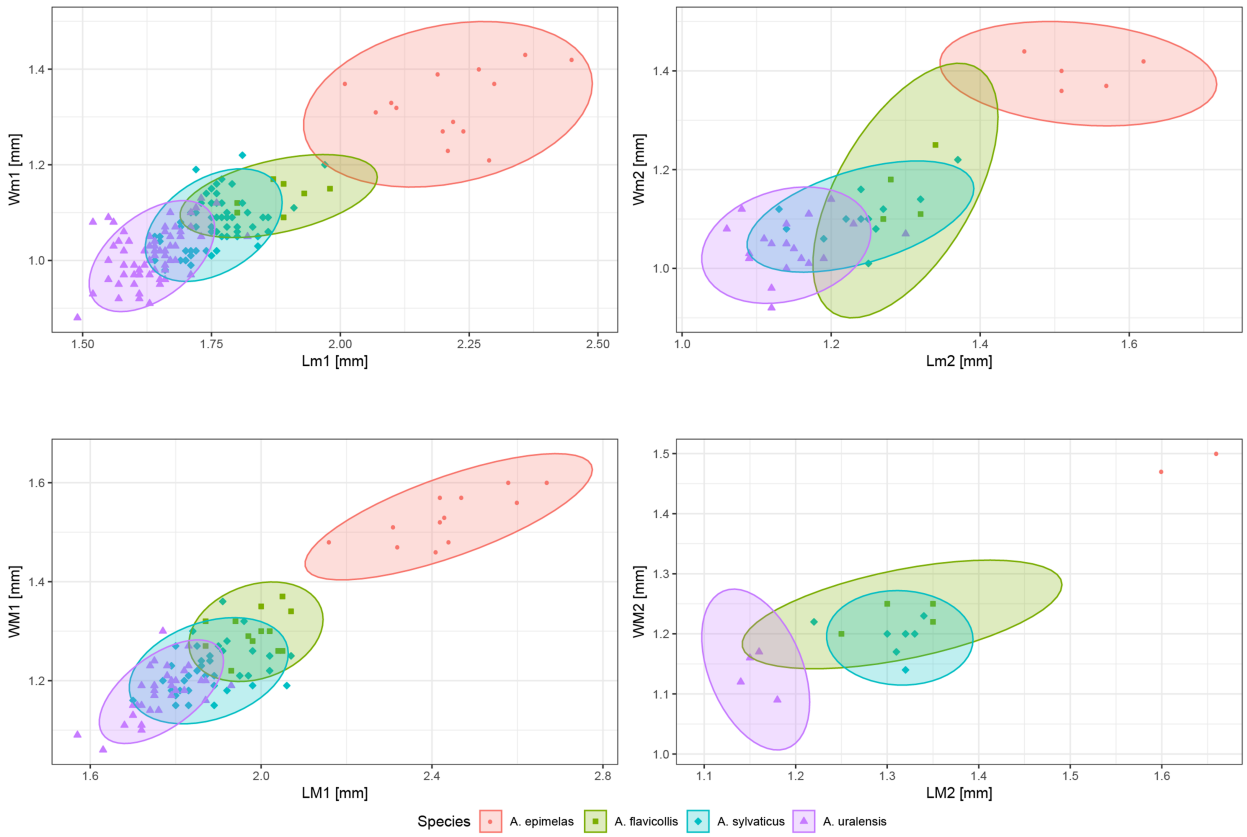


Figure 53. Scatter plot diagrams and 95% confidence ellipses of length (L) versus width (W) of upper (M1, M2) and lower (m1, m2) molars of *Apodemus* species from Kozarnika.

Apodemus uralensis Pallas, 1811

Figure 54I–K and Figure 55G,J–L)

Studied material—Biozone B: L11a: 1 m2, 24 m1, 6 m2 10 M1; L11a1: 1 M1, L11b: 2 m1, 1 M1; L12: 7 m1, 3 m2, 7 M1, 1 M2; L12: 7 m1, 3 m2, 7 M1, 1 M2; L13a: 6 m1, 5 m2, 4 M1, 1 M2; L13b: 4 m1, 2 m2, 5 M1, 1 M2; L13b: 4 m1, 2 m2, 5 M1, 1 M2; L13c: 12 m1; 3 m2, 6 M1, 1 M2. Biozone A: L10a: 1 m1, 1 M1; L5b: 1 m1, L5c: 2 m1, L6/7: 4 m1, 1 m2, 1 M1; L9ab: 1 m1.

Description—Teeth that fall within the lower limit of variability for *A. sylvaticus* or below were attributed to this species.

M1. t7 is small, often elongated, and rarely appears as a small conical tubercle. t12 is absent or expressed only faintly in unworn teeth. t7 and t9 are not connected, except in teeth with advanced wear. In most cases, t9 is less developed than t6. Among the 24 teeth with preserved roots in this size group, 17 have three roots, and the remaining six have four.

m1. The acc is usually minor, not isolated, and does not protrude in front of the line connecting the front walls of the anterior, labial, and lingual tubercles. The additional tubercles of the labial cingulum, located in front of c1, are weakly expressed or absent.

m2. The anterolabial tubercle is small or moderately developed.

Measurements—Table 34.

Remarks—Teeth falling below the lower limit of variability in *Apodemus sylvaticus* are very similar in occlusal-surface structure to those of the fossil species *A. maastrichtiensis* and the modern *A. uralensis*. They differ from the fossil species in lacking an isolated acc of m1. In terms of the great relative proportion of teeth with three roots, they are very similar to the Late Pleistocene population from the nearby Cave 16, which no doubt belongs to the modern species [38].

Table 34. Measurements [mm] of molars of *Apodemus* species from Kozarnika.

Species	Molar	N	L				W			
			X	SD	Min	Max	X	SD	Min	Max
A. uralensis	m1	66	1.63	0.060	1.49	1.82	1.01	0.054	0.88	1.13
	m2	22	1.14	0.054	1.06	1.30	1.05	0.053	0.92	1.14
	M1	36	1.77	0.071	1.57	1.93	1.18	0.050	1.06	1.30
	M2	4	1.16	0.017	1.14	1.18	1.14	0.037	1.09	1.17
A. sylvaticus	m1	60	1.76	0.064	1.64	1.97	1.08	0.054	0.98	1.2
	m2	11	1.25	0.06	1.14	1.37	1.11	0.055	1.01	1.2
	M1	36	1.88	0.079	1.7	2.07	1.22	0.049	1.15	1.4
	M2	7	1.31	0.04	1.22	1.34	1.19	0.03	1.14	1.2
A. cf. *flavicollis*	m1	6	1.86	0.053	1.8	1.93	1.13	0.05	1.09	1.2
	m2	5	1.27	0.082	1.13	1.34	1.15	0.1	1.1	1.3
	M1	9	2	0.053	1.93	2.07	1.27	0.04	1.19	1.3
	M2	3	1.5	0.156	1.35	1.66	1.32	0.2	1.22	1.5
A. epimelas	m1	14	2.21	0.122	1.98	2.45	1.31	0.083	1.15	1.43
	m2	5	1.53	0.062	1.46	1.62	1.40	0.033	1.36	1.44
	M1	12	2.44	0.138	2.16	2.67	1.53	0.050	1.46	1.60
	M2	1	1.60				1.47			

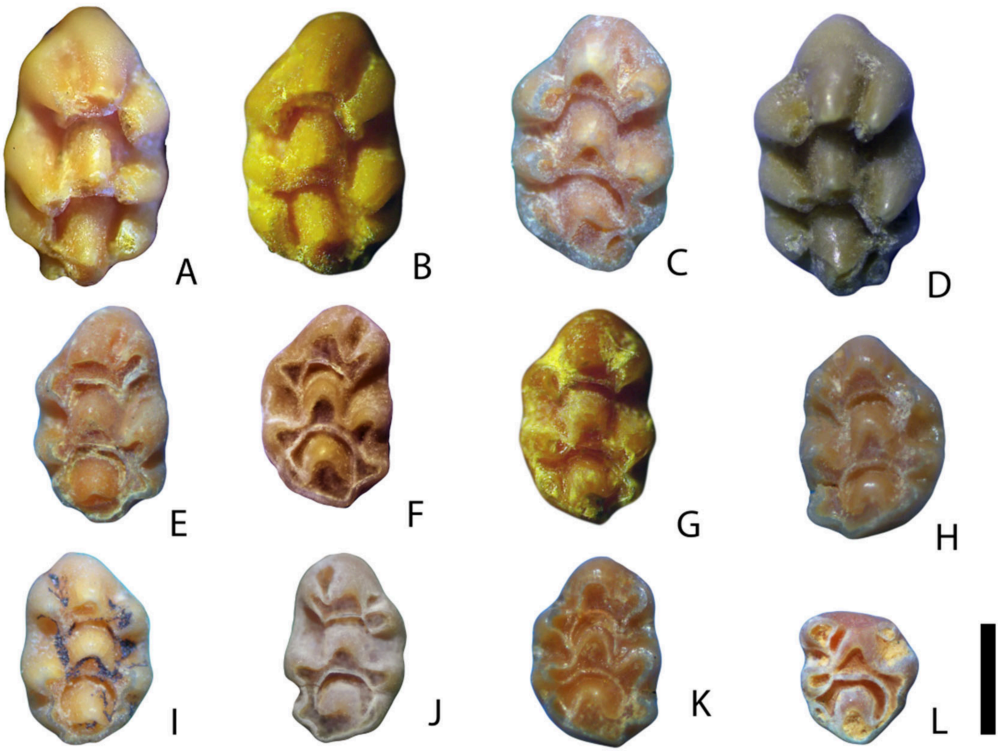


Figure 54. *Apodemus epimelas* (**A**–**C**), *Apodemus flavicollis* (**E**), *Apodemus sylvaticus* (**F**–**H**,**L**), *Apodemus uralensis* (**I**–**K**). Occlusal views of upper molars ((**A**–**K**) M1, (**L**) M2). (**A**)—kz1422, L11b, (**B**)—BG-IBER-FMC-000004068, L11a; (**C**)—BG-IBER-FMC-000017756, L11b; (**D**)—BG-IBER-FMC-000019919,

L12, (**E**)—BG-IBER-FMC-000019917, L12, (**F**)—BG-IBER-FMC-000019924, L12, (**G**)—BG-IBER-FMC-000004067, L11a, (**H**)—BG-IBER-FMC-000018409, L13a, (**I**)—BG-IBER-FMC-000017096, L12, (**J**)—BG-IBER-FMC-000016899, L12, (**K**)—BG-IBER-FMC-000018416, L13a, (**L**)—BG-IBER-FMC-000019940,L12. Scale bar = 1 mm.

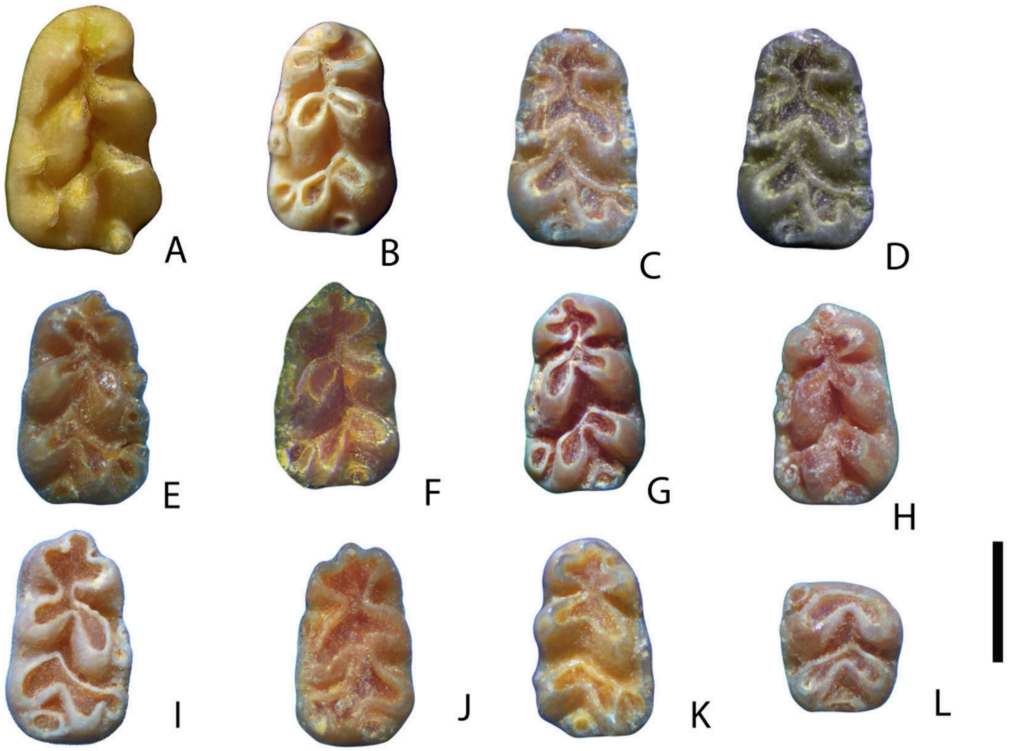


Figure 55. *Apodemus epimelas* (**A**), *Apodemus* cf. *flavicollis* (**C**,**D**), *Apodemus sylvaticus* (**B**,**D**–**F**,**H**,**I**), *Apodemus uralensis* (**G**,**J**–**L**). Occlusal views of lower molars ((**A**–**J**) M1, (**L**) M2). (**A**)—BG-IBER-FMC-000005279, L11b; (**B**)—BG-IBER-FMC-000007486, L11a1; (**C**)—BG-IBER-FMC-000019916-1,L12; (**D**)—BG-IBER-FMC-000019916-2, L12; (**E**)—BG-IBER-FMC-000017095, L12; (**F**)—BG-IBER-FMC-000000012, L11b; (**G**)—BG-IBER-FMC-000018422, L13a; (**H**)—BG-IBER-FMC-000017097, L12; (**I**)—BG-IBER-FMC-000017759, L11b; (**J**)—BG-IBER-FMC-000019932, L12; (**K**)—BG-IBER-FMC-000018413, L13a; (**L**)—BG-IBER-FMC-000019941, L12. Scale bar = 1 mm.

Apodemus sylvaticus (Linnaeus, 1758)

(Figure 54F–H,L and Figure 55B,D–F,H,I)

Studied material—Biozone B. L11b: 1 m2; L11b: 1 M2, 4 M1, 5 m1; L12: 1 M2, 2 m2, 9 M1, 16 m1; L13a: 2 m2, 5 M1, 9 m1; L13b: 3 M2, 5 m2, 6 M1, 11 m1; L13c: 1 m1, 1 M1; Biozone A. L9ab: 4 m1.

Description—M1. t7 is well developed. t12 is absent or very weakly expressed in unworn teeth. t7 and t9 are widely separated except in teeth in very advanced stages of wear. t9 is less developed than t6 in only about half of the teeth in this size group. The posterior spur on t3 is absent or short and weakly expressed. Of the 20 teeth with preserved roots, six have three roots, while the remaining have four.

M2. t3 is large. t7 can be observed on only one tooth and is well developed. t9 is small on the two teeth where it is visible.

m1. acc is most often well developed, isolated, and protruding forward, well in front of the line connecting the anterior walls of the anterior, labial, and lingual tubercles. The accessory tubercles of the labial cingulum, located anterior to c1, are well expressed.

m2. The anterolabial tubercle is most often moderately developed.

Measurements—Table 34.

Remarks—The molars in this size group differ from those of the similarly sized fossil species, *Apodemus atavus*, in that they have predominantly four roots and lack t12 and the posterior spur on t3 of M1. Apparently, the Kozarnika population is more evolutionarily advanced and is therefore considered a modern species. The presence of a three-rooted M1 can be interpreted as a sign of primitiveness.

Apodemus cf. *flavicollis* (Melhior, 1834).

(Figures 54E and 55C,D)

Studied material—Biozone B. L13—Lower: 3 m1; L13c: 1 M2, 3 m2, 4 M1; L13b: 1 M1, 5 M2, 1 m1, 2 m2; L13a: 1 M1, 1 m2, 1 m1, 2 M2, 6 m; L12: 1 M1; L12: 1 m2, 3 m1; L11b: 2 M1, 16 m; L11a: 1 m1, 3 m2; Biozone A. L9ab: 1 m1.

Description—M1—larger than those in modern *A. sylvaticus*; t1 is displaced posteriorly relative to t2–t3; t4–t7 are separated, rarely connected. Out of seven M1, four possess 3 roots, two possess 4, and one possesses 5 roots.

M2—t1 often extends posteriorly through a small enamel protrusion; the posterior cingulum is often absent or reduced to a small enamel bump along the edge of t8. t9 is reduced.

m1. The acc is usually minor or moderately developed and does not protrude beyond the line connecting the front walls of the anterior, labial, and lingual tubercles. The additional labial cingular tubercles located in front of c1 are poorly developed.

m2—reduced marginal cingulum.

Measurements—Table 34.

Remarks—The large teeth and the relatively simple structure of m1 are similar to those of the recent *Apodemus flavicollis* and the fossil *A. dominans*. They differ from the latter species in having a relatively large proportion of M1 with four roots and in lacking t12 on M1. Since the sample is very small, it is difficult to assess the taxonomic status of the available molars; therefore, their assignment to modern species is tentative.

Apodemus epimelas Nehring, 1902

(Figure 54A–C and Figure 55A)

Studied material—Biozone B. L13—Lower: 1 M1; L13c: 1 M1, 1 M2; L13c: 2 m1, 9 m; L13b: 2 m2, 4 m1, 4 M1, 30 m; L13a: 2 m1, 3 M1, 26 m; L12: 1 m1, 2 M1, 2 m2, 10 m; L11c: 2 m; L11b: 5 M1, 6 m1, 9 m; L11a1: 1 m2, 18 m; L11a: 1 m2, 3 M1, 4 m1, 10 m.

Description—M1. t7 is well developed, in some cases large; t12 is strongly expressed; t7 and t9 are widely separated; 4 roots.

M2. t12 and t3 are well developed.

m1. The crown is quite high. The development of the acc and labial accessory tubercles varies, but they are most often moderate or well-pronounced.

m2. The anterolabial tubercle varies in size, ranging from poorly developed to very large.

Measurements—Table 34.

Remarks—In addition to its large size, the presence of T12 on M1 and M2 indicates that this material belongs to the subgenus *Karstomys*, which includes two recent species: *Apodemus mystacinus* and *A. epimelas*. Their specific identity has been debated for a long time. However, modern genetic data indicate that they are distinct allopatric species that diverged more than 4 million years ago [189]. Therefore, the remains were attributed to the European species *A. epimelas*.

Family Spalacidae Gray, 1821

Genus *Nannospalax* Palmer, 1903

The terminology of the morphology of the occlusal surface of lower and upper molars is shown in the Figure 56.

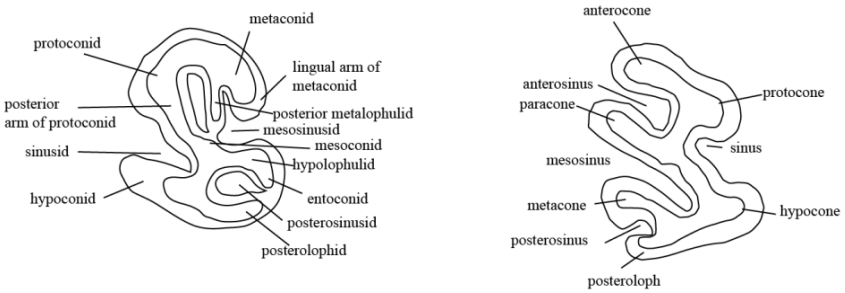


Figure 56. Terminology of upper (M1) and lower (m1) molars of Spalacidae, compiled from [17–19].

Nannospalax sirakovi sp. nov.
(Figures 57–59)

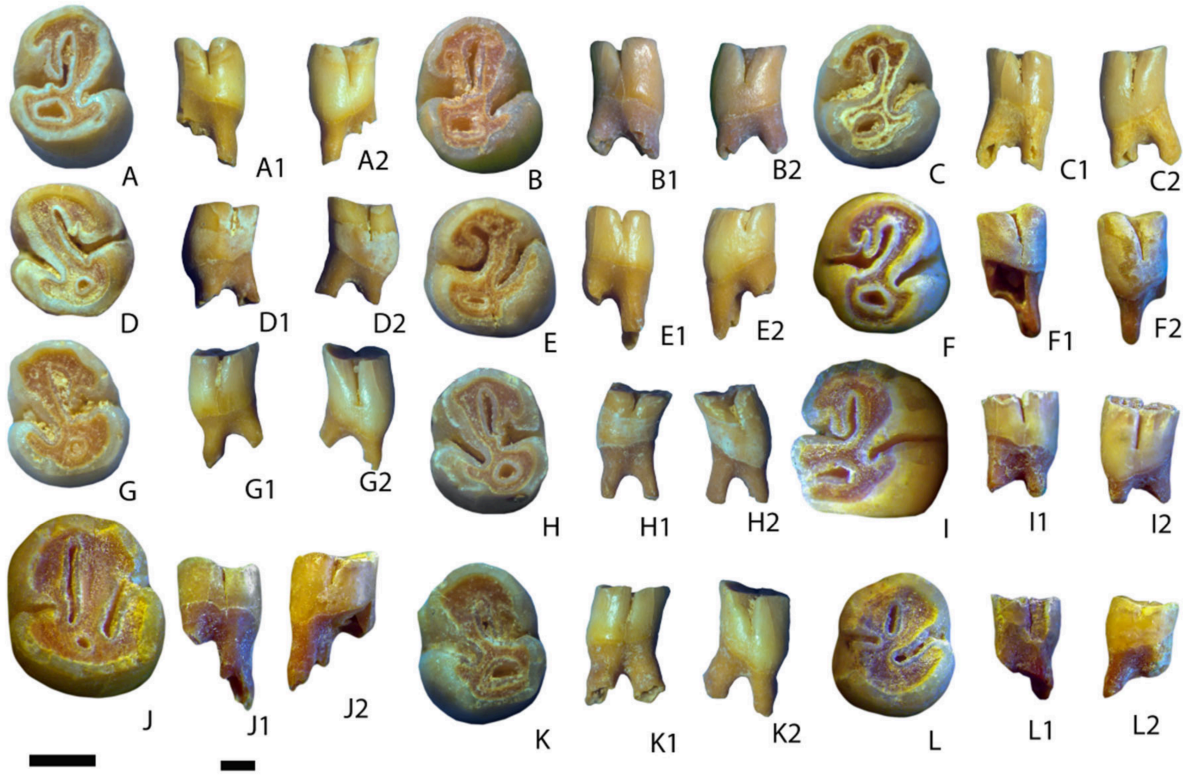


Figure 57. First lower molars of *Nannospalax sirakovi* sp. nov. (**A**), holotype; (**B**–**L**), paratypes. Scale bars represent 1 mm. (**B**)—BG-IBER-FMC-000017040, L12; (**C**)—BG-IBER-FMC-000020295, L12; (**D**)—BG-IBER-FMC-000018778, L13a; (**E**)—BG-IBER-FMC-000020288, L12; (**F**)—BG-IBER-FMC-000015033, L11b; (**G**)—BG-IBER-FMC-000020309, L12; (**H**)—BG-IBER-FMC-000020298, L12; (**I**)—BG-IBER-FMC-000015030, L11b; (**J**)—BG-IBER-FMC-000015032, L11b; (**K**)—BG-IBER-FMC-000020296, L12; (**L**)—BG-IBER-FMC-000015034, L11b. (**A**–**L**)—occlusal, (**A1**–**L1**)—lingual, (**A2**–**L2**)—buccal views. Scale bars = 1 mm.

Derivato nominis. Dedicated to Dr. Nikolai Sirakov (Archaeological Institute, Sofia), who co-directed fieldwork at Kozarnika and made significant contributions to the collection of small-mammal remains during excavations from 2000 to 2009.

Holotype: m1, catalog number BG-IBER-FMC-000020292 (Figure 57A).

Diagnosis. Small size (holotype, Lm1 × Wm1 = 2.1 × 1.69 mm). On the first lower molar, the posterior metalophulid is, in most cases, long and almost parallel to the longitudinal axis of the tooth until the most advanced stages of erosion (Figure 57A,F,I). In the process of tooth wear, it merges with the hypolophulid, in which the inner part of the mesosinusid closes in the form of an enamel island, elongated in the longitudinal direction

(Figure 57B,H,J,L). The posterosinusid is deep and extends well along the height of the crown. As a result, the enamel islet formed by the inner part of the posterosinusid remains large until the latest stages of crown wear.

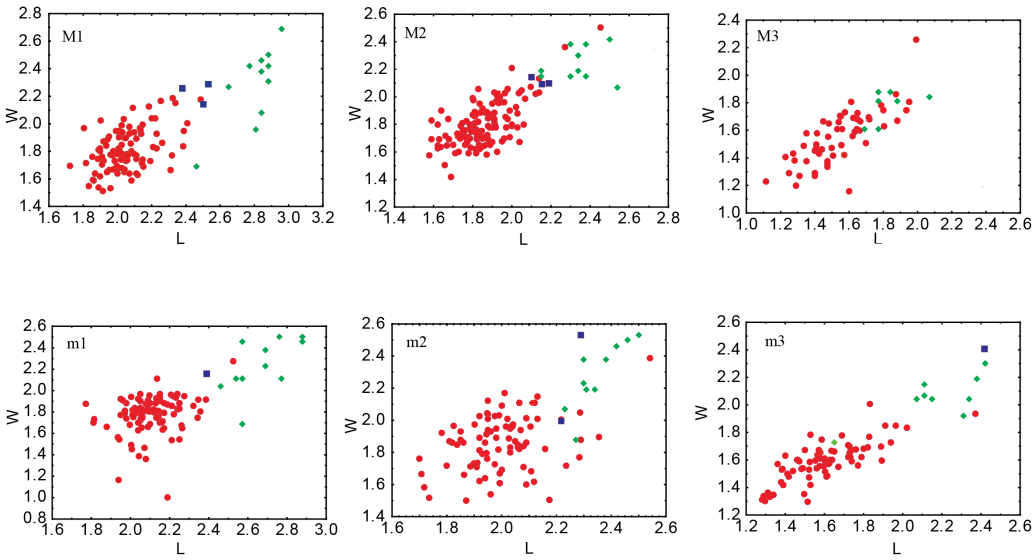


Figure 58. Scatter plot diagrams of length (L, mm) versus width (W, mm) for upper (M1–M3) and lower (m1–m3) molars in *Nannospalax sirakovi* sp. nov. from Biozone B2 of Kozarnika (red circles), *N. leucodon* from Biozone A1 (blue squares), and recent specimens from Bulgaria (green diamonds).

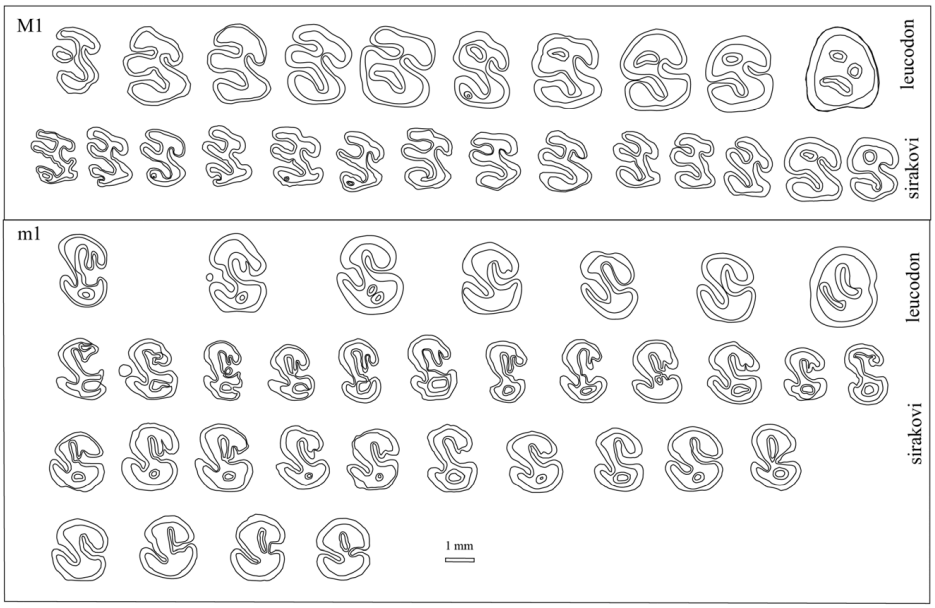


Figure 59. Variability in the structure of the occlusal surface of M1 and m1 in *Nannospalax sirakovi* from Kozarnika and the modern species *N. leucodon* from Bulgaria. For comparability, the upper teeth are rotated to the right, and the lower ones to the left. The individual's age, or the degree of abrasion of the occlusal surface, increases from left to right. Scale bar = 1 mm.

Differential diagnosis. Smaller than the Pliocene *Nannospalax macoveii* (Simionescu, 1930) and *N. odessanus* Topacevski, 1969; the Middle Pleistocene *Spalax chalkidikae* Kretzoi, 1977; the modern and Late Pleistocene *N. leucodon* (Nordmann, 1840), (Figure 58); and the modern *N. xanthodon* (Nordmann, 1840). The new species has a more complex structure of the first lower molar compared to *N. leucodon* and *N. xanthodon*. In these species, the posterior metalophulid is less developed. It disappears quickly with the wear of the crown,

in which a large anterior island, elongated anteroposteriorly, is rarely formed, as in the new species. The postero-lingual enamel islet forms early, is smaller, and disappears quickly with tooth abrasion. The structure of the lower molar of the new species somewhat resembles that of *N. ehrenbergi* (Nehring, 1897). However, in the latter species, in young individuals, the posterosinusid remains open, and the islet is formed at the latest stages of erosion. The posterior metalophulid in *N. ehrenbergi* is shorter; therefore, the anterior enamel islet is smaller and not elongated anteroposteriorly.

Locus typicus—Kozarnika Cave, NW Bulgaria.

Stratum typicum—Kozarnika, Biozone B, layer 12, Late Biharian.

Figured paratypes—Figure 57B–L.

Further material—Biozone B. L13ower: 8 m; L13c: 1 m1; L13c: 1 m3; L13c: 114 m; L13c: 2 M1; L13b: 400 m; L13a: 15 m1; L13a: 2 m2; L13a: 1 m2; L13a: 6 m3; L13a: 296 m; L13a: 5 M1; L13a: 1 M1; L13a: 5 M2; L13a: 5 M3; L12: 12 m1; L12: 10 m1; L12: 1 m1; L12: 12 m2; L12: 5 m2; L12: 1 m2; L12: 10 m3; L12: 1 m3; L12: 1 m3; L12: 379 m; L12: 11 M1; L12: 1 M1; L12: 9 M1; L12: 2 M1; L12: 1 M1; L12: 22 M2; L12: 9 M2; L12: 1 M2; L12: 1 M2; L12: 3 M2; L12: 1 M3; L12: 8 M3; L12: 1 M3; L11c: 117 m; L11b: 34 m1; L11b: 6 m1; L11b: 10 m1; L11b: 1 m1; L11b: 1 m1; L11b: 7 m1; L11b: 56 m2; L11b: 1 m2; L11b: 6 m2; L11b: 37 m3; L11b: 2 m3; L11b: 1 m3; L11b: 7 m3; L11b: 316 m; L11b: 39 M1; L11b: 3 M1; L11b: 2 M1; L11b: 2 M1; L11b: 3 M1; L11b: 1 M1; L11b: 1 M1; L11b: 20 M1; L11b: 65 M2; L11b: 1 M2; L11b: 1 M2; L11b: 2 M2; L11b: 1 M2; L11b: 12 M2; L11b: 25 M3; L11b: 8 M3; L11a1: 1 m1; L11a1: 1 m3; L11a1: 1 m3; L11a1: 369 m; L11a1: 2 M1; L11a: 6 m1; L11a: 1 m1; L11a: 3 m2; L11a: 13 m3; L11a: 1 m3; L11a: 342 m; L11a: 11 M1; L11a: 9 M2; L11a: 2 M2; L11a: 7 M3.

Measurements—Table 35.

Table 35. Measurements [mm] of molars of *Nannospalax* species from Kozarnika.

Species	Molar	N	L				W			
			X	SD	Min	Max	X	SD	Min	Max
N. leucodon	lm1	4	2.56	0.135	2.39	2.72	2.15	0.126	2.02	2.32
	lm2	4	2.33	0.106	2.22	2.47	2.23	0.221	1.99	2.53
	lm3	2	2.27	0.211	2.12	2.42	2.12	0.409	1.83	2.41
	uM1	14	2.54	0.129	2.25	2.75	2.21	0.135	1.93	2.40
	uM2	12	2.16	0.130	1.92	2.42	2.14	0.104	2.01	2.36
	uM3	1	1.61	0.000	1.61	1.61	1.81	0.000	1.81	1.81
N. sirakovi	lm1	100	2.1	0.13	1.7	2.5	1.8	0.176	1.0	2.3
	lm2	87	1.99	0.145	1.70	2.54	1.85	0.175	1.45	2.39
	lm3	79	1.63	0.220	1.28	2.37	1.60	0.160	1.29	2.15
	uM1	100	2.04	0.140	1.72	2.49	1.79	0.235	0.00	2.19
	uM2	132	1.87	0.146	1.58	2.45	1.80	0.154	1.42	2.50
	uM3	55	1.55	0.200	1.11	1.99	1.55	0.197	1.16	2.26

Description—The variability of the occlusal surface of the first lower and first upper molars is presented in Figures 57 and 59.

M1. The paracone remains free until the late stages of tooth abrasion. The posterosinus in unworn teeth is well expressed. In moderately worn teeth, it closes into a mark that disappears later during the crown wear than in the modern species. Three roots.

M2. The anterior enamel islet is formed in the early stages of tooth wear. The metacone fuses with the posteroloph, forming a posterior mark (preserved up to old age) in the very

early stages of tooth wear. The tooth has one outer and one inner reentrant fold. During wear, the outer fold closes first, before the inner one. Three roots—a massive inner and two weakly developed outers.

M3. Even in young specimens, the protocone and hypocone fuse, resulting in a C-shaped occlusal surface that, as the crown wears away, becomes a centrally located island. The tooth has two roots, and in old specimens, where the roots are well developed, the anterior one is often massive and results from the fusion of two roots.

m1. The mesoconid is mostly absent, but in some young specimens it may be present as a protrusion on the anterior wall of the entoconid (Figure 57). The fusion of the entoconid and metaconid and the formation of an anterior enamel islet occur at very advanced stages of tooth erosion. The entoconid and posterior metalophulid fuse during the earliest stages of abrasion, resulting in a large enamel island that persists throughout most of life. It has two roots.

m2. The entoconid fuses with the posterolophid in the early stages of wear, resulting in a posterior enamel island present throughout life. It has two roots.

m3. The chewing surface is S-shaped. Closure of the internal invading fold into an islet occurs only at very late stages of wear. Three roots, one massive posterior and two small anterior.

Remarks—Regarding the structure of the molar occlusal surface, especially that of the first lower molar, the new species occupies an intermediate position between the Pliocene species *Nannospalax macoveii* and the modern species *N. leucodon* and *N. xanthodon*. It shows some similarity to *N. odessanus* in this regard, as evidenced by the massive complex of the hypolophulid and entoconid, as well as the large posterior islet, which persists until the latest stages of tooth wear. However, unlike the Pliocene species, the new species has three roots on M1, more closely resembling modern species. According to Topachevsky [17], the Pliocene species *N. odessanus* is the ancestral form of the modern *N. leucodon* and *N. xanthodon*. In this context, based on its distinct tooth-structure features, particularly those of the first lower molar, the new species can be viewed as an intermediate stage in this phylogenetic lineage. Conversely, genetic data [189] suggest that the divergence between *Nannospalax xanthodon* and *N. leucodon* occurred between 11.88 and 26.10 Mya. Therefore, *N. odessanus* is likely a primitive side branch, not directly related to either of the recent species. The resemblance of the new species to *N. odessanus* in some features indicates a lower evolutionary level rather than an ancestor-descendant relationship.

Nannospalax leucodon Nordmann, 1840

(Figure 60)

Studied material—Biozone A. L10b: 1 m; L10a: 1 M3,1 m2,1 m1,3 M1, 3 M2, 10 m; L9c: 2 m; L9ab: 1 m3, 2 m, 2 m2, 3 m1, 8 M2, 9 M1; L6/7: 5 m; L5c: 7 m; L5b: 1 m3; L5b: 2 M1, 21 m; L5a:1 m,1 m2, 3 M2.

Description—m1. The available tooth from layer 10a, which shows a moderate level of crown erosion, is intermediate in size between the modern species and the new species from Biozone B, described above as *N. sirakovi*. The posterior metalophulid is well developed, and the posterior enamel island is small, situated on the medial axis of the occlusal surface.

m2 has a simplified S-shaped occlusal surface.

m3. Tooth erosion yields an e-shape.

M1. Simplified structure. The available teeth are in an advanced stage of erosion, and the paracone and anterocone are fused or almost fused. The mesosinus is open.

M2. The paracone fuses with the anterocone, and the anterior mark appears relatively early.

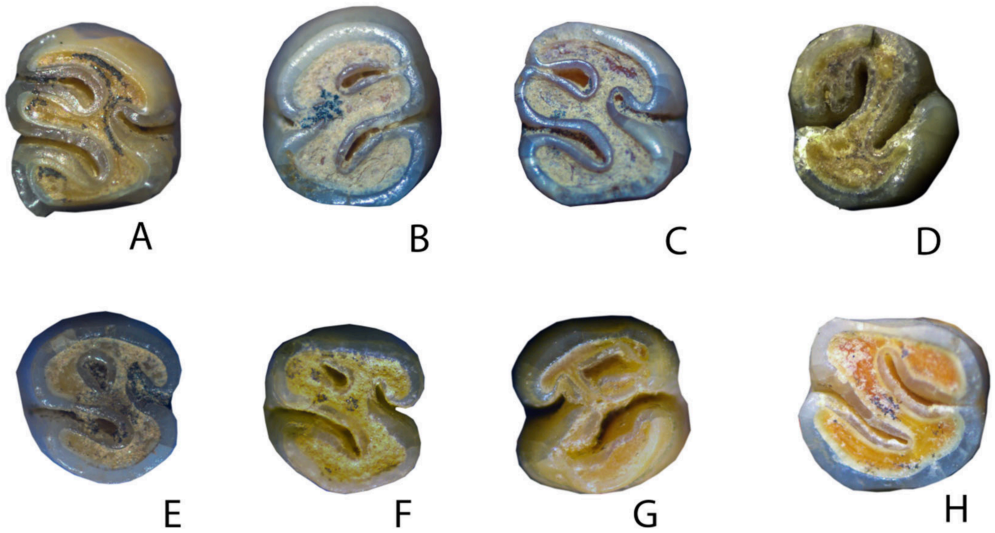


Figure 60. *Nannospalax leucodon*, molars in occlusal view. (**A**)—M1, BG-IBER-FMC-000008835, L5b; (**B**)—M1, BG-IBER-FMC-000013711, L10a; (**C**)—M1, BG-IBER-FMC-000015436, L5b; (**D**)—m1, BG-IBER-FMC-000013519, L10a; (**E**)—M2, BG-IBER-FMC-000009185, L5a; (**F**)—M2, BG-IBER-FMC-000009525, L5a; (**G**)—M2, BG-IBER-FMC-000013517, L10a; (**H**)—m2, BG-IBER-FMC-000013518, L10a. Scale bar = 1 mm.

Measurements—Table 35.

Remarks—The available molars from the upper layers of Kozarnika (Biozone A) differ from those in Biozone B, belonging to *Nannospalax sirakovi* sp. n., by their larger size (Figures 58 and 59) and a simplified occlusal surface. They are very similar to the Late Pleistocene *N. leucodon* from Cave 16 [38] and the comparative material of the modern species from Bulgaria.

Family Gliridae Muirhead, 1819

Subfamily Glirinae (Muirhead, in Brewster, 1819) Thomas, 1897

Genus *Glis* Brisson, 1762

Glis sackdillingensis (Heller, 1930)

(Figure 61L–T)

Studied material—Biozone B. L13—Lower 1 t; L13c: 1 t; L13c: 2 M1/2; L13c: 1 M2; L13c: 1 1m2; L13c: 1 m1; L13c: 4 M1/2; L13c: 4 m1/2; L13c: 7 t; L13c: 1 M3; L13c: 1 M1; L13c: 1 P4; L13c: 2 M1/2; L13c: 2 m1; L13c: 10 t; L12: 2 M3; L12: 2 M2; L12: 2 M1; L12: 4 m1; L12: 7 t; L11b: 4 t; L11a1: 1 P4; L11a1: 20 t; L11a: 1 M2; L11a: 1 m3; L11a: 1 m1; L11a: 2 m2; L11a: 8 t.

Description—P4. Viewed occlusally, the nearly round shape. One specimen has six transverse ridges (missing the additional anterior ridge). The middle additional ridge is fused with the protoloph on the lingual side. In the other tooth, both the anterior and posterior additional ridges are absent.

M1. The occlusal surface is flat. Its outline is a rounded square or a rounded trapezoid with a slightly oblique anterior edge. There are seven ridges—four main ones: anteroloph, protoloph, metaloph, and posteroloph—and three additional ridges located in the valleys between them. On the labial side, the valleys are open except for the anterior one, which is closed due to the fusion of the anteroloph with the paracone. On the lingual side, the posterior valley is closed due to the fusion of the posteroloph and mesoloph at the protocone. It has three roots.

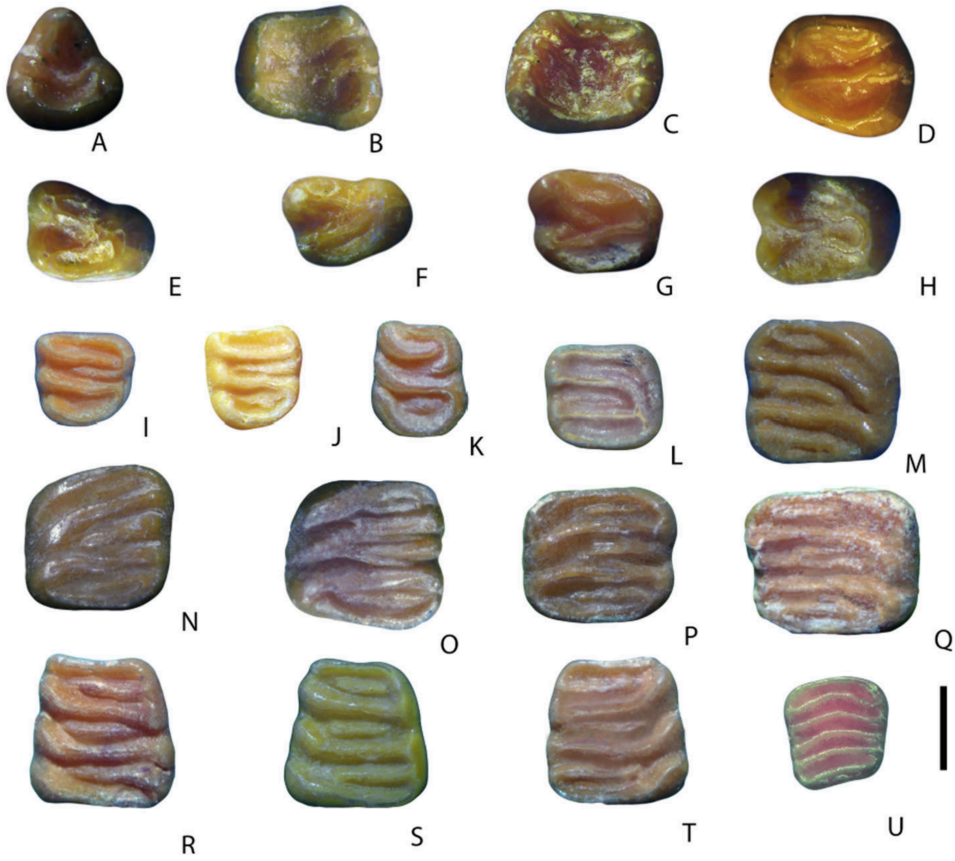


Figure 61. *Eliomys* cf. *quercinuis* (**A**–**H**), *Myomimus* cf. *roachi* (**I**–**L**), *Glis sackdillingensis* (**M**–**P**), *Muscardinus avellanarius* (**U**), cheek teeth in occlusal view. (**A**)—p4, BG-IBER-FMC-000004223, L11a; (**B**)—m1/2, BG-IBER-FMC-000001387, L11a; (**C**)—m1/2, BG-IBER-FMC-000001370,L11a; (**D**)—m3, BG-IBER-FMC-000001372, L11a; (**E**)—P4, BG-IBER-FMC-000001359,L11a; (**F**)—P4, BG-IBER-FMC-000001388, L11a1; (**G**)—M1, BG-IBER-FMC-000004342,L11a; (**H**)—M2, BG-IBER-FMC-000001358, L11a; (**I**)—m3, BG-IBER-FMC-000020285, L12; (**J**)—m3, BG-IBER-FMC-000000011, L11b; (**K**)—m2, BG-IBER-FMC-000017029, L12; (**L**)—M1/2, BG-IBER-FMC-000018596,L13a; (**N**)—M1, BG-IBER-FMC-000016912, L12; (**O**)—M1, BG-IBER-FMC-000016913,L12; (**P**)—M1/2, BG-IBER-FMC-000016562, L12; (**Q**)—M1/2, BG-IBER-FMC-000017112, L12; (**R**)—m1, BG-IBER-FMC-000019031, L12; (**S**)—m1, BG-IBER-FMC-000018434, L13a; (**T**)—m1, BG-IBER-FMC-000019030, L12; (**U**)—m2, BG-IBER-FMC-000004065, L11a. Scale bar = 1 mm.

M2. Similar to the first molar, but with a rounded rectangular shape, wider than long. The anterior two valleys are open labially, and the posterior one is closed due to the fusion of the posteroloph with the metacone. On the lingual side, the anterior and posterior valleys are closed due to fusion of the protoloph with the anteroloph and the metatoloph with the posteroloph, respectively. In one tooth, there are two additional ridges between the protoloph and the metaloph. Three roots.

m1. Viewed occlusally, the shape is rounded-trapezoidal, with a flat occlusal surface and seven transverse ridges—four primary (anterolophid, metalophid, mesolophid, and posterolophid) and three secondary. The valleys between the main ridges are open labially.

p4. Rounded triangular shape in occlusal view, with six transverse ridges.

Measurements—Table 36.

Table 36. Dental Measurements [mm] of *Glis sackdillingensis* from Kozarnika.

Tooth	N	L				W			
		X	SD	Min	Max	X	SD	Min	Max
lm1	8	1.82	0.091	1.64	1.92	1.90	0.139	1.75	2.18
lm1/2	3	1.71	0.096	1.64	1.82	1.65	0.277	1.48	1.97
lm2	2	1.83	0.177	1.70	1.95	1.78	0.156	1.67	1.89
lm3	1	1.97	0.000	1.97	1.97	1.70	0.000	1.70	1.70
uM1	3	1.79	0.067	1.71	1.83	1.91	0.080	1.83	1.99
uM1/2	8	1.79	0.065	1.67	1.87	1.91	0.125	1.75	2.10
uM2	4	1.73	0.062	1.65	1.80	1.93	0.048	1.88	1.98
uM3	3	1.36	0.215	1.19	1.60	1.41	0.338	1.20	1.80
uP4	2	1.33	0.078	1.27	1.38	1.48	0.071	1.43	1.53

Remarks—The teeth from Kozarnika tend to be smaller than those of recent *Glis glis* from Bulgaria and align well with *G. sackdillingensis* from the type locality (Figure 62). The last species was described from lower teeth, with particular emphasis on its smaller size relative to the modern species. A distinctive feature of this species is the fusion of the posteroloph with the metaloph of M1/2, whereas in modern species they remain separate [190]. The available material, in terms of size and features of the occlusal surface, matches the characteristic features of *Glis sackdillingensis*. They are similar to, but slightly larger than, the material from Varbeshnitsa, identified as *Glis* cf. *sackdillingensis* [48].

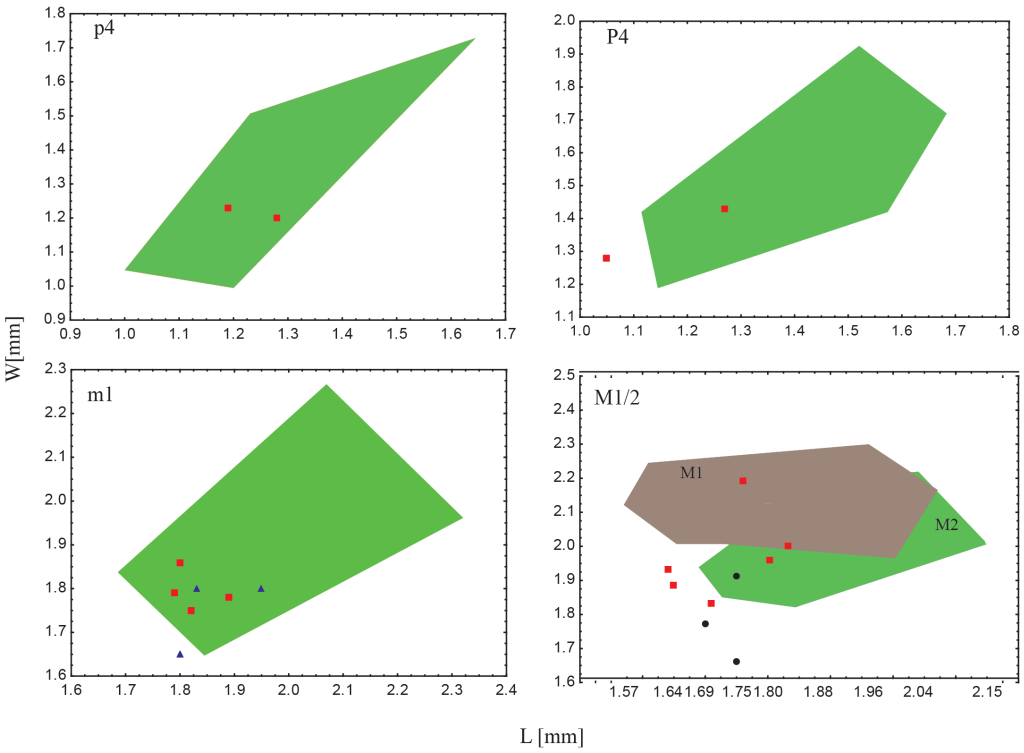


Figure 62. Biplots of the length (L) and width (W) of cheek teeth of *Glis sackdillingensis* and *G. glis*; red squares—Kozarnika, black circles—Varbeshnitsa, Bulgaria, Late Biharian [48], blue triangles—Sackdillingen Höhle, Germany, Pleistocene [191]; polygons represent the variability of the recent species from Bulgaria.

Glis minor Kowalski, 1956

Studied material and Measurements [mm]—Biozone B. L12: 1 m1 (1.65 × 1.55), (BG-IBER-FMC-000022005).

Remarks—The available tooth is very similar to those of *Glis sackdillingensis*, but it is smaller, falling within the variability range of *G. minor*. It is slightly larger than the two molars from the nearby Pliocene site Muselievo [74].

Subfamily Leithiinae Lydekker, 1895

Genus *Eliomys* Wagner, 1840

Eliomys quercinus cf. *helleri* Jánossy, 1962

(Figure 61A–H)

Studied material and measurements (L × W, mm). Biozone B. L11a: M1 (1.32 × 1.65); M2 (1.37 × 1.78); 2P4 (1.55 × 1.25, 1.16 × 1.58); p4 (1.49 × 1.39); 2 m1/2 (1.43 × 1.83, 1.50 × 1.74); m3 (1.46 × 1.72).

Description—p4 has a triangular outline in occlusal view. The mesoconid and mesolophid are well developed. There is no additional ridge between the mesolophid and posterolophid.

P4. Presence of proto-, meta-, and posteroloph, short antero- and centroloph.

M1/M2: More or less pronounced development of the lophs arising, respectively, from the posterior margin of the paracone and the anterior margin of the metacone. These lophs sometimes fuse.

m1/2. One of the two teeth (right, BG-IBER-FMC-000001370) is slightly worn and has a relatively complex occlusal surface, but generally matches the basic structure of *Eliomys*. The occlusal surface is concave. The labial and lingual tubercles are high and well-defined. The mesolophid does not reach the entoconid. The centrolophid is bent forward with a weak branch in the middle toward the metalophid. The metalophid is bent forward in its middle. There are traces of an additional posterior ridge. The other tooth (right, BG-IBER-FMC-000001387) is worn, which simplifies the structure of the chewing surface. A trace of an additional ridge is present between the meso- and posterolophid.

m3 (BG-IBER-FMC-000001372). The occlusal surface is concave. The three main labial tubercles—protoconid, mesoconid, and hypoconid—are tall and well-defined, with valleys opening on the labial side. The lingual tubercles (protoconid and metaconid) are shorter but still well developed. There are three prominent ridges: anterolophid, mesolophid, and posterolophid. The other transverse ridges (centrolophid, metalophid, and anterior additional ridge) are less developed. The centrolophid does not reach the mesial edge of the occlusal surface. In the valley between the mesolophid and the posterolophid, there are traces of an additional posterior ridge.

Remarks—The evolutionary paths of the genus *Eliomys* suggest a transition from the large species of the Late Pliocene, *Eliomys intermedius* Friant, 1953 (type locality Breche de Sete), to the current small species, *Eliomys quercinus quercinus*, through *Eliomys quercinus helleri* Jánossy, 1962, which is common in Pleistocene sites [84]. The latter, besides its intermediate size, is also distinguished by the presence of accessory enamel ridges between the mesolophid and posterolophid ridges and prominently developed tubercles and transverse ridges. The presence of an additional posterior ridge varies among individual populations, with its frequency decreasing toward the Late Pleistocene [84]. The available lower teeth, which display faint traces of an additional posterior ridge between the posterolophid and the mesolophid, as well as well-developed tubercles and ridges, align them more closely with the intermediate form (*Eliomys quercinus helleri*), corresponding to the age of the deposits. In terms of size, the current teeth fall within the overlap zone between Pleistocene and modern populations [84,192]. The limited material restricts more comprehensive comparisons and prevents precise subspecific identification.

Genus *Muscardinus* Kaup, 1829

Muscardinus avellanarius (Linnaeus, 1758)

(Figure 61U)

Studied material and Measurements [mm]. Biozone B. L11a: m2 (1.36 × 1.33), L13a: m2 (1.42 × 1.34).

Description—The present teeth are rounded trapezoidal in shape, slightly wider anteriorly, with six main transverse ridges, slightly bent forward, especially well expressed in the first three.

Remarks—In terms of the size and structure of the occlusal surface, the present material falls within the range of variability of modern species and the Late Pleistocene population from Cave 16 [38] and is smaller than *Muscardinus dacicus* Kormos, 1930 [193].

Genus *Myomimus* Ognev, 1924

Myomimus cf. *roachi* (Bate, 1937)

(Figure 61I–L)

Studied material and Measurements [mm]—Biozone B. L11b: m3 (1.23 × 1.22). L12: M1/2 (1.28 × 1.41), m1/2 (1.41 × 1.13), m3 (1.15 × 1.23)

Description—M1/2. The occlusal surface has a rounded square outline. It is simple and has four transverse ridges (anterior loph, protoloph, metaloph, and posteroloph), with no centroloph. It has three roots.

m1/2. The tooth has a rounded, elongated shape, slightly narrowed at the front. The anterolophid is relatively short and does not connect with the protoconid. The centrolophid is also short and does not reach the middle of the occlusal surface. The mesolophid and posterolophid are well developed, merging near the entoconid, forming a wide lingual valley containing a well-developed posterior extra ridge and three roots.

m3. Rounded trapezoidal shape. The ridges are similar to those in m1/2, but the anterolophid and centrolophid are longer. Only one of the two teeth has an additional posterior ridge in the valley between the mesolophid and posterolophid.

Remarks—Since the Pliocene, the genus *Myomimus* has shown a pattern of evolutionary change toward simpler occlusal surfaces, characterized by shortening of some transverse ridges and the gradual reduction and disappearance of the posterior extra ridge on the lower teeth [194]. Given its geological age, the available material aligns well with this trend. It clearly exhibits more simplified teeth, especially the upper molar, compared to the Pliocene specimen from Muselievo, described as *Myomimus complicidentatus* Popov, 2004 [74]. The upper molar, with its simplified structure, resembles material from the modern species *M. roachi* from Bulgaria. However, the lower teeth differ in that two of them have additional posterior ridges, which are absent in the modern species. In this regard, the material resembles specimens from the Biharian site Kalymnos-Xi, labeled as *M. roachi* [195]. Due to the small sample size, which limits more detailed analysis and comparison, the material is tentatively assigned to the modern species *M. roachi*.

Family Castoridae Batsch, 1788

Genus *Castor* Linnaeus, 1758

Castor plicidens Forsyth Major, 1875

(Figure 63G–I)

Studied material and Measurements [mm] (L × W)—Biozone B. L11b: M1/2 (6.9 × 7.87); L12: M1/2 (7.38 × 7.56); L13c: M1/2 (8.1 × 8.65).

Description—The folds of the available molars are filled with crown cementum. The teeth are in an advanced stage of wear—likely belonging to older individuals, probably over 4 years old [196].

M1–2. The occlusal surface has a rounded trapezoidal shape, with the posterior side inclined relative to the anterior one. The paraflexus and hypoflexus practically do

not overlap along the tooth axis. As a result, the dentine field between them is slightly stretched out anterolingually. The mesoflexus, along its greater length, develops almost perpendicular to the mesiodistal axis of the occlusal surface, and after passing it, curves backward and nearly touches the posterior wall, but a narrow dentine field remains between them. The anterior enamel wall of the mesoflexus is broadly crenulated. The metaflexus is straight, perpendicular to the mesiodistal axis throughout its length; only at the very end does it bend backward at a right angle; the enamel walls are smooth. The hypostria reaches the base of the crown.



Figure 63. *Hystrix refossa* (**A**–**F**), *Castor plicidens* (**G**–**I**). (**A**)—left M1/2, BG-IBER-FMC-000006350, L13b; (**B**)—m1, BG-IBER-FMC-000000659, L13b; (**C**)—right m1, BG-IBER-FMC-000021535, L13a; (**D**)—right M1/2, BG-IBER-FMC-000017113, L12; (**E**)—left m2, BG-IBER-FMC-000005262, L11b; (**F**)—right dp4, BG-IBER-FMC-000005281, L11b; (**G**)—right M1/2, BG-IBER-FMC-000015054, L11b; (**H**)—left M1/2, BG-IBER-FMC-000003575, L13c; (**I**)—left M1/2, BG-IBER-FMC-000017114, L12; Scale bar represents 5 mm.

m1/2. The paraflexid develops almost perpendicular to the anteroposterior axis of the occlusal surface and extends significantly beyond it toward the labial side. The mesoflexid is slightly curved anteriorly but does not touch the paraflexid; therefore, no enamel island forms between them. In specimen BG-IBER-FMC-000017114, the metaflexid and hypoflexid meet in the middle of the occlusal surface, leaving a narrow, short dentine field between them that develops obliquely anterolingually. In specimen BG-IBER-FMC-000003575, the tips of the para- and metaflexid overlap, leaving a relatively long dentine field between them that is strongly inclined in the anterior–posterior direction. The posterior enamel wall of the metaflexid is broadly folded. Lingual striids reach the crown base, and the mesostriid is slightly longer than the para- and metastriids.

Remarks—The available teeth are distinguished from those of *Trogontherium* by the presence of cement in the reentrant folds and the degree of development of the striae, which reach the base of the crown, in contrast, for example, to *Trogontherium cuvieri* Fischer de Waldheim, 1809, from the early Middle Pleistocene of Kozi Grzbiet [197]. In the Pliocene *C. praefiber* Depéret, 1890 the striae also do not reach the base of the crown.

In size, the available upper molars fall within the range of variability of fossil and modern populations of *Castor* [11,197–200]. The teeth are relatively broad. This is because the teeth belong to older individuals. It is known that in modern and fossil beavers, the upper molars become shorter but broader as a result of attrition [198].

From the Upper Valdarno Basin in Italy, the form *Castor plicidens* has been described, characterized by pronounced secondary enamel folds on the premolar and molar occlusal surfaces [201–203]. The available teeth, especially the lower molars, resemble this form, but the secondary folds are fewer, wider, and shallower. A similar morphotype has been noted in adult specimens from Early Pleistocene layers of Gran Dolina (level TD6), assigned to *Castor fiber* [189]. *C. fiber* cf. *plicidens* has been reported from the Late Villafrancian (MNQ19) in Romania [203], which is visually very similar to the Kozarnika. Evidence of age variability suggests that secondary enamel folds may have appeared during tooth abrasion, raising questions about the specific identity of *C. plicidens* [204]. According to [200], the form "*plicidens*" may have been a semi-isolated geographical subspecies characteristic of the Apennine Peninsula that later disappeared at the beginning of cooling in the Late Biharian, as a result of hybridization with northern migrants. The available material, in the context of data for Italy, Spain, GB, and Romania, corresponds with the view of Friant [202] that *C. plicidens* was a species that lived in Europe during the warm Quaternary periods through the beginning of the Neolithic.

Family Hystricidae Fischer de Waldheim, 1817

Genus *Hystrix* Linnaeus, 1758

Hystrix refossa Gervais, 1852

(Figure 63A–F)

Studied material—Biozone B. L13: Lower: 1 t; L13c: 11 t; L13b: 1 m1, 24 t, 1 M1/2; L13a: 20 t, 2 M1/2; L12: 3 m1–2, 18 t, 4 M1–2; L11c: 17 t; L11b: 5 m2, 2 p4, 14 t, 4 M1–2; L11a1: 14 t; L11a: 2 t.

Description—All well-developed but unworn teeth have high crowns. The roots are small.

Upper dentition. On unworn teeth, there are well-defined three labial reentrant folds—paraflexus, mesoflexus, and metaflexus. With tooth wear, they, or parts of them, close sequentially to become the parafossette and mesofossette, which have elongated, often irregular shapes. As the gridding surface wears down further, they disintegrate, forming additional enamel islets. Finally, the hypoflexus closes. The most worn teeth have four enamel islets.

Lower dentition. Unworn teeth have three lingual reentrant folds—paraflexid, mesoflexid, and metaflexid. On the labial side, there is a well-developed hypoflexid, which extends to the base of the crown. With wear of the tooth, the folds close in marks, with the metafossetid forming earliest and the hypofossetid forming latest. The most worn teeth have five enamel islands.

Measurements [mm] (L × W; N, Min–Mean–Max). M1/2: 9, 5.75–7.8–9.7 × 5.76–7.23–9.01; m1/2: 3, 7.84–8.72–10.2 × 6.13–6.8–7.99; p4: 2, 8.66–9.26–9.9 × 6.2–6.68–7.15.

Remarks—Broad intraspecific variability and limited morphological markers complicate taxonomic assignments of the porcupine fossil remains [205]. Weers [206] provides a comprehensive taxonomic revision, based on dental characteristics, with particular emphasis on tooth size, crown height, and wear patterns, synonymizing *Hystrix major*, *H. etrusca*, *H. makapensis*, and *Hystrix angressi* with *Hystrix refossa*, and further reducing other named taxa to synonyms of *H. primigenia* and *H. vinogradovi*. Lately, Weers [207] has extended this revision, reducing the number of recognized Euro-Asiatic *Hystrix* species. Several Asian taxa (*Hystrix crassidens*, *H. gigantea*, *H. magna*) were synonymized with *Hystrix refossa*, and the European *Hystrix vinogradovi* was considered a synonym of *Hystrix brachyura*. Rook

and Sardella [205] recognize *Hystrix major* and *H. etrusca* as junior synonyms of *H. refossa*, following the revisions of Weers [206], and note the inclusion of other taxa such as *H. angressi* and *H. makapanensis* within *H. refossa*. Based on detailed metric data, they note that *H. refossa* is larger and more hypsodont than extant *H. cristata* and other fossil species. In terms of the lengths of the upper and lower molars, measured on well-preserved and moderately worn teeth, the Kozarnika material falls within the middle range of *H. refossa* and the upper range of modern *H. cristata*, far exceeding those of *H. vinogradovi* [137,206–208]. These features, together with the relatively high degree of hypsodonty, indicate that the material belongs to *H. refossa*.

5. Biostratigraphy and Paleoecology

5.1. Taphonomy

The sediments in the entrance chamber of Kozarnika cave, uncovered during the archaeological excavations, proved to be extremely rich in small-mammal bones (Figure 64). The bone assemblages are very similar across different layers. They are characterized by the extraordinary abundance of cranial and postcranial remains; the teeth are, in general, in a good stage of preservation (complete, without signs of rolling), and although many of them are isolated, there are a lot that are in their corresponding mandibles; the number of right and left anatomical elements is quite similar in each taxon. All these features indicate that the bones of small mammals were not subjected to a significant secondary transport. In many samples, which represent sediments from 1 square meter with a thickness of 5 cm, rare species such as hare, hedgehog, mole, etc., are represented by left and right anatomical elements, or consecutive teeth, which, based on their characteristics such as shape peculiarities, degree of tooth wear, can confidently be attributed to a single individual (e.g., Figure 9B,C and Figure 11B,C). Figure 64C shows the abnormal shapes of the left and right m1s of *Microtus arvalidens* from sample (kz1692) in layer 12, which most likely belong to one individual.

During sorting of the material, the degree of digestion of determinable teeth was specifically marked according to the categories of Andrew [209]. Over 95% belong to the first category. About 2–3% belong to the second category (Figure 46C). The rest belong to the third category. The first category is characteristic of the Barn Owl (*Tyto alba*). The second category characterizes several other owl species, as well as the degree of wear of the Barn Owl during nesting. Based on this, it can be said that the bones of small rodents are primarily accumulated by this owl. A smaller part likely results from predation by the Eagle owl (*Bubo bubo*). Remains of larger species, such as hares, hedgehogs, and mole rats, confirm this. These owls are opportunistic hunters and are sedentary, so their prey spectrum is assumed to be a good representation of the ecosystem in which they live.

Most of the marmot remains belong to young individuals that died during hibernation in their burrows, which were identified in some places within the sediments (Figure 1). Since the traces of digging are associated with Biozone B, they are concentrated in the lowest layers near the cave's bedrock. It can be assumed that they are synchronous with the upper layers of this biozone. This is also supported by the fact that they are predominantly light in color and much less eroded and fragmented compared to the other remains in the lowest layers.



Figure 64. Bone assemblages from Biozone A (**A**) and Biozone B (**B**). (**C**) Anomalous first lower molars (m1) of *Microtus arvalidens* from the sediment sample kz1692 from layer 12, probably belonging to a single individual.

5.2. Biostratigraphy

Species richness (number of species) is a key indicator of biodiversity. To assess species richness in stratigraphic assemblages, the rarefaction method was used [210]. This is a standardization technique that allows fair comparison of richness observed at different times or locations, based on samples of varying sizes (number of individuals). It shows the dependence between the number of identifiable remains and the number of species and, in this way, indirectly allows an assessment of the representativeness of the samples in reflecting the species composition within a given assemblage. It is evident that, in terms of species richness, stratigraphic assemblages form two groups (Figure 65). Those from Biozone B have

nearly twice the species richness as those from Biozone A. Layer 11c from Biozone B occupies an intermediate position. From the shape of the curves, it can be seen that for species-rich assemblages (those from Biozone B), the number of identifiable remains required to represent 90% of the species is about 3000, whereas for the poorer ones (Biozone A), it is 500. Based on this, most stratigraphic assemblages can be considered representative in terms of species richness, and the absence of certain species can be interpreted from a biological perspective. Exceptions are the assemblages from layers L13–Lower, L10b, and L9c.

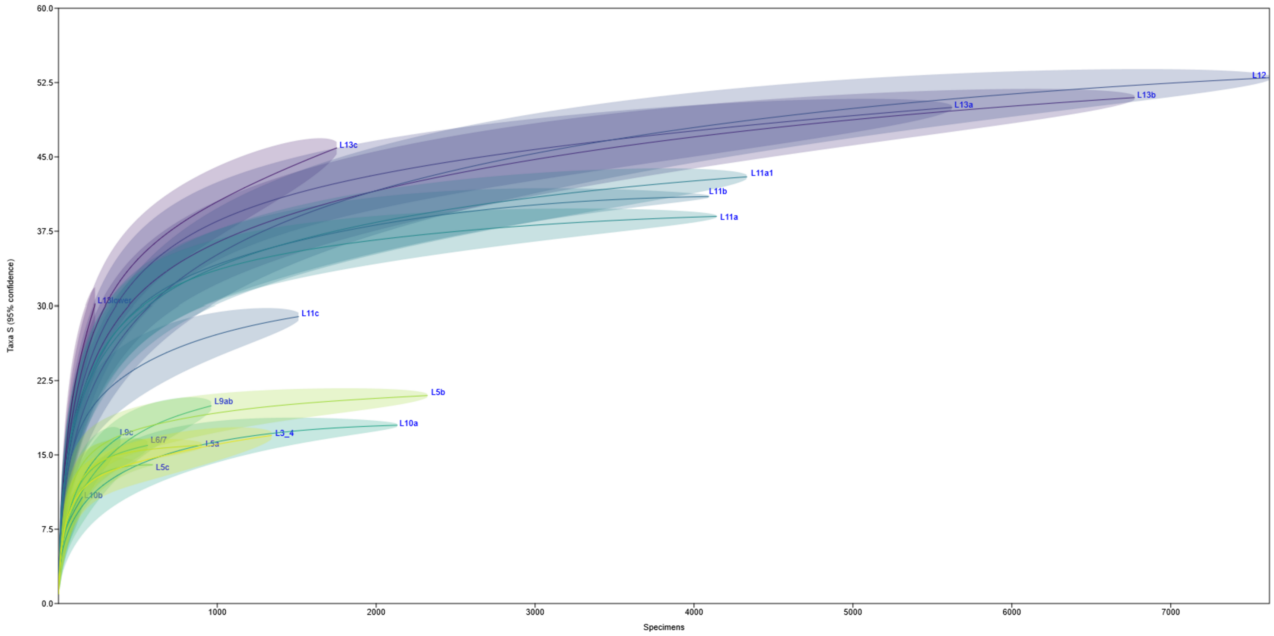


Figure 65. Rarefaction curves and 95% confidence intervals of cumulative species richness of stratigraphic small mammal assemblages plotted against the number of identified specimens.

The stratigraphic features of the paleontological material of small mammals have been analyzed using TWINSPAN [211]. This is a hierarchical, divisive classification method used to produce a double-classified species-by-sample table. It clusters layer assemblages and species into ecologically interpretable groups (hereafter LSG and SSG, respectively), thereby revealing assemblage patterns along a stratigraphic gradient. At the first level, the stratigraphic assemblages form two groups, which correspond to the already established biozones, A and B, representing Biharian and Toringian, respectively (Table 37). The second and third grouping levels within these biozones vary. In biozone B, three groups of stratigraphic assemblages are distinguished. Two of them (LSG010 and LSG011) are stratigraphically compact and cover the lower (L13c-L12) and upper (L11b-L11a) parts of the biozone, respectively. The third group (LSG00) includes the lowest layer, L13-Lower, and the middle layer in this biozone, layer L11c. This group, which is not stratigraphically compact, differs from the others in having fewer species. Regarding layer L13-Lower, this is obviously due to the small sample size (Figure 65). For layer 11c, represented by a large sample, this is a real feature. The low species richness in layer 11c is due to the complete absence of the rarest species, which make up groups SSG000 and SSG001 (Table 37). Half of the species from group SSG000 do not reappear in the upper layers—LSG011. It can be assumed that layer 11c represents a period of climate change, probably cooling. After this period, species diversity increases but remains lower than in the earlier period, as represented by the layers in LSG010 (Figure 65).

Table 37. TWINSPAN classification of small-mammal stratigraphic assemblages. Species relative abundance is coded by the cut levels set at 2, 5, 10, and 20% NISP—number of identified specimens. The single, double, and triple lines represent the three levels of division. The layers (assemblages) are arranged in stratigraphic order, while the colors reflect their grouping according to the analysis

Species Stratigraphic Group (SSG)	Layer Stratigraphic Group (LSG)	00	010	010	010	010	00	011	011	011	10	10	10	10	111	111	110	111	111
	Layer	L13-L	L13c	L13b	L13a	L12	L11c	L11b	L11a1	L11a	L10b	L10a	L9c	L9ab	L6/7	L5c	L5b	L5a	L3_4
	NISP	247	1767	6785	5632	7639	1527	4109	4342	4150	162	2146	404	973	573	609	2332	917	1358
	Number of species	31	46	51	50	53	29	41	43	39	11	18	17	20	16	14	21	16	16
000	*Borsodia newtoni*		1	1	1														
000	*Drepanosorex praearaneus*			1															
000	*Glis minor*				1														
000	*Prolagurus pannonicus*		1	1	1	1													
000	*Talpa minor*					1													
000	*Tamias orlovi*					1													
000	*Ungaromys nanus*					1													
000	*Villanyia* cf. *exilis*		1	1		1													
000	*Allophaiomys* cf. *burgondiae*		1	1	1	1			1										
000	*Mimomys* cf. *tornensis*		1	1	1	1			1										
000	*Muscardinus avellanarius*		1	1	1					1									
000	*Ochotona* cf. *transcaucasica*			1	1	1			1										
000	*Sciurus* sp.			1	1	1			1										
001	*Neomys* cf. *newtoni*								1										
001	*Castor plicidens*		1			1		1											
001	*Allocricetus ehiki*			1	1	1		1	1	1									
001	*Eliomys quercinus*		1	1	1			1	1	1									
001	*Lepus* cf. *terraerubrae*					1		1											
001	*Microtus arvalinus*			1	1	1		1		1									
010	*Allophaiomys deucalion*	2	1	1	1	1		1	1										
010	*Asoriculus gibberodon*	1				1													
010	*Beremendia fissidens*	1		1	1	1	1		1										
010	*Hypolagus* cf. *petenyi*	1		1	1				1										
010	*Apodemus* cf. *flavicollis*	1	1	1	1	1		1		1				1					
010	*Allocricetus bursae*	4	5	5	4	4	3	3	4	4									
010	*Asoriculus thenii*	1	1	1	1	1			1										
010	*Borsodia arankoides*	1	1	1	1	1		1	1	1									
010	*Erinaceus* sp.		1	1	1	1	1	1	1	1									
010	*Glis sackdillingensis*	1	1	1	1	1		1	1	1									
010	*Mimomys pitymyoides*		1	1	1	1	1	1	1										
010	*Pliomys coronensis*		1	1	1	1	1	1	1	1									
010	*Sorex runtonensis*		1	1	1	1	1	1	1	1									
010	*Apodemus* sp.	2	3	3	2	2	1	1	2	2		1	1				1		
010	*Allophaiomys gregaloides*	3	2	3	3	3	3	2	2	3									
010	*Allophaiomys* cf. *pliocaenicus*	1	1	1	1	1	1	1	1	1									
010	*Apodemus epimelas*	1	1	1	1	1	1	1	1	1									
010	*Clethrionomys hintonianus*	1	1	1	1	1	1	1	1	1									
010	*Dinaromys dalmatinus*	1	1	1	1	1	1	1	1	1									
010	*Hystrix refossa*	1	1	1	1	1	1	1	1	1									
010	*Lagurus arankae*	2	1	1	1	1	1	1	1	1									
010	*Marmota marmota*	2	1	2	1	1	2	1	1	1									
010	*Microtus arvalidens*	4	5	5	5	5	5	5	5	5									
010	*Mimomys blanci*	1	1	1	1	1	1	1	1	1									

Table 37. *Cont.*

010	*Myomimus* cf. *roachi*	1	1	1	1	1	1	1	1	1									
010	*Pliomys episcopalis*	1	1	1	1	1	1	1	1	1									
010	*Lagurus transylvanicus*	5	4	4	4	4	5	4	4	4									
010	*Alexandromys nivalinus*	2	1	1	1	1	1	1	1	2									
010	*Microtus nivaloides*	2	2	2	2	2	3	2	3	3									
010	*Mimomys savini*	1	1	1	1	1	2	2	1	1									
010	*Nannospalax sirakovi*	2	3	3	3	3	3	4	3	3									
010	*Ochotona* sp.	1	1	1	1	1	1	2	2	2									
011	*Apodemus sylvaticus*		1	1	1	1		1	1	1	1			1					
011	*Cricetus cricetus*	1	1	1	1	1	1	2	2	2			1	1			1		
011	*Crocidura leucodon*		1	1						1					1				
011	*Sicista subtilis*		1	1	1	1	1	1	1	1		1	1				1		
10	*Apodemus uralensis*		1	1	1	1		1	1	1		1	1	1	1	1	1		
110	*Sorex minutus*		1	1	1	1		1		1	1	1	1	1	1	1	1	1	1
110	*Spermophilus citellus*	1	2	2	2	2	2	2	2	2	2	2	2	3	2	2	2	1	1
110	*Sorex araneus*	1	1	1		1	1			1	1	1	1	1	1		2	1	2
110	*Sorex minutissimus*		1													1			1
110	*Talpa europaea*				1	1		1						1	1		1		1
111	*Nannospalax leucodon*										1	1	1	2	1	1	1	1	
111	*Neomys* cf. *fodiens*											1							
111	*Alexandromys oeconomus*											1	1	1			1	1	1
111	*Arvicola amphibius*										2	1	1	1	1	1	1	1	1
111	*Lagurus lagurus*										4	5	5	5	3	4	4	4	4
111	*Mesocricetus newtoni*				1	1		1	1	1	4	3	4	5	3	2	4	2	2
111	*Microtus* ex gr. *arvalis*										5	5	5	5	5	5	5	5	5
111	*Nothocricetulus migratorius*										1	1	1	1	1	2	2	1	1
111	*Ochotona pusilla*											1		1			1	1	1
111	*Chionomys nivalis*										4	3	2	2	3	3	4	4	4
111	*Clethrionomys glareolus*												1	1	1	1	1	1	1
111	*Microtus subterraneus*											1		1	1	1	1	1	1
111	*Stenocranius gregalis*											1	1	1	1	1	1	1	2
111	*Allactaga major*																1	1	

The stratigraphic assemblages from biozone A also form three groups: two of which are stratigraphically coherent—LSG10 and LSG111—and one, composed of a single layer (L5b), is inserted between LSG10 and LSG111 and, in terms of species composition, is more of a variant of LSG10. The differences between the groups are less pronounced than those in biozone B, in both the structure of the stratigraphic assemblages and species richness. These differences are probably due to weak climatic fluctuations.

The summary of faunal dynamics presented in the profile of the Kozarnika Cave is shown in Figure 66. The lowest layers from both biozones, L13-Lower and L10b, are not presented due to their small sample sizes. A well-defined faunal reorganization is observed in the layers from the lower part of the profile—Biozone B. It is expressed as the disappearance of species during the period marked by layers L13b-L11c. The species that are gradually disappearing are *Prolagurus pannonicus*, *Villanyia* cf. *exilis*, *Asoriculus gibberodon*, *Talpa minor*, *Tamias orlovi*, *Ungaromys nanus*, *Borsodia newtoni*, *Glis minor*, and *Drepanosorex praearaneus*.

The species that disappear after them, in the interval 11c–11a, are *Mimomys pitymyoides*, *Allophaiomys deucalion*, *Beremendia fissidens*, *Asoriculus thenii*, *Allophaiomys* cf. *burgondiae*, *Mimomys* cf. *tornensis*, *Ochotona* cf. *transcaucasica*, *Sciurus* sp., *Hypolagus* cf. *petenyi*, *Neomys* cf. *newtoni*, *Talpa europaea*, *Castor plicidens*, *Lepus* cf. *terraerubrae*. These two groups include most of the species traditionally considered characteristic of earlier periods, with some regarded as indicator species whose disappearance marks the end of the Villanian,

while others are thought to mark the boundary between the Early and Late Biharian, e.g., [22,212–214]. The species that disappear during the period between the two biozones, i.e., the species that are not found during the Late Pleistocene, are *Muscardinus avellanarius*, *Allocricetus ehiki*, *Eliomys quercinus*, *Microtus arvalinus*, *Borsodia arankoides*, *Erinaceus* sp., *Glis sackdillingensis*, *Pliomys coronensis*, *Sorex runtonensis*, *Allophaiomys* cf. *pliocaenicus*, *Apodemus epimelas*, *Clethrionomys hintonianus*, *Dinaromys dalmatinus*, *Hystrix refossa*, *Lagurus arankae*, *Marmota marmota*, *Mimomys blanci*, *Myomimus* cf. *roachi*, *Pliomys episcopalis*, *Mimomys savini*, *Alexandromys nivalinus*, *Ochotona* sp., *Allophaiomys gregaloides*, *Microtus nivaloides*, *Nannospalax sirakovi*, *Allocricetus bursae*, *Lagurus transylvanicus*, and *Microtus arvalidens*. This group also includes the most abundant species, which dominate in number and/or occur across most layers of Biozone B. Most of these species are characteristic of the Early-to-Middle Pleistocene transition. This group also includes *Mimomys blanci*. This species can be considered a more progressive variant of *M. pusillus*. The last appearance of *M. pusillus* is regarded as a marker for the boundary between the Early and Late Biharian. From this, it follows that the presence of the closely related but more progressive species *M. blanci*, which is sometimes indistinguishable from *M. pusillus*, does not contradict the assignment of the fauna of Biozone B to the Late Biharian. The upper boundary of the Late Biharian is marked by the last appearance of *M. pusillus*, about 650,000 years ago [8]. This species occurs in all layers of Biozone B. Based on this, it can be said that this age is the possible upper limit of the depositional time interval for Biozone B layers. It should also be noted that within this group, there are species considered characteristic of earlier periods, but their number is low: *Borsodia arankoides*, *Allophaiomys* cf. *pliocaenicus*, and *Lagurus arankae*.

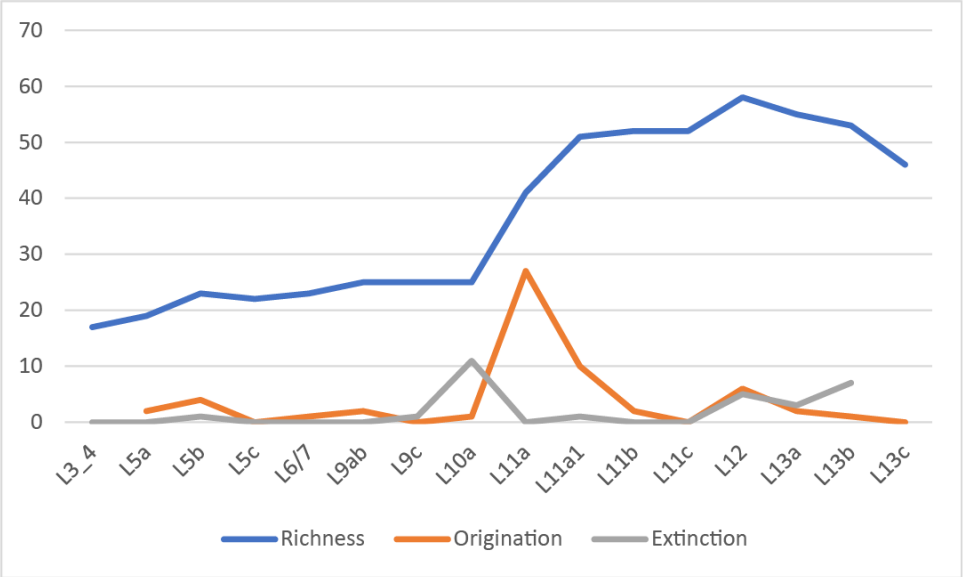


Figure 66. Faunal turnover, illustrated by diversity (species richness), origination, and extinction curves by layer. The values are calculated using the range-through option in the PAST package, which fills in any gaps between the first and last appearances of each species.

The emergence of new species in the layers of Biozone B is gradual, but intensifies after layer 11c. There is a smaller peak of newly appeared species in layer 12, which, combined with the extinctions that have not yet reached the final stages, expressed in layer 11c, leads to the greatest species richness in layer 12. After that, the emergence of new species does not offset the extinctions, and species diversity declines, reaching its lowest point for the Biozone B in layer 11a. Among the species that appear earliest are *Allocricetus ehiki*, *Microtus arvalinus*, *Ochotona* cf. *transcaucasica*, *Sciurus* sp., *Drepanosorex praearaneus*,

followed by *Mesocricetus newtoni*, *Talpa europaea*, *Lepus* cf. *terraerubrae*, *Talpa minor*, *Tamias orlovi*, *Ungaromys nanus*, *Neomys* cf. *newtoni*, and *Glis minor.* Since most of these species are rare, their appearance in one layer or another may be due to chance. These species disappear before layer 11a. Noteworthy is *Mesocricetus newtoni*, whose appearance in layer 13a marks the earliest appearance of the species. In Biozone B, it remains rare, but in Biozone A, it is one of the dominant species.

The emergence of new species declines sharply during the transition between the two biozones, which, combined with the extinction of species characteristic of the Early Pleistocene, leads to a drastic reduction in species diversity. The small number of newly appearing species is a result of Biozone B already containing species characteristic of the Late Pleistocene—Biozone A: *Sorex araneus*, *S. minutus*, *S. minutissimus*, *Talpa europaea*, *Apodemus sylvaticus*, *A. flavicollis*, *A. uralensis*, *Cricetus cricetus*, *Spermophilus citellus*, *Crocidura leucodon.* In biozone A, they are added by *Nannospalax leucodon*, *Neomys fodiens*, *Alexandromys oeconomus*, *Arvicola amphibius*, *Lagurus lagurus*, *Nothocricetulus migratorius*, *Ochotona pusilla*, *Chionomys nivalis*, *Clethrionomys glareolus*, *Microtus subterraneus*, *Stenocranius gregalis*, and *Allactaga major.*

5.3. Paleoecology

The probable cause of the faunal turnover is climate change. To test this hypothesis, paleontological data were analyzed in relation to changes in Mean Annual Temperature (MAT) over the last 800,000 years [215,216]. The model data are spaced 1000 years apart. This resolution is too detailed for analyzing paleontological data, even when absolute datings are available. To better align with the paleontological evidence, the model data were averaged by consecutive Marine Isotope Stages (MIS). For Biozone B, the interval from MIS19 to MIS16 was selected. The lower boundary of this range is based on paleomagnetic data [217]. The upper limit is chosen according to the assumed Late Appearance Date (LAD) of *Mimomys pusillus/blanci* [8]. For Biozone A, based on the available datings, the periods chosen for temperature assessment were MIS6 and MIS2–MIS3, respectively, for layer 10a and layers 5–3-4. It can be seen that temperature trends correspond to changes in species diversity resulting from faunal turnover (Figure 67).

A reconstruction of the average annual temperature based on species identified as modern has been made to establish a closer link between the modeled climate data and the available faunal data. The reconstruction was based on averaging the medians of the species' temperature tolerances [218]. The medians, in the context of the parabolic curve of thermal tolerance, represent the optimal temperature conditions for the species. The average optimum for species in Biozone A is 3 °C, which is lower than the modeled range of 4–6 °C (Figure 67). This is because the tolerance of some species that today have a limited distribution (e.g., *Mesocricetus newtoni*, *Chionomys nivalis*) is probably broader. Given that the current MAT in the area is 10 °C, paleontological data indicate a significantly colder climate during the periods represented by the sediments in Biozone A. For Biozone B, the reconstructed MAT based on small mammals corresponds well with the model temperatures (Figure 67). These comparisons suggest that the deposits in Biozone B most likely span the isotopic stages MIS17–MIS19 (i.e., a period from 790 to 676 Ka [219]). The relatively low species diversity recorded in layer 11c may indicate that it corresponds to the cooling period of MIS18.

Relatively high temperatures, similar to modern ones, reconstructed from indicator species of small terrestrial mammals, are also corroborated by the bat fauna. Their remains are abundant in the deposits of Biozone B and very scarce in those of Biozone A. According to preliminary identifications [101], the dominant species in Biozone B are *Rhinolophus ferrumequinum* Schreber, 1774; *R.* cf. *mehelyi* Matschie, 1901; *Myotis blythii* Tomes, 1857; and

Miniopterus schreibersii Kuhl, 1817. These species are characteristic of southern Europe and are widely distributed throughout Bulgaria today.

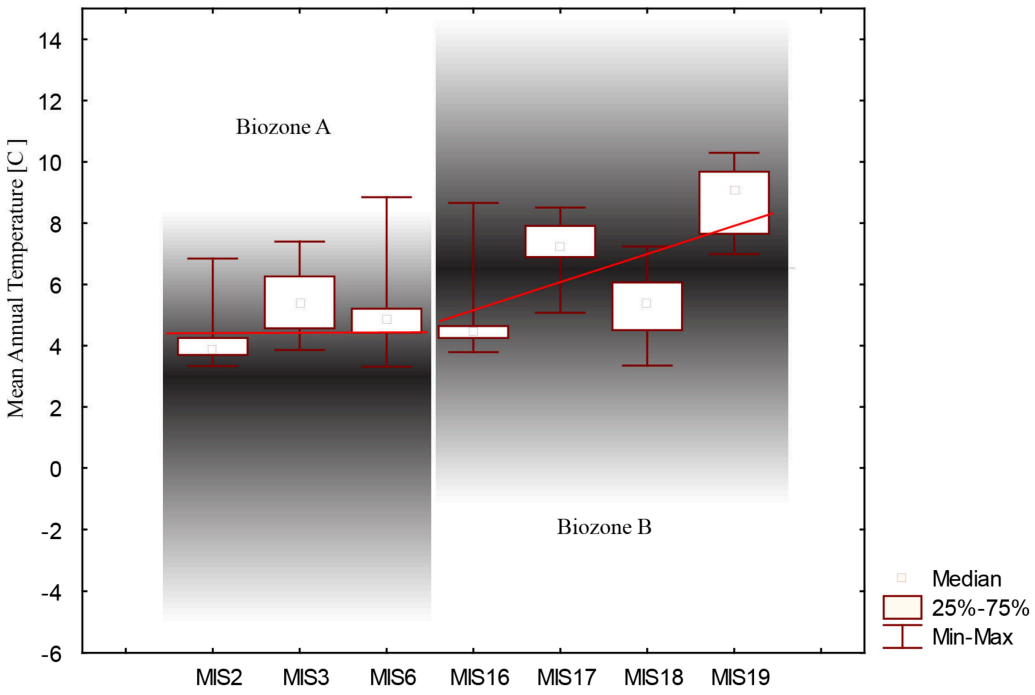


Figure 67. Statistical parameters of mean annual temperatures by isotope stages, presented in each biozone. The gradient shading indicates the overall suitability for indicator species based on their temperature optima, with the highest density marking the average value. The red lines show temperature trends within each biozone.

To understand habitat changes in the cave surroundings in the context of paleotemperature variations, the ecological spectra of stratigraphic assemblages of small mammals were analyzed. Many of the species in Biozone A have close relatives in Biozone B, such as *Nannospalax sirakovi*—*N. leucodon*, *Clethrionomys hintonianus*—*C. glareolus*, *Lagurus transylvanicus*—*L. lagurus*, *Ochotona* sp.—*Ochotona pusilla*, *Allocricetus bursae*—*N. migratorius*, *Microtus arvalidens*—*M. subterraneus*, *M. arvalinus*—*M. arvalis*, *Alexandromys nivalinus*—*A. oeconomus*. It can be assumed that these pairs of species also have similar ecological requirements. These species, along with those classified as modern species but found only in Biozone A, make up 60% of the fauna in the Kozarnika layers. They offer an opportunity for paleoenvironmental reconstructions based on the principle of actualism. For this purpose, they were classified into several eco-geographical groups according to their current distribution and association with regionally specific biotic complexes—biomes and sub-biomes—characterized by the dominance of a particular habitat type, formed under the influence of a combination of the primary climate factors—temperature and humidity [220].

Cryooro Tundras of the temperate alpine belt (CO): *Chionomys nivalis*, *Marmota marmota*. These species prefer low mean annual temperatures, as in the lowland tundra of the polar regions, but with lower thermic and luminic seasonality.

Cold (Boreal) forest (BF): *Neomys fodiens*, *Sorex minutissimus*, *Alexandromys nivalinus*, *A. oeconomus*, *Arvicola amphibius*. These species inhabit a predominantly conifer forest, with some broad-leaved trees, ericoid shrubs, and an herb layer of sedges and grasses, in a cold climate with high temperature seasonality, featuring long, cold winters in which temperatures reach extreme negative values; moderate precipitation, ranging from 500 mm to over 1000 mm, and no summer drought.

Temperate (Nemoral) deciduous forests (TDF): *Apodemus flavicollis*, *Apodemus* sp., *Apodemus sylvaticus*, *Clethrionomys glareolus*, *C. hintonianus*, *Crocidura leucodon*, *Eliomys quercinus*, *Muscardinus avellanarius*, *Sorex araneus*, *Sorex minutus*, and *Talpa europaea*. These species prefer habitats that include a variety of forests, groves, bushes, and grasslands in areas with moderate mean annual temperatures and clearly distinct hot summers and cold winters.

Temperate forest steppe (TFS): *Apodemus uralensis*, *Microtus arvalidens*, *Microtus arvalinus*, *Microtus ex gf. arvalis*, *Microtus subterraneus*. These species are indicative of landscapes consisting of a mosaic of forest and grassland vegetation, covering a large extent between eastern Central Europe and East Asia, occupying an intermediate spatial position between the closed forests (taiga or Nemoral forests) and the treeless steppes, under transitional climatic conditions.

Steppes (S): *Allactaga major*, *Cricetus cricetus*, *Lagurus lagurus*, *Allocricetus bursae*, *Nothocricetulus migratorius*, *Ochotona pusilla*, *Lagurus transylvanicus*, *Sicista subtilis*, *Stenocranius gregalis*. These species are indicative of grassland or dwarf-shrubland in a highly continental climate with a large annual temperature range, which usually implies very cold winters, moderate or low precipitation, mainly in summer, and no or moderate drought in the growing season.

Mediterranean (M): *Apodemus epimelas*, *Myomimus roachi*. These species inhabit landscapes dominated by trees, shrubs, and scrub, with reduced, hard leaves, under relatively high mean annual temperatures and arid summer conditions.

Submediterranean forest steppe (SFS): *Spermophilus citellus*, *Nannospalax leucodon*, *N. sirakovi*, *Mesocricetus newtoni*. These species preferred habitats consist of dry grassland and open broad-leaved woodland in areas with relatively high temperatures and moderate to high continentality, with winter temperatures frequently falling below zero.

Regarding the species composition (Figure 68B), the stratigraphic eco-geographic spectra are relatively homogeneous and correspond to the geographical location. It should be noted that there is an increase in the relative share of Boreal species in Biozone A, especially well expressed in layers 10a and 3–4, and a disappearance of Mediterranean species, which are absent in Biozone A. These features indicate a cooling of the climate, most clearly manifested in layers 10a and 3–4. Concerning the relative abundance of species of particular eco-geographical groups, all layers are dominated by species that inhabit open spaces (Figure 68A). Since these species are preferred prey for owls, this is not particularly informative about the dominant habitat type in the cave surroundings. However, comparing stratigraphic changes can provide some insight into the relative proportions of habitats and, by extension, paleoecological changes. The differences are most evident in the relative abundances of mountain (CO), steppe (S), and temperate forest-steppe (TFS) species. This is especially well expressed in layers 10a, 5a, and 3–4. The forest-steppe species also increase at the expense of steppe species in the uppermost layers, from layer 6–7 to layer 3–4. These changes probably reflect increased humidity under relatively cool climatic conditions. In biozone B, the ratio between eco-geographical groups remains relatively stable, showing a consistent dominance of steppe and forest-steppe habitats. It should be noted that there is an increase in cold-loving species in layer 11c.

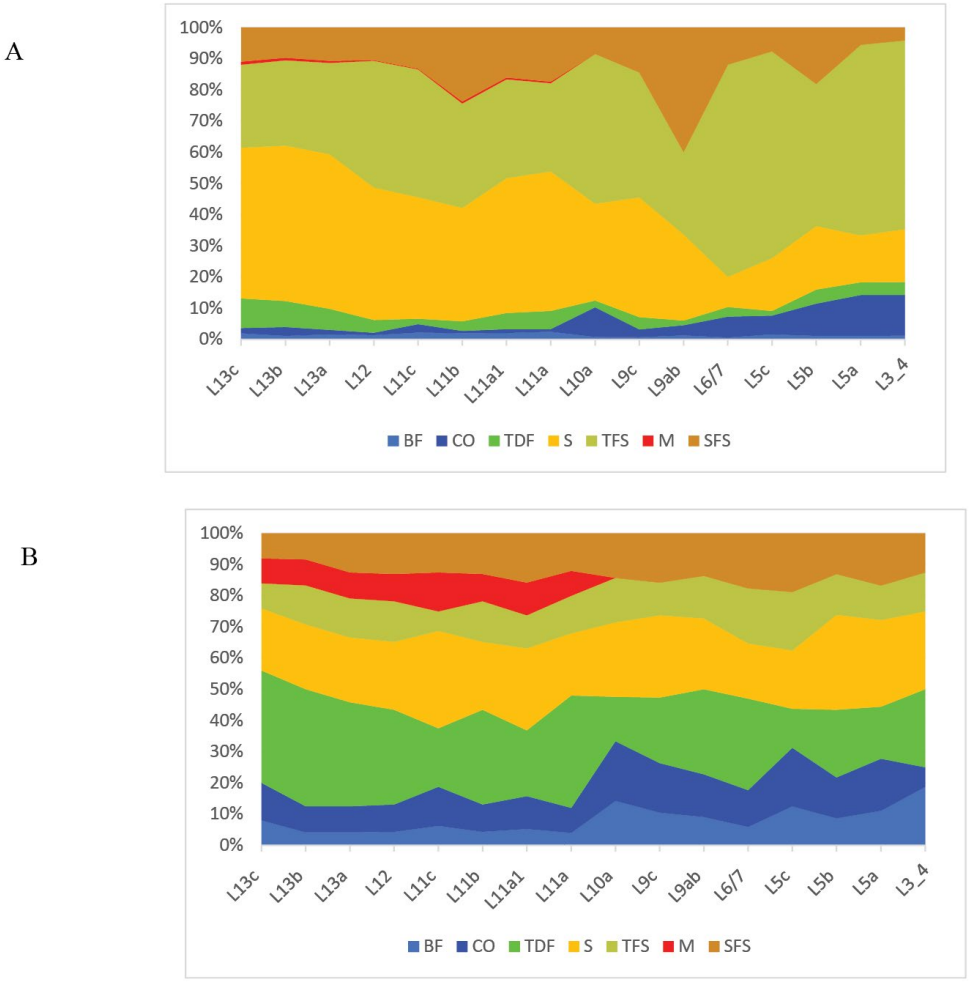


Figure 68. Eco-geographical spectra of stratigraphic small-mammal assemblages based on the number of identified individuals (**A**) and species (**B**). CO—Cryooro Tundras of the temperate alpine belt, BF—Cold (Boreal) forest, TDF—Temperate (Nemoral) deciduous forests, TFS—Temperate forest steppe, S—Steppes, M—Mediterranean, SFS—Submediterranean forest steppe.

5.4. Biostratigraphic Correlations

Without other reliable absolute dating methods available, magnetostratigraphy remains the primary technique applicable to Early and early Middle Pleistocene sites in Europe. Layers with fossils that can be matched to the palaeomagnetic timescale provide an independent means of verifying biostratigraphic correlations [139]. At Kozarnika, as discussed in our earlier publication, the small-mammal record, according to standard biostratigraphy, should span nearly the entire Brunhes Chron in a continuous sequence, cross the Brunhes–Matuyama boundary, and extend into the Jaramillo normal-polarity Subchron [4]. Later, the Brunhes–Matuyama boundary was discovered in the upper part of Layer 13-Lower [5], confirming the age inferred from small mammals. As mentioned above, based on biostratigraphic data, the upper boundary of the deposits in Biozone B cannot be older than 650 Kya. These data allow comparisons with faunas for which reliable age estimates from paleomagnetic data are available. Several sites in Europe, according to available paleomagnetic data, fall within an interval just above the Brunhes–Matuyama boundary, up to 600 Kya [135,139].

The West Runton Freshwater Bed (WRFB) in East Anglia, England, represents the Cromerian interglacial, dating to early MIS 17. Its microfauna includes species such as *Clethrionomys hintonianus*, *Pliomys episcopalis*, *Mimomys savini*, *Microtus 'arvalinus'*, *M. 'rattiepoides'*, *M. gregaloides*, and *M. arvalidens*. Similarly, the Voigtstedt fauna in central Germany,

an important early Brunhes assemblage, shares several taxa with WRFB, including *Microtus arvalinus*, *M. ratticepoides*, and *Mimomys savini*. Morphometric evidence suggests Voigtstedt is slightly younger, with paleoecological data indicating warmer conditions, possibly during the Cromerian climatic optimum. Deposits at Přezletice, Czech Republic, yield vole species such as *Microtus arvalinus*, *M. arvalidens*, *M. gregaloides*, *M. ratticepoides*, and *Mimomys savini*, and their faunal profile resembles that of West Runton. The mammal fauna from Kozi Grzbiet, Poland, contains more continental species, and morphometric data imply that Přezletice and Kozi Grzbiet are somewhat older than Voigtstedt. At Mahlis, Central Germany, the Matuyama–Brunhes boundary lies beneath the fossiliferous layers, which contain a sparse micromammal fauna including *Microtus arvalinus*, *M. ratticepoides*, and *Mimomys savini*. In Únětice, Czech Republic, the boundary is also below the vole layer with *Microtus* sp. (A/L value 50.3; n = 2) and *Mimomys savini*. In Pakefield, England, deposits contain *Mimomys savini* and *M. pusillus* alongside *Microtus ex gr. arvalis* in normally polarized layers. At Rifreddo (San Lorenzo Cycle), Southern Italy, layers have yielded rodents such as *Iberomys* ex gr. *huescarensis-brecciensis*, *Microtus arvalidens*, and *Mimomys savini*, indicating temperate conditions. In Spain, at the multilayer site Trichera Dolina, in layer TD8, representing the very bottom of the Brunhes magnetic polarity zone, against the background of *Mimomys savini*, *Pliomys episcopalis*, *Microtus gregaloides*, *M. seseae*, *Iberomys huescarensis*, *Microtus oeconomus* appears for the first time.

Several Eastern European localities with small mammals correspond to the beginning of the Brunhes paleomagnetic epoch. The small mammal fauna near the settlement of Priazovsky (Taman Peninsula) includes *Spermophilus* sp., *Mimomys pusillus*, *M. savini*, *Lagurodon arankae*, *Microtus (Stenocranius) hintoni*, *M.* ex gr. *oeconomus*. This fauna is similar in evolutionary level to the vole genera *Mimomys*, *Lagurodon*, and *Microtus* from earlier sites (correlating with the end of the Matuyama epoch), Petropavlovka, and Karay-Dubina. It appears that small-mammal faunas at this evolutionary level persisted throughout the late Matuyama and early Brunhes epochs. At the Litvin site (Krasnodar Krai, Taman Peninsula, species such as *Ochotona* sp., *Allactaga* sp., *Mimomys savini*, *Borsodia fejervaryi*, *Prolagurus pannonicus*, *Eolagurus simplicidens gromovi*, *Allophaiomys pliocaenicus nutiensis*, *Microtus (Stenocranius) hintoni*, and *Microtus arvalinus* have been found. The fauna from the Nagornoe 1 section (Ukraine, Kagul lagoon, VII terrace of the Danube) includes *Mimomys savini*, *Prolagurus pannonicus*, *Allophaiomys pliocaenicus*, *Microtus (Stenocranius) hintoni-gregaloides*, and *M. oeconomus*, among others.

All these localities are characterized by the presence of *Mimomys savini*, while *M. pusillus* has been identified only in one of them. The species found in all these localities correspond to the group of dominant or frequently occurring species in the lower layers of Kozarnika. However, a significant difference is the absence of Villanyian and early Biharian elements in these faunas, which, although with a low relative abundance, are found in all layers of the lower series of Kozarnika deposits. Nevertheless, it should be noted that in some nearby localities, in the northwestern Black Sea region, species from these groups are present, including *Allophaiomys pliocaenicus*, *A. pliocaenicus nutiensis*, *Borsodia fejervaryi*, *Lagurodon arankae*, and *Microtus (Stenocranius) hintoni*. Completely absent, however, are other early species such as *Mimomys pitymyoides*, *M. tornensis*, *Villanyia exilis*, and *Borsodia arankoides*. Considering that in Kozarnika these species have very low relative abundance in the stratigraphic assemblages, it can be assumed that their absence in the mentioned localities is partly due to the small sample sizes from those sites. In general, the situation in Kozarnika corresponds with what is known about the fauna of large mammals in Europe during this time, where, during the intervals of colder climate, the southern regions of Europe (the Apennine, Balkan, and Iberian peninsulas) often served as refugia for some thermophilous Villafranchian taxa typical of earlier times [132].

The faunal change registered in Biozone B, when viewed alongside paleomagnetic data and climate shifts during the MIS19 to MIS17 interval, indicates that it reflects the mid-Pleistocene transition (MPT, around 1200 to 500 Kya). This period was marked by significant changes in Earth's climate, shifting from low-amplitude 41,000-year obliquity-driven cycles to high-amplitude, roughly 100,000-year fluctuations that define the later Pleistocene and Holocene [221]. Starting around 900 Kya, major glaciations, particularly in the Northern Hemisphere, dramatically affected both biota and the physical environment. The Matuyama–Brunhes magnetic Chron boundary (approximately 773 Kya) aligns with a major glacial event, occurs roughly in the middle of the MPT, and is a common marker in marine and land sediments [222].

Repeated climate oscillations altered vegetation structure, shifting from forests to steppe and grasslands during glacial-interglacial cycles, and consequently modified the structure of faunal assemblages. Faunal renewal accelerated with the dispersal of taxa with warm-humid affinities during interglacial events and with cold-steppe affinities during glacial events. At the same time, the southern parts of Europe began to play a more important role as a refuge for temperate Early Pleistocene taxa that were already extinct in more northern areas during stadial phases [223,224]. These faunal changes are known as the Villafranchian–Galerian transition. It can be assumed that the dispersal of humans in Europe is part of this faunal turnover. In this way, the recorded dynamics of the small mammal fauna in Biozone B, together with its paleoecological context and archaeological findings, support the Galerian migration hypothesis of human invasion in Europe [216].

6. Conclusions

This study is based on an exceptionally rich material (45,672 identifiable remains) collected through precise sampling at 5-cm intervals in the sediments and washed through screens with a 1-cm mesh. The sediments are well-dated. For the upper part of the deposits, Biozone A, corresponding to the Toringian, absolute dates are available, indicating that they span two periods: MIS 3–4 and MIS 6. Paleomagnetic data, combined with biostratigraphic data based on small mammals, allow the lower part of the deposits, Biozone B, to be attributed to the upper Biharian, spanning the chronological interval from the Brunhes–Matuyama boundary to about 650,000 years ago and covering MIS 17–19. Based on this, it can be assumed that there is a temporal hiatus of about 470,000 years between the two biozones.

The taphonomic features of the material indicate that the majority of small-mammal remains were accumulated through owl predation, most likely by the Barn Owl (*Tyto alba*), and, to a lesser extent, by the Eagle Owl (*Bubo bubo*) and the Tawny Owl (*Strix aluco*). The morphological and anatomical features of the bone assemblages indicate that they have not undergone significant secondary transport and re-deposition. They are practically in situ, with fragmentation resulting from natural weathering and decay of the less durable bone structures, as well as from mechanical pressure and temperature changes acting during different stages of the burial of the bone assemblages.

In this context, the morphological features and evolution of 75 species of small mammals were analyzed in detail. An important feature of the site is that the fauna in the upper layers (Biozone A) consists of species that still live today. This enables many of their morphological features—such as variability, size, and qualitative traits—to act as references and starting points for morphological analysis and taxonomic decisions. This is especially important for species in the lower deposit series, which often differ from modern species and have conflicting taxonomic classifications. It proves particularly useful in defining taxonomic boundaries between closely related species and in objectively measuring their differences from modern relatives.

Geometric analysis of mass species of "grey" voles (Microtina) and steppe lemmings (*Lagurus)* has clarified the controversial taxonomic positions of some species. It confirmed that *Microtus arvalinus* is a distinct species different from *Microtus nivaloides*. Rapid evolution in *Lagurus transylvanicus* towards *L. lagurus* has been demonstrated.

In all layers of Biozone B, two key guide fossils, *Mimomys savini* and *M. blanci*, occur, indicating the second stage of the Early Biharian. This predates the Brunhes/Matuyama reversal and contradicts paleomagnetic data and the evolutionary levels of mass-vole species, which indicate a Late Biharian age. Additionally, several species characteristic of the Early Pleistocene (Villanyian and Early Biharian) have been identified, including *Borsodia newtoni*, *B. arankoides*, *Lagurus arankae*, *Prolagurus pannonicus*, *Villanyia* cf. *exilis*, *Mimomys pitymyoides*, *M. tornensis*, *Allophaiomys deucalion*, *A.* cf. *pliocaenicus*, *and A.* cf. *burgondiae*. Although rare, these species are regularly found in Biozone B, which is composed mainly of Late Biharian species such as *Allophaiomys gregaloides*, *Microtus arvalidens*, *M. nivaloides*, and *Lagurus transylvanicus*.

Some of the above-mentioned "archaic" species represent a notable aspect of the faunal composition in Biozone B at Kozarnika: the coexistence of primitive species that occur in low numbers with more abundant species believed to be their descendants. *Allophaiomys deucalion*, considered to be at the base of the radiation of more advanced forms within the subtribe Microtina, is found alongside its "descendants," including *Allophaiomys* cf. *pliocaenicus*, *A.* cf. *burgondiae*, *A. gregaloides*, *Alexandromys nivalinus*, *Microtus arvalidens*, and *M. nivaloides*. In the tribe Lagurini, forms at different evolutionary stages coexist, including *Borsodia arankoides/Lagurus arankae*, *L. arankae/L. transylvanicus*, and *Borsodia newtoni/Prolagurus ternopolitanus* (as a morphotype)—*P. pannonicus.* These cases challenge the common view of gradual evolution and suggest that evolution within these two clades is not purely anagenetic. Instead, they support the punctuated equilibrium model, which accounts for the persistence of ancestral species alongside their descendants. Consequently, the macroevolutionary trend appears to be driven by species selection rather than by natural selection within populations. Various phylogenetic lineages show different chronological ranges across geographic regions. Throughout much of the Holarctic, primitive forms tend to disappear quickly—likely due to global cooling and competition from more advanced, better-adapted relatives. However, in some regions, primitive forms, such as those at Kozarnika, persist longer.

The Kozarnika case illustrates that the anagenetic model, which relies primarily on the successive replacement of specific forms for biostratigraphic subdivision, is not well suited to large-scale correlations. Comparisons with faunas dated by paleomagnetism suggest that the mass species composition and their evolutionary stages, determined through quantitative morphological criteria, are more reliable for biostratigraphic correlations.

The presence of *Mesocricetus newtoni* and *Spermophilus citellus* marks their earliest known occurrence in Biozone B.

In the lower series of deposits, a species from the genus *Nannospalax* is abundantly represented, distinguished from the modern species *N. leucodon* by a significantly smaller size and a more complex chewing surface, and described as a new species, *N. sirakovi*.

The ecological spectra of the stratigraphic assemblages indicate that in both biozones, inhabitants of open habitats, steppes, and forest-steppes predominate. The differences between the two biozones are mainly determined by temperature, as Biozone B includes thermophilic Mediterranean species such as *Apodemus epimelas*, *Myomimus* cf. *roachi*, and *Hystrix refossa*. The number of species associated with closed habitats, forests, and shrublands (*Sorex* spp., murids, glirids) in this zone is also significant.

The faunal turnover in the lower deposits has been examined thoroughly. A restructuring of fauna resulted from the gradual disappearance of Early Pleistocene species.

Paleoecological reconstructions based on small mammal assemblages suggest that this faunal change is linked to paleoclimatic shifts during MIS19–MIS17, reflecting a reorganization of the biota associated with the mid-Pleistocene transition. This period saw significant climatic changes, shifting from low-amplitude 41,000-year cycles driven by obliquity to high-amplitude, roughly 100,000-year fluctuations characteristic of the later Pleistocene and Holocene.

Supplementary Materials: The following supporting information can be downloaded at https://www.mdpi.com/article/10.3390/fossils4030023/s1. Table S1: Catalog of studied specimens with links to available photos.

Funding: This research received no external funding.

Informed Consent Statement: Not applicable.

Data Availability Statement: A catalog of the specimens studied, with links to available photos, is provided in the Supplementary Materials.

Acknowledgments: This study was based on specimens deposited in the Fossil Mammals Collection of the Institute of Biodiversity and Ecosystem Research—Bulgarian Academy of Sciences, upgraded in the framework of the project DiSSCo-BG (Upgrade of the Research Infrastructure "Distributed System of Scientific Collections—Bulgaria") funded by the National Roadmap for Research Infrastructures, Ministry of Education and Science of the Republic of Bulgaria. Kozarnika cave fieldwork is funded by the National Institute of Archaeology and Museum of the Bulgarian Academy of Sciences (N. Sirakov) and UMR5199 CNRS PACEA (J.-L. Guadelli), financially supported by the Advisory Committee of the Archaeological Research abroad of the French Ministry of Foreign Affairs (Mission Paléolithique de Bulgarie directed by J.-L. Guadelli). I thank the excavation teams at the Kozarnika site for their work.

Conflicts of Interest: The author declares no conflict of interest.

References

1. Guadelli, J.-L.; Sirakov, N.; Ivanova, S.; Sirakova, S.; Anastassova, E.; Courtaud, P.; Dimitrova, I.; Djabarska, N.; Fernandez, P.; Ferrier, C. Une Séquence Du Paléolithique Inférieur Au Paléolithique Récent Dans Les Balkans: La Grotte Kozarnika à Orechets (Nord-Ouest de La Bulgarie). In *Les Premiers Peuplements en Europe*; Archaeopress: Oxford, UK, 2005; Volume 1364, pp. 87–103.
2. Sirakov, N.; Guadelli, J.-L.; Ivanova, S.; Sirakova, S.; Boudadi-Maligne, M.; Dimitrova, I.; Ph, F.; Ferrier, C.; Guadelli, A.; Iordanova, D.; et al. An Ancient Continuous Human Presence in the Balkans and the Beginnings of Human Settlement in Western Eurasia: A Lower Pleistocene Example of the Lower Palaeolithic Levels in Kozarnika Cave (North-Western Bulgaria). *Quat. Int.* **2010**, *223–224*, 94–106. [CrossRef]
3. Hopkins, R.; Guadelli, J.-L.; White, D.; Stringer, C.; Vegh, E.; Buckley, M.; Guadelli, A.; Ph, F.; Sirakov, N.; Higham, T. A Refined Chronology for the Middle–Upper Paleolithic Transition at Kozarnika Cave (Bulgaria) 40–50,000 Years Ago. New AMS Radiocarbon Dates and Implications for Early *Homo sapiens* in Europe. *PaleoAnthropology* **2026**, *1*, 82–98.
4. Popov, V.; Marinska, M. An Almost One Million Year Long (Early to Late Pleistocene) Small Mammal Succession from the Archaeological Layers of Kozarnika Cave in Northern Bulgaria. *Cour. Forsch.-Inst. Senckenberg* **2007**, *259*, 79–92.
5. Muttoni, G.; Sirakov, N.; Guadelli, J.-L.; Kent, D.V.; Scardia, G.; Monesi, E.; Zerboni, A.; Ferrara, E. An Early Brunhes (<0.78 Ma) Age for the Lower Paleolithic Tool-Bearing Kozarnika Cave Sediments, Bulgaria. *Quat. Sci. Rev.* **2017**, *178*, 1–13. [CrossRef]
6. Tillier, A.; Sirakov, N.; Guadelli, A.; Fernandez, P.; Sirakova, S.; Dimitrova, I.; Ferrier, C.; Guérin, G.; Heidari, M.; Krumov, I.; et al. Evidence of Neanderthals in the Balkans: The Infant Radius from Kozarnika Cave (Bulgaria). *J. Hum. Evol.* **2017**, *111*, 54–62. [CrossRef] [PubMed]
7. Fernandez, P.; Crégut-Bonnoure, E. Les Caprinae (Rupicaprini, Ovibovini, Ovini et Caprini) de la séquence pléistocène de Kozarnika (Bulgarie du Nord): Morphométrie, biochronologie et implications phylogéniques. *Rev. Paléobiol.* **2007**, *26*, 425–503.
8. Maul, L.C.; Markova, A.K. Similarity and Regional Differences in Quaternary Arvicolid Evolution in Central and Eastern Europe. *Quat. Int.* **2007**, *160*, 81–99. [CrossRef]
9. Kawamura, Y.; Takai, M. Pliocene Lagomorphs and Rodents from Udunga, Transbaikalia. *Asian Paleoprimatology* **2009**, *5*, 15–44.
10. Weerd, A. Rodent Faunas of the Mio-Pliocene Continental Sediments of the Teruel-Alfambra Region, Spain. Ph.D. Thesis, Utrecht University, Utrecht, The Netherlands, 1976.

11. Barisone, G.; Argenti, P.; Kotsakis, T. Plio-Pleistocene Evolution of the Genus Castor (Rodentia, Mammalia) in Europe: *C. fiber plicidens* of Pietrafitta (Perugia, Central Italy). *Geobios* **2006**, *39*, 757–770. [CrossRef]
12. Dirnberger, M.; Peláez-Campomanes, P.; López-Antoñanzas, R. Phylogenetic Relationships of Neogene Hamsters (Mammalia, Rodentia, Cricetinae) Revealed under Bayesian Inference and Maximum Parsimony. *PeerJ* **2024**, *12*, e18440. [CrossRef] [PubMed]
13. Wang, B.Y. Zapodidae (Rodentia, Mammalia) from the Lower Oligocene of Qujing, Yunnan, China. *Mainz. Geowiss. Mitteilungen* **1985**, *14*, 345–367.
14. De Bruijn, H. Some New Miocene Gliridae (Rodentia Mammalia) from the Calatayud Area (Province of Zaragoza, Spain). *I. K. Ned. Akad. Van Weteschappen-Proc. Ser. B-Phys. Sci.* **1966**, *69*, 1–21.
15. Bosma, A.A. The Influence of Attrition on the Dental Pattern of Pleistocene Acanthion Brachyurus (Hystricidae, Rodentia, Mammalia) from Java. *Proc. K. Ned. Akad. Wet.* **1968**, *71*, 336–341.
16. Reumer, J.W.F. Ruscinian and Early Pleistocene Soricidae (Insectivora, Mammalia) from Tegelen (The Netherlands) and Hungary. *Scr. Geol.* **1984**, *73*, 1–173.
17. Topachevskyi, V.A. *Mole Rats. Spalacidae*; Fauna USSR. Mammals; Nauka: Moscow, Russia, 1969; Volume 3.
18. Erten, H. Spalax Denizliensis sp. nov.(Spalacidae, Rodentia) from an Early Pleistocene-Aged Locality in the Denizli Basin (Southwestern Turkey). *Turk. J. Zool.* **2018**, *42*, 62–67. [CrossRef]
19. Erdal, O.; Erturaç, M.K.; Dalfes, H.N.; Sen, S. Rodents from the Middle Pleistocene of Niksar Basin (Tokat-Turkey): Implications on Palaeoenvironment and the North Anatolian Fault. *Neues Jahrb. Für Geol. Paläontol. Abh.* **2018**, *289*, 77–111. [CrossRef]
20. Sinitsa, M.V.; Pogodina, N.V. The Evolution of Early Spermophilus in Eastern Europe and the Antiquity of the Old World Ground Squirrels. *Acta Palaeontol. Pol.* **2019**, *64*, 643–667. [CrossRef]
21. Van der Meulen, A.J. Middle Pleistocene Smaller Mammals from the Monte Peglia (Orvieto, Italy) with Special Reference to the Phylogeny of Microtus (Arvicolidae, Rodentia). *Quaternaria* **1973**, *17*, 1–144.
22. Rabeder, G. Die Arvicoliden (Rodentia, Mammalia) Aus Dem Pliozän Und Dem Älteren Pleistozän von Niederösterreich. *Beitr. Paläontol. Osterr.* **1981**, *8*, 1–373.
23. Carls, N.; Rabeder, G. Die Arvicoliden (Rodentia, Mammalia) Aus Dem Ältest-Pleistozän von Schernfeld (Bayern). *Beitr. Paläontol. Osterr.* **1988**, *14*, 123–237.
24. Tesakov, A.S. Biostratigraphy of the Middle Pliocene-Eopleistocene of Eastern Europe. *Trans. Geol. Inst.* **2004**, *554*, 1–248. [CrossRef]
25. Martin, R.A. Notes on the Classification and Evolution of Some North American Fossil *Microtus* (Mammalia; Rodentia). *J. Vertebr. Paleontol.* **1987**, *7*, 270–283. [CrossRef]
26. Cuenca-Bescós, G.; Laplana, C.; Canudo, J.I. Biochronological Implications of the Arvicolidae (Rodentia, Mammalia) from the Lower Pleistocene Hominid-Bearing Level of Trinchera Dolina 6 (TD6, Atapuerca, Spain). *J. Hum. Evol.* **1999**, *37*, 353–373. [CrossRef] [PubMed]
27. Hutchison, J.H. Notes on Type Specimens of European Miocene Talpidae and a Tentative Classification of Old World Tertiary Talpidae (Insectivora: Mammalia). *Geobios* **1974**, *7*, 211–256. [CrossRef]
28. Popov, V.V. Late Pliocene Erinaceidae and Talpidae (Mammalia: Insectivora) from Varshets (North Bulgaria). *Acta Zool. Cracoviensia* **2004**, *47*, 61–80.
29. Lippi, P.; Masini, F.; Maul, L.; Abbazzi, L. Evolutionary Changes of Enamel Differentiation in Pleistocene Mediterranean and Middle European Populations of Microtus (Rodentia, Arvicolidae). *Paludicola* **1998**, *2*, 50–61.
30. Masini, F.; Maul, L.C.; Abbazzi, L.; Petruso, D.; Savorelli, A. Independent Water Vole (Mimomys Savini, Arvicola: Rodentia, Mammalia) Lineages in Italy and Central Europe. *Foss. Impr.* **2020**, *76*, 59–83. [CrossRef]
31. Rohlf, F.J. *tpsDig, Digitize Landmarks and Outlines*; Department of Ecology and Evolution, State University of New York at Stony Brook: Stony Brook, NY, USA, 2004.
32. Sheets, H.D. Integrated Morphometrics Package (IMP) 8, 2014. Available online: https://www.animal-behaviour.de/imp/ (accessed on 20 September 2016).
33. Rohlf, F.J. Morphometric Spaces, Shape Components and the Effects of Linear Transformations. In *Advances in Morphometrics*; Springer: Boston, MA, USA, 1996.
34. Rohlf, F.J. *TPSRELW: Relative Warps*, version 1.20; New York State University at Stony Brook: Stony Brook, NY, USA, 1998.
35. Dryden, I.L.; Mardia, K.V. *Statistical Shape Analysis*; Wiley: Hoboken, NJ, USA, 1998.
36. Hammer, O.; Harper, D.A.T.; Ryan, P.D. PAST: Paleontological Statistics Software Package for Education and Data Analysis. *Palaeontol. Electron.* **2001**, *4*, 9.
37. Scrucca, L.; Fop, M.; Murphy, T.B.; Raftery, A.E. Mclust 5: Clustering, Classification and Density Estimation Using Gaussian Finite Mixture Models. *R J.* **2016**, *8*, 289. [CrossRef]
38. Popov, V.V. The Small Mammals (Mammalia: Insectivora, Chiroptera, Lagomorpha, Rodentia) from Cave 16 (North Bulgaria) and the Paleoenvironmental Changes during the Late Pleistocene. *Temnata Cave Excav. Karlukovo Karst Area Bulg.* **2000**, 2, 159–240.

39. Botka, D.; Mészáros, L. *Crocidura* (Mammalia, Soricidae) Remains from the Late Early Pleistocene Somssich Hill 2 Locality (Villány Hills, Southern Hungary). *Fragm. Palaeont. Hung.* **2015**, *32*, 67–98. [CrossRef]
40. Rzebik-Kowalska, B. Insectivora [Mammalia] from the Early and Early Middle Pleistocene of Betfia in Romania. I. Soricidae Fischer von Waldheim, 1817. *Acta Zool. Cracoviensia* **2000**, *43*, 1–53.
41. Rzebik-Kowalska, B. Fossil History of Shrews in Europe. In *Evolution of Shrews*; Mammal Research Institute Polish Academy of Sciences: Białowieża, Poland, 1998; pp. 23–92.
42. Reumer, J.W. Notes on the Soricidae (Insectivora, Mammalia) from Crete, Part I. The Pleistocene Species Crocidura Zimmermanni. *Bonn. Zool. Beitr.* **1986**, *37*, 161.
43. Popov, V.V. Middle Pleistocene Small Mammals (Insectivora, Lagomorpha, Rodentia) from Morovitsa Cave (North Bulgaria). *Acta Zool. Cracoviensia* **1989**, *32*, 561–588.
44. Popov, V. Late Pliocene Soricidae (Insectivora, Mammalia) from Varshets (North Bulgaria). *Acta Zool. Cracoviensia* **2003**, *46*, 43–72.
45. Rzebik-Kowalska, B. Pliocene and Pleistocene Insectivora (Mammalia) of Poland, VIII Soricidae: Sorex Linnaeus 1758, Neomys Kaup, 1829, Macroneomys Fejfar, 1966, Paenelimnoecus Baudelot, 1972 and Soricidae Indeterminata. *Acta Zool. Cracoviensia* **1991**, *34*, 323–424.
46. Heller, F. Eine Neue Altquartäre Wirbeltierfauna von Erpfingen (Schwäbische Alb). *Neues Jahrb. Geol. Paläontol.* **1958**, *107*, 1–102.
47. Jammot, T.D. Les Insectivores (Mammalia) Du Gisement Pléistocène Moyen Des Abîmes de La Fage à Noailles (Corrèze). *Nouv. Arch. Mus. d'Histoire Nat.* **1973**, *11*, 41–51. [CrossRef]
48. Popov, V.V. Middle Pleistocene Small Mammals (Mammalia: Insectivora, Lagomorpha, Rodentia) from Varbeshnitsa (Bulgaria). *Acta Zool. Cracoviensia* **1988**, *31*, 193–234.
49. Jánossy, D. Stratigrafische Auswertung Der Europäischen Mittelpleistozänen Wirbeltierfauna. *Berichte Dtsch. Ges. Geol. Wiss.* **1969**, *14*, 573–643.
50. Harrison, D.L. Systematic Status of Kennard's Shrew [Sorex Kennardi Hinton, 1911, Insectivora: Soricidae]: A Study Based on British and Polish Material. *Acta Zool. Cracoviensia* **1996**, *39*, 201–212.
51. Hinton, M.A.C. I.—The British Fossil Shrews. *Geol. Mag.* **1911**, *8*, 529–539. [CrossRef]
52. Mais, K.; Rabeder, G. Das Grobe Höhlensystem Im Pfaffenberg Bei Bad Deutsch-Altenburg (Niederösterreich) Und Seine Fossilen Faunen. *Die Hölle* **1984**, *35*, 213–230.
53. Clot, A.; Chaline, J.; Jammot, D.; Mourier-Chauvire, C.; Rage, J.C. Les Poches Ossifiées Du Pleistocène Moyen et Inférieur de Mountoussé (Hautes-Pyrénées). *Bull. Société Hist. Nat. Toulouse* **1976**, *112*, 146–161.
54. Osipova, V.A.; Rzebik-Kowalska, B.; Zaitsev, M.V. Intraspecific Variability and Phylogenetic Relationships of the Pleistocene Shrew *Sorex runtonensis* (Soricidae). *Acta Theriol.* **2006**, *51*, 129–138. [CrossRef]
55. Rofes, J.; Moya-Costa, R.; Bennàsar, M.; Blain, H.-A.; CuencaBescós, G. Biostratigraphy, Palaeogeography and Palaeoenvironmental Significance of *Sorex runtonensis* Hinton, 1911 (Mammalia, Soricidae): First Record from the Iberian Peninsula. *Palaeogeogr. Palaeoclimatol. Palaeoecol.* **2016**, *459*, 508–517. [CrossRef]
56. Rzebik-Kowalska, B. Erinaceomorpha and Soricomorpha (Mammalia) from the Late Pleistocene and Holocene of Krucza Skała Rock Shelter and Komarowa Cave (Poland). *Acta Zool. Cracoviensia* **2006**, *49*, 83–118. [CrossRef]
57. Marchetti, M.; Parolin, K.; Sala, B. The Biharian Fauna from Monte La Mesa [Verona, Northeastern Italy]. *Acta Zool. Cracoviensia* **2000**, *43*, 79–105.
58. Harrison, D.L.; Parfitt, S.A. Fossil Remains of Shrews (Soricomorpha: Soricidae) and Desmans (Talpidae: Desmaninae) from Norfolk, England, with Biostratigraphic Implications for the Plio-Pleistocene Boundary in East Anglia. *Acta Zool. Cracoviensia Ser. A Vertebr.* **2009**, *52*, 61–79. [CrossRef]
59. Rzebik-Kowalska, B. The Pliocene and Early Pleistocene Lipotyphla (Insectivora, Mammalia) from Romania. *Acta Zool. Cracoviensia* **2002**, *45*, 251–281.
60. Mezhzherin, V.A. Shrews (Sorex, Insectivora, Mammalia) from Pleistocene deposits of the USSR. In *Tjeriologija*; Nauka: Novosibirsk, Russia; Volume 1, pp. 117–130.
61. Rabeder, G. Die Insectivoren Und Chiropteren (Mammalia) Aus Dem Altpleistozän von Hundsheim (Niederösterreich). *Ann. Naturhist. Mus. Wien* **1972**, *76*, 375–474.
62. Botka, D.; Mészáros, L. Asoriculus and Neomys (Mammalia, Soricidae) Remains from the Late Early Pleistocene Somssich Hill 2 Locality (Villány Hills, Southern Hungary). *Fragm. Palaeontol. Hung.* **2017**, *34*, 105–125. [CrossRef]
63. Malez, M.; Rabeder, G. Neues Fundmaterial von Kleinsäugern Aus Der Altpleistozänen Spaltenfüllung Podumci 1 in Norddalmatien (Kroatien, Jugoslawien). *Beitr. Paläontol. Osterr.* **1984**, *11*, 439–510.
64. Rofes, J.; Cuenca-Bescós, G. First Record of *Beremendia fissidens* (Mammalia, Soricidae) in the Pleistocene of the Iberian Peninsula, with a Review of the Biostratigraphy, Biogeography and Palaeoecology of the Species. *Comptes Rendus Palevol* **2009**, *8*, 21–37. [CrossRef]
65. Maul, L.C.; Parfitt, S.A. Micromammals from the 1995 Mammoth Excavation at West Runton, Norfolk, UK: Morphometric Data, Biostratigraphy and Taxonomic Reappraisal. *Quat. Int.* **2010**, *228*, 91–115. [CrossRef]

66. Marchetti, M. Talpa Masinii n. sp., a New Fossil Mole Species from the Late Villanyian Fauna of Rivoli Veronese (North-Eastern Italy) in the Context of the European Fossil Record of Genus Talpa. *Foss. Impr.* **2024**, *80*, 285–311. [CrossRef]
67. Maul, L.C. Die Kleinsäugerreste (Insectivora, Lagomorpha, Rodentia) Aus Dem Unterpleistozän von Untermassfeld. In *Das Pleistozän von Untermassfeld bei Meiningen (Thüringen)*; Propylaeum: Heidelberg, Germany, 2001; Volume 3, pp. 783–887.
68. Van Cleef-Roders, J.T.; Hoek Ostende, L.V.D. Dental Morphology of Talpa Europaea and Talpa Occidentalis (Mammalia: Insectivora) with a Discussion of Fossil Talpa in the Pleistocene of Europe. *Zool. Meded.* **2001**, *75*, 51–67. [CrossRef]
69. Sansalone, G.; Kotsakis, T.; Piras, P. Talpa Fossilis or Talpa Europaea? Using Geometric Morphometrics and Allometric Trajectories of Humeral Moles Remains from Hungary to Answer a Taxonomic Debate. *Palaeontol. Electron.* **2015**, 18.2.42A. [CrossRef] [PubMed]
70. Koenigswald, W. von Mittelpleistozäne Kleinsäugerfauna Aus Der Spaltenfüllung Petersbuch Bei Eichstätt. *Mitt. Bayer. Staatssamml. Paläontol. Hist. Geol.* **1970**, *10*, 407–432.
71. Rzebik-Kowalska, B. *Sorex bifidus* n. sp. and the Rich Insectivore Mammal Fauna (Erinaceomorpha, Soricomorpha, Mammalia) from the Early Pleistocene of Żabia Cave in Poland. *Palaeontol. Electron.* **2013**, *16*, 1–35. [CrossRef] [PubMed]
72. Berto, C.; Luzi, E.; Marchetti, M.; Pereswiet-Soltan, A.; Sala, B. Faunal Renewals during the Early Pleistocene on the Northern Italian Peninsula: Climate and Environment Reconstructions Inferred from the Rivoli Veronese Small Mammal Assemblage (Adige River Valley, Verona, Italy). *Quat. Int.* **2022**, *633*, 134–153. [CrossRef]
73. Fostowicz-Frelik, Ł. Revision of *Hypolagus* (Mammalia: Lagomorpha) from the Plio-Pleistocene of Poland: Qualitative and Quantitative Study. *Ann. Zool.* **2007**, *57*, 541–590.
74. Popov, V.V. Pliocene Small Mammals (Mammalia, Lipotyphla, Chiroptera, Lagomorpha, Rodentia) from Muselievo (North Bulgaria). *Geodiversitas* **2004**, *26*, 403–491.
75. Čermák, S. The Plio-Pleistocene Record of *Hypolagus* (Lagomorpha, Leporidae) from the Czech and Slovak Republics with Comments on Systematics and Classification of the Genus. *Bull. Geosci.* **2009**, *84*, 497–524. [CrossRef]
76. Kretzoi, M. Die Altpleistozänen Wirbeltierfaunen Des Villanyer Gebirges. *Geol. Hung. Ser. Palaeontol.* **1956**, *27*, 1–264.
77. López Martínez, N. Les Lagomorphes (Mammalia) Du Pléistocène Supérieur de Jaurens. *Nouv. Arch. Muséum D'histoire Nat. Lyon* **1980**, *18*, 5–16. [CrossRef]
78. Markova, A.K. Micromammals from the Paleolithic Cave of Azyh. *Paleontol. Sbor.* **1982**, *19*, 14–28. (In Russian)
79. Erbaeva, M.A. *Cenozoic Pikas (Taxonomy, Systematics, Phylogeny)*; Nauka: Moscow, Russia, 1988.
80. Vekua, A.K. A New Representative of Lagomyidae from the Paleolithic of Georgia. *Soobšč. Akad. Nauk GSSR* **1967**, *15*, 139–143. (In Russian)
81. Fostowicz-Frelik, Ł.; Frelik, G.J.; Gasparik, M. Morphological Phylogeny of Pikas (Lagomorpha: Ochotona), with a Description of a New Species from the Pliocene/Pleistocene Transition of Hungary. *Proc. Acad. Nat. Sci. Phila.* **2010**, *159*, 97–118. [CrossRef]
82. Erbajeva, M.A.; Montuire, S.; Chaline, J. New Ochotonids (Lagomorpha) from the Pleistocene of France. *Geodiversitas* **2001**, *23*, 395–409.
83. Popov, V.V. Quaternary Small Mammals from Deposits in Temnata-Prohodna Cave System. *Temnata Cave Excav. Karlukovo Karst Area Bulg.* **1994**, *1*, 11–53.
84. Chaline, J. Les Rongeurs Du Pléistocène Moyen et Supérieur de France: Systématique-Biostratigraphie-Paléoclimatologie. In *Cahiers de Paléontologie*; C.N.R.S.: Paris, France, 1972; pp. 1–410.
85. Maul, L. Die Kleinsaugerreste (Insectivora, Lagomorpha, Rodentia) Aus Dem Unterpleistozän von Untermassfeld. *Das Pleistozän Untermassfeld Bei Meining.* **2001**, *3*, 783–887. [CrossRef]
86. Heinrich, W.D. Biometrische Untersuchungen an Fossilen Kleinsäugetieren Aus Einer Jungpleistozänen Deckschichtenfolge Über Dem Interglazialen Travertin von Burgtonna in Thürungen. *Quartärgeologie* **1978**, *3*, 255–268. [CrossRef]
87. Heinrich, W.D.; Janossy, D. Fossile Säugetierreste Aus Einer Jungpleistozänen Deckschichtenfolge Über Dem Interglazialen Travertin von Burgtonna in Thüringen. *Quartärpaläontologie* **1978**, *3*, 231–254. [CrossRef]
88. Kormos, T. Die Säugetiere Der Felsnische Pilisszántó in Systematischer Zoogeographischer Und Hylogenetischer Hinsicht. *Mitteilungen Jahrb. K. Ung. Geol. Reichsanst.* **1916**, *23*, 331–523.
89. Kowalski, K.; Nadachowski, A. Rodentia. In *Excavation in the Bacho Kiro Cave*; Polish Scientific Publishers: Warsaw, Poland, 1982.
90. Sinitsa, M.V.; Virág, A.; Pazonyi, P.; Knitlová, M. Redescription and Phylogenetic Relationships of *Spermophilus citelloides* (Rodentia: Sciuridae: Xerinae), a Ground Squirrel from the Middle Pleistocene—Holocene of Central Europe. *Hist. Biol.* **2021**, *33*, 19–39.
91. Storch, G. Eine Mittelpleistozäne Nager-Fauna von Der Insel Chios, Ägäis (Mammalia: Rodentia). *Senckenberg. Biol.* **1975**, *56*, 165–189.
92. Popova, L.V.; Maul, L.C.; Zagorodniuk, I.V.; Veklych, Y.M.; Shydlovskiy, P.S.; Pogodina, N.V.; Bondar, K.; Strukova, T.V.; Parfitt, S.A. Good Fences Make Good Neighbours': Concepts and Records of Range Dynamics in Ground Squirrels and Geographical Barriers in the Pleistocene of the Circum-Black Sea Area. *Quat. Int.* **2019**, *509*, 103–120. [CrossRef]
93. Danukalova, G.; Yakovlev, A.; Kosintcev, P.; Agadjanian, A.; Alimbekova, L.; Eremeev, A.; Morozova, E. Quaternary Fauna and Flora of the Southern Urals Region (Bashkortostan Republic). *Quat. Int.* **2009**, *201*, 13–24. [CrossRef]

94. Czernielewski, M. *Rodents (Rodentia, Mammalia) from the Late Pliocene Site of Węże 2: Systematics, Biogeography and Ecomorphology*; Instytut Paleobiologii Polskiej Akademii: Warsaw, Poland, 2024.
95. Sulimski, A. Pliocene Lagomorpha and Rodentia from Węże I (Poland). *Acta Palaeontol. Pol.* **1964**, *9*, 149–244.
96. Rekovets, L.; Nadachowski, A. Pleistocene Voles (Arvicolidae) of the Ukraine. *Paleontol. Evol.* **1995**, *28–29*, 145–245. [CrossRef]
97. Kowalski, K. Pleistocene Rodents of Europe. *Folia Quat.* **2001**, *72*, 3–389.
98. Kormos, T. Diagnosen Neuer Säugetiere Aus Der Oberpliozänen Fauna Des Somlyóberges Bei Püspökfürdő. *Ann. Musei Natl. Hung.* **1930**, *27*, 237–246.
99. Pucek, Z. Familie Zapodidae Coues, 1875-Hüpfmäuse. In *Handbuch der Säugetiere Europas*; Akademische Verlagsgesellschaft: Wiesbaden, Germany, 1982; Volume 2, pp. 497–583.
100. Kalthoff, D.C.; Mörs, T.; Tesakov, A. Late Pleistocene Small Mammals from the Wannenköpfe Volcanoes (Neuwied Basin, Western Germany) with Remarks on the Stratigraphic Range of Arvicola Terrestris. *Geobios* **2007**, *40*, 609–623. [CrossRef]
101. Popov, V. Pliocene-Quaternary Small Mammals (Eulipotyphla, Chiroptera, Lagomorpha, Rodentia) in Bulgaria: Biostratigraphy, Paleoecology and Evolution. In *The Pleistocene*; Nova Science Publishers: New York, NY, USA, 2018; pp. 109–235.
102. Hír, J. Allocricetus Ehiki Schaub, 1930 (Rodentia, Mammalia) Finds from Villány 3 and Osztramos 3 (Hungary). *Fragm. Mineral. Palaeontol.* **1993**, *16*, 61–80.
103. Fahlbusch, V. Pliozäne Und Pleistozäne Cricetinae (Rodentia, Mammalia) Aus Polen. *Acta Zool. Cracoviensia* **1969**, *14*, 99–137.
104. Pradel, A. Fossil Hamsters (Cricetinae, Rodentia) from the Pliocene and the Quaternary of Poland. *Acta Zool. Cracoviensis* **1988**, *31*, 235–296.
105. Horáček, I.; Lebedová, K. Cricetinae in the Quaternary Fossil Record of the Czech Republic and Slovakia (Rodentia: Cricetidae). *Lynx* **2023**, *53*, 365–415. [CrossRef]
106. Kurtén, B. *Pleistocene Mammals of Europe*; Weidenfeld & Nicolson: London, UK, 1968.
107. Mayhew, D. Late Pleistocene Small Mammals from Amissa (Macedonia, Greece). *Proc. K. Ned. Akad. Van Wetenschappen. Ser. B* **1978**, *81*, 302–323. [CrossRef]
108. Hír, J. Cricetulus Migratorius (Pallas, 1773) (Rodentia, Mammalia) Population from the Toros Mountains (Turkey) (with a Special Reference to the Relation of Cricetulus and Allocricetus Genera). *Folia Hist.-Nat. Musei Matra.* **1993**, *18*, 17–34.
109. Hír, J. Cricetids (Rodentia, Mammalia) of the Early Pleistocene Vertebrate Fauna of Somssich-Hegy 2 (Southern Hungary, Villány Mountains). *Ann. Hist.-Nat. Musei Natl. Hung.* **1998**, *90*, 57–90.
110. Sesé, C.; Soto, E. Los Micromamíferos (Rodentia, Insectivora y Lagomorpha). En: La Cueva de Ambrosio (Almería, Spain) y Su Posición Cronoestratigráfica En El Mediterráneo Occidental. *BAR Int. Ser.* **1988**, *462*, 157–168.
111. Jánossy, D. *Pleistocene Vertebrate Faunas of Hungary*; Elsevier: Amsterdam, The Netherlands, 1986; Volume 8.
112. Povoas, L.; Zilhao, J.; Chaline, J.; Brunet-Lecomte, P. La Faune de Rongeurs Du Pléistocène Supérieur de La Grotte de Caldeirao (Tomar, Portugal). *Quaternaire* **1992**, *3*, 40–47. [CrossRef]
113. Cuenca-Bescós, G. Análisis Filogenético de Allocricetus Del Pleistoceno (Cricetidae, Rodentia, Mammalia). *Coloq. Paleontol.* **2003**, *1*, 95–113. [CrossRef]
114. Paunovic, M.; Rabeder, G. Early Pleistocene micromammal faunas of Razvodje and Tatinja draga in South-Croatia. *Beitr. Paläontol.* **1996**, *21*, 69–84.
115. Hír, J. A Short Sketch of the Evolution and Stratigraphy of the Plio-Pleistocene Cricetids (Rodentia, Mammalia) in Hungary. *Folia Hist.-Nat. Musei Matra.* **1997**, *22*, 43–49.
116. Santel, W.; Von Koenigswald, W. Preliminary Report on the Middle Pleistocene Small Mammal Fauna from Yarimburgaz Cave in Turkish Thrace. *EG Quat. Sci. J.* **1998**, *48*, 162–169. [CrossRef]
117. Hinton, M.A.C. *Monograph of the Voles & Lemmings (Microtinae) Living and Extinct*; Order of the Trustees of the British Museum: London, UK, 1926; Volume 1.
118. Escudé, E.; Montuire, S.; Desclaux, E.; Quéré, J.-P.; Renvoisé, E.; Jeannet, M. Reappraisal of «chronospecies» and the Use of *Arvicola* (Rodentia, Mammalia) for Biochronology. *J. Archaeol. Sci.* **2008**, *35*, 1867–1879. [CrossRef]
119. Bol'shakov, V.N.; Vasileva, I.A.; Maleyeva, A.G. *Morphotypic Variability of Vole Teeth*; Nauka: Moscow, Russia, 1980.
120. Hinton, M.A. Diagnoses of Species of Pitymys and Microtus Occurring in the Upper Freshwater Bed of West Runton, Norfolk. *J. Nat. Hist.* **1923**, *12*, 541–542. [CrossRef]
121. Forsyth Major, C.I. Exhibition of, and Remarks upon Some Jaws and Teeth of Pliocene Voles (Mimomys Gen. Nov.). *Proc. Zool. Soc.* **1902**, *1*, 102–107.
122. Nadachowski, A. Comments on Variation, Evolution, and Phylogeny of Chionomys (Arvicolidae). In *International Symposium Evolution, Phylogeny and Biostratigraphy of Arvicolids (Rodentia, Mammalia)*; Geological Survey: Prague, Czech Republic, 1990; pp. 353–368.
123. Kretzoi, M. New Names for Arvicolid Homonyms. *Ann. Hist.-Nat. Musei Natl. Hung.* **1958**, *50*, 55–58.
124. Nadachowski, A. Systematics, Geographic Variation, and Evolution of Snow Voles (Chionomys) Based on Dental Characters. *Acta Theriol.* **1991**, *36*, 1–45. [CrossRef]

125. Kretzoi, M. Skizze Einer Arvicoliden-Phylogenie Stand. *Vertebr. Hung. Musei Hist.-Nat. Hung.* **1969**, *11*, 155–193.
126. Van der Meulen, A.; Zagwijn, W.H. Microtus (Allophaiomys) Pliocaenicus from the Lower Pleistocene near Brielle, The Netherlands. *Scr. Geol.* **1974**, *21*, 1–12.
127. Garapich, A.; Nadachowski, A. A Contribution to the Origin of Allophaiomys [Arvicolidae, Rodentia] in Central Europe: The Relationship between Mimomys and Allophaiomys from Kamyk [Poland]. *Acta Zool. Cracoviensia* **1996**, *39*, 179–184.
128. Laplana, C.; Montuire, S.; Brunet-Lecomte, P.; Chaline, J. Révision des Allophaiomys (Arvicolinae, Rodentia, Mammalia) des Valerots (Côte-d'Or, France). *Geodiversitas* **2000**, *22*, 255–267.
129. Ünay, E.; Emre, Ö.; Erkal, T.; Keçer, M. The Rodent Fauna from the Adapazarı Pull-Apart Basin (NW Anatolia): Its Bearings on the Age of the North Anatolian Fault. *Geodin. Acta* **2001**, *14*, 169–175. [CrossRef]
130. van der Meulen, A.J. *Microtus (Allophaiomys)* Deucalion (Kretzoi, 1969), (Arvicolidae, Rodentia) from the Upper Villányian (Lower Pleistocene) of Villány-5, S. Hungary. *Koninkl. Nedrl. Akad. Wet.* **1974**, *77*, 259–266.
131. Markova, A.K. Eastern European Rodent (Rodentia, Mammalia) Faunas from the Early–Middle Pleistocene Transition. *Quat. Int.* **2005**, *131*, 71–77. [CrossRef]
132. Markova, A.K.; Vislobokova, I.A. Mammal Faunas in Europe at the End of the Early—Beginning of the Middle Pleistocene. *Quat. Int.* **2016**, *420*, 363–377. [CrossRef]
133. Hir, J.; Venczel, M. New Allophaiomys Material from Betfia. *Meded. Ned. Inst. Toegepaste Geowet. TNO* **1994**, *60*, 305–312.
134. Alcalde, G.; Agustí, J.; Villalta, J.D. Un Nuevo Allophaiomys (Arvicolidae, Rodentia, Mammalia) En El Pleistoceno Inferior Del Sur de España. *Acta Geológica Hispánica* **1981**, *16*, 203–205.
135. Cuenca-Bescos, G.; Rofes, J.; López-García, J.M.; Blain, H.A.; De Marfá, R.J.; Galindo-Pellicena, M.A.; Bennásar-Serra, M.L.; Melero-Rubio, M.; Arsuaga, J.L.; de Castro, J.M.B.; et al. Biochronology of Spanish Quaternary Small Vertebrate Faunas. *Quat. Int.* **2010**, *212*, 109–119. [CrossRef]
136. Nadachowski, A.; Zagorodnyuk, I. Recent Allophaiomys-like Species in the Palaearctic: Pleistocene Relicts or a Return to an Initial Type. *Acta Zool. Cracoviensia* **1996**, *39*, 387–394.
137. Petronio, C.; Angelone, C.; Atzori, P.; Famiani, F.; Kotsakis, T.; Salari, L. Review and New Data of the Fossil Remains from Monte Peglia (Late Early Pleistocene, Central Italy). *Riv. Ital. Paleontol. Stratigr.* **2020**, *126*, 791–819. [CrossRef] [PubMed]
138. Cuenca-Bescós, G.; Rofes, J.; López-García, J.M.; Blain, H.-A.; Gabal-Garcés, R.; Sauqué, V.; Arsuaga, J.L.; Bermúdez de Castro, J.M.; Carbonell, E. The Small Mammals of Sima Del Elefante (Atapuerca, Spain) and the First Entrance of Homo in Western Europe. *Quat. Int.* **2013**, *295*, 28–35. [CrossRef]
139. Maul, L.C.; Heinrich, W.-D.; Parfitt, S.A.; Paunescu, A.-C. Comment on the Correlation between Magnetostratigraphy and the Evolution of *Microtus* (Arvicolidae, Rodentia, Mammalia) during the Early and Early Middle Pleistocene. *Cour. Forsch.-Inst. Senckenberg* **2007**, *259*, 243–263.
140. Cuenca-Bescós, G.; Canudo, J.I.; Laplana, C. Los Arvicólidos (Rodentia, Mammalia) de Los Niveles Inferiores de Gran Dolina (Pleistoceno Inferior, Atapuerca, Burgos, España). *Rev. Esp. Paleontol.* **1995**, *10*, 202–218.
141. Maul, L.; Masini, F.; Abbazzi, L.; Turner, A. The Use of Different Morphometric Data for Absolute Age Calibration of Some South- and Middle European Arvicolid Populations. *Palaeontogr. Ital.* **1998**, *85*, 111–151.
142. Terzea, E. Remarques Sur La Morphologie Dentaire et La Répartition de Microtus Nivalis Martins (Rodentia, Mammalia) Dans Le Pléistocène de Roumanie. *Trav. Inst. Spéol. Emile Racovitza* **1972**, *11*, 271–298.
143. Nadachowski, A. *Late Quaternary Rodents of Poland with Special Reference to Morphotype Dentition Analysis of Voles*; Panstwowe Wydawnictwo Naukowe: Warsaw, Poland, 1982.
144. Baca, M.; Popović, D.; Lemanik, A.; Fewlass, H.; Talamo, S.; Zima, J.; Ridush, B.; Popov, V.; Nadachowski, A. The Tien Shan Vole (Microtus Ilaeus; Rodentia: Cricetidae) as a New Species in the Late Pleistocene of Europe. *Ecol. Evol.* **2021**, *11*, 16113–16125. [CrossRef] [PubMed]
145. Heller, F. Die Wühlmäuse (Mammalia, Rodentia, Arvicolidae) des Ältest-und Altpleistozäns Europas: Eine Übersicht über die bisher bekannten Gattungen und Arten. *Quartär – Int. Jahrb. Zur Erforsch. Des Eiszeitalt. Und Der Steinzeit* **1968**, *19*, 23–53.
146. Stuart, A.J. The Vertebrate Fauna of the Type Cromerian. *Boreas* **1975**, *4*, 63–76. [CrossRef]
147. Markova, A.K. Paleolandscape Reconstruction of Likhvin Interglacial by the Data of Eastern European Small Mammals. *Izv. RAN Ser. Geogr.* **2004**, *2*, 39–51.
148. Prost, S.; Guralnick, R.P.; Waltari, E.; Fedorov, V.B.; Kuzmina, E.; Smirnov, N.; Van Kolfschoten, T.; Hofreiter, M.; Vrieling, K. Losing Ground: Past History and Future Fate of Arctic Small Mammals in a Changing Climate. *Glob. Change Biol.* **2013**, *19*, 1854–1864. [CrossRef] [PubMed]
149. Baca, M.; Popović, D.; Lemanik, A.; Baca, K.; Horáček, I.; Nadachowski, A. Highly Divergent Lineage of Narrow-Headed Vole from the Late Pleistocene Europe. *Sci. Rep.* **2019**, *9*, 17799. [CrossRef] [PubMed]
150. Jánossy, D.; van der Meulen, A.J. On Mimomys (Rodentia) from Osztramos-3, North Hungary. *Nederl. Akad. Wet. Proc. B* **1975**, *78*, 381–391.

151. Bachelet, B. Muridae et Arvicolidae (Rodentia, Mammalia) Du Pliocène Du Sud de La France: Systématique, Évolution, Biochronologie. Ph.D. Thesis, Université des Sciences et Techniques du Languedoc, Montpellier, France, 1990.
152. Aguilar, J.-P.; Bachelet, B.; Lesage, J.-L.; Michaux, J. Le Gisement Karstique Du Grand Serre (Commune de Montclus, Gard). Données Nouvelles Sur Les Faunes de Rongeurs Du Pliocène Terminal Dans Le Sud de La France. *Geobios* **1993**, *26*, 633–640. [CrossRef]
153. Mayhew, D.F.; Stuart, A.J. Stratigraphic and Taxonomic Revision of the Fossil Vole Remains (Rodentia, Microtinae) from the Lower Pleistocene Deposits of Eastern England. *Philos. Trans. R. Soc. Lond.* **1986**, *1986*, 431–485. [CrossRef]
154. van Kolfschoten, T. Review of the Pleistocene Arvicolid Faunas from the Netherlands. In *International Symposium on Evolution, Phylogeny, Biostratigraphy of Arvicolids*; Geological Survey: Prague, Czech Republic, 1990; pp. 255–274.
155. Galobart, A.; Agustí, J. Los Micromamíferos de Los Yacimientos Del Pleistoceno Inferior de Incarcal (Girona, NE de La Península Ibérica). *Paleontol. Evol.* **2003**, *34*, 63–67.
156. Popov, V.V. Early Pleistocene Small Mammals (Eulipothyphla, Chiroptera, Lagomorpha and Rodentia) from Futjova Cave, North Bulgaria. *Acta Zool. Bulg.* **2017**, *69*, 263–282.
157. Tesakov, A.S. Voles of the Tegelen Fauna. *Meded. Ned. Inst. Toegepaste Geowet. TNO* **1998**, *60*, 71–134.
158. Mayhew, D.F. West European Arvicolid Evidence of Intercontinental Connections during the Early Pleistocene. *Quat. Int.* **2013**, *284*, 62–73. [CrossRef]
159. Serdyuk, N.V. Some of the Small Mammals from Haarstrang Site (Germany). *Geol. Paläontol. Westfal.* **2010**, *76*, 75–81.
160. Siori, M.S.; Sala, B. The Mammal Fauna from the Late Early Biharian Site of Castagnone (Northern Monferrato, Piedmont, NW Italy). *Geobios* **2007**, *40*, 207–217. [CrossRef]
161. Rabeder, G. *Mimomys malezi* n. sp., Ein Neuer Arvicolide (Rodentia) Aus Dem Altpleistozän von Dalmatien. *Beitr. Paläontol. Osterr.* **1983**, *10*, 1–13.
162. Kościów, R.; Nadachowski, A. Type Populations of Some Mimomys Species (Arvicolidae, Rodentia) at the Pliocene/Pleistocene Boundary in Central Europe. *Folia Zool.* **2002**, *51*, 93–104.
163. Van Den Hoek Ostende, L.W.; Diepeveen, F.; Tesakov, A.; Saraç, G.; Mayhew, D.; Alçiçek, M.C. On the Brink: Micromammals from the Latest Villanyian from Bıçakçı (Anatolia). *Geol. J.* **2015**, *50*, 230–245. [CrossRef]
164. Tesakov, A.S. Evolution of Small Mammal Faunas and Late Cenozoic Continental Biostratigraphy of Southern Eastern Europe and Western Asia. Doctoral Dissertation, Geological Institute of the Russian Academy of Sciences, Moscow, Russia, 2021.
165. Nadachowski, A. Biharian Voles (*Arvicolidae*, *Rodentia*, *Mammalia*) from Kozi Grzbiet (Central Poland). *Acta Zool. Cracoviensia* **1985**, *29*, 13–28.
166. Bartolomei, G.; Chaline, J.; Fejfar, O.; Jánossy, D.; Jeannet, M.; Koenigswald, W.; Kowalski, K. Pliomys Lenki Heller 1930 (Rodentia, Mammalia) En Europe. *Acta Zool. Cracoviensa* **1975**, *20*, 393–467.
167. Terzea, E. *Pliomys lenki* (Heller, 1930) (Rodentia, Mammalia), Dans Le Pléistocène de Roumanie. *Trav. Inst. Spéol. «E. Racovitza»* **1983**, *22*, 65–80.
168. Sala, B. Dinaromys Allegranzii n.sp.[Mammalia, Rodentia] from Rivoli Veronese [Northeastern Italy] in a Villanyian Association. *Acta Zool. Cracoviensia* **1996**, *39*, 469–472.
169. Nesin, V.A.; Skorik, A.F. First Find of Dinaromys Vole (Rodentia, Microtinae) in the USSR. *Vestn. Zool.* **1989**, *5*, 14–17.
170. Kormos, T. Über Eine Neuentdeckte Forestbed-Fauna in Dalmatien. *Palaeobiologica* **1931**, *4*, 113–136.
171. Kormos, T.; Mimomys Newtoni, F. Major Und Lagurus Pannonicus Kormos, Zwei Gleichzeitig Verwandte Wühlmäuse von Verschiedener Phylogenetischer Entwicklung. *Mathem. Naturwissenschaft. Anz. Ung. Akad. Wiss.* **1938**, *57*, 353–379.
172. Terzea, E. Chronologie de Faunes de Mammifères Pléistocènes Du Nord-Ouest de La Roumanie et Évolution Des Lagurinés (Rodentia). *Trav. Inst. Spéol. «Émile Racovitza»* **1995**, *34*, 171–186.
173. Popov, V.V. Early Pleistocene Rodentia (Mammalia) from the (Temnata Dupka) Cave near Karlukovo (North Bulgaria). *Acta Zool. Bulg.* **1986**, *30*, 3–14.
174. Jablonski, D. Species Selection: Theory and Data. *Annu. Rev. Ecol. Evol. Syst.* **2008**, *39*, 501–524. [CrossRef]
175. Mayhew, D.F. Revision of the Fossil Vole Assemblage (Mammalia, Rodentia, Arvicolidae) from Pleistocene Deposits at Kisláng, Hungary. *Palaeontol* **2012**, *55*, 11–29. [CrossRef]
176. Terzea, E. Les Arvicolides (Rodentia, Mammalia) Du Pléistocène Moyen de Chiscau-1 (Depart. de Bihor, Roumanie). *Trav. l'Institut Spéol. "Emile Racovitza"* **1989**, *28*, 57–72.
177. Terzea, E. Biochronology of the Pleistocene Deposits at Betfia (Bihor, Romania). *Acta Zool. Cracoviensia* **1996**, *39*, 531–540.
178. Mayhew, D.F. The Type Material and the Enamel Structure of Villanyia Exilis Kretzoi, 1956 (Arvicolidae, Rodentia). *Acta Zool. Cracoviensia-Ser. A Vertebr.* **2009**, *52*, 81–94. [CrossRef]
179. Pasquier, L. Dynamique Évolutive d'un Sous-Genre de Muridae, Apodemus (Sylvaemus). Étude Biométrique Des Caractères Dentaires de Populations Fossiles et Actuelles d'Europe Occidentales. Ph.D. Thesis, Université de Montpellier, Montpellier, France, 1974.
180. Freudenthal, M.; Martín-Suárez, E. Size Variation in Samples of Fossil and Recent Murid Teeth. *Scr. Geol.* **1990**, *93*, 1–34.

181. Knitlová, M.; Horáček, I. Late Pleistocene-Holocene Paleobiogeography of the Genus Apodemus in Central Europe. *PLoS ONE* **2017**, *12*, e0173668. [CrossRef] [PubMed]
182. Knitlová, M.A.; Horáček, I. Genus Apodemus in the Pleistocene of Central Europe: When Did the Extant Taxa Appear. *Foss. Impr.* **2017**, *74*, 460–481. [CrossRef]
183. Cai, B.; Qiu, Z. Murid Rodents from the Late Pliocene of Yangquan and Yuxian, Hebei. *Vertebr. Palasiat.* **1993**, *31*, 267–293.
184. Martín-Suárez, E.; Mein, P. Revision of the Genera Parapodemus, Apodemus, Rhagamys and Rhagapodemus (Rodentia, Mammalia). *Geobios* **1998**, *31*, 87–97. [CrossRef]
185. Minwer-Barakat, R.; Madurell-Malapeira, J.; Alba, D.M.; Aurell-Garrido, J.; De Esteban-Trivigno, S.; Moyà-Solà, S. Pleistocene Rodents from the Torrent de Vallparadís Section (Terrassa, Northeastern Spain) and Biochronological Implications. *J. Vertebr. Paleontol.* **2005**, *31*, 849–865.
186. Rietschel, S.; Storch, G. Aussergewöhnlich Erhaltene Waldmäuse (Apodemus Atavus Heller, 1936) Aus Dem Ober-Pliozän von Willershausen Am Harz. *Senckenberg. Lethaea* **1974**, *54*, 491–519.
187. Fejfar, O.; Storch, G. Eine Pliozäne (Ober-Ruscinische) Kleinsäugerfauna Aus Gundersheim, Rheinhessen. 1. Nagetiere: Mammalia, Rodentia. *Senckenberg. Lethaea* **1990**, *71*, 139–184.
188. de Bruijn, H.; van der Meulen, A.J. The Early Pleistocene Rodents from Tourkobounia-1 (Athens, Greece). *Proc. K. Ned. Akad. Wet. B* **1975**, *78*, 314–338.
189. Kumar, S.; Suleski, M.; Craig, J.E.; Kasprowicz, A.E.; Sanderford, M.; Li, M.; Stecher, G.; Hedges, S.B. TimeTree 5: An Expanded Resource for Species Divergence Times. *Mol. Biol. Evol.* **2022**, *39*, msac174. [CrossRef] [PubMed]
190. Pazonyi, P.; Szentesi, Z.; Trembeczki, M.; Hír, J.; Mészáros, L. A New Middle Pleistocene Small Vertebrate Fauna from the Nagyharsány Crystal Cave (Villány Hills, Southern Hungary). *Fragm. Palaeontol. Hung.* **2021**, *37*, 101–126. [CrossRef]
191. Heller, F. Eine Forest-Bed-Fauna Aus Der Sackdillinger Hôhle (Oberpfalz). *Neues Jahrb. Mineral. Geol. Palaontol. Beil.-Band* **1930**, *63*, 247–298.
192. Paunesco, A.-C.; Abbassi, M. Les Variations d'Eliomys (Myoxidae, Rodentia) Durant Le Quaternaire. *Bull. Mus. Anthropol. Préhist. Monaco* **2000**, *242*, 3–13.
193. Kowalski, K. The Pliocene and Pleistocene Gliridae (Mammalia, Rodentia) from Poland. *Acta Zool. Cracoviensia* **1963**, *8*, 533–567.
194. Daams, R. The Dental Pattern of the Dormice Dryomys, Myomimus, Microdyromys and Peridyromys. *Utrecht Micropaleontol. Bull. Spec. Publ.* **1981**, *3*, 1–115.
195. Kuss, S.; Storch, G. Eine Säugetierfauna (Mammalia: Artiodactyla, Rodentia) Des Älteren Pleistozänsvon Der Insel Kalymnos (Dodékanes; Griechenland). *Neues Jahrb. Geol. Paläontol. Monatshefte* **1978**, *4*, 206–227.
196. Heinrich, W.-D.; Maul, L.C. Mortality Profiles of Castor and Trogontherium (Mammalia: Rodentia, Castoridae), with Notes on the Site Formation of the Mid-Pleistocene Hominin Locality Bilzingsleben II (Thuringia, Central Germany). *Foss. Impr.* **2020**, *76*, 40–58. [CrossRef]
197. Fostowicz-Frelik, Ł. First Record of Trogontherium Cuvieri (Mammalia, Rodentia) from the Middle Pleistocene of Poland and Review of the Species. *Geodiversitas* **2008**, *30*, 765–778.
198. Stefen, C. Intraspecific Variability of Beaver Teeth (Castoridae: Rodentia). *Zool. J. Linn. Soc.* **2009**, *155*, 926–936. [CrossRef]
199. Cuenca-Bescós, G.; Ardévol, J.R.; Morcillo-Amo, Á.; Galindo-Pellicena, M.Á.; Santos, E.; Costa, R.M. Beavers (Castoridae, Rodentia, Mammalia) from the Quaternary Sites of the Sierra de Atapuerca, in Burgos, Spain. *Quat. Int.* **2017**, *433*, 263–277. [CrossRef]
200. Van Laere, G.; Mörs, T. Beavers and Flying Squirrels (Rodentia: Castoridae, Pteromyini) from the Late Pliocene of Hambach 11C, Germany. *Geodiversitas* **2023**, *45*, 223–241. [CrossRef]
201. Forsyth Major, C.F. On the Mammalian Fauna of the Val d'Arno. *Q. J. Geol. Soc.* **1885**, *41*, 1–8. [CrossRef]
202. Friant, M. A European Castor of the Quaternary Era, Castor Plicidens F. Maj. *J. Palaeontol. Soc. India* **1959**, *4*, 75–77. [CrossRef]
203. Terhune, C.E.; Curran, S.; Croitor, R.; Drăgușin, V.; Gaudin, T.; Petculescu, A.; Robinson, C.; Robu, M.; Werdelin, L. Early Pleistocene Fauna of the Olteţ River Valley of Romania: Biochronological and Biogeographic Implications. *Quat. Int.* **2020**, *553*, 14–33. [CrossRef]
204. Kotsakis, T. Turolian and Ruscinian Castorids: Some Observations. *Boll. Della Soc. Paleontol. Ital.* **1989**, *28*, 271–276.
205. Rook, L.; Sardella, R. Hystrix Refossa Gervais, 1852 from Pirro Nord (Early Pleistocene, Southern Italy). *Riv. Ital. Paleontol. Stratigr.* **2005**, *111*, 489. [CrossRef] [PubMed]
206. Van Weers, D.J. The Porcupine Hystrix Refossa Gervais, 1852 from the Plio-Pleistocene of Europe, with Notes on Other Fossil and Extant Species of the Genus Hystrix. *Scr. Geol.* **1994**, *106*, 35–52.
207. Van Weers, D.J. A Taxonomic Revision of the Pleistocene Hystrix (Hystricidae, Rodentia) from Eurasia with Notes on the Evolution of the Family. *Contrib. Zool.* **2005**, *74*, 301–312. [CrossRef]
208. Monchot, H.; Fernandez, P.; Gaillard, J.M. Paleodemographic Analysis of a Fossil Porcupine (Hystrix Refossa Gervais, 1852) Population from the Upper Pleistocene Site of Geula Cave (Mount Carmel, Israel). *J. Archaeol. Sci.* **2012**, *39*, 3027–3038. [CrossRef]

209. Andrews, P. *Owls, Caves and Fossils: Predation, Preservation and Accumulation of Small Mammal Bones in Caves, with an Analysis of the Pleistocene Cave Faunas from Westbury-Sub-Mendip, Somerset, UK*; University of Chicago Press: Chicago, IL, USA, 1990.
210. Gotelli, N.J.; Colwell, R.K. Quantifying Biodiversity: Procedure and Pitfalls in the Measurement and Comparison of Species Richness. *Ecol. Lett.* **2001**, *4*, 379–391. [CrossRef]
211. Hill, M.O. Twinspan: A Fortran Program for Arranging Multivariate Data in an Ordered Two-Way Table by Classification of the Individuals and Attributes. In *Ecology and Systematica*; Cornell University: Ithaca, NY, USA, 1979.
212. Fejfar, O.; Heinrich, W.D. Muroid Rodent Biochronology of the Neogene and Quaternary in Europe. In *European Neogene Mammal Chronology*; NATO ASI Series; Springer: Boston, MA, USA, 1990; Volume 180, pp. 91–117.
213. Tessakov, A. *Biostratigraphy of the Middle Pliocene-Eopleistocene of Eastern Europe*; Nauka: Moscow, Russia, 2004.
214. Markova, A.K. Pleistocene Mammal Faunas of Eastern Europe. *Quat. Int.* **2007**, *160*, 100–111. [CrossRef]
215. Krapp, M.; Beyer, R.; Edmundson, S.L.; Valdes, P.J.; Manica, A. A Statistics-Based Reconstruction of High-Resolution Global Terrestrial Climate for the Last 800,000 Years. *Sci. Data* **2021**, *8*, 228. [CrossRef] [PubMed]
216. Leonardi, M.; Hallett, E.Y.; Beyer, R.; Krapp, M.; Manica, A. Pastclim 1.2: An R Package to Easily Access and Use Paleoclimatic Reconstructions. *Ecography* **2023**, *2023*, e06481. [CrossRef]
217. Muttoni, G.; Scardia, G.; Kent, D.V. Early Hominins in Europe: The Galerian Migration Hypothesis. *Quat. Sci. Rev.* **2018**, *180*, 1–29. [CrossRef]
218. Watson, M.J.; Kerr, J.T. rTPI: An R Package for Calculating Thermal and Aridity Position Indices for Terrestrial Vertebrates. *Ecol. Evol.* **2026**, *16*, e73397. [CrossRef] [PubMed]
219. Bassinot, F.C.; Labeyrie, L.D.; Vincent, E.; Quidelleur, X.; Lancelot, Y. The Astronomical Theory of Climate and the Age of the Brunhes-Matuyama Magnetic Reversal. *Earth Planet. Sci. Lett.* **1994**, *B126*, 91–108. [CrossRef]
220. Loidi, J.; Navarro-Sánchez, G.; Vynokurov, D. Climatic Definitions of the World's Terrestrial Biomes. *Veg. Classif. Surv.* **2022**, *3*, 231–271. [CrossRef]
221. Shackleton, N.J. New Data on the Evolution of Pliocene Climatic Variability. In *Paleoclimate and Evolution, with Emphasis on Human Origins*; Yale University Press: New Haven, CT, USA; pp. 242–248.
222. Head, M.J.; Pillans, B.; Farquhar, S.A. The Early–Middle Pleistocene Transition: Characterization and Proposed Guide for the Defining Boundary. *Epis. J. Int. Geosci.* **2008**, *31*, 255–259. [CrossRef]
223. Masini, F.; Sala, B. Large- and Small-Mammal Distribution Patterns and Chronostratigraphic Boundaries from the Late Pliocene to the Middle Pleistocene of the Italian Peninsula. *Quat. Int.* **2007**, *160*, 43–56. [CrossRef]
224. Koenigswald, W.V.; Heinrich, W.D. Biostratigraphische Begriffe Aus Der Säugetierpaläontologie Für Das Pliozän Und Pleistozän Deutschlands. *EG Quat. Sci. J.* **2007**, *56*, 96–117. [CrossRef]

Disclaimer/Publisher's Note: The statements, opinions and data contained in all publications are solely those of the individual author(s) and contributor(s) and not of MDPI and/or the editor(s). MDPI and/or the editor(s) disclaim responsibility for any injury to people or property resulting from any ideas, methods, instructions or products referred to in the content.